CRPP

CENTRE DE RECHERCHES EN PHYSIQUE DES PLASMAS
FACULTÉ DES SCIENCES DE BASE
ASSOCIATION EURATOM - CONFÉDÉRATION SUISSE

ÉCOLE POLYTECHNIQUE
FÉDÉRALE DE LAUSANNE

ANNUAL REPORT

2010

Table of contents

Préface

Cher Lecteur,

C'est pour moi un grand privilège de vous présenter le Rapport Annuel 2010 du Centre de Recherches en Physique des Plasmas.

Nos activités principales, dans le domaine de la fusion, ont pour but la construction d' ITER, de s'assurer de son exploitation scientifique et de poser les bases d'une future centrale électrique de démonstration. Elles couvrent la physique des plasmas expérimentale, en particulier celle du tokamak, la modélisation numérique et la Recherche & Développement technologique, y compris les contributions de la Suisse dans le cade de « l'approche élargie ». Vous en trouverez les principales réalisations effectuées durant l'année 2010 dans ce rapport.

En plus de la recherche en fusion, le développement des procédés industriels utilisant le plasma a constitué une part importante de notre Recherche & Développement. Comme par le passé, ces activités ont attiré un grand intérêt de l'industrie.

Dernier point, mais non des moindres, l'éducation et la formation de jeunes scientifiques et ingénieurs, si importante considérant qu'il s'agira de la « génération ITER », a continué d'être une de nos forces.

A cette occasion, je voudrais remercier tous mes collègues, dont l'engagement nous a permis d'obtenir la richesse des résultats qui sont présentés dans ce rapport.

Toutes nos activités ont bénéficié du financement de plusieurs institutions publiques et privées. Sans leur support, bien des succès obtenus n'auraient pas été possibles, et je voudrais leur exprimer mes remerciements les plus sincères

Prof. M.Q. Tran
Directeur Général

Foreword

Dear Reader,

It is a great privilege for me to present the Annual Report for 2010 of the Centre de Recherches en Physique des Plasmas.

Our main activities in the field of fusion are aimed towards the construction of ITER, securing its scientific exploitation and laying the foundations of a demonstration power plant. They cover tokamak and experimental plasma physics, numerical modeling and technology R&D, which include the contributions of Switzerland in the frame of the Broader Approach. You will find in the report the main achievements during 2010.

Besides fusion research, the development of industrial processes based on plasmas has remained an important part of our R&D, which, as in the past, attracted great interest from the industry.

Last but not least, education and training of young scientists and engineers, specially of the ITER generation, has been and continued to be our strong point.

I would like to take this opportunity to thank all my colleagues, whose commitment has allowed us to achieve the wealth of results presented in the report.

All our activities have benefited from the funding of many public and private institutions: without their support many achievements would not have been possible and I would like to express my most sincere thanks to all of them.

Prof. M.Q. Tran
General Director

Vorwort

Liebe Leserin, lieber Leser,

Es ist für mich ein grosses Privileg, Ihnen hiermit den Jahresbericht 2010 des Centre de Recherches en Physique des Plasmas (CRPP) vorlegen zu können.

Unsere Hauptbetätigungsfelder im Bereich der Kernfusion sind der Bau von ITER, dessen erfolgreiche wissenschaftliche Ausbeute sowie die Grundsteinlegung für eine zukünftige Demonstrationsanlage zur Produktion von Elektrizität mittels Kernfusion. Diese Aktivitäten umfassen die experimentelle Plasmaphysik (insbesondere des Tokamaks), die numerische Modellierung sowie die Forschung und Entwicklung im Bereich der Fusionstechnologie. Dazu gehört ebenfalls der Beitrag der Schweiz zum erweiterten Forschungsprogramm „Broader Approach". Wir stellen die wichtigsten Ergebnisse unserer Arbeit im Jahre 2010 im vorliegenden Bericht vor.

Neben der Fusionsforschung sind unsere Anstrengungen im Bereich der industriellen Anwendung der Plasmaphysik ein wichtiges Standbein. Wie bereits in der Vergangenheit ist dieses Geschäftsfeld auf grosses Interesse seitens der Industrie gestossen.

Nicht zu vergessen ist natürlich die Aus- und Weiterbildung junger Studenten, Doktoranden, Wissenschaftler und Ingenieure – die „ITER-Generation" schlechthin. Sie ist selbstverständlich weiterhin eine unserer Prioritäten und Stärken.

An dieser Stelle möchte ich meinen Kollegen und Mitarbeitern für Ihren unermüdlichen Einsatz herzlich danken – ohne Sie könnte ich Ihnen nicht einen derart reichhaltigen Jahresbericht präsentieren.

Zahlreiche Institutionen aus dem öffentlichen und privaten Bereich haben unsere Tätigkeiten gefördert. Ohne Ihre Unterstützung und Treue wären viele der hier rapportierten Erfolge nicht möglich gewesen. Dafür möchte ich mich an dieser Stelle nochmals ausdrücklich bedanken.

Prof. M. Q. Tran
Generaldirektor

Prefazione

Caro lettore,

È per me un grande privilegio presentare il Rapporto Annuale 2010 del Centre de Recherches en Physique des Plasmas.

Le nostre attività principali nel campo della fusione mirano alla costruzione di ITER, ad assicurare il suo sfruttamento scientifico e a gettare le fondamenta per la costruzione di una centrale elettrica dimostrativa. Queste attività comprendono lo studio della fisica del tokamak e della fisica sperimentale del plasma, la modellizzazione numerica e la ricerca e lo sviluppo tecnologico. Esse includono inoltre il contributo della Svizzera nell'ambito del Broader Approach. I principali risultati conseguiti nell'anno 2010 possono essere trovati all'interno del rapporto.

A parte la ricerca nel campo della fusione, lo sviluppo di processi industriali basati sui plasmi è rimasto una parte importante del nostro programma di ricerca e sviluppo. Tale attività ha attirato grande interesse dall'industria, come nel passato.

Non da ultimo, l'educazione e la formazione di giovani scienziati e ingegneri, mi riferisco in particolare alla "generazione ITER", sono stati e continuano ad essere il nostro punto di forza.

Vorrei cogliere l'opportunità per ringraziare tutti i miei colleghi, il cui impegno ci ha permesso di raggiungere i numerosi risultati presentati nel rapporto.

Tutte le nostre attività hanno tratto beneficio dai fondi di molte istituzioni pubbliche e private: senza questo supporto, molti risultati non sarebbero stati possibili. Vorrei esprimere i miei più sinceri ringraziamenti a tutte queste istituzioni.

Prof. M.Q. Tran
Direttore Generale

1 INTRODUCTION

1.1 The international frame and its relation to the Swiss programme

1.1.1 ITER

The ITER Council approved in 2010 the ITER Baseline, a reference document that includes the project specifications, its schedule and objectives. In this baseline, the first plasma is foreseen towards the end of 2019. The scientific phase with operation in a D-T yielding 500MW fusion power is scheduled for 2026.

Important changes in the ITER project leadership occurred in 2010. Prof. Osamu Motojima, former director of the Japanese project Large Helical Device, was appointed Director General. He is assisted by Dr. Remmelt Haange as Deputy Director General in charge of the construction of ITER. Dr. Haange was responsible for the technical part of the large project W7-X of the Association Euratom - Max Planck Institute of Plasma Physics.

In Europe, the Joint Undertaking Fusion for Energy, which is responsible for the European contribution to ITER, was also re-organised under a new director, Dr. Franck Briscoe. The total budget for the European contribution to the in kind and in cash contribution to ITER construction is capped at 6.6 billions (2008 value). The budget 2012-2013 of the Euratom programme needs an increase of 1.3 billions . This budget increase is supported at all European levels, and proposal on how to finance it has been put forward. A final political discussion on funding instruments is being held among the concerned European institutions (Commission, Council and Parliament).

1.1.2 Euratom

As mentioned in the 2009 Annual Report, the funding of the Association Euratom – Swiss Confederation has continued to decrease in 2010, and this decrease is continuing in 2011. To define a national strategy, the CEPF has launched an audit of the CRPP with respect to its scientific contribution within the international programme, to its funding perspectives and the general governance of the Swiss fusion programme. The CRPP scientific achievements were highly praised by the international audit committee and its strategic vision, including its plans for upgrading the TCV tokamak, strongly endorsed. The audit will serve as a basis for the CEPF to define its strategy regarding fusion. The outcome of the CEPF assessment is expected in 2011.

In 2010, Switzerland has signed the High Performance Computer Implementing Agreement (IA) within the European Fusion Development Agreement (EFDA). A new IA covering fusion Power Plant Physics and Technology (PPPT-IA) was proposed in 2010. It will cover activities in physics needed to design a demonstration fusion power plant (called DEMO), which will produce significant electricity power to the grid.

Major JET enhancement projects were implemented in 2010, in particular to install a first wall similar to that foreseen for ITER, and the scientific operation will resume in 2011.

1.2 A brief summary of the CRPP activities

The general strategy of the CRPP in the field of fusion was endorsed by many international panels and its implementation was continued in 2010. The main lines are a contribution to the construction of ITER and the advancement of plasma science for ITER scientific exploitation. Regarding DEMO, the CRPP not only contributes to its physics basis but also to the key material science and technology developments. As part of the contract work given by the Swiss Government, it also performs R&D in the frame of the Broader Approach (BA).

The Annual Report 2010 will provide the readers with the details of all our achievements. Here below are just a few highlights:

- In TCV, a novel divertor configuration ("The Snowflake") was obtained and explored for the first time.

- In Torpex, a basic plasma physics device, the space and time characterisation of plasma filaments generation and evolution has brought new physics insight on heat and particle transport in magnetized plasmas.

- In the field of plasma simulations, evidence of spontaneous symmetry breaking in a tokamak (with an application to TCV) was analysed.

- Important contributions of the CRPP in the ITER construction were obtained in the field of superconductivity, electron cyclotron heating and magnetic diagnostics.

- Significant contributions were provided to the BA by CRPP, among which the design of a test cell for IFMIF, the development of the small sample test technology and of high voltage power supply for gyrotrons.

- The development of processes using plasma has been pursued in 2010 and continues to attract great interest from industry thanks to the high quality of the group.

1. INTRODUCTION

1.1 La situation internationale en relation avec le programme Suisse

1.1.1 ITER

Le Conseil d'ITER a pprouvé en 2010 le "ITER Baseline", qui est un document de référence incluant les spécifications du projet, son calendrier et ses objectifs. Selon cette base, le premier plasma est prévu pour la fin 2019, et la phase scientifique d'opération dans le deutérium-tritium, produisant 500MW de puissance de fusion, est attendue en 2026.

D'importants changements dans la direction du projet ont eu lieu en 2010. Prof. Osamu Motojima, ancien directeur du projet japonais « Large Helical Device », a été nommé Directeur Général. Il est assité du Dr Remmelt Haange, Directeur Général Adjoint en charge de la construction d'ITER. Dr Haange était, avant sa nomination, responsable de la technologie du grand projet W7-X de l'Association Euratom – Institut Max Planck de Physique des Plasmas.

En Europe, l'entreprise commune « Fusion for Energy », qui est responsable de la contribution européenne à ITER, a également été réorganisée sous une nouvelle direction, le Dr Franck Briscoe. Le budget total pour la contribution de l'Europe à la construction d'ITER, en nature et en espèces, est plafonnée à 6.6 milliards d' (valeur 2008).Le budget 2012-2013 du programme fusion de l'Euratom a besoin d'une augmentation de 1.3 milliards d' . Cette augmentation est soutenue à tous les niveaux européens, et une proposition de financement a été formulée. Une discussion finale sur les instruments de financement se tient parmi les institutions européennes concernées, soit la Commission, le Conseil et le Parlement.

1.1.2 Euratom

Le financement de l'Association Euratom – Confédération Suisse a poursuivi sa décrue, et cette décroissance continuera en 2011. Afin de définir une stratégie nationale, le CEPF a procédé à un audit du CRPP concernant sa contribution scientifique au programme international, ses perspectives de financement et la gouvernance générale du programme suisse de fusion. Le comité international d'audit a fait l'éloge appuyé des résultats scientifiques accomplis par le CRPP. Il a également donné son plein appui à sa vision stratégique. Cet audit servira de base au CEPF pour définir sa stratégie concernant la fusion. Le résultat de l'évaluation du CEPF est attendu pour 2011.

En 2010, la Suisse a signé un accord de mise en œuvre (Implementing Agreement, IA) sur le calcul à haute performance)High Perfromance Computing, HPC). Un nouvel IA couvrant la physique et la technologie d'une centrale électrique à fusion (Power Plant Physics and Technology, PPPT-IA) a été soumis en 2010. Il couvrira les activités de physique nécessaire au design d'une centrale électrique à fusion de démonstration, appelée DEMO, qui produira une puissance électrique substantielle sur le réseau.

Plusieurs projets d'amélioration ont été implémentés dans le tokamak JET, en particulier l'installation d'une première paroi similaire à celle prévue pour ITER. L'opération scientifique va reprendre en 2011.

1.2 Un bref résumé des activités du CRPP

La stratégie générale du CRPP dans le domaine de la fusion a été appuyée par plusieurs jurys internationaux, et son implémentation a continué en 2010. Les lignes principales en sont une contribution à la construction d'ITER et l'avancement de la science du plasma en vue de l'exploitation scientifique d'ITER. En ce qui concerne DEMO, le CRPP contribue non seulement à ses bases physiques, mais également aux développements de secteurs clés de la science des matériaux et de la technologie. Faisant partie du mandat de prestations du gouvernement Suisse, le CRPP accomplit aussi de la Recherche & Développement dans le cadre de « l'approche élargie » (Broader Approach, BA).

Le lecteur trouvera dans les pages qui suivent plus de détails sur nos résultats. Ci-dessous, seuls quelques points forts sont résumés:

- Dans TCV, une configuration nouvelle du divergeur, appelée « The Snowflake », a été obtenue et explorée pour la première fois au monde.

- Dans Torpex, une installation de physique des plasmas de base, la caractérisation spatio-temporelle de la génération et de l'évolution de filaments de plasma a apporté de nouvelles idées sur la physique du transport de chaleur et de particules dans les plasmas magnétisés.

- Dans le domaine de la simulation numérique des plasmas, une brisure spontanée de symétrie dans un tokamak a été mise en évidence et analysée, avec une application au TCV.

- D'importantes contributions à la construction d'ITER ont été obtenues par le CRPP dans les domaines de la supraconductivité, du chauffage électronique cyclotronique et des diagnostics magnétiques.

- Le CRPP a fourni des contributions substantielles à « l'approche élargie », parmi lesquelles le design d'une cellule de test pour IFMIF, le développement de la technologie de test de petits échantillons et le générateur de haute puissance pour les gyrotrons.

- Le développement des procédés plasmas s'est poursuivi en 2010 et a continué d'attirer un grand intérêt de la part de l'industrie, grâce à la haute qualité du groupe.

1 EINLEITUNG

1.1 Das internationale Umfeld und dessen Einfluss auf das schweizerischen Forschungsprogramm

1.1.1 ITER

Der ITER-Rat hat im Jahre 2010 die sogenannte ITER-Baseline genehmigt. Dieses Dokument enthält die Spezifikationen, die Ziele und den Zeitplan des ITER-Projekts. Nach aktuellem Planungsstand wird das erste ITER-Plasma gegen Ende 2019 erwartet. Die wissenschaftliche Betriebsphase mit D-T-Brennstoff, welche 500 MW Fusionsleistung erzielen soll, ist für aktuell für 2026 geplant.

Im Jahre 2010 gab es einige wichtige Änderungen in der ITER-Projektführung: Prof. Osamu Motojima, ehemaliger Direktor des japanischen Projekts Large Helical Device, wurde zum Generaldirektor ernannt. Dr. Remmelt Haange steht ihm als stellvertretender Generaldirektor zur Seite und ist verantwortlich für den Bau von ITER. Dr. Haange war vormals technischer Verantwortlicher des Grossprojekts W7-X des Max-Planck-Instituts für Plasmaphysik, EURATOM Association.

Die europäische ITER-Agentur, das sogenannte “Joint Undertaking Fusion for Energy”, wurde 2010 unter seinem neuen Direktor Dr. Frank Briscoe ebenfalls reorganisiert. Das Gesamtbudget des europäischen Beitrags zum Bau von ITER (Geld- und Sachleistungen), wurde auf 6.6 Mia. gedeckelt (Preisstand 2008).
Das Budget für das EURATOM-Programm 2012-2013 benötigt eine Aufstockung um 1.3 Mia. , welche von allen Europäischen Instanzen gutgeheissen wird und dessen Finanzierung bereits skizziert wurde. Die finale politische Diskussion der Finanzierungsinstrumente ist im Gange (Europäische Kommission, Europarat und Europäisches Parlament).

1.1.2 Euratom

Wie bereits in den Jahresberichten der Vorjahre erwähnt, wurde die finanzielle Zuwendung an die Association EURATOM – Confédération Suisse im Jahre 2010 erneut deutlich reduziert. Der Rückgang wird auch im Jahr 2011 anhalten.

Mit dem Ziel, eine nationale Strategie zu definieren, hat der ETH-Rat ein Audit des CRPP veranlasst. Dieses nahm den wissenschaftlichen Beitrag des CRPP ans internationale Forschungsprogramm, dessen Finanzierungsperspektiven sowie die allgemeine Governance des schweizerischen Forschungsprogrammes unter die Lupe.

Nach getaner Arbeit war das internationale Audit-Komitee des Lobes voll über die erzielten wissenschaftlichen Resultate des CRPP. Den strategischen Zielen, insbesondere den Ausbauplänen für den Tokamak TCV, wurde vollumfänglich beigepflichtet. Dieses Audit dient nun dem ETH-Rat als Grundlage für die Definition seiner Strategie bezüglich der Kernfusion. Die Resultate der Evaluierung durch den ETH-Rat werden im Laufe des Jahres 2011 erwartet.

Ausserdem hat die Schweiz im Jahre 2010 die Vereinbarung für Hochleistungsrechner, das "High Performance Computer (HPC) Implementing Agreement" (IA), im Rahmen des EFDA-Abkommens (European Fusion Development Agreement) unterzeichnet. Ein weiteres IA, jenes für "Power Plant Physics and Technology" (PPPT), wurde 2010 eingereicht. Dieses umfasst die grundlegenden physikalischen und technologischen Arbeiten zum Entwurf eines Demonstrationsfusionskraftwerks (DEMO), welches erstmals eine erhebliche elektrische Leistung ins Stromnetz einspeisen soll.

Am JET wurden 2010 ebenfalls bedeutende Verbesserungen realisiert – unter anderem ist die Installation einer ITER-ähnlichen Innenhülle des Torus zu erwähnen. Der wissenschaftliche Betrieb von JET wird 2011 wiederaufgenommen.

1.2 Eine Zusammenfassung der Forschungsergebnisse des CRPP

Die allgemeine Strategie des CRPP im Bereich der Kernfusion wurde durch zahlreiche internationale Gremien bestätigt und damit im Jahre 2010 weiterverfolgt. Die Eckpfeiler dieser Strategie sind die Beiträge zum Bau von ITER und das Vorantreiben der Plasmaphysik im Hinblick auf den wissenschaftlichen Betrieb von ITER. Die Mitwirkung am DEMO-Projekt ist vielfältig: Insbesondere die Beiträge zu dessen physikalischen Grundlagen, die Anstrengungen zum Meistern der technologischen Herausforderungen und die Ausübung einer Schlüsselrolle im Bereich der Materialwissenschaft sind hervorzuheben. Im Auftrag der Schweizer Regierung kümmert sich das CRPP ebenfalls um die Forschungs- und Entwicklungsprojekte im Rahmen des erweiterten Programms zur Fusion, „Broader Approach“ (BA).

Der Geschäftsbericht 2010 gibt einen Überblick über unsere Tätigkeiten und beschreibt detailliert die erzielten Resultate. Herausragende Ergebnisse sind:

- Erstmals weltweit wurde im Tokamak TCV eine neue Divertor-Konfiguration, genannt „Schneeflocke“, erzielt und anschliessend studiert;
- Im TORPEX-Experiment für Grundlagenforschung in Plasmaphysik wurden die Erzeugung und das Verhalten von Plasmafäden in Raum und Zeit charakterisiert. Diese Arbeiten brachten neue Erkenntnisse über die Gesetzmässigkeiten von Wärme- und Teilchentransport in magnetisierten Plasmen;
- Mittels numerischer Plasmasimulationen wurde die spontane Symmetriebrechung im Tokamak bewiesen und auf TCV angewendet;
- In den Gebieten der Supraleitung, der Heizung mittels Elektronen-Zyklotronwellen sowie der magnetischen Diagnostik leistete das CRPP wichtige Beiträge zum Bau von ITER;
- Das CRPP lieferte substanzielle Beiträge zum erweiterten Programm (BA), unter anderem die Entwicklung einer Testzelle für IFMIF, die Entwicklung der Technologie zur Materialprüfung an kleinen Testobjekten sowie der Hochspannungsversorgung des Gyrotrons;
- Erfolgreiche Weiterentwicklung von Prozessen in der Plasmatechnologie. Dank der herausragenden Qualität dieses Geschäftsfeldes stossen diese Aktivitäten nach wie vor auf grosses Interesse seitens der Industrie.

1 INTRODUZIONE

1.1 La situazione internazionale e il suo rapporto con il programma Svizzero.

1.1.1 ITER

L'ITER Council ha approvato nel 2010 la "ITER Baseline", un documento di riferimento che include le specifiche del progetto, il suo programma e i suoi obiettivi. Secondo questo documento, il primo plasma è previsto per la fine nel 2019. La fase scientifica con operazioni in D-T per produrre 500MW di potenza è prevista per il 2026.

Cambiamenti importanti alla guida di ITER sono avvenuti nel 2010. Il Prof. Osamu Motojima, in precedenza direttore del progetto giapponese "Large Helical Device", è stato nominato Direttore Generale. È assistito dal Dr. Remmelt Haange, come vice Direttore Generale a capo della costruzione di ITER. Il Dr. Haange era il responsabile della parte tecnica del progetto W7-X della Associazione Euratom - Max Planck Institute of Plasma Physics.

In Europa, il Joint Undertaking Fusion for Energy, che è responsabile del contributo europeo a ITER, è stato riorganizzato sotto la nuova direzione del Dr. Franck Briscoe. Il bilancio totale (diretto e indiretto) per il contributo Europeo alla costruzione di ITER è stato coperto con 6,6 miliardi di Euro (valore del 2008). Il bilancio 2012-2013 del programma Euratom richiede un aumento di 1,3 miliardi di Euro. Questo aumento di bilancio è sostenuto in Europa a tutti i livelli, ed una proposta sul metodo di finanziamento è stata avanzata. Una discussione politica finale sulla metodologia del finanziamento sta avvenendo tra le istituzioni europee interessate (Commissione, Consiglio e Parlamento).

1.1.2 Euratom

Come menzionato nel rapporto annuale 2009, il finanziamento dell'Associazione Euratom – Confederazione Svizzera è continuato a diminuire nel 2010 e questa diminuzione sta continuando nel 2011. Per definire una strategia nazionale, il CEPF ha avviato una verifica del CRPP riguardante il suo contributo scientifico nell'ambito del programma internazionale, le prospettive di finanziamento e il controllo generale del programma svizzero di fusione. I risultati scientifici del CRPP sono stati notevolmente elogiati dal comitato internazionale di verifica e la visione strategica del CRPP, che include i piani di potenziamento del tokamak TCV, sono stati caldamente raccomandati. La verifica servirà come base al CEPF per definire la sua strategia riguardo alla fusione. Il risultato della valutazione del CEPF è atteso nel 2011.

Nel 2010, la Svizzera ha firmato l'"High Performance Computer Implementing Agreement (IA)" nell'ambito dell'European Fusion Development Agreement (EFDA). Un nuovo IA concernente la "Power Plant Physics and Thecnology (PPPT-IA) è stato proposto nel 2010. Esso coprirà le attività necessarie per la progettazione di una

centrale a fusione dimostrativa (chiamata DEMO), che produrrà una significativa quantità di energia immessa nella rete.

Rilevanti potenziamenti del JET sono stati realizzati nel 2010, in modo particolare per installare una prima parete simile a quello prevista per ITER. Le attività scientifiche riprenderanno nel 2011.

1.2 Un breve riassunto delle attività del CRPP

La strategia generale del CRPP nel campo della fusione è stata approvata da molte commissioni internazionali, e la sua attuazione è continuata nel 2010. Le linee principali sono il contributo alla costruzione di ITER e l'avanzamento della fisica del plasma, al fine di poter sfruttare i risultati di ITER. Per quanto riguarda DEMO, il CRPP non solo contribuisce allo studio della fisica legata a questa macchina, ma anche agli sviluppi chiave per quanto riguarda i materiali e la tecnologia. Secondo il contratto di lavoro stipulato con il Governo Svizzero, il CRPP lavora anche per lo sviluppo e la ricerca nel quadro del Broader Approach (BA).

Il rapporto annuale 2010 fornisce ai lettori i dettagli di tutti i nostri risultati. Qui sono soltanto evidenziati alcuni punti:

- nel tokamak TCV, una nuova configurazione (lo "snowflake") è stata ottenuta ed esplorata per la prima volta;

- in TORPEX, un esperimento di fisica di base del plasma, la caratterizzazione spaziale e temporale della generazione ed evoluzione di filamenti di plasma ha portato ad una nuova comprensione del trasporto di particelle e di calore nei plasmi magnetizzati;

- nel campo delle simulazioni del plasma, evidenze di una rottura della simmetria in un tokamak (con applicazioni a TCV) è stata analizzata;

- contributi importanti del CRPP nella costruzione di ITER sono stati ottenuti nel campo della superconduttività, del riscaldamento ciclotronico elettronico e delle diagnostiche magnetiche;

- contributi significativi sono stati forniti al BA dal CRPP, tra i quali la progettazione di una cella di test per l'IFMIF, lo sviluppo di una tecnologia per piccoli campioni di test, e di un alimentatore di alto voltaggio per i girotroni;

- lo sviluppo di processi industriali con l'impiego del plasma è continuato nel 2010, e continua ad attrarre grande interesse dalle industrie, grazie alla alta qualità del gruppo.

2 RESEARCH ACHIEVEMENTS OF THE CRPP IN 2010

2.1 The TCV tokamak

The TCV tokamak has the dual mission of supporting ITER and exploring alternative paths to a fusion reactor. Its most unique tools are a 4.5-MW ECRH system with 7 real-time controllable launchers and a plasma control system with 16 independent shaping coils. Additional ECRH power, ion heating sources, and in-vessel MHD control coils are now envisaged. Recent upgrades in temperature, density, and rotation diagnostics are being followed by new turbulence and suprathermal electron diagnostics, and a new digital real-time network has been commissioned.

The year 2010 represented a very intense period of operation for TCV, with only minor interventions on the machine and a few weeks long summer break. Experiments in 2010 completed the campaign defined in 2008 and initiated in 2009. Most scientific missions defined in 2009 were led to successful completion. In addition, following a pattern that is typical of TCV mode of operation, which remains extremely flexible and open to the insertion of new ideas along the experimental campaigns, a good fraction of the approximately 100 sessions run in 2010 were dedicated to the exploration of ideas that were not foreseen in the original run plan.

As detailed below, the 2010 campaign led to very significant progress. The shape control flexibility of TCV has enabled the generation and control of the first “snowflake” divertor, characterized by a null point in which both the poloidal field and its gradient vanish. The predicted increases in flux expansion and edge magnetic shear have been verified experimentally, and stable EC-heated snowflake ELMy H-modes have been obtained and characterized. ECCD modulation techniques have been used to study the role of the current profile in energy transport, and simulations reproduce the results robustly. L-mode impurity transport increases strongly with triangularity, similar to energy transport. The relation between impurity and electron density gradients is explained in terms of neoclassical and turbulent drives. Studies of rotation in the absence of externally applied torque have continued, highlighting the important role of MHD and sawtooth relaxations in determining the rotation profiles. A newly predicted mechanism for turbulent momentum transport associated with up-down plasma asymmetry has been verified in TCV. Trapped electron mode turbulence measured by correlation ECE increases with increasing power and triangularity, consistent with the concomitant increase in anomalous transport and in qualitative agreement with quasi-linear mixing-length estimates. Sawtooth period control, NTM control, and soft X-ray emission profile control have been demonstrated in TCV using the new digital control hardware, as a step on the way to more complex applications.

The operation cycle of TCV will start in 2011 with a new set of missions, in a variety of themes. These missions represent the result of a general brainstorming discussion, held at the end of 2010 within the TCV team at CRPP, as well as with a number of collaborators from European and international institutions.

2.1.1 Scenarios with internal transport barriers

A few experimental sessions were devoted in 2010 to reproducing previously achieved steady-state scenarios with no external current injection. This is the only reported type of stable tokamak discharge entirely sustained by the internally generated bootstrap current. One of the goals of the more recent experiments was to explore the effect of initial conditions, particularly density, on the ultimate self-organized state reached by the plasma, which entails a transport barrier in the inner core of the discharge. The discharge path cannot be directly controlled, as it is dictated by the effect of the current profile on transport, and thus on the pressure profile, which in turn completely determines the current profile itself under these conditions. Path variations and even bifurcations in response to varying initial conditions are thus to be expected. A fairly wide database now exists and is currently being analyzed.

A second goal was to observe a recharging of the Ohmic transformer by imposing a constant plasma current in bootstrap overdrive conditions. This was indeed observed, but thus far only transiently, as the excessive edge current profile peeling-off ends up destroying the scenario equilibrium and disrupting the plasma.

2.1.2 H-mode physics

During the 2010 campaign experiments on H-mode physics concentrated on making an in depth characterisation of the edge pedestal, developing H-mode at negative triangularity ($\delta<0$) and investigating power threshold in the presence of electron cyclotron heating (ECH). These studies made extensive use of the third harmonic ECH system (X3) and a fraction of the second harmonic system (X2).

Figure 2.1.1 shows two discharges typical of cases at positive upper triangularity (#40103) and negative upper triangularity (#40350), subject of the investigations detailed below.

Characterisation of the edge pedestal

An H-mode plasma target was designed so that its shape and position optimised the edge Thomson scattering diagnostic coverage. At the same time, its electron density was controlled to ensure good X3 electron cyclotron resonance heating. In so doing it was possible to make detailed measurements of edge pedestal parameters in type-I and type-III ELMy discharges.

By establishing a technique to predict, in real-time, the likely next occurrence of an ELM in an H-mode discharge it was also possible to trigger the Thomson scattering diagnostic with respect to the ELM. Therefore, coherent averaging techniques could be used to improve the signal to noise ratio of measurements made of the ELM itself and of the pedestal parameters around the time of an ELM. A picture of the temporal evolution of the pedestal temporal evolution during an ELM cycle was, thereby, constructed.

The pedestal width ($\Delta\rho_{ped}$) has been found to scale with the poloidal beta in the pedestal, $\beta_{pol,ped}$: $\Delta\rho_{ped} \propto 0.13 \times (\beta_{pol,ped})^{0.26\pm0.11}$. It will be necessary to extend the

parameter space toward higher beta and density values to improve our estimation of the scaling parameters.

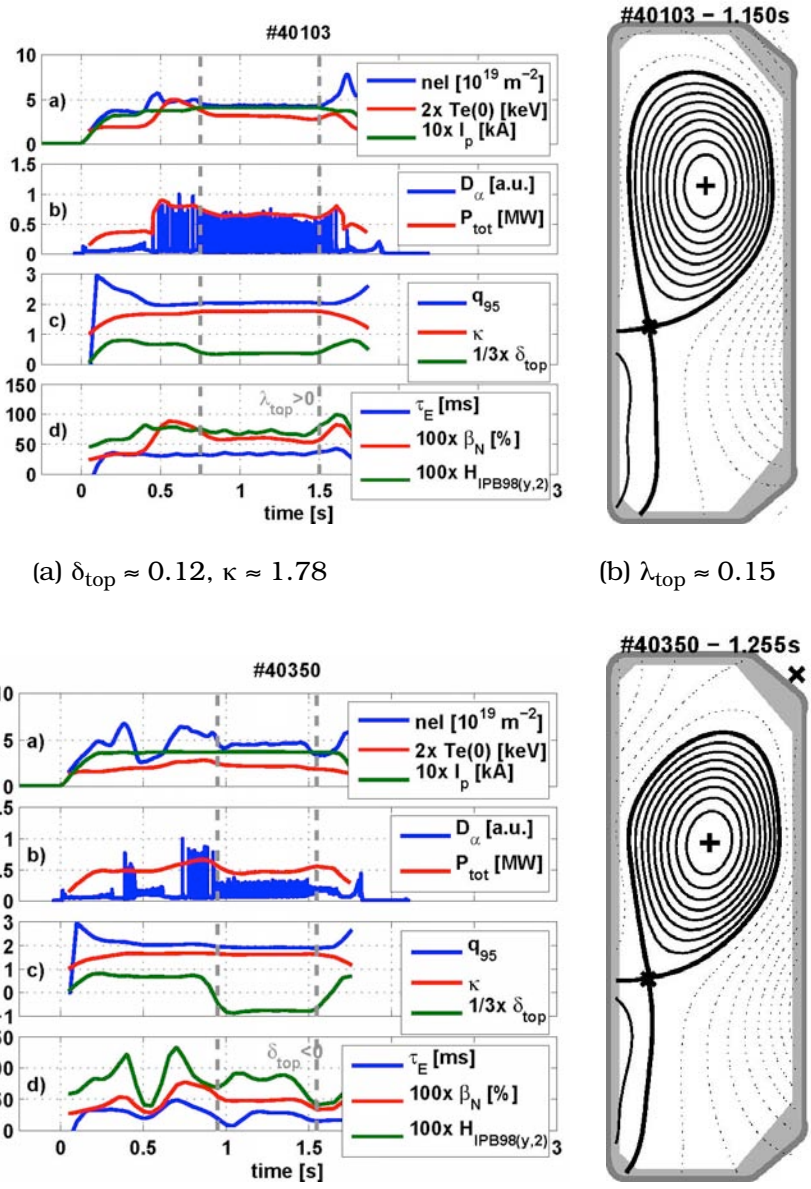

(a) $\delta_{top} \approx 0.12$, $\kappa \approx 1.78$ (b) $\lambda_{top} \approx 0.15$

(c) $\delta_{top} \approx 0.12$, $\kappa \approx 1.78$ (d) $\lambda_{top} \approx 0.15$

Fig. 2.1.1 *Temporal evolution and shape of two separate H-mode discharges at positive and negative upper triangularity. The dashed vertical lines delimit the time interval where the plasma equilibrium had the shape discribed*

The edge pedestal characteristics were also studied as a function of plasma shape, elongation (κ) and triangularity (δ). By increasing κ, the maximum pedestal pressure gradient could be increased, while changes in triangularity and squareness had pronounced effects on ELM frequency and particle exhaust. Ideal MHD stability limit calculations agree well with these experimental observations.

Figure 2.1.2 shows pedestal profiles obtained by coherent averaging of the experimental measurements through a Type-I ELM cycle. Detailed measurements of

the temporal evolution of the ELM cycle show that the pedestal pressure gradient saturates shortly before the ELM onset and that a large pedestal pressure gradient is necessary but not sufficient to explain the ELM event.

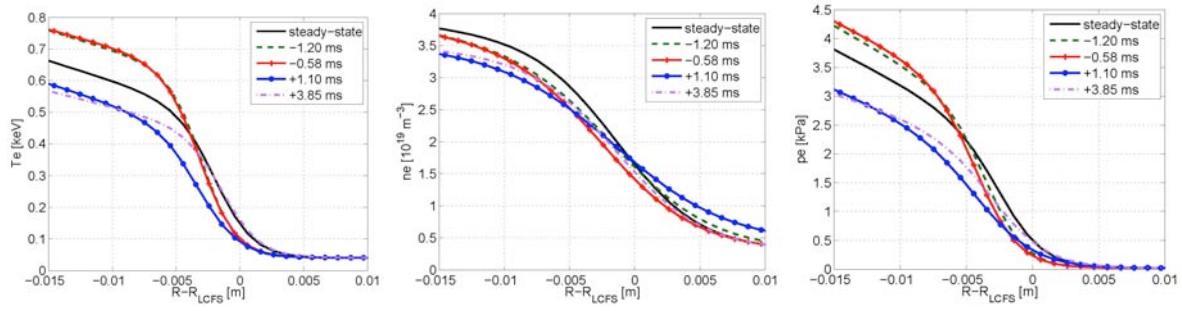

(a) (b) (c)

Fig. 2.1.2 *Temporal evolution of the pedestal during a type-I ELM cycle. Shown are the electron temperature (a), density (b) and pressure (c) profiles as a function of a radial coordinate. R_{lcfs} is the approximate location of the last closed flux surface. Negative times correspond to pre-ELM while positive times correspond to post-ELM.*

Analyses of the radial displacement of the pedestal during a type-I ELM indicate that the pedestal moves outward during the post-ELM phase and inward during the pre-ELM phase. These movements have an impact on the edge stability.

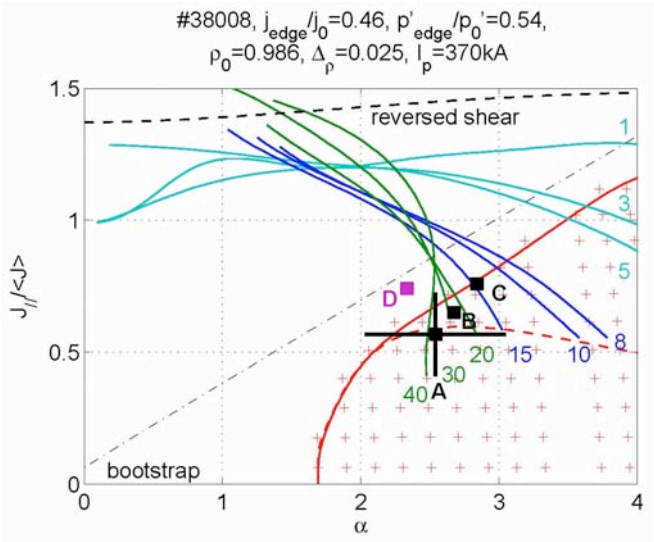

Fig. 2.1.3 *Ideal MHD stability map for a TCV H-mode plasma with type-I ELMs. Shown is the experimental point A, which corresponds to the profile of the inter-ELM phase. Points B, C and D refer to the times $t\text{-}t_{ELM}$={5.0, -1.0, +1.5}msec in the ELM cycle with respect to the Dα peak. Negative times are before the peak and positive times after the peak.*

Figure 2.1.3 shows the evolution of the ideal-MHD stability map during a Type-I ELM. The ideal-MHD calculations agree rather well with experimental data. This gives confidence in the interpretation that medium-n current driven kink modes and large-n pressure driven modes play important roles in limiting achievable

pedestal pressure gradient in Type-I ELMs, where the resistivity is low. Ideal MHD theory is less successful at explaining the stability of Type-III ELMy H-modes.

Development of H-modes at negative triangularity

Core-plasma confinement has been seen to improve, in TCV, in low density L-mode discharges at negative δ. At the same time it is known that, in H-mode, both the pedestal height and ELM size increase as δ increases. It is of great interest to explore properties of H-modes at negative δ, in particular to verify the dependence of confinement on negative δ values, to assess the ELM behaviour and to investigate the pedestal properties.

In TCV, initial experiments have established a diverted negative δ discharge (δ=-0.6), with an X-point close to the continuous LFS wall, with the bottom leg extending to the tokamak floor, vertically stable at an elongation of κ=1.7. So far, these discharges have always been hampered by MHD mode activity, due to the low q_{95} used, aiming at the Ohmic H-mode transition. There appears to be an optimum to find between high plasma current, low-q_{95} discharges, with good vertical stability properties and high Ohmic input power to enter into Ohmic H-mode (κ=1.7, δ_{up}=-0.4, δ_{bot}=-0.8, q_{95}=2.2, I_p=425kA), and lower plasma current, higher q_{95} to reduce mode activity (κ=1.77, δ_{up}=-0.2, δ_{bot}=-0.7, q_{95}=3.8, I_p=240kA). Additional EC heating, to avoid too low-q operation, should be further developed to reduce MHD activity.

H-modes with negative upper triangularity, but positive lower triangularity with the X-point on the HFS wall, have recently been produced in TCV. They are studied for their ELM and pedestal characteristics: a first indication shows that when δ_{up} is made negative (κ =1.65, δ_{up}=-0.3, δ_{bot}=+0.6, q_{95}=2.2, I_p=370kA), ELMs are getting faster and smaller (see Figure 2.1.1). It is likely that the change in the sign of δ provokes the change in ELM frequency, although an effect of a lower coupled additional heating power causing a transition from type-I to type-III ELM regime cannot be excluded at this stage.

Further work is required to maintain additional heating during the transition from positive upper δ to negative upper δ, as well as to create H-mode targets with both upper and lower negative δ.

L-mode to H-mode transitions

L- to H-mode transitions are regularly obtained in TCV discharges. Most of them were obtained without additional heating, in a relatively wide variety of plasma conditions. The L-H threshold power was investigated with EC heating at the second harmonic (X2) a few years ago. On the other hand, ohmic H-mode plasmas have been heated with the third harmonic (X3) ECH system. However, inducing L-H transitions by injection of X3 ECH has never been addressed. Preliminary experiments were performed in the frame of the Joint International Experiment (JEX/TC-2), an experimental collaboration dealing with power hysteresis in H-mode plasmas.

Different levels of X3 ECH power were applied to diverted L-mode plasmas to measure the threshold power. The plasma current and the plasma density were varied from shot to shot to vary the ohmic power and search for the minimum value of the threshold power. This minimum was found at a density of about $3.6 \times 10^{19} m^{-3}$.

The search for this so-called roll-over was driven by previous studies during which stationary ELMy H-modes were preferentially obtained close to the corresponding density. However, none of these discharges led to a stationary ELMy H-mode. This might be due to a decrease in the X3 ECH power absorption, which is itself due to the spontaneous increase of the plasma density occurring in H-mode.

2.1.3 Plasma rotation

Introduction

Plasma rotation studies on TCV rely on the performance of the Diagnostic Neutral Beam (DNB) and the associated spectroscopic beam observation and analysis. During the last year, the DNB has performed almost faultlessly after the upgrade of the high voltage capacitor bank and the installation of a fresh arc source. Operation near 50keV ensured an optimal charge exchange cross section for the C^{6+} ions radiating at 530nm. The beam current was often well above 2.5A. On the spectroscopic side, the original CCD detector modules were upgraded with new cameras that are capable of operating at higher speeds and are equipped with on-chip electronic amplification. These back lit CCD chips have a quantum efficiency above 85%; the on-chip amplification allows data read-out at high speed without over compromising the S/N ratio due to the additional noise intrinsic to the fast read-out process. The result was an exceptional year for ion temperature, density and rotation measurements with the whole diagnostic system operating reliably over many thousand plasma discharges.

The increased diagnostic spatial resolution, introduced in 2009, was exploited in detailed profile measurements for a variety of plasma shapes and conditions. The increased temporal resolution and detector sensitivity was used to reconstruct rotation profiles across fast events such as sawteeth. In the following, three specific investigations on the behaviour of plasma rotation and/or momentum transport are reported.

Momentum transport induced by an up-down asymmetric magnetic equilibrium

Following the study reported in 2009, experiments were continued, in collaboration with Warwick University, UK, of changes in the toroidal rotation profile with a symmetric change in the plasma squareness shape parameter. As before, mirror discharges were produced in the TCV vessel for which there was a predicted change in the parallel momentum transport. This was motivated by the theoretical discovery of ion-scale turbulent momentum transport depending on asymmetries in the outer part of the plasma. Fig. 2.1.4 shows a summary of measured toroidal rotation profiles, together with the calculated bulk ion rotation profiles and the compared plasma shapes. Physical considerations predict that inverting the plasma current and/or the magnetic field should also change the sign of the predicted up-down asymmetry flux. This comparison was successfully performed and proved that the observed rotation profile change was not ascribable to the TCV machine itself-(machine distortion, error field etc.)

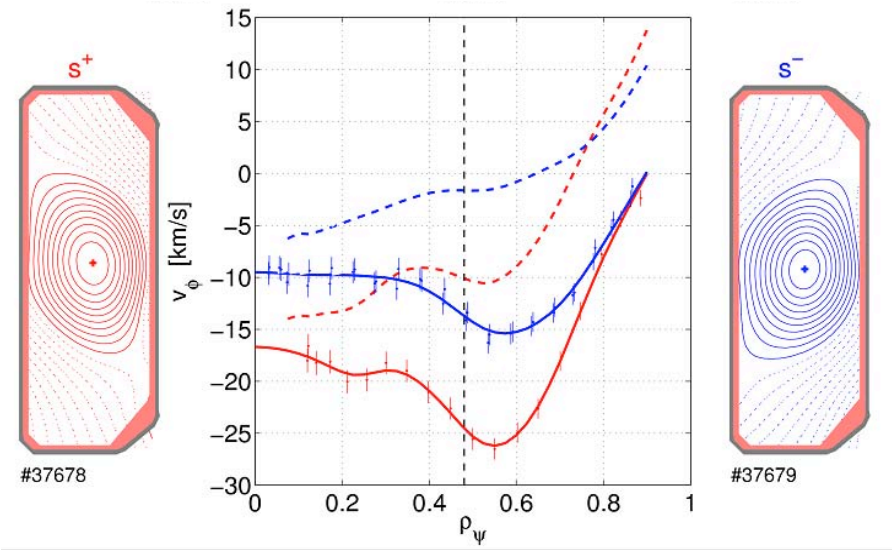

Fig. 2.1.4 *Toroidal Rotation profiles for two different up/down asymmetric configurations. Dashed lines indicate the predicted rotation for the plasma bulk, which shows a similar effect.*

Linear calculations of the turbulent momentum flux were performed with the gyrokinetic flux tube code GKW (Fig. 2.1.5). Three kinetic species (electron, deuterium and carbon) were included with electrostatic fluctuations considered in the collisionless limit. Figure 2.1.6 shows the predicted rotation difference between the configurations at three different radii shown in Fig. 2.1.5 as a function of the turbulent wave number. It is encouraging to note that, though collisions and ExB shearing are not included for a quantitative comparison, the general features and in particular the sign, of the experimental observation are well described.

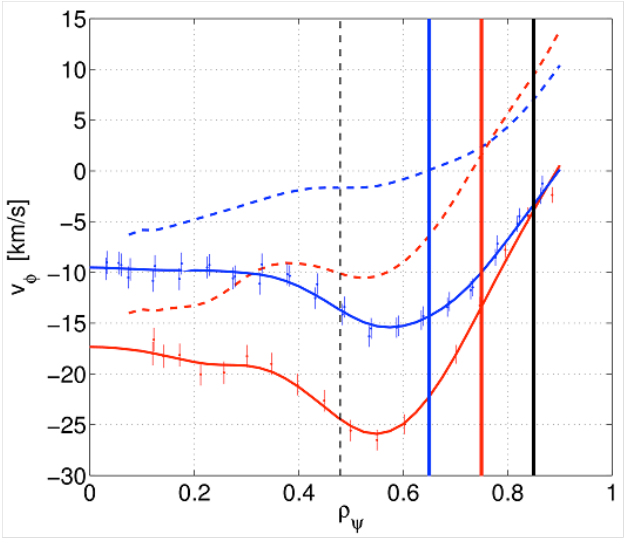

Fig. 2.1.5 *GKW analysis of the turbulent contribution to the plasma torque at three radii indicated by vertical lines*

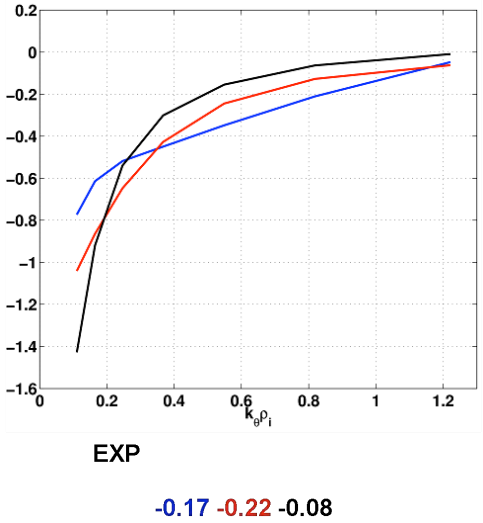

Fig. 2.1.6 *Difference across squareness change for each radius as a function of the turbulence wave-number. Caption shows experimental values.*

Momentum Transport Across Sawteeth Events

Using the real-time triggering, together with ECH partially stabilised sawteeth, the rotation profiles across sawteeth events were measured. The sawteeth period was lengthened from ~3-5ms to above 14ms and was monitored by the real-time plasma control system that generates a stream of up to 8 triggers for the CXRS diagnostic every 2ms after each sawtooth. By conditionally re-sampling the resulting spectra over many sawteeth, the characteristic evolution of the toroidal plasma rotation was measured with a 2ms time resolution. Figure 2.1.7 shows a plot of the toroidal rotation profile at three times in the phase between sawteeth and the time history of the toroidal rotation at three radial locations across a sawtooth cycle. This work was initially prompted by the observation of a "flattening" of the toroidal rotation profile inside the sawtooth inversion radius and a slight acceleration in the co-current plasma direction within the flattened region. The preliminary results show a sharp plasma acceleration in the co-current direction in the core at the sawtooth crash followed by a slower momentum transport across the whole plasma.

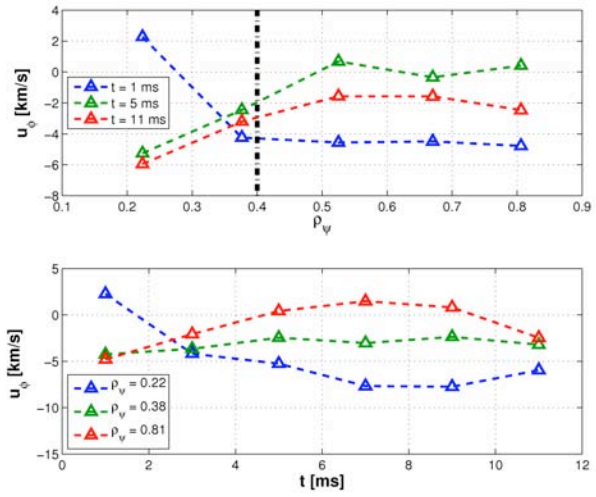

Fig. 2.1.7 *Top: Toroidal Rotation Profiles just after (1ms) to close to the end of the sawtooth cycle (11ms)- Bottom: Evolution of the Toroidal Rotation at three radial positions across the complete sawtooth cycle.*

With the installation of the new, faster, Andor CCD cameras in 2010, it was possible to increase the radial resolution to the full 20 chords whilst maintaining the 2ms time resolution. Figure 2.1.8 shows a very recent measurement of the rotation profiles performed using the new cameras. The core acceleration at the sawtooth crash now appears to have structure within the profile-flattened region itself. Although these conclusions are still preliminary, the role of MHD on the final rotation profile has been clearly demonstrated and must be included in any prediction of plasma rotation in future devices such as ITER.

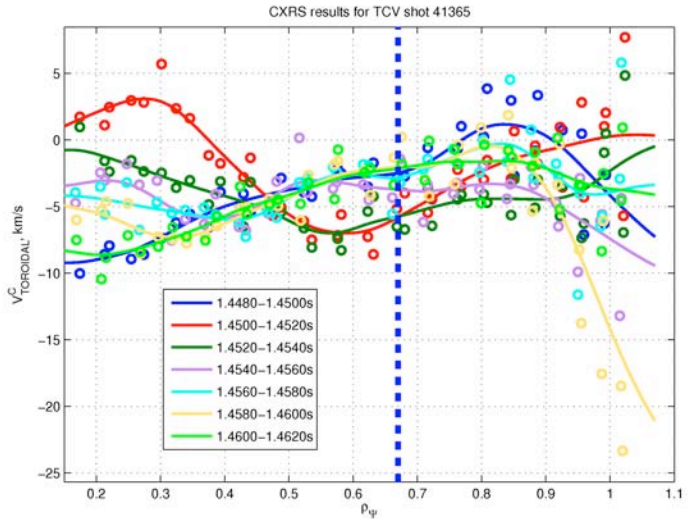

Fig. 2.1.8 *Toroidal rotation profile across a sawtooth period. Across the crash (Blue->Red) there is strong co-current acceleration that is well within the reconstructed q=1 surface (vertical dashed line). Profile in plasma edge is still unreliable and there is a possible offset in the absolute velocity values.*

Effects of ECH/ECCD on tearing modes and link to rotation profile

Specific experiments were preformed to better separate the momentum transport properties that can be attributed to micro-instabilities from those related to MHD activity. Together with the observations above that sawteeth (n=1, m=1 modes) can affect the rotation profile, higher order rational surfaces together with the sawteeth can lead to non-monotonic rotation profiles. During the formation of diverted plasmas, it was noted that the plasma configuration went through a phase with a rapid decrease in the overall poloidal cross-section. At constant plasma current, this results in configurations with an edge safety factor that passes close to q~3. By forming the divertor at lower plasma current, q~4.5-5, and at relatively low plasma density, this phase was avoided, which considerably diminished the subsequent MHD activity.

A fine current scan was performed with a series of discharges each containing a limited and a diverted configuration phase. This more detailed comparison between the configurations shows that both behave similarly, Fig. 2.1.9, Fig. 2.1.10. At lower plasma current, the toroidal rotation is counter-current in both cases with a significant momentum pinch sustaining a peaked profile. The momentum transport properties of this pinch are not modified by increasing the plasma current outside the sawtooth mixing radius. At higher plasma current, local gradients of the

toroidal profile are modified significantly, enough to change eventually the rotation direction. This effect is seen when the sawtooth activity affects the whole minor radius.

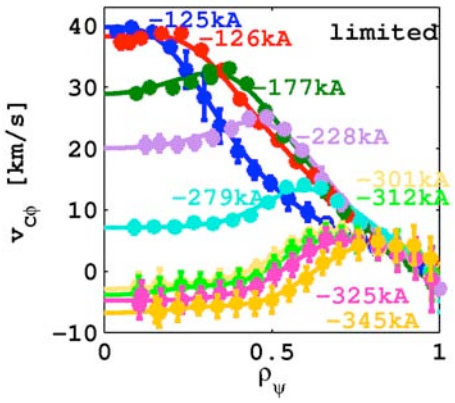

Fig. 2.1.9 *Rotation profiles as a function of plasma current for limited discharges.*

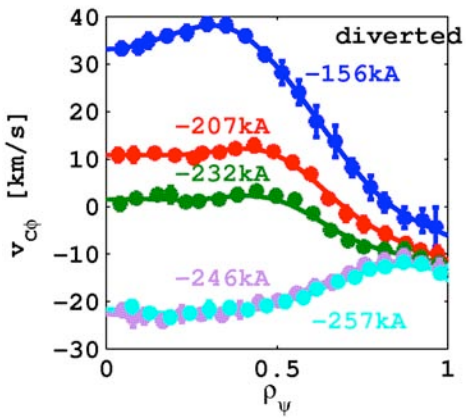

Fig. 2.1.10 *Same for diverted configurations in the absence of strong MHD behaviour.*

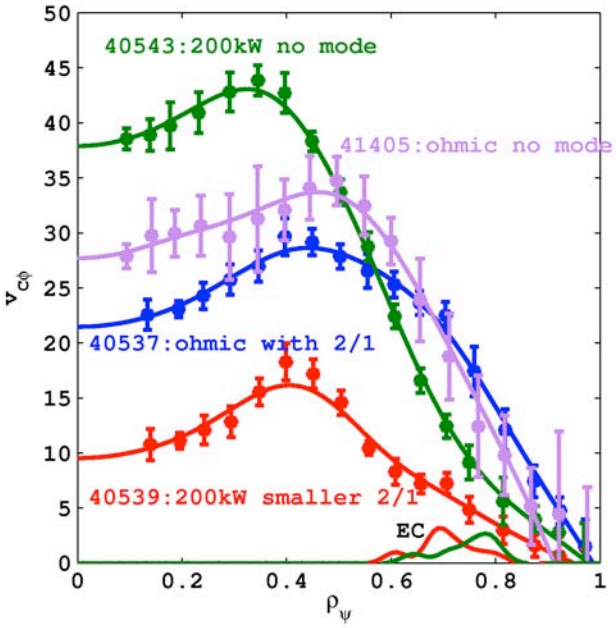

Fig. 2.1.11 *Toroidal Rotation profiles for Ohmic discharges with (40537) and without (41405) 2/1 mode- With EC and smaller 2/1 mode (40539) and with EC stabilised mode outside q=1 (40543)- Although EC appears to increase the radial transport, mode stabilisation allows it to peak further. The strongest rotation is achieved with the 2/1 mode stabilised by ECCD with power outside q=1.*

The presence of a tearing mode can further affect the toroidal rotation profile. In the case shown in Fig. 2.1.11, a discharge was chosen in which a 2/1 tearing mode was unstable from 0.5s until the end of the discharge. Adding ~200kW of EC at the q=2 surface partially stabilised the mode. Since it is already known that EC can affect

the rotation, the comparison is made with the profiles measured where, following mode stabilisation, the EC power is turned off and the measurement performed before the mode re-appears, 200ms later. Finally, also shown in Fig. 2.1.11, adding off-axis co-CD to stabilise the mode resulted in plasma rotation profile that is even more peaked than in the EC case that only partially stabilised the 2/1 mode. The effect of ECCD, with or without the presence of the 2/1 mode, is strong, although the pressure, not shown, varies by ~30%, the local electron temperature is ~2x higher with EC and the significance of the collisionality effect remains to be investigated.

Collaboration with Alcator C-Mod

A further session on the Alcator C-Mod device was performed this year to see if the toroidal rotation reversal, first observed on TCV could be reproduced on another tokamak device whose intrinsic rotation is not dominated by high power Neutral Beam Heating. Complementary to previous experiments, configurations with clearly distinct limited and diverted phases were measured for a range of plasma currents. As in TCV, for diverted plasmas, a toroidal rotation profile reversal was observed over a small range of plasma density. TCV was operated with a toroidal magnetic field of 1.43T, while the C-Mod experiments were performed at their medium 5T field. The reversal of the rotation profile phenomena are currently being analysed and compared to the TCV case uniting the diagnostic information available from both machines.

2.1.4 Heat and particle transport in TCV

Effect of triangularity on heat transport and turbulence measured by correlation ECE

Plasma shaping is one of the fundamental tools that can modify the instabilities driving the turbulent state and core energy transport. In low collisional TCV plasmas, the transition from positive to negative triangularity reduces the energy transport by up to a factor of two. Such clear changes of transport found in the experiment represent valuable test cases for the validation of plasma transport modelling.

Turbulence correlation-ECE measurements have been extended further into the plasma core with a good coverage of the mid-radius range, where the plasma is fully optically thick, thus allowing pure temperature fluctuations to be collected. Spectra for δ=±0.45 are shown in Fig. 2.1.12(left) for a radial position ρ_V=0.42. Plasma profiles and collisionality are maintained similar for both triangularity values through adequate EC heating. The frequency spectra (CSD = cross-spectral density) correspond to the expected trapped electron mode (TEM) frequency range. The relative temperature fluctuations (integrated over the CSD) decrease by more than a factor of two from δ=+0.45 to δ=-0.45. Most of the reduction in the fluctuation spectra occurs at frequencies below 80kHz. The spectra increase in amplitude with lower density, and thus lower collisionality, as expected in the TEM range. Thus the robustness of the results strongly depends on the density control.

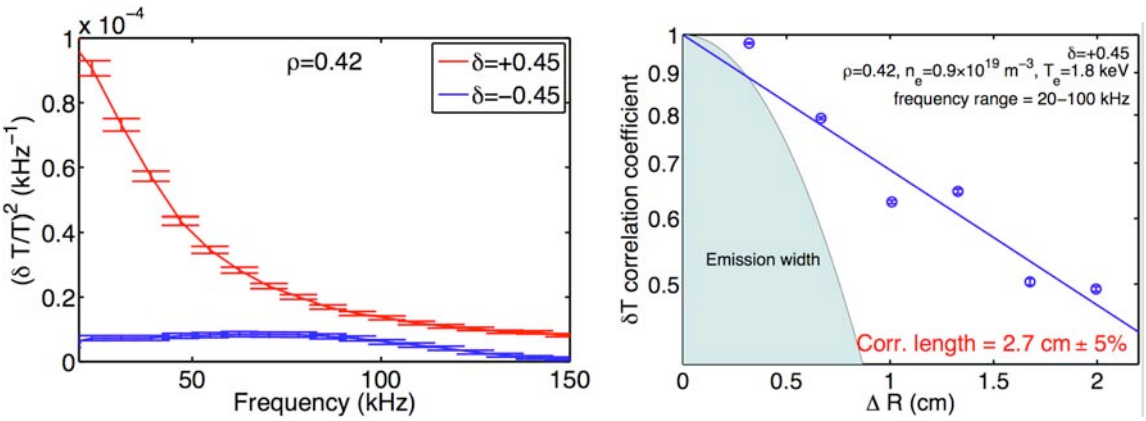

Fig. 2.1.12 *Left: Electron turbulence spectra for positive (red) and negative triangularity (blue). Right: correlation coefficient for positive triangularity (δ=+0.45) as a function of probing volumes separation, yielding a correlation length of 2.7cm.*

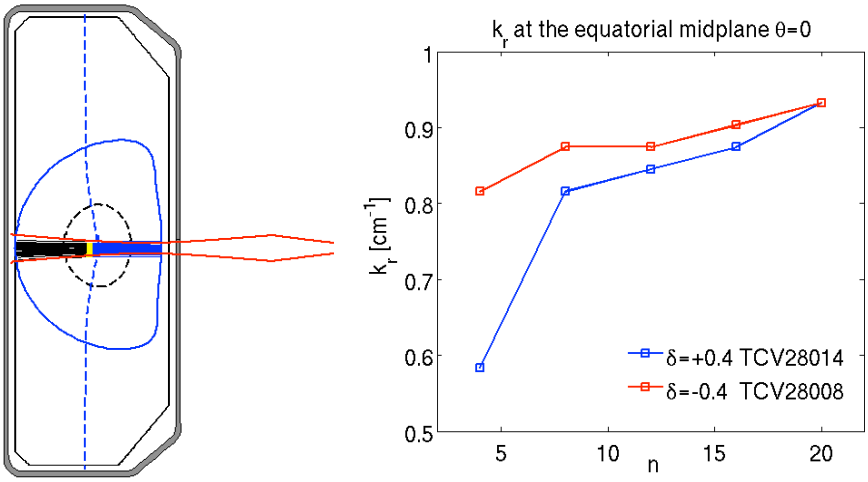

Fig. 2.1.13 *Left: Correlation ECE view showing the effect of the focusing lens on the low field side (region that can be probed is in blue), together with a negative triangularity plasma. Right: Linear global gyrokinetic calculation of the radial wave vector k_r as a function of the toroidal mode number, indicating a reduction of the characteristic radial wavelength at negative triangularity.*

Important for the comparison of experiments and gyrokinetic modelling is the clear definition of the probing volumes. The width of the ECE beam, see Fig. 2.1.13(left), is set by the focusing lens and defines the poloidal wave vector accessible range, k_θ 0.5-0.8cm^{-1}, i.e. $k_\theta \rho_s$ 0.3-0.5, covering most of the expected TEM spectra playing a role in transport. The radial resolution is given by the EC resonance thermal Doppler broadening, indicated as 'EC emission width' in Fig. 2.1.12(right), which is well resolved by the instrumental frequency resolution. This allows measuring the correlation length L_c at both triangularities, as already shown in Fig. 2.1.12(right) for δ=+0.45, to be compared with the result of global gyrokinetic simulations. Linear runs using ORB5 predict a decrease of the characteristic radial wavelength – an increase of k_r – for negative triangularity plasmas, in the low toroidal mode number low frequency TEM domain, as shown in Fig. 2.1.13(right).

Particle and impurity transport

The dependence of carbon density profile on plasma current has been investigated further, in particular with respect to additional electron heating. In Fig. 2.1.14 we show the carbon profile normalized to its value at ρ_ψ=0.8 for positive and negative triangularity cases. In both cases, one gyrotron is coupled to the plasma, 450kW, and the deposition location is moved slowly from outside the inversion radius to inside the inversion radius. The time at which the EC deposition is near and then inside the q=1 radius is well determined from the SXR time trace. It correlates directly with the two types of profiles as shown in Fig. 2.1.14. EC is therefore observed to enhance the effect of sawtooth activity on the carbon density profile. This shows that the role of MHD and sawteeth on particle transport has to be considered in details in order to extract the dependencies related to turbulence.

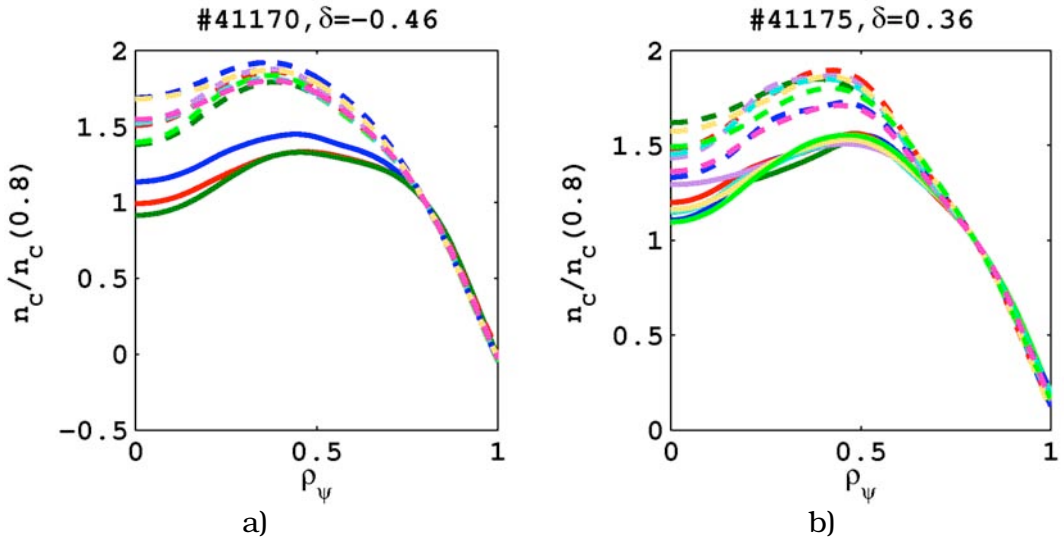

Fig. 2.1.14 *Normalized carbon density profile for EC scan from outside (dashed lines) to inside (solid) the q=1 radius for (a) negative triangularity (b) positive triangularity shape.*

Density profiles in electron-heated H-modes

It was clear from the very first X3 EC heated experiments that strongly electron heated TCV H modes show flatter electron core density profiles than those with purely ohmic heating (see Fig. 2.1.15). This behaviour seems to contradict the observations on AUG and JET, where density peaking increases with decreasing collisionality, but it is very similar to that observed on FTU fully non-inductive, electron heated plasmas.

In recent experimental campaigns, new data have been collected in ohmic and ECH H-modes, repeating the very first experiments and also exploring wider parameter ranges. These experiments, where special attention was made to the quality of the collected data, allow us to more reliably compare experiments and theory. The observed experimental dependencies can be explained in the framework of a recently proposed quasi-linear gyrokinetic model, and the previous apparent contradictions can be resolved.

The difference in the observed behaviour stems from the powerful electron heating applied on these H-mode plasmas. With the addition of the ECH the electron temperature and the electron temperature gradients are increased, while the ion temperature profiles remain basically unaffected. The theory predicts a decrease in density peaking when the T_e/T_i ratio increases, mainly due to a reduction in the thermo-diffusive pinch. Similarly, the slightly increasing electron temperature gradient enhances the trapped electron modes, to which outward flux is attributed, and the stationary value of the density gradient is found at a lower value. It turns out that these effects are stronger than the effect of collisionality. In addition, the neoclassical Ware-pinch can contribute significantly to the density peaking. This effect is non-negligible in the ohmic cases and explains further why TCV ohmic highly collisional H-modes are characterised by a higher value of R/L_{ne}.

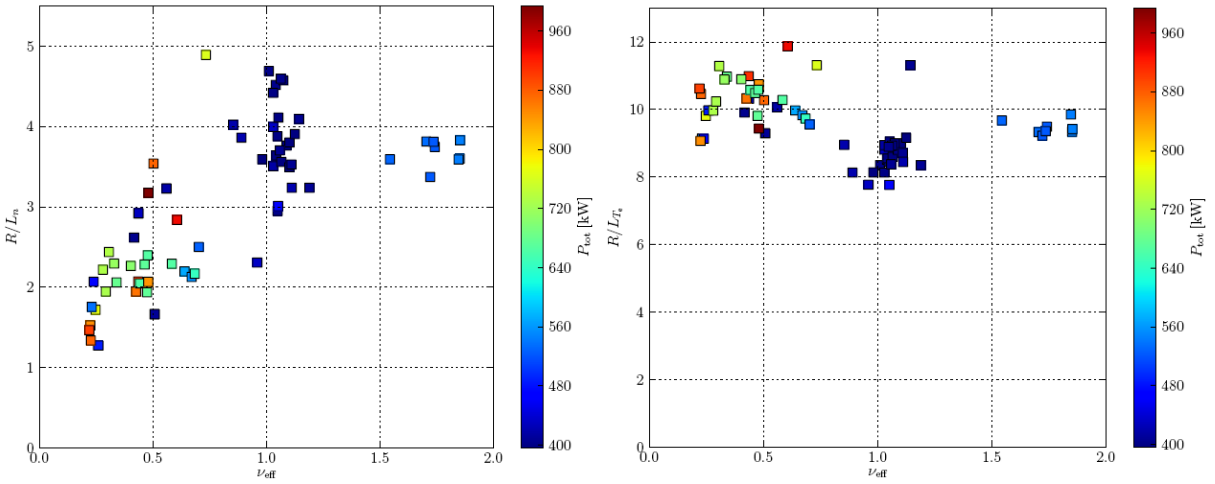

Fig. 2.1.16 *(a) R/L_{ne} and (b) R/L_{Te} versus effective collisionality for TCV H-modes. The colorbar reflects the total input power, the lowest values relate to ohmic discharges. A significant increase of R/L_{ne} versus collisionality is observed.*

2.1.5 Physics of ECH, ECCD and of suprathermal electrons

Real-time control using EC actuators

The use of real-time control of the EC actuators (power, angles) has advanced rapidly. In particular, thanks to the ease of programming the control algorithms by using SIMULINK within the MATLAB environment, the power waveforms have been modulated at high frequency (many kHz) with phase-locking to magnetic probe signals using a digital phase-locked-loop (PLL). This opens the possibility to deposit energy within magnetic island structures. The first application of this has been to study the stabilization of neoclassical tearing modes, as described in the following subsection.

The availability of this application instigated an investigation of full on/off power modulation of the X2 gyrotrons that are nominally rated for 70% RF power modulation with 23% beam power modulation. It has been demonstrated that by modulating the accelerating voltage to below a certain value, deleterious RF generation in the intermediate beam power range can be avoided, so that 100% RF power modulation becomes possible with a 33% modulation of the beam power. Furthermore, modulation frequencies of up to ~15kHz are possible.

EC stabilization of Neoclassical Tearing Modes

The stabilization of neoclassical tearing modes (NTMs) is a key issue for ITER. The detailed physics of the mode stabilization and the control methods to affect that stabilization are being investigated using the real-time digital control system and a newly developed real-time poloidal flux diffusion simulation code, RAPTOR.

The experimental studies on EC control of tearing modes have rapidly expanded. Event-based control is implemented, in which MHD activity is detected, the power and/or angles of various gyrotrons are modified in real-time, and the frequency and the phasing between the mode and the gyrotron modulation are tracked in real-time. The latter can be changed from shot to shot, or scanned within one shot.

Target plasmas in which the tearing modes are destabilized systematically have been developed. The power deposition location of one cluster of gyrotrons is varied until the mode is created; subsequently, these gyrotrons return to a predetermined 'nominal' position to establish a reproducible starting condition for the mode stabilization portion of the experiments. Using these targets, gyrotron beams from a second cluster are moved across the mode position by poloidal angle steering to investigate "metastable" islands at or near the self-stabilizing limit.

In recent experiments, the stabilizing beams have been moved towards the resonance layer from either side, which allows a precise determination of the width of the region within which the mode can be fully stabilized. Comparisons between the stabilizing effects of co- / counter- ECCD and ECH have begun, both with CW and partially modulated power waveforms. Initial indications are that stabilization by heating effects dominates in these plasmas. Initial phase scans of modulated power indicate that modulation has a small but visible effect in some cases. Detailed investigations are planned for 2011, with the aim of eventually including real-time simulations of NTM physics in RAPTOR. The relative ease with which the experimental control algorithms can be modified, coupled with the ability to compare shot-to-shot scans with single shot parameter sweeps and, finally, the enhanced productivity that is inherent in real-time control and simulations, will allow us to perform very detailed studies of complex phenomena with a minimum amount of machine time.

Suprathermal electrons

Experiments were specially designed in TCV to study the synergy between EC power absorption at both the second and third harmonic resonances (using the 82.7GHz, so-called X2 gyrotrons). This is accomplished by sweeping the toroidal magnetic field so that both resonances are at nearly the same flux surface (high-field side, HFS, and low-field side, LFS, of the plasma centre, respectively) while doing ECCD. Synergy is evidenced by an increase in HXR and ECE signals. These experiments have been analyzed with the help of the LUKE quasi-linear Fokker-Planck code and compared with linear results. Excess X3 absorption is predicted on the LFS (3^{rd} harmonic) due to the generation of a suprathermal electron population by HFS (2^{nd} harmonic) absorption. HXR and ECE emission trends are found to be in good agreement with simulated synergy levels. A parametric dependence of the X2/X3 synergy during density and power scans has also been analyzed. A key concern is modelling the transport in velocity space and physical (radial) space. Tailoring of the transport is expected to improve the match between simulations and present experiments as well and is the subject of ongoing research.

2.1.6 Electron Bernstein Wave Heating and Current Drive

The efficiency of electron Bernstein wave heating (EBH) and current drive (EBCD) via O-X-B mode conversion is explored in overdense H-mode TCV plasmas. The injection direction for optimal mode conversion is calculated using the AMR code solving the cold full-wave equations in a 1D plasma slab. The existence and position of the optimum injection angle were successfully checked in experiments with 2^{nd} harmonic EC power in O-mode polarization for quasi-horizontal injection at the plasma midplane and poloidally oblique injection from below the plasma midplane. In the latter case, agreement with the numerical simulations was achieved.

Depending on the launching scheme, off-axis or central power deposition can be achieved. In the case of poloidally oblique injection, the electrostatic mode undergoes a strong upshift of its parallel index of refraction, as shown by ray-tracing simulations with the AMR code. As a consequence, the power is absorbed far off-axis due to strong Doppler shift. The power deposition location was confirmed experimentally by standard Fourier analysis of the soft X-ray response to square modulations in the ECH power amplitude (MECH).

In the case of equatorial injection, the Doppler shift is reduced and the wave can reach the cyclotron resonance on-axis where the sawtooth activity is strong due to the high Ohmic power level needed for the transition to high-density H-mode. When sawteeth are present, standard Fourier analysis techniques of MECH experiments are hampered and the Break-In-Slope (BIS) analysis method is used to determine the radius of power deposition with promising results. In its simplest form, the BIS method assumes that the locally absorbed EC power is proportional to the break in the slope of the temperature time-trace at the EC power step times, providing an estimated power deposition profile at a time rate equal to the power modulation frequency. The BIS technique thus allows one to track time-evolving power deposition locations in non-stationary conditions, a feature of particular interest for real-time control experiments. Single and double X2 power beam deposition locations were successfully tracked in non-stationary plasmas by this BIS technique, confirming the deposition location predicted by the LUKE code.

In order to determine the amount of absorbed EC power, the total plasma kinetic energy is extracted from the plasma toroidal flux. The latter is measured by a set of diamagnetic loops (DML) on the TCV vacuum vessel. The global power absorption can thus be evaluated by harmonic analysis of the plasma response to MECH. Scans of the ECH modulation frequency were performed for central deposition of both X2 and X3. In all cases, the experimental DML transfer function is best fitted with the model transfer function H_{22} derived from the electron energy evolution equation taking into account the EC power, the energy confinement time and the electron deflection time. Unexpectedly, the transfer function exhibits a resonance around 200Hz (see Fig. 2.1.16). Thus, physical parameters such as the EC power absorption cannot be extracted from the fit without further improvements in the plasma energy response model. The pernicious effect of the sawtooth modulation on the plasma frequency response makes it a good candidate for the energy transport involved in this resonance.

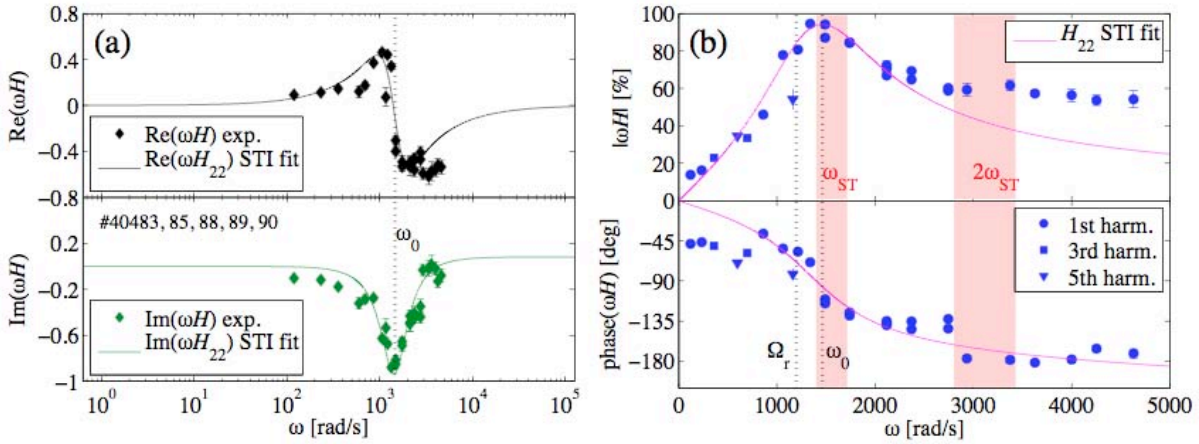

Fig. 2.1.16 *(a) Real and imaginary parts, (b) amplitude and phase of the experimental DML transfer function versus ECH modulation angular frequency. The experimental data are fitted using a rational function of complex polynomials. The amplitude corresponds to the power absorption estimator, which was expected to saturate at the actual absorption efficiency for high modulation frequencies. Instead, the transfer function exhibits a resonance at the proper angular frequency ω_0=1461rad/s (close to the sawtooth frequency ω_{ST}=1558rad/s) with quality factor Q=1.23.*

The possibility of EBCD in TCV was addressed using AMR ray-tracing results coupled to the LUKE Fokker-Planck code for the wave-particle interaction. When the EC resonance passes through the plasma centre, the maximum current drive efficiency is found for slightly off-midplane injection, yielding moderate parallel refractive index upshift and mid-radius power deposition. In this case, the effects of decreasing electron temperature at the deposition location when increasing the parallel refractive index upshift are balanced. Nevertheless, the amplitude of the driven current is small, of the order of 1% of the Ohmic plasma current (i.e. 4kA for 500kW of injected EC power). Preliminary modulated EBCD experiments show plasma current modulations of too small amplitude to unambiguously distinguish between resistivity modulations and a direct EBCD effect.

In the O-X-B mode conversion process, the X-mode converts into EBW in a wave-wave interaction at the upper-hybrid resonance (UHR). Approaching the UHR, the wave electric field grows and part of the power is lost into lower-hybrid (LH) waves due to a non-linear parametric instability (LHPI). These decay waves have been detected using a loop-antenna in TCV EBW experiments, with major peaks around 600MHz and 725MHz, in the expected LH frequency range (see Fig. 2.1.17). As expected, the LHPI amplitude is correlated with the conditions for an effective O-X mode conversion i.e. a steep density gradient at the O-mode cut-off. When the wave-plasma coupling is good, indicated by low stray power level, the loop antenna detects LH decay waves. ELMs and back transitions to L-mode induce sudden drops of the edge density gradient, thus yielding wave-plasma coupling losses and decreases of the LHPI signal amplitude.

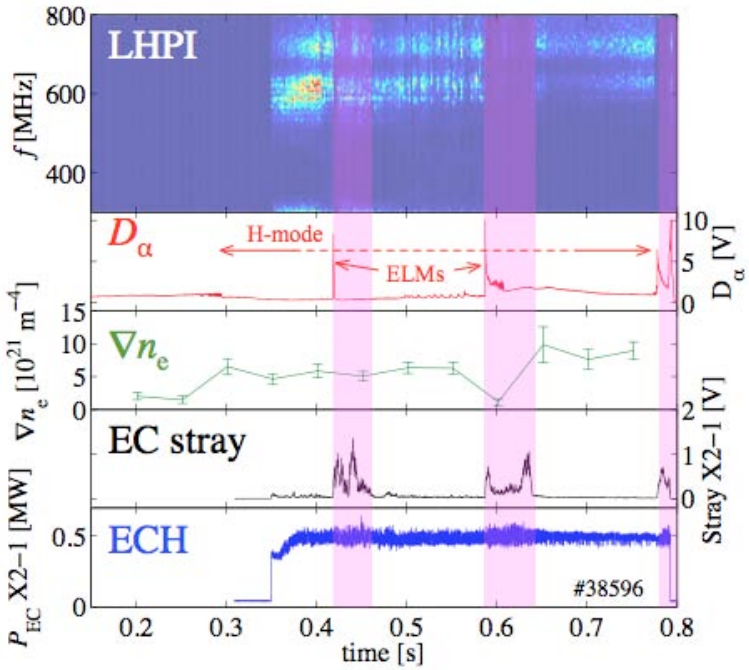

Fig. 2.1.17 *From top to bottom: LHPI spectra versus time, D_α light, gradient of the electron density profile pedestal (Thomson scattering), EC stray power, injected O2 EC power. The O2 power injection starts (at t=0.35s) after the plasma transition to H-mode (at t=0.3s, see D_α trace). Magenta bands indicate time intervals of low O-X conversion efficiency due to ELMs and back-transitions to L-mode.*

2.1.7 Exploration of new shapes and configurations: snowflake divertor

In the tokamak approach to magnetic confinement nuclear fusion, the divertor configuration has emerged as the preeminent solution to managing power exhaust and core impurity content. In the presence of a magnetic X-point, where the poloidal field vanishes, energy and particle losses are channelled primarily into a divertor region that is separated from the confined plasma region. The drawback of this approach is the high power flux impinging on the divertor plates, which may consequently overheat and undergo destructive erosion. This is particularly true during edge localized modes (ELMs) occurring in the high-confinement H-mode, which cause repetitive, violent, and potentially highly damaging ejections of energy and particles onto the divertor surfaces. Heat flux management in the tokamak divertor and, in particular, the control of ELMs, remain therefore a primary goal of magnetic fusion research.

A “snowflake” (SF) divertor configuration has recently been proposed to reduce the plasma-wall interaction by changing the divertor poloidal magnetic field topology. The feasibility of this configuration was demonstrated for the first time in the TCV tokamak. The X-point of a SF configuration features a second order null-point, i.e. both the poloidal magnetic field and its spatial first derivatives vanish. By perturbing this configuration, a SF+ configuration or SF- configuration is obtained with two contiguous X-points that, for the SF-, are both located at the separatrix. The distance between the X-points normalized to the plasma minor radius (σ) parameterizes the proximity to an ideal SF configuration. SF plasmas feature a

longer scrape-off layer (SOL) connection length and higher flux expansion in the null-point region compared with conventional single-null configuration (SN). Additionally, the increased magnetic shear in the edge region is predicted to influence ELM behaviour.

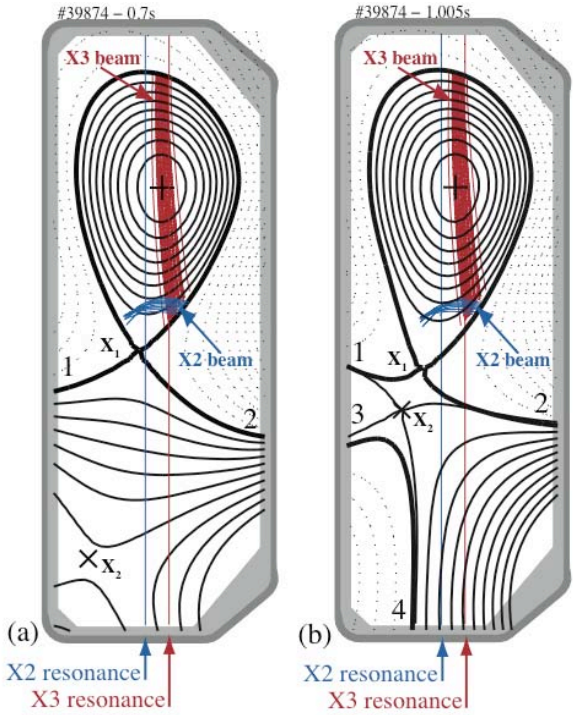

Fig. 2.1.18 *SN configuration (a) and SF+ configuration (b). Red lines: ECH-X3 beam injected from the top of TCV. Blue lines: ECH-X2 beam injected from the low-field side. The positions of the second and third harmonic resonances are represented together with the strike point and null-point positions.*

Stationary ELMy H-modes are obtained with a SF+ divertor in TCV and a significant change in the ELM frequency is observed, compared to an equivalent SN divertor plasma, demonstrating the potential of SF plasmas to lead to a new type of high confinement scenario with better edge properties.

The SF+ configuration studied is shown in Fig. 2.1.18(b). The chosen configuration is a compromise between the enhancement of the magnetic properties and the stable sustainment of the configuration by the TCV poloidal coil array and control system. For this study, the SF+ is compared with the SN configuration (Fig. 2.1.18(a)). The SN shape is tuned to match the shape and wall separations of the SF+ configuration. Differences between the two shapes are only significant in the null point region where the larger flux expansion of the SF+ configuration results in a small modification of the plasma separatrix geometry.

In these scenarios, the $\boldsymbol{B}\cdot\nabla\boldsymbol{B}$ ion-drift direction is towards the null-point, the plasma current is $300kA$ and the toroidal magnetic field at the TCV major radius ($R0$=$0.88m$) is $1.43T$. In addition to the ohmic power, the plasma is heated with 1.5MW X-mode Electron Cyclotron Heating (ECH). The ECH beam geometry is shown in Fig. 2.1.18: 1MW is injected at the 3rd electron cyclotron harmonic (X3) from the top of TCV and 0.5MW is injected from the low-field side (LFS) at the 2nd harmonic (X2). The absorbed fraction computed by the ray tracing code TORAY-GA

is 75% for the X3, primarily in the core region, and 100% for the X2, localized near the plasma edge.

Figure 2.1.19 shows plasma signals during an H-mode with a SN established between 0.28*s* and 0.7*s*, and a SF+ stationary phase between 0.8*s* and 1.64*s*. ECH is injected from 0.3*s* to 1.7*s*. This reproducible discharge featuring both SN and SF+ configurations within the same plasma pulse is used to examine the differences and similarities in the H-mode and ELM behaviours. Operated at low plasma density to avoid the ECH cutoff, these plasmas are well below the ohmic H-mode TCV density threshold and undergo a transition to H-mode only when the ECH power is applied, identified by the characteristic drop in *Hα* emission (Fig. 2.1.19(a)) and the development of an edge transport barrier in the pressure profile measured by Thomson scattering. The H-mode features steady ELMs, starting immediately after the transition. Figure 2.1.19(b,c) shows the temporal evolution of the volume averaged temperature and the line averaged electron plasma density. The volume averaged plasma temperature increases by ~15% during the SN to SF+ transition as the second X-point is moved between the positions shown in Fig. 2.1.19. The pedestal temperature does not change (Fig. 2.1.22(a)). The total plasma energy, confinement time and H-factor increase by ~15% in the steady-state SF+ phase. This relatively small enhancement may be consistent with the variation of the global plasma shape parameters (e.g. the ~30% increase in the lower triangularity) between SN and SF+ configurations.

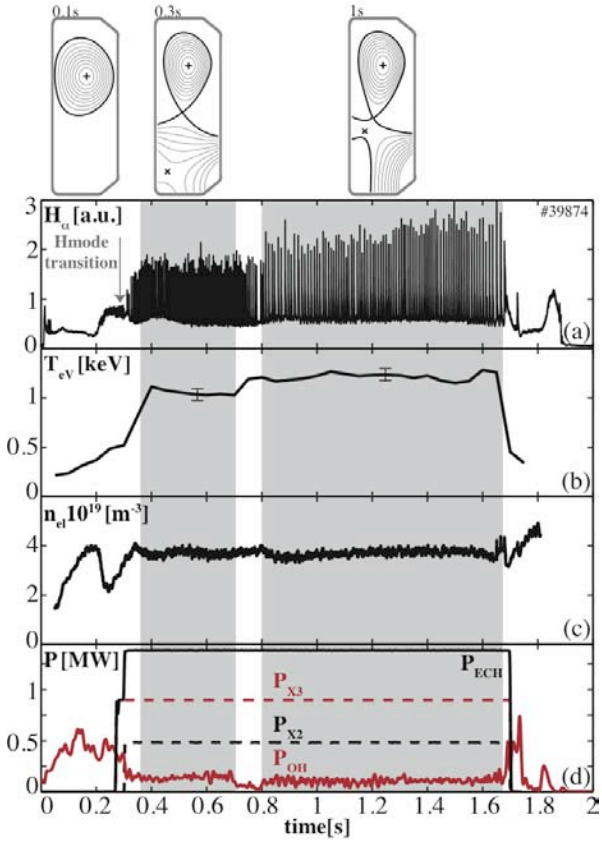

Fig. 2.1.19 *(a) Hα edge emission detected by a wide-angle filtered photodiode at the top of the vessel; (b) volume averaged electron plasma temperature; (c) line averaged electron plasma density; (d) ohmic power (red solid line), ECH-X2 power (black dashed line), ECH-X3 power (red dashed line), and total ECH power (black solid line).*

The L-H power threshold and the ELM dynamics are crucial properties of H-mode plasmas and their understanding is regarded as an urgent need for controlled fusion. The L-H mode threshold power for the two configurations is identified with a sequence of discharges with increasing heating power. Figure 2.1.20 shows the minimum heating power necessary to establish an H-mode as a function of the volume averaged plasma density n_eV. Above $n_eV \sim 5 \cdot 10^{19} m^{-3}$, H-mode access is possible with ohmic heating power alone. The power threshold is similar for the two configurations, so the change in magnetic topology does not appear to influence the H-mode threshold as one might expect from the increase in shear just inside the separatrix. This is an important result since one of the purposes of snowflake divertors is to open a new regime for ELMy H-modes.

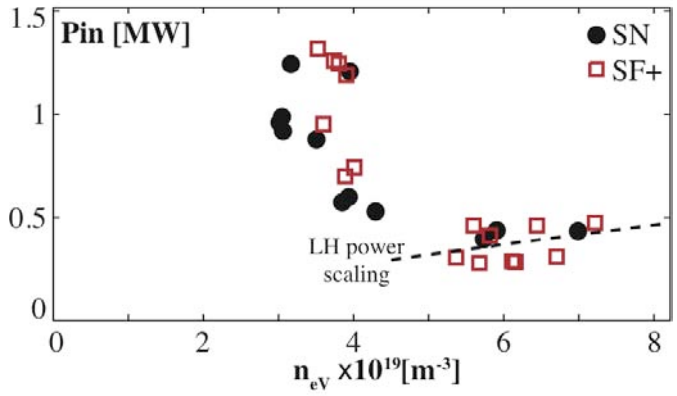

Fig. 2.1.20 *H-mode input power threshold vs volume averaged electron plasma density for the SN (black circles) and the SF+ (red squares) configurations. The dashed line represents the L-H mode transition scaling from the international H-mode threshold database.*

In H-modes, ELMs are readily observed as spikes on *Hα* radiation from the plasma edge. The vertical *Hα*-filtered photodiode, Fig. 2.1.19(a), has a field of view that covers all the strike points. A clear change is observed at the SN-SF+ transition with a reduction in the ELM frequency and an increase in the amplitude of the *Hα* peaks and their integrated intensity across the ELM by ~30%. The ELMing phases are compared for a sequence of discharges with stepwise increase of the heating power. Figure 2.1.21 shows the ELM frequency (ν_{ELM}) versus the input power (*Pin*) for both configurations with quantities averaged over a power step held for 200*ms*, i.e. long enough compared to the confinement time and to ensure regular ELM activity. The vertical error bars depict the scatter in the computed ELM period and the horizontal error bars are mainly due to 15% uncertainties in the absorbed fraction of the ECH-X3 power. The ELM frequency increases with heating power, a behaviour typically associated with Type I ELM regimes. The high input power compared with P_{thrLH} and the absence of a detectable magnetic precursor oscillation also favor a Type I classification. For both configurations, the average energy drop at each ELM ($\Delta W_{ELM} > 1.6$ *kJ*, $\Delta W_{ELM}/W_p > 10\%$) is comparable to, or larger than, that of Type I ELMs in other devices. Strikingly, the ELM frequency for the SF+ configuration is 2-3 times lower than for the SN configuration whereas the normalized energy loss at each ELM increases by 20-30% only. The ELM behaviour is thus indeed strongly modified by the SF+ configuration and results in improved plasma performance. The significant reduction of ν_{ELM} with a relatively smaller increase of ΔW_{ELM} causes a decrease of the normalized ELM power loss ($\nu_{ELM} \Delta W_{ELM}/P_{in}$), changing from 30% for the SN to ~12% for the SF+ configuration.

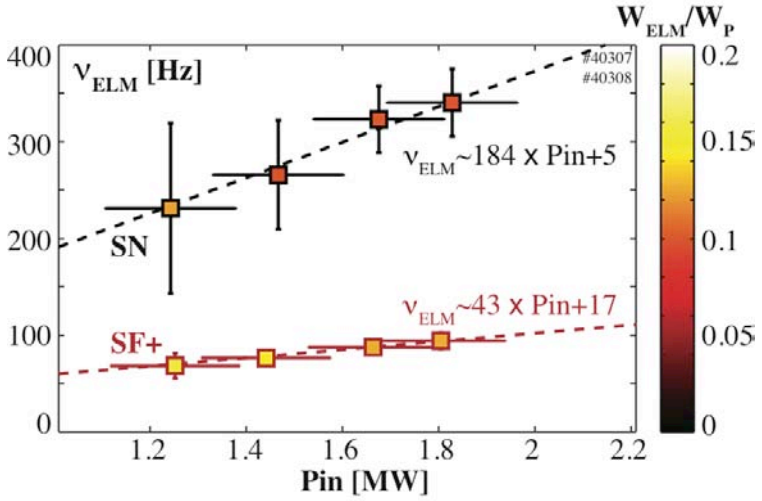

Fig. 2.1.21 *ELM frequency variation as a function of the total input power for the SN and the SF+ configurations. The colour parameterizes the ELM energy loss normalized to the plasma energy.*

An analysis of the stability of the plasma edge was undertaken to assess the nature of the ELMs for the two configurations. Figure 2.1.22(a,b) show the temperature and density pedestal profiles for the SN and the SF+ configurations, demonstrating no significant difference in the pedestal profiles, except for the slightly steeper temperature gradient of the SF+ configuration just inside the pedestal region (leading to a 15% increase in T_{e0}). The magnetic shear is computed for the two configurations using the CHEASE code and is shown in Fig. 2.1.22(b). The edge bootstrap current, calculated from the electron temperature and density profiles, is fully taken into account. The SF+ configuration has higher magnetic shear just inside the plasma separatrix and a slightly lower bootstrap current fraction.

Figure 2.1.22(c) shows the MHD stability space diagram of normalized parallel current density in the pedestal ($J\|/\langle J\rangle$) vs. the normalized pressure gradient α computed with the KINX code. The squares represent the experimental profiles derived from the Thomson scattering data in Fig. 2.1.22(a,b). The ion temperature is taken to be equal to the electron temperature, as indicated by the Charge eXchange Recombination Spectroscopy (CXRS) measurements near the plasma edge. The experimental points for both configurations are close to the kink-ballooning stability boundary, as expected for Type I ELMy H-modes. The second stability region is slightly larger for the SF+ configuration, i.e. coupled kink-ballooning modes at intermediate-high toroidal mode numbers are more stable. This is a general feature of SF configurations and is confirmed also when calculating the stability diagram with identical profiles.

One of the most unusual features of the SF SOL is the presence of two additional divertor legs (strike points 3 and 4 in Fig. 2.1.18(b)). The properties of the strike point 4 of the SF+ configuration are analyzed with a fast vertical infra-red (VIR) camera monitoring the floor tiles. Figure 2.1.23 shows the coherently averaged ELMs spatial profiles of the heat flux and temperature at the strike point 4 measured with the VIR camera. The peaks of the $H\alpha$ signal are used as reference for the coherent averaging. A considerable amount of power reaches this strike zone, even though this divertor leg is not directly connected to the main plasma region. Cross-field transport, which is important in the vicinity of the X-points, may explain

this observation. The total energy deposited at strike point 4 is inferred by integrating the heat flux profile. On average, ~15% of the total energy lost by the plasma at each ELM (measured with a Diamagnetic Loop) impinges on strike point 4, supported by independent calorimetry analysis based on thermocouples in the divertor tiles. No significant broadening of the profiles during the ELM is observed, in contrast with typical observations for the outer strike point of a SN plasma.

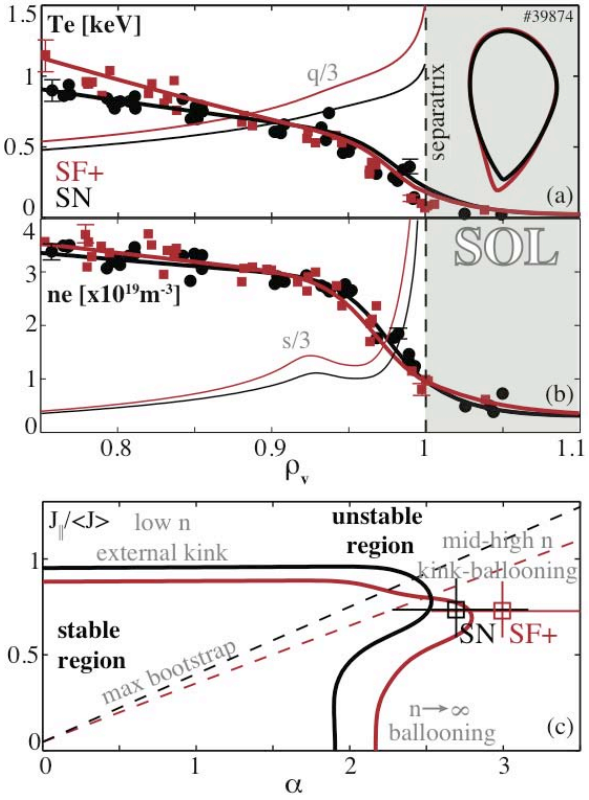

Fig. 2.1.22 *(a) Electron temperature and (b) density pedestal profiles for the SN and the SF+ configurations (solid lines) together with the Thomson scattering measurements (dots) as functions of ρv. The error bars of the Thomson scattering measurements for the innermost core and pedestal regions are indicated. Thin lines represent (a) the q/3 profile and (b) the magnetic shear s/3. The LCFS of the two configuration is shown in (a) on the right. (c) Stability diagrams of the SN and the SF+ configurations. The collisional bootstrap current is represented by dashed lines together with the experimental points for both configurations (squares).*

In conclusion, a type I ELMy H-mode regime has been successfully achieved in a snowflake configuration and compared to an equivalent single-null discharge. The most striking difference is in the ELM frequency, reduced by a factor 2-3 in the snowflake, while $\Delta W_{ELM}/W_P$ is only increased by 20-30%. This opens the way to the study of the effect of the new magnetic topology on ELMs.

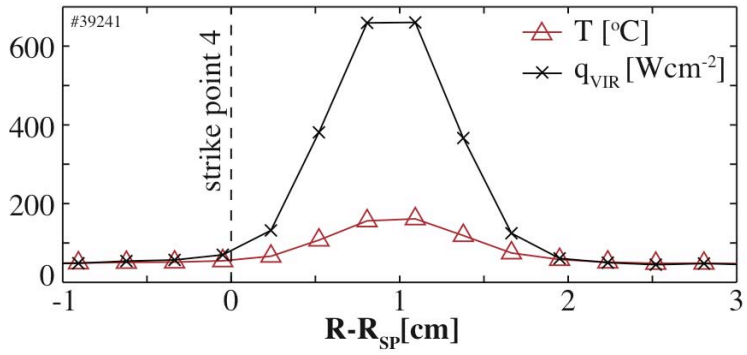

Fig. 2.1.23 *Temperature T and heat flux q_{VIR} profiles at the strike point 4 vs the distance from the strike point at the time of the ELM Hα spike. The profiles are coherently averaged over 30 ELMs.*

2.1.8 Exploration of new shapes and plasma configurations: doublets

A doublet shaped plasma is a tokamak MHD equilibrium characterized by two plasma currents confined with nested magnetic flux surfaces (Fig. 2.1.24(b)). Since the two plasma currents have the same toroidal direction, a magnetic X-point is present between the two plasma axis. The magnetic flux surface that crosses the X-point is the separatrix.

In a conventional diverted single-axis plasma (Fig. 2.1.24(a)), the X-point defines the position of the separatrix that corresponds to the plasma boundary. Outside the separatrix, the magnetic field lines are opened and intersect the divertor plates through the Scrape-O Layer (SOL). In a doublet shaped plasma, outside the internal separatrix there is a region with closed magnetic field lines (mantle) delimited externally by the plasma boundary and the SOL (Fig. 2.1.24(b)).

The vertical stability of symmetric and asymmetric doublets has been studied using the equilibrium code CAXE and the stability code KINX. A characteristic feature of the doublet n=0 stability is the presence of two unstable modes. The most unstable mode features a mirror symmetric displacement of the two domains inside the separatrix. The most stable mode is characterized by a displacement of the two plasma columns toward the same vertical direction. A comparison shows that the n=0 mode growth rate is much lower for doublets than for a single-axis plasmas with the same overall elongation, with a larger difference for asymmetric doublets.

A simple model to analyze the vertical stability of a droplet/doublet configuration is described using a linear electromagnetic model of a system of two plasmas surrounded by the TCV vacuum vessel. The two plasmas can move inside the vacuum vessel but no deformation is allowed (Rigid Model). The plasma inertia is neglected since it does not play an important role for low growth rates of the unstable modes, i.e. controllable by the real-time control system on TCV. The two plasmas can only rigidly shift vertically inside the vacuum vessel. The current in the PF coils is supposed to be constant and the variation of the plasma current is neglected. The TCV vacuum vessel is modeled with 38 filaments magnetically coupled.

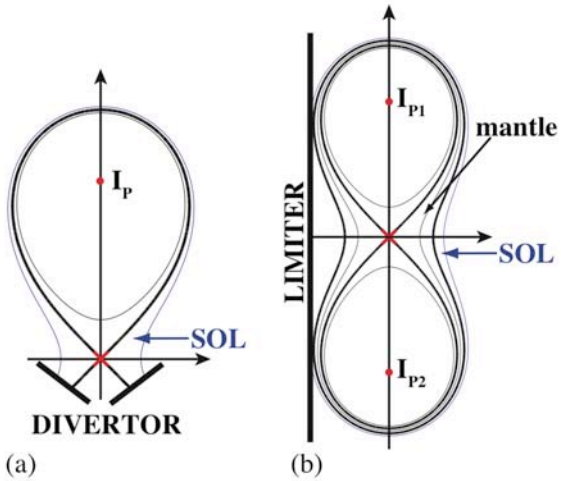

Fig. 2.1.24 *Conventional single-axis diverted plasma (a) and doublet shaped plasma (b) in a straight filamentary tokamak model. The red circles represent the current laments and the red crosses the X-points.*

The growth rate of the unstable vertical modes of a doublet plasma computed using the rigid model (RM) are compared with those evaluated with the KINX code. The reference equilibrium is computed with the CAXE code, in shown in Fig. 2.1.25(a). A current-less pressure-less mantle is considered. Starting from this equilibrium, the comparison is done changing the thickness of the mantle (Fig. 2.1.25(b)) and the distance of the two plasmas from the inner wall (Fig. 2.1.25(c)).

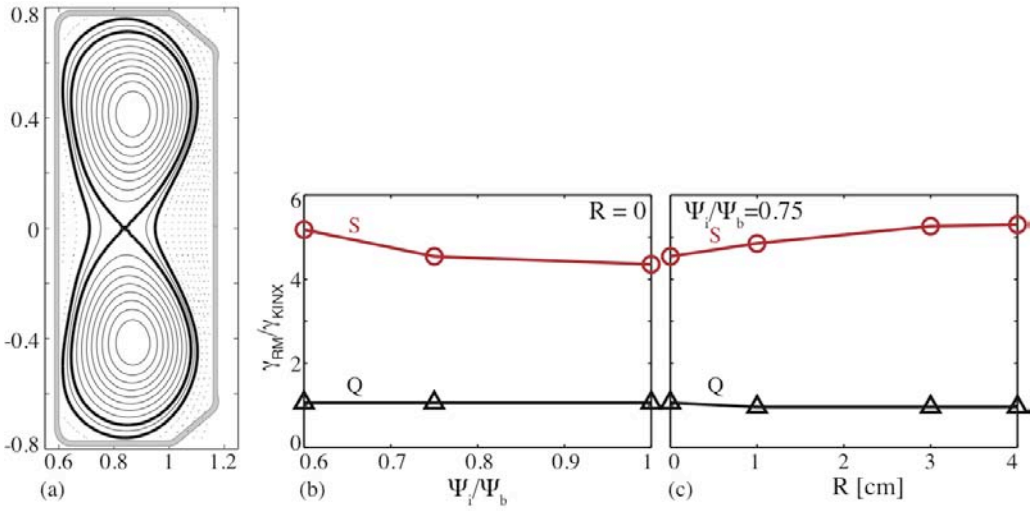

Fig. 2.1.25 *MHD equilibrium of a symmetric doublet computed with the CAXE code (a); ratio of the vertical instability growth rate computed with the rigid model and the KINX code for the symmetric mode (red) and anti-symmetric mode (black) as a function of mantel thickness (b) and distance from wall (c).*

Independently of the thickness of the doublet mantle there is a good agreement between the growth rate computed by the RM and the KINX code for the anti-symmetric mode. A similar result is obtained when the distance from the inner wall is changed (Fig. 2.1.25(c)). Conversely, there is a large difference between the

growth rate of the symmetric mode computed with the RM and the KINX code. The RM gives a growth rate approximately 5 times higher than the one computed with the KINX code, showing a stabilizing influence of the doublet mantle and the stabilizing effects of the conductive wall. The large difference in the predicted growth rate of the symmetric unstable mode between the two codes is due to the nature of the plasma displacements, which inevitably lead to a plasma shape deformation. The rigid model by definition cannot take into account this effect. Plasma deformation induces a plasma current that flows along the magnetic field lines in the plasma edge. This current has a stabilizing effect, reducing the effective growth rate of the vertically unstable mode. The current is mainly localized in the mantle. A reduction of the mantle thickness lead therefore to an increase of the unstable growth rate and a reduction of the discrepancy between the growth rate computed with the RM and KINX, as shown in Fig. 2.1.25.

To create a doublet by merging two droplet-shaped plasmas, the stability of the droplet configuration needs to be analyzed. The KINX code cannot analyze the stability of a droplet plasma. Conversely, the MHD-NX code computes the ideal MHD stability of plasma equilibrium configurations with arbitrary topology of axisymetric magnetic surfaces, including doublets and droplets. A sequence of up-down symmetric droplet equilibria is computed with the free-boundary equilibrium solver MGAMS/FBTE. Each equilibrium consists in two limited plasmas. The relative position of the two plasmas is changed and the stability of each equilibrium is computed. A direct comparison between the RM and the MHD-NX code is not possible, since the RM computes the resistive growth rate and the MHD-NX code the ideal stability, i.e. with a perfect conductive wall surrounding the plasma. However, a qualitative comparison may be useful to identify general trends and behaviors of droplet plasmas. A comparison between the stability region computed with the RM and MHD-NX shows a good qualitative agreement. The RM predicts an ideal instability for higher distance between the two plasmas compared to the MHD-NX code. This is probably due to the effect of the surface currents in the droplet edge configuration.

The stability should be considered when programming the discharge evolution. During the droplet phase, the two plasmas should be kept as far as possible from each other to reduce the vertical growth rate, especially during the early phase, when the active control system is less effective due to the low plasma current in the two lobes. The two plasmas should grow close to the HFS vacuum vessel, where the conducting wall contributes to stabilize the two plasmas.

2.1.9 Plasma edge characterisation and modelling

The main focus of the edge studies in TCV in 2010 was to characterise the new snowflake configuration. This configuration has four divertor legs (instead of two in conventional single-null plasmas) and features increased flux expansion, at least in the region of the divertor itself. Since the TCV vessel and coil systems are not optimised for this shape, the unexpected effect of the increased flux expansion was to re-focus some of the divertor legs by the time they reached the machine wall.

This effect was sufficiently strong that the Langmuir probe spacing on the inner, outer and floor of the TCV vessel was insufficient to resolve the spatial distribution of the divertor legs. This will be the subject of a reviewed Langmuir probe implementation (see below). Furthermore, the current Langmuir probe design intercept too many field lines resulting in a saturation of the characteristic currents during strong events such as H-mode ELMs, Fig. 2.1.26.

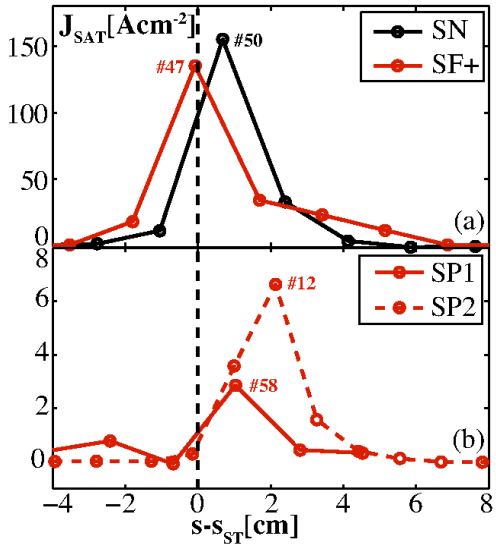

Fig. 2.1.26 *Top - Profiles of the Langmuir ion saturation currents for ELMs in Single Null (SN) and Snowflake (SF) configurations on the inner wall strike point. The solid dots show the probe positions on the vessel as a function of their distance from the divertor leg strike point. Clearly the available spatial resolution is not sufficient to resolve any structure within the strike point region. Bottom - Saturation currents for two of the new strike points in the Snowflake configuration that also indicate the limited spatial resolution of the probe arrays.*

Despite this, a qualitative comparison of the ELM characteristics of plasmas with diverted and snowflake configurations was achieved by adapting the Langmuir probe electronics to double their maximum current limit. A high-speed Infra-Red camera was simultaneously able to measure the power reaching the floor of the TCV vessel during the ELMs for comparison. In preliminary observations, a considerable proportion of the power expulsed during an ELM event in a snowflake configuration reaches the vessel floor.

Experiments involving H-mode TCV discharges with negative triangularity require that the divertor leg be placed on the outside TCV wall. By operating at specific heights, it is possible to avoid the diagnostic port apertures, but the inner divertor leg will inevitably interact with the outer wall carbon protection tiles that are not designed for these powers.

In view of these considerations, we are embarking on the design phase of new outer wall protection tiles to accommodate the negative triangularity H-mode and simultaneously upon a re-design of the Langmuir probe and their spacing. In view of the upgrades proposed for TCV that also include modifications to the outside wall, progress will depend on the advancement of all these projects. Finally, modifications to the IR camera optics are being envisaged to observe all the divertor leg wall interactions of the snowflake configuration to measure this configuration's ability to distribute the exhausted power.

2.2 Theory and numerical simulation

Research activities in theory and numerical simulations of magnetically confined fusion plasmas pursue three general objectives: (1) the basic understanding of fundamental physics processes occurring in such systems; (2) the analysis and prediction of specific tokamak and stellarator experiments; (3) the investigation and optimisation of novel confinement systems.

A vigorous continuing effort has been devoted to the problem of anomalous transport of heat, particles and momentum caused by the quasi-ubiquitons presence of turbulence in magnetically confined plasmas (section 2.2.1). The application of RF waves and their consistent modelling in the presence of fast ions is presented in section 2.2.2. Tokamak operational limits imposed by macroscopic stability are analyzed in section 2.2.3.

Optimization studies of 3D configurations have been pursued (section 2.2.4). Progress has also been made for the integrated tokamak modelling (ITM) in the frame of the EFDA-ITM task force (section 2.2.5). A new field of investigations has been opened with the discovery of spontaneous symmetry breaking in nominally axisymmetric tokamak configurations that, under certain conditions, undergo a bifurcation to an equilibrium exhibiting a 3D helical core (section 2.2.6). Finally, modelling of discharge evolution of ITER plasmas has been further studied (section 2.2.8).

2.2.1 Physics underlying anomalous transport

Size scaling of turbulent-induced transport

Simulations from the two global codes ORB5 and GENE have revisited the issue of size scaling and have confirmed that in the limit of small ρ^* (ρ^* = Larmor radius / minor radius of tokamak) one indeed converges to the results obtained with the local, so-called flux-tube, model, in which the heat diffusivity scales like gyro-Bohm ($\chi_{GB}=\rho^*\rho_s c_s/a$). This study pointed out the importance of correctly implementing magnetic geometry, which is not ensured by the implementation of the so-called s-α model in flux-tube gyrokinetic codes. By independently varying the Larmor radius and the width of the gradient profiles with respect to the system size, it was also shown that the turbulent effective heat diffusivities, estimated in Gyro-Bohm units, depends on the radial width of the strong gradient profile and not on system size only: it could be expressed in terms of the effective parameter ρ^*_{eff} defined as the ratio of the ion sound Larmor radius to the width of the linearly unstable region, see Fig. 2.2.1. In addition, it was shown for the first time that Lagrangian and Eulerian codes do agree on the size scaling issue, thus resolving a longstanding controversy in the fusion plasma theory community.

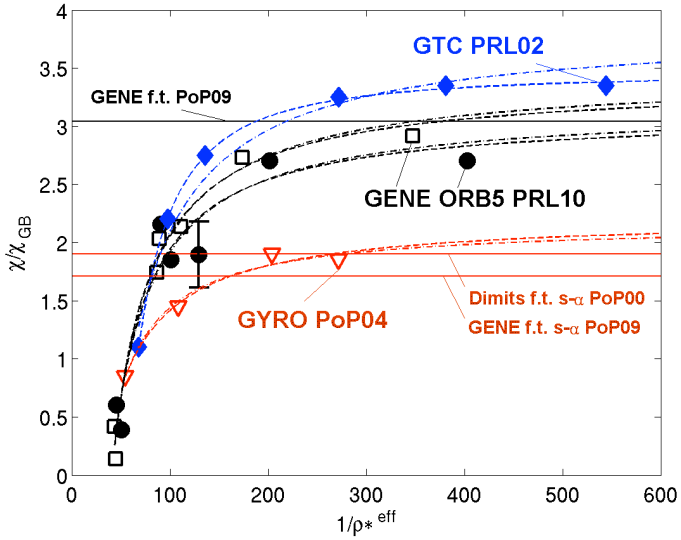

Fig. 2.2.1 *Size scaling of Ion Temperature Gradient (ITG) turbulent heat transport obtained with various global gyrokinetic codes.*

Detailed benchmark comparison of the ORB5 and GENE global gyrokinetic codes

Besides the remarkable agreement in finite size scaling effects mentioned above, the global version of the Eulerian gyrokinetic code GENE has been thoroughly benchmarked against the global PIC code ORB5 for simulating microturbulence in the ITG regime using the reduced adiabatic electron model. These comparisons have been pushed to an unprecedented level of detail: not only the heat fluxes have been compared, but also the detailed mode structures, the nonlinear spectra, the Geodesic Acoustic Modes (GAM), the zonal flow damping behaviour, the structure of avalanches and bursts show remarkable agreement. Cases without and with heat sources have been considered. In the former case, the profiles rapidly relax to marginally stable gradients while in the latter case gradients are maintained above critical levels in a quasi-stationary microturbulent state. Such a quasi-stationary state is particularly valuable for code comparisons as it enables to acquire statistically relevant estimates of the fluctuating turbulent fluxes from the different simulations.

Dealing with chaos: ensemble of statistically independent simulations of turbulence

Turbulent processes are characterized by a chaotic behaviour, often accompanied by bursts and avalanches. A measurable fraction of the heat flux is carried by large, avalanche-like events. Performing ensemble averages of statistically independent simulations using the ORB5 code, starting from different initial conditions, in order to assess the intrinsic variability of turbulent fluxes, have resulted in reliable estimates of their standard deviation. Figure 2.2.2 (top) shows the instantaneous heat diffusivities from a set of 10 simulations identical except for a tiny variation on the initial condition. Figure 2.2.2 (bottom) shows the same quantities but averaged over a time window of fixed size. Finally the standard deviation of the results as a function of the time-averaging window size Δt_w decreases as $1/\sqrt{\Delta t_w}$.

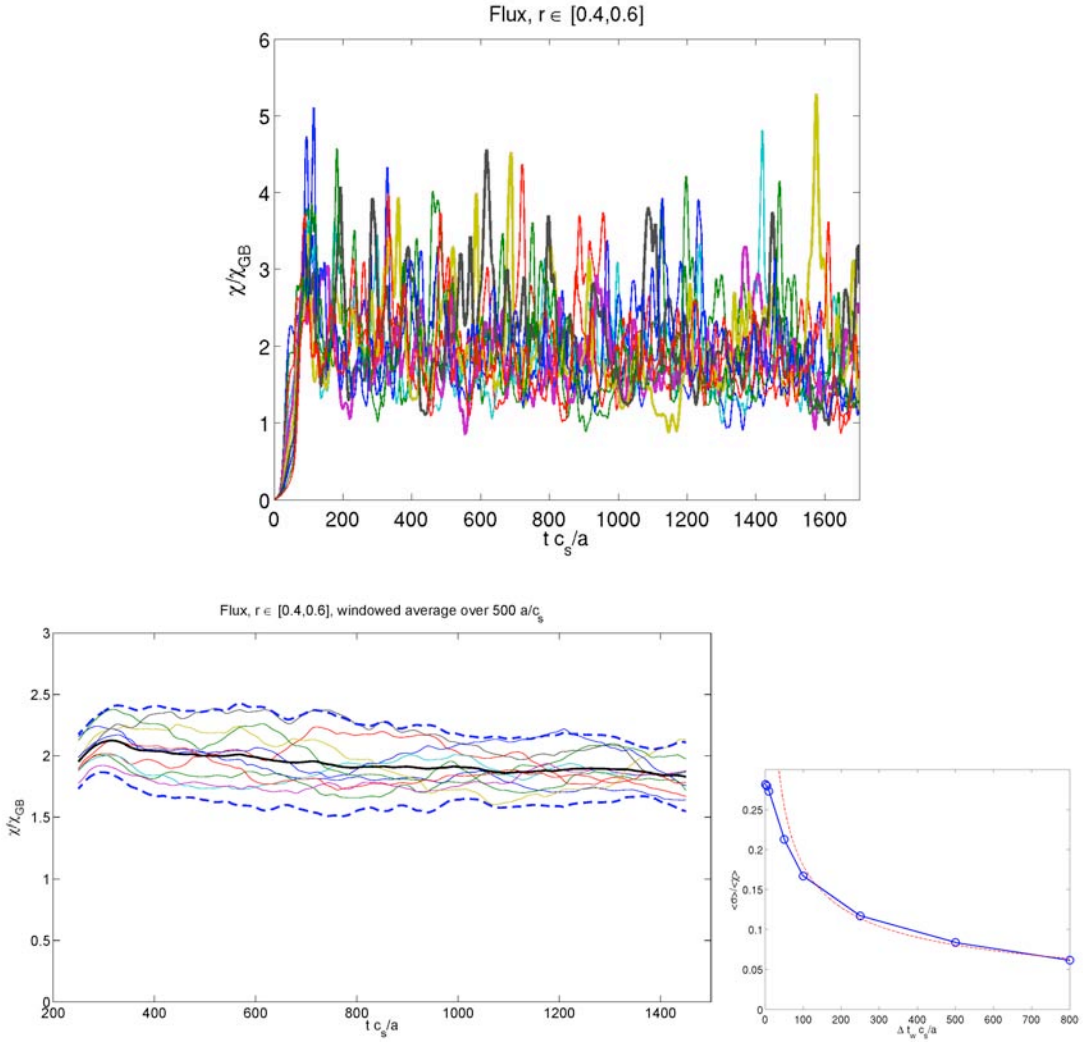

Fig. 2.2.2 *Time traces of turbulent heat diffusivity from a set of 10 independent global gyrokinetic ORB5 simulations differing only in their initial small perturbation. Top: instantaneous values. Bottom left: time window averaged values, with the thick line showing the ensemble average and the dotted lines two standard deviations from the average.Bottom right: standard deviation of the ensemble as a function of time averaging window size.*

Particle transport in electron internal transport barriers of TCV

The GENE code has been applied for carrying out simulations of turbulent particle transport under conditions relevant to electron internal transport barriers (e-ITB's) in the TCV tokamak. In a first approach, results were obtained using the flux-tube model. It has been shown that typical electron and ion profiles are such that both ITG (= Ion Temperature Gradient) and TEM (= Trapped Electron Modes) are simultaneously unstable and respectively lead to inward and outward contributions to the particle transport which may cancel each other, thus enabling a state of zero particle flux even for the steep gradients found in the barrier region. The electron heat transport computed from the simulations is more than twice as high as those experimentally measured. First global simulations seem to point out the significant importance of finite ρ^*_{eff} effects on heat transport in these transport barriers. A numerical instability, which at first affected global GENE simulations with kinetic

passing electrons, prevented the thorough investigation of these finite ρ^*_{eff} effects. This numerical issue appears to have now been solved thanks to an improved discretization scheme which better accounts for the symmetries and conservation properties of the underlying equations.

Resonant behaviour near mode rational surfaces

A study of the effect of kinetic passing electrons on ITG and TEM turbulence has been initiated using the GENE code. It is observed how the non-adiabatic electron response near mode rational surfaces may lead to fine structures in the radial envelope of linear eigenmodes (Fig. 2.2.3). One of the purposes of this study is to investigate whether such structures survive in the non-linear regime with the potential of significantly affecting the turbulent fluxes. So as to more systematically point out the role played by passing electrons, a hybrid model, which evolves trapped particles kinetically and passing particles adiabatically, is being implemented. This reduced electron model will allow us to "turn off" the kinetic response of passing particles.

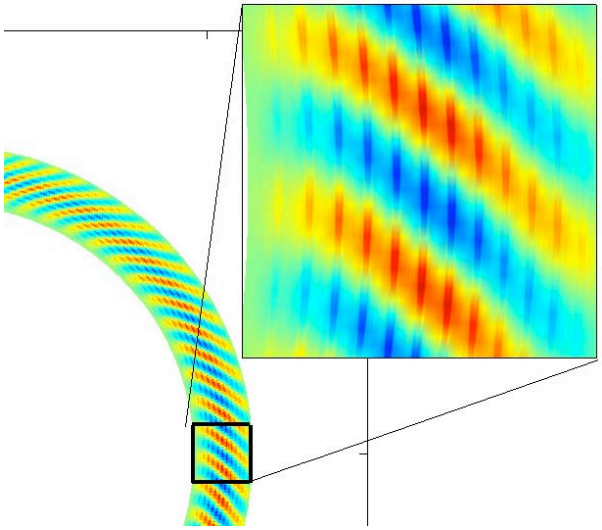

Fig. 2.2.3 *Trapped Electron Mode (TEM) computed with the GENE code including non-adiabatic electron response. The sharp radial structures correspond to mode-rational surfaces.*

Implementation of collisions in Eulerian Vlasov codes

The implementation of linearized Landau collision operators in ($V_{parallel}$, V_{perp}) velocity variables has been carried out using a finite element approach. A novel, implicit time integration scheme, which enables to preserve mass, momentum and kinetic energy to round-off machine precision, has been derived. As a test case, the effect of collisional detrapping of electrons on linear and non-linear Landau damping of Langmuir waves was considered. The implementation of non-linear self-collisions has been initiated as well. To this end, algorithms for computing the Rosenbluth potentials by solving the corresponding Poisson-like equations with appropriate boundary conditions have been developed. Time-stepping of the non-linear collision operators remains to be addressed.

Implementation of collisions in the gyrokinetic PIC code ORB5

A Langevin approach has been considered for implementing approximate forms of the linearized Landau collision operators into the global gyrokinetic delta-f PIC code ORB5. Various numerical procedures have been applied for reducing the accumulation of numerical noise, including a coarse-graining scheme, as well as a novel background switching scheme, which alternatively considers a canonical Maxwellian background for carrying out the collisionless dynamics and a local Maxwellian background for carrying out the linearized collision dynamics. The collisional ORB5 code has been benchmarked by carrying out neoclassical transport simulations both within and beyond the standard neoclassical ordering. These simulations have been compared both to analytical results as well as to results obtained from other codes. Neoclassical equilibrium states obtained with ORB5 provide a sound starting point for carrying out global microturbulence simulations including collisional effects. First simulations of this type have been carried out. Of particular interest will be the study of ion-ion collisional effects on zonal flow dynamics, as well as the effect of electron-ion collisions in the TEM turbulent regime.

High Performance Computing (HPC) issues: field-aligned solver in ORB5

In view of the optimization of the parallelization scheme, the implementation of field-aligned coordinates in ORB5 has been initiated. The aim is to reduce by orders of magnitude the grid size requirement for the 3D field solver, thus reducing the all-to-all inter-processor communication, which is not scalable to very high processor numbers. Solving the Poisson equation in a sheared cylindrical magnetic configuration with arbitrary radial safety factor profile has been first considered as a test case in view of solving the quasi-neutrality equation in a tokamak system using field-aligned coordinates. Currently, a finite element method, using B-splines of arbitrary order, was successfully implemented for solving the Poisson equation in a cylindrical annulus and considering radial Dirichlet boundary conditions. The issue with field-aligned coordinates of correctly accounting for the periodic boundary conditions within the magnetic surface has been solved.

Effects of externally applied large scale poloidal and toroidal flows on turbulence

Both externally applied and self-consistently driven shear flows are known to impact transport in tokamaks. The introduction of arbitrary initial flow profiles into the code ORB5 allows the convenient studies of how these two types of flows both influence transport levels and self-consistently evolve. A formulation has been devised which preserves the canonical structure of the background particle distribution when either toroidal or poloidal flows are introduced, and benchmarks have been made against previous results. A series of numerical investigations have been performed, to determine how the structure of an imposed flow shear influences transport levels and the quantitative structure of the turbulence. Turbulence suppression is possible above a certain shearing rate magnitude for homogeneous shear flows, and little evolution of the shearing rate is seen. However, when a flow with a zone boundary, where the shearing rate reverses at mid-radius, is introduced, the shear flow evolves substantially during the simulation. E×B shear flows with a zone boundary of a positive sign decay to a saturation amplitude, consistent with the well known saturation of turbulently generated zonal flows. Unlike the E×B flow, toroidal momentum transport is shown to be roughly

consistent with a local model, where momentum flux is proportional to the local parallel flow.

Turbulent transport of fast ions

Preliminary analyses on the anomalous transport of energetic species have been extended by linking the gyrokinetic GENE code to the single particle guiding centre code VENUS.

Numerical simulations with the GENE code, focused on the ITER steady state scenario, reveal the presence of a rich mixture of microturbulent modes in this important plasma configuration. In particular, the presence of unstable ITG, TEM and ETG modes has been observed in linear simulations. Nonlinearly, only the former two are shown to be important. The electromagnetic turbulent fields resulting from the saturation of these small scale instabilities are shown to create transport levels larger than estimates based on Coulomb collisions, especially for passing particles. The transport characteristics of suprathermal ions have been obtained by employing a novel definition of a velocity space dependent particle diffusivity, which has then been employed in a single particle following framework.

The VENUS code has been updated and a neutral beam deposition model developed. The injection of high-energy beams in fusion plasmas has been modelled by taking into account the magnetic geometry and the interaction between neutral particles and ionized plasma. The numerical particles representative of NBI ions are then evolved in time with the inclusion of collisional effects (both slowing down and pitch angle scattering) and turbulent transport (including the particle diffusivity simulated with the GENE code). Results show that the 1MeV NNBI in ITER will be affected only to a small extent by the presence of turbulent fields (Fig. 2.2.4). In contrast, ions generated from lower energy NBI would be significantly redistributed, and this in turn might affect plasma stability and transport. Such findings are consistent with inefficient current drive schemes reported in a number of present day machines.

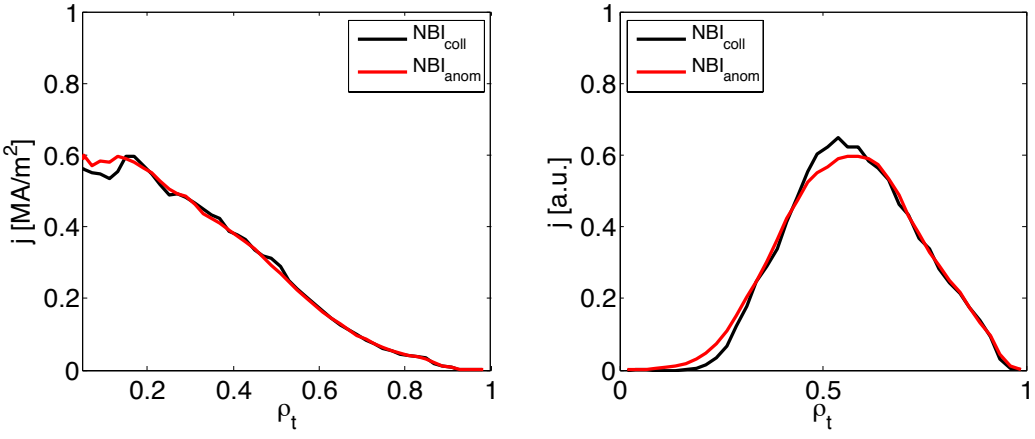

Fig. 2.2.4 *Left panel: current density driven by the on-axis 1MeV NNBI in the ITER steady state scenario in presence of collisional transport (black) and with the addition of microturbulent fields (red). Right panel: current density driven by the off-axis NNBI at 300keV in ITER simulated with the VENUS code. The anomalous redistribution (red curve) is more important given the lower energy beam.*

Gyrokinetic codes benchmarking with kinetic electrons and MHD equilibria

A set of equilibria and profiles has been developed in order to extend the CYCLONE benchmark case to non-circular shapes and kinetic electrons. This is important before using such codes for simulating electron transport particularly in TCV. A set of five equilibria has been developed, Figs 2.2.5 and 2.2.6, starting from the CYCLONE circular concentric case, up to a single-null DIII-D type equilibria with elongation, triangularity, up-down asymmetry and Shafranov shift. In addition they all have the same local values of q and shear at r/a=0.5 as the CYCLONE test case. Thus it is possible to compare local and global codes and to evaluate shaping effects on the CYCLONE base case. Linear results have been obtained with the GS2 and GYRO codes. These results show in particular that since shaping and shear can have contradictory effects on the modes growth rates, comparing only two cases is not sufficient to fully check the codes consistency.

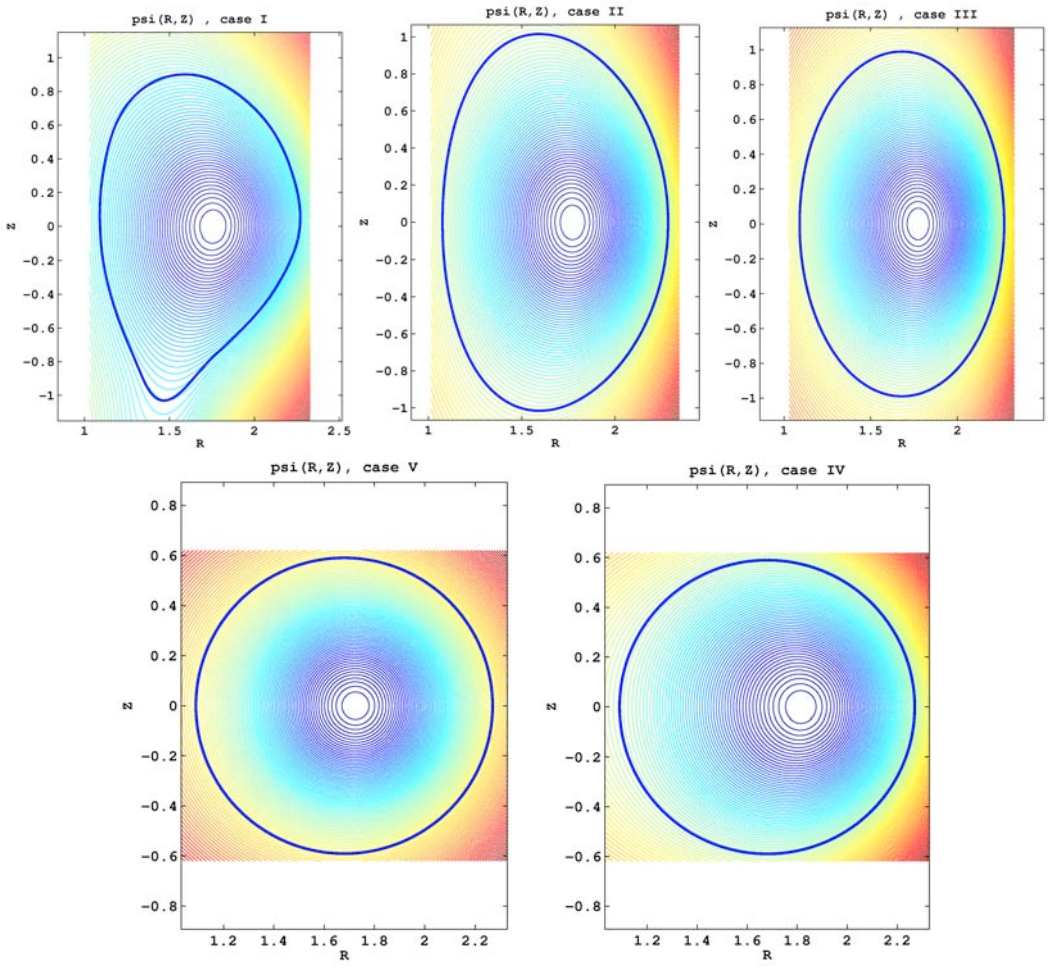

Fig. 2.2.5 *Set of five equilibria starting from CYCLONE-base circular concentric (case V), with Shafranov shift (case IV), elongation (case III), triangularity (case II), single-null (case I).*

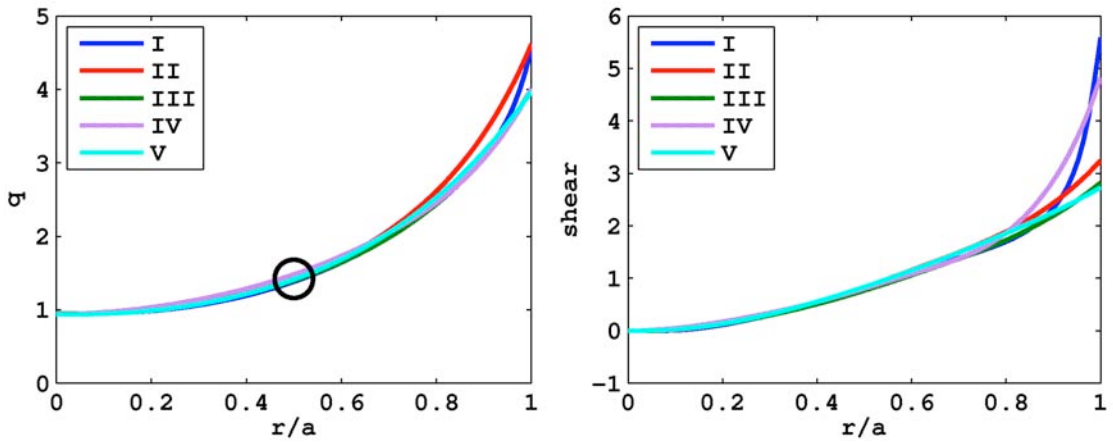

Fig. 2.2.6 *(a) q profiles and (b) magnetic shear profiles for the five equilibria shown above. The current density profile was adjusted, using CHEASE, to yield very similar profiles and allow a better comparison with the effects on turbulence. The circle marks the local value at r/a=0.5 used for flux tube calculations with GS2 and GYRO.*

Particle transport modeling

A database of TCV H-mode discharges with good electron temperature and density profiles has been assembled in view of studying particle transport. The density peaking is observed to decrease with decreasing collisionality, contrary to the usual trend, and a number of gyrokinetic simulations have been started in order to explain this behaviour. Preliminary results show that collisionality has a little effect, but the combination of ohmic versus EC heated cases and high versus low density, lead to T_e/T_i effects and Ware pinch contribution, which can explain the observed trend. An important result emerging from this study is that it is a combination of effects, impacting the ITG and/or TEM turbulence, which lead to the global observation.

2.2.2 RF waves

ICRF waves in 2D and 3D configurations

The code package SCENIC, comprising the codes VMEC for MHD equilibria, LEMan for wave fields and VENUS for distribution function evolution, has been completed. The benchmark efforts against SELFO from KTH, started 2009, have been continued and allowed for thorough testing. As a direct result, important improvements to SCENIC could be implemented.

Applications of SCENIC to 3MW He^3 minority heating cases showed that the iterated scheme converges and is indeed necessary for finding self-consistent solutions to RF heating scenarios. Furthermore, comparisons between the raw distribution functions from VENUS and the analytical model bi-Maxwellian used in the equilibrium and wave field calculations show that the particular bi-Maxwellian applied to these problems is appropriate and yields very satisfying results. High power (12MW) heating of a lighter hydrogen minority at different locations shows that dramatic changes in both the equilibrium and the dielectric tensor can

happen. These changes are due to highly energetic particles with the resulting non-standard wide orbit effects, and can significantly change global stability parameters such as the second derivative of the Shafranov shift and the ballooning parameter, which is related to the radial pressure derivative. Figures 2.2.7 shows the RF induced current densities (without the background Ohmic current), split into contributions from passing and trapped particles, and the perpendicular ballooning parameter at the end of a converged simulation for 12MW injected power and a 3% hydrogen minority in a deuterium background plasma. The resonant layer is on the low field side, around R=3.5m.

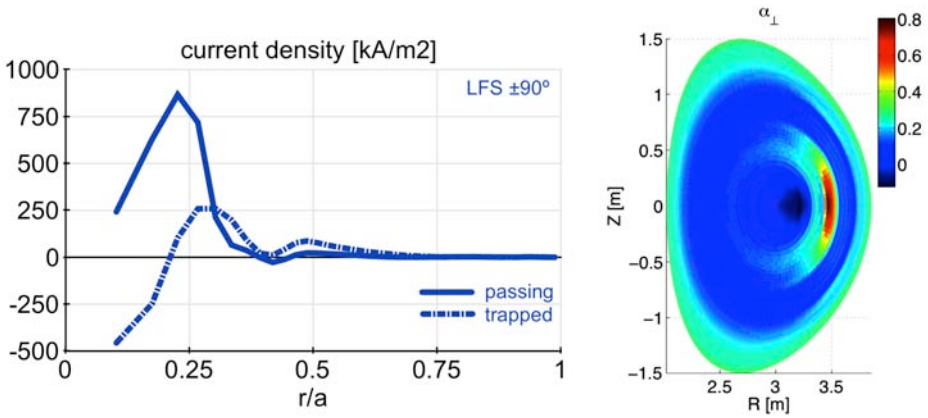

Fig. 2.2.7 *RF induced current densities (without the background Ohmic current), split into contributions from passing and trapped particles (left), and the perpendicular ballooning parameter (right) at the end of a converged simulation for 12MW injected power and a 3% hydrogen minority in a deuterium background plasma.*

2.2.3 Operational limits

MHD equilibria and stability computations of TCV plasmas

In support of the preparation of doublet plasma experiments in the TCV tokamak, doublet and droplet plasma equilibrium and stability were studied with the CAXE, KINX and MHD_NX codes. The influence of perturbed surface currents on the n=0 stability was quantified by comparison with the results of a rigid displacement model (RZIP2). The n=0 growth rates for a conventional doublet configuration inside the TCV wall are about 5 times higher in RZIP2 compared to KINX for the most unstable mode (opposite displacements of two plasma columns). The limits of operational space for doublet formation in TCV set by n=0 instability may thus be considerably extended due to the presence of perturbed surface currents at the plasma boundary. New versions of the KINX-BFX3 code suitable for the edge stability calculations in fixed boundary doublet equilibria with high pressure gradient and current density at the internal separatrix and of the KINX-NW3 code with a possibility of n=0 resistive wall mode calculations both for doublet and droplet plasmas have been produced.

In support of the TCV experimental campaign aiming at studying H-mode plasmas with various separatrix shapes, including negative triangularity and snowflake (SF) divertor, free boundary equilibrium and stability calculations have been performed. In particular, equilibrium configurations with a prescribed position of the second order null of the poloidal magnetic field and PF coil currents within TCV hardware constraints were investigated. It was shown that SF configurations with negative

triangularity of the null point can be produced in the TCV tokamak. An increase of the pedestal in the SF configuration keeping fixed values of PF coil currents results in a splitting of the null point and formation of the SF-"minus" configuration. The n=0 resistive wall mode growth rates are very sensitive to the plasma shape near the null point at the low field side for the negative triangularity SF equilibria. The n=0 growth rates go down by a factor of 3 for self-consistent free boundary SF equilibria with pedestal compared to the equilibrium without pedestal. Such n=0 mode stabilization in an ideal plasma is mostly related to the existence of perturbed surface currents for strongly up-down asymmetric plasma cross-sections. A milder (tens of percent) improvement of edge kink/ballooning mode stability limits was observed with the shape effect under pedestal variations.

The analysis of specific upper positive/lower negative triangularity equilibria with negative triangularity affecting the plasma edge stability has been initiated. A possible advantage of such positive/negative triangularity configurations is to obtain H-mode without ELM activity, possibly due to the lack of kink/ballooning mode second stability access in the pedestal region, while preserving positive triangularity in the plasma core.

Equilibrium and stability of tokamak equilibria with islands

The MHD_NX unstructured grid stability code was tested for external and internal kink mode computations, including Kruskal-Shafranov n=1 stability limit for equilibrium with islands. The adaptive grid option was implemented in the code with different types of monitor function for grid refinement. However, an efficient adaptive grid operation is only possible if the numerical scheme accuracy does not degrade for irregular and highly anisotropic unstructured grids.

Equilibrium sequences with axisymmetric island chains (relevant to the AC tokamak operation and current hole regimes) computed with a perturbative equilibrium code were used for n=0 stability studies under variations of high order harmonics of the plasma geometry. It was found that only sufficiently high squareness (4^{th} harmonic) results in n=0 fixed boundary mode stabilization. It is in accordance with stable analytic equilibria with square cross-section found earlier. The stability computations for essentially nonlinear equilibrium solutions with islands will be pursued in future studies.

MHD Stability and Kinetic effects

An extended region of small or vanishing magnetic shear is susceptible to interchange, quasi-interchange or infernal mode instability when respectively q<1, q=1 or q>1 in the low shear region. An MHD eigenvalue equation has been developed that encompasses all three cases. This has enabled analytical derivation of the mode structure, the growth rates and stability criteria of these important instabilities. Collaborative work on this topic with experimentalists and theorists at Culham has led to a recent publication on infernal modes in the MAST spherical tokamak. Moreover, further work will investigate the numerous kinetic modes that exist simultaneously. On another topic, the effect of toroidal plasma rotation on these modes has been studied. Two recent publications have combined analytic theory, sophisticated numerical MHD simulations and MAST experiments, with surprisingly consistent results. In broad terms it was found that internal kink and sawtooth stability are governed by an extremely complicated combination of density and equilibrium velocity profiles. An important development was finding that a newly discovered geodesic acoustic mode, existing in the continuum, and solely

generated in a toroidally rotating equilibrium, plays an important role in governing the stability of the discrete internal kink mode.

Sawtooth behaviour and internal stability in the presence of fast ions

New calculations of the internal kink stability have been performed which take into account the finite orbit widths of passing ions that intersect the q=1 surface. This analytical work has been extended and compared favourably with numerical simulations. The work has enabled understanding of the extreme sensitivity of sawteeth to the exact location of counter- and co- toroidally propagating ICRF waves. Favorable comparison with previous experiments led to the work being published in Physical Review Letters. Following this, a round of dedicated JET experiments, with He3 minority ions, and resonance on the high field side of the tokamak, have been undertaken in order to test the new theory against an alternative classical theory involving the change in the shear at the q=1 surface. A key result from these studies was the expected observation showing that the minority ICRF concentration must be low in order that sawteeth are effectively controlled. This helped to further verify the proposed fast ion mechanism. Shown in Figure 2.2.8 are experimental results and comparison with simulation. Reduction in the minority concentration increases the orbit widths of the energetic ions, thereby increasing the magnitude of the fast ion mechanism that controls the sawteeth. Nevertheless, if the concentration becomes too low, coupling to the minority ions becomes inefficient, and the control mechanism is lost, as confirmed by the simulations. Finally, direct ITER simulations, with realistic ITER equilibria and RF antenna, have been undertaken. Initial results indicate that the lower relative orbit widths in ITER mean that fast ion control of sawteeth in ITER will be more challenging than in JET. Nevertheless, by positioning the resonance on the low field side (LFS), it may be possible to nullify the stabilising effect of alpha particles. It is hoped that JET experiments with LFS resonance of He^3, possibly conducted in 2012, may confirm the efficiency of this technique.

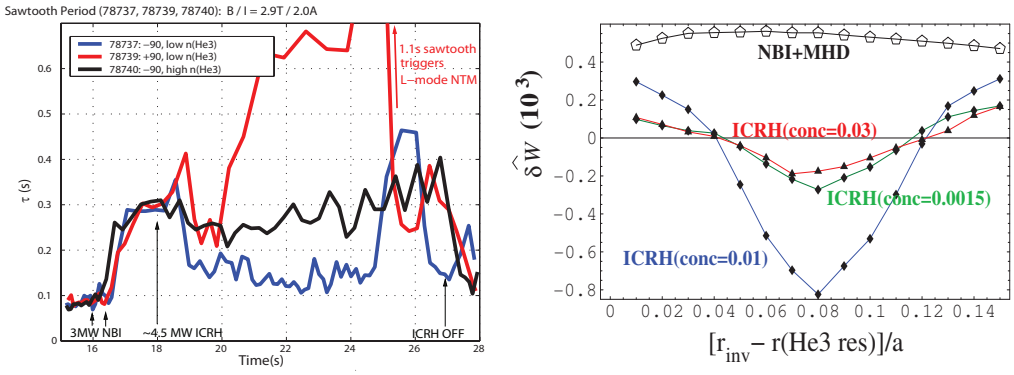

Fig. 2.2.8 *Showing on the left JET experiments using He^3 minority with resonance on the high field side close to q=1 surface. The red curve employs +90 phasing, and the resulting long sawteeth trigger an NTM. The black and blue curve compare the destabilizing effect of employing -90 phasing ICRF; low concentration of minority He^3 gives the strongest effect due to larger fast ion orbit widths. On the right, simulations evaluate the fast ion contribution to the internal kink potential energy. The simulations agree with experiment, but it is shown that if the He^3 minority concentration is too low, the control mechanism is lost due to inefficient heating.*

2.2.4 Optimization of 3D configurations

Optimisation of quasi-isodynamic stellarator configurations

An optimised 4-field period quasi-isodynamic stellarator configuration has been obtained computationally. The shape of the B-contours near its maximum value is hyperboloidal. Closed contours of the second adiabatic invariant exist for the entire range of deeply to barely trapped particle orbits. Alpha particles born within 2/3 of the plasma radius are very well confined. The parallel current density remains enclosed within each field period and the equivalent neoclassical ripple is small, Ideal MHD stability becomes marginal when $<\beta> \sim 6\%$ and is unstable to ballooning structures at $<\beta>=7.5\%$.

Neoclassical transport in 3D stellarators

The bootstrap current in LHD configurations has been calculated with the VENUS+delta f code. The LHD discharge with vacuum magnetic axis at 3.90m has a measured current of 10kA. VENUS+delta f recovers this value with a 20% error bar. The total number of particles followed was 6.4 million. A discharge with the magnetic axis at 4.05m has negative 14kA, while the VENUS+delta f prediction is -8+-2kA. This value is closer than the corresponding result of any other model considered.

Energetic particle physics

Initial benchmark calculations for n=1 and n=2 Toroidal Alfvén Eigenmodes (TAE) with VENUS+delta f that includes contributions from the NOVA-k, CAS3D-k and TAEFL codes has been undertaken on a simple circular cross section aspect ratio 3 tokamak. The perturbed electrostatic and electromagnetic fields employ the Chen-White approximation to determine the impact on the energetic particle orbits. A rough agreement between the four codes tested to the linear n=1 TAE growth rate is obtained for particle charge number $Z > 1$. However, all codes diagree when $Z < 1$ is investigated and for n=2 TAE modes.

3D ballooning stability in stellarators

An estimate of marginal stability has been computed using a theory based on classical and quantum chaos (Weyl formula) for kinetic ballooning mode ray trajectories in an inward shifted LHD configuration with fast particle driven pressure anisotropy. Finite hot particle drifts displace the minimum value of the Weyl number to lower frequencies, but its magnitude remains higher than when these energetic particle drifts are neglected.

2.2.5 Integrated Tokamak Modelling ITM (ITM)

In the frame of the EFDA Integrated Tokamak Modeling (ITM) Task Force, the versions of the equilibrium code CAXE and ideal MHD stability code KINX with input parameters in XML format and the corresponding actors for the KEPLER

workflow manager were built and tested on the ITM TF gateway computer for the ITM data structure and Uniform Access Layer (UAL) version 4.08a. The Kepler workflows with the developed actors were tested for conventional shots from the IMP#12 “Equilibrium and Linear stability” project databases. The equilibrium and stability CAXE and KINX integrated to the ITM data structures are ready for further verification and validation in the frame of IMP#12 project.

The equilibrium code CHEASE has also been integrated within the ITM database using Consistent Physical Objects (CPO) and KEPLER environment. In addition, numerical tools that allow to run CHEASE on a series of equilibria or to fit just the plasma boundary, for example, have been developed for the community.

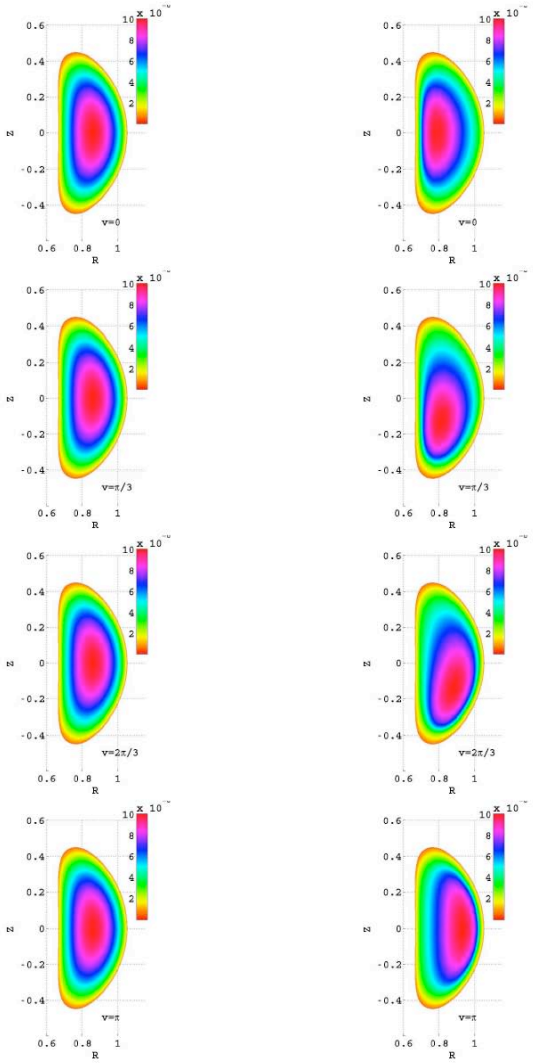

Fig. 2.2.9 *The bifurcated equilibrium toroidal magnetic flux contours at 4 cross sections covering half the torus obtained with the ANIMEC code for the axisymmetric branch (left column) and the helical branch (right column) in a TCV-like configuration*

The efficient and versatile cubic spline interpolation routine, interpos, has also been well integrated within the ITM framework.

Modules required for the transport simulations and such as to be coupled with the European Transport Solver (ETS) solver code have been further developed. The sawteeth module has been tested within the ETS solver. The documentation and cleaning up of the code is now required but all the interfaces and functionalities are implemented. The NTM module is well advanced as well. It actually consists of mainly three modules, to check if there is a tearing mode, to advance the island

width, frequency and phase, and to modify the transport coefficients accordingly. Composite actors have been built for each of the modules and for the NTM module as well. Next year, the integration with the ETS will be tested, a NTM CPO will be developed and the documentation provided.

2.2.6 Tokamak simulations with 3D field effects

MHD equilibrium states with an imposed axisymmetric boundary develop bifurcated solutions when the equilibrium has reversed core magnetic shear (or very flat shear) with q_{min} around unity. One solution is the standard axisymmetric state. The other displays a 3D helical core similar to a saturated ideal internal kink. These results have been obtained in a model TCV tokamak prescribing the pressure and rotational transform profiles using the 3D ANIMEC MHD equilibrium code which computes 3D equilibrium states with nested magnetic flux surfaces (Fig. 2.2.9).

2.2.7 Edge simulations

Development of a fluid code for Scrape Off Layer (SOL) simulation

The development of a fluid code to simulate SOL turbulence was started. This is based on the GBS two-fluid code that was initially developed for the simulation of the TORPEX device.

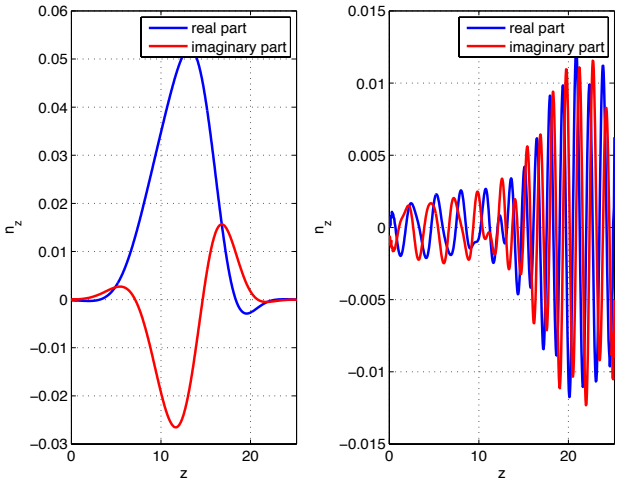

Fig. 2.2.10 *Typical eigenfunctions for the density, plotted as a function of the parallel coordinate, in the case of ballooning mode (left panel) and of drift wave instability (right panel).*

Porting the code to the SOL configuration has required including a number of effects that were not considered in the TORPEX simulation. First, a simple SOL geometry was implemented by considering a *s*-α tokamak geometry. Second, electromagnetic effects have been included. Finally, ion temperature effects have been analytically derived and will be implemented in the code next year.

Initial simulation results have been carried out and have displayed the transition from a drift-wave driven turbulence to a resistive ballooning-driven turbulence if the plasma resistivity and q are increased.

In order to interpret the simulation results, a linear code has been written to evaluate the growth rate of the instabilities present in the system. This code has shown what are the parameter regimes where the drift wave instability, the resistive ballooning mode, and the ion temperature gradient mode dominate, respectively. It has also been useful to identify the eigenfunctions, which is particularly important to characterize the modes present in the non-linear simulations. In Fig. 2.2.10 we show the example of such eigenfunctions, related to a resistive ballooning mode and a drift wave mode, respectively.

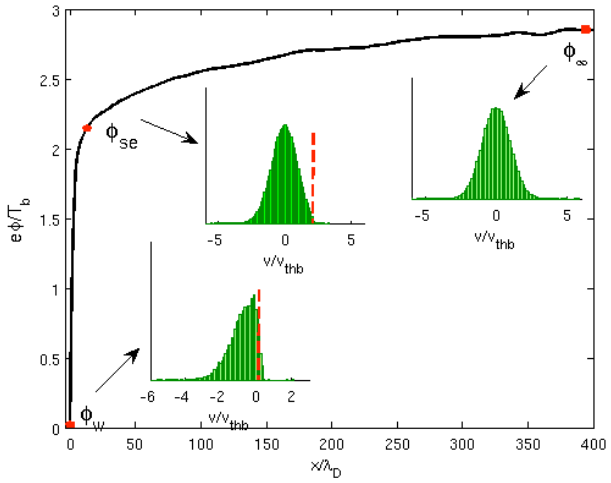

Fig. 2.2.11 *Potential profile in the vicinity of the wall. The electron distribution function is shown at the bulk, at the sheath edge, and at the wall.*

Investigation of the sheath dynamics

The determination of the boundary conditions to be applied to SOL fluid simulation code at the sheath edge is of extreme importance, since they strongly affect the plasma dynamics and determine the plasma losses at the vessel. Since a kinetic approach is needed in order to study the plasma dynamics in the proximity of a solid wall, a 1D3V particle-in-cell (PIC) code has been developed.

The simplest case of a magnetic field perpendicular to the wall has been first explored. In this regime, the magnetic field does not affect the plasma-wall transition, and an electrostatic sheath is present where the plasma quasi neutrality is broken. A combined fluid and kinetic description of the plasma, supported by the numerical results, has been used to rigorously derive the position of the sheath entrance and to understand how the fluid quantities are related at this point. In particular, it has been found that the Bohm criterion, stating that ions need to be accelerated up the sound speed c_s in order for a sheath to exist, is valid in floating potential conditions or in the presence of ion current to the wall, but fails to describe the transition to the non-neutral region in the presence of an electron current to the wall. In fact, the electron velocity distribution function is a Maxwellian that is progressively truncated approaching the wall (Fig. 2.2.11), which can have a strong effect on the ion velocity at the sheath edge, in the case of a large electron current. The more general situation of a magnetic field oblique to the wall

is now being studied in detail, using the same PIC code and a similar analytical procedure.

2.2.8 Full tokamak modelling of ITER

On the physics side of full tokamak modelling of ITER, a master project was carried out. Modulating the auxiliary power has long been a tool to study power deposition and transport. Modulating the loop-voltage has been used to validate plasma response models. The work explored the cross-coupling between these two forms of modulation of the plasma. To handle modulation concerning both heat transport and variations of the poloidal field (PF), the DINA-CH full tokamak simulation code, combined with CRONOS, has been used for the ITER geometry.

Sinusoidal modulation of additional electron cyclotron heating (ECH) power was made at an angular frequency ω with a period of 0.5-12s, steered by 3 upper launcher ECH antennae. It led to very clean synchronous electron temperature responses with the expected local minimum in phase and a peak in the modulation amplitude at the deposition zone at mid-radius. There was negligible 2ω modulation of the current density or electron temperature.

Sinusoidal modulation of the PF coil system at the same frequencies led to clean synchronous current density responses with the amplitude dropping off rapidly and the phase increasing with penetration depth. The signal was still clean at $\rho \sim 0.8$ at the lower frequencies and again, there was little sign of 2ω effects.

A scan of the upper launcher angle to deposit the ECH power further out produced a spatial overlap of the electron temperature modulation and the electric field modulation and resulted in a clean 2ω response of the plasma current density as expected. This response is attributed to the non-linear cross terms between the linearised conductivity response and the linearised electric field response, leading to a 2ω peak-to-peak current density modulation of the order of 40% of the local target plasma current density. This modulation amplitude could be translated into a period-averaged offset by selecting the phase between the two modulation sources, to be confirmed in simulations currently in progress.

This work served both to explore these phenomena and to further verify the behaviour of the DINA-CH&CRONOS coupling.

2.3 Operation of a specialised basic plasma physics device, TORPEX

Questions related to turbulence and transport in tokamaks dictate the dynamical plasma behaviour both in the plasma core and at the edge. In the core, turbulence regulates the transport of energy and particles, i.e. the confinement, and consequently the fusion power for a given plasma size. At the edge, turbulence plays a twofold role. On the one hand, it affects the local profiles by determining the transport, particularly in high-confinement regimes in which edge transport barriers exist. These barriers provide boundary conditions for the self-organized plasma state that characterizes the core and thus affects the overall discharge performance. On the other hand, turbulence may have an even more dramatic impact on the reactor function by causing rapid bursts of energy and particles that

can produce significant local damages on the first wall. Controllable levels of edge turbulence could also play a beneficial role in removing exhaust particles that, if accumulated, would lead to fuel dilution, quenching the fusion reactivity.

Edge turbulence is typically characterized by very high relative fluctuation levels, leading to strong nonlinear effects and to the formation of macroscopic structures, often referred to as blobs (or filaments, due to their oblong, field-aligned shape). The study of edge turbulence represents a significant part of the plasma physics efforts for fusion. In high performance fusion devices, these investigations are hindered by their complex interplay with atomic effects and by the intrinsic difficulty in diagnosing fusion grade plasmas with adequate temporal and spatial resolution, even at the plasma boundary.

The research programme of the basic plasma physics group at CRPP, conducted on the TORPEX device, has been motivated by these limitations, and focuses on the study of the basic physics aspects of edge turbulence, in plasma environments that are qualitatively similar to, yet much simpler than those of the edge of burning plasmas. Such similarity is found in the normalised plasma parameters and in important elements of the magnetic configuration, namely magnetic field curvature and cross-field pressure gradients, the major ingredients for the drift-interchange turbulence expected to play a role at the edge of burning plasmas. The simple magnetized plasmas produced in TORPEX contain such ingredients, while presenting the advantage of being relatively easily diagnosed throughout its volume by a large number of probing channels for the plasma and wave (turbulence) parameters with adequate spatial and temporal resolution, and of being affected by a number of well defined external control parameters. Plasmas are confined in TORPEX by a toroidal magnetic field up to B_T=0.1T, and a vertical field, B_v~50mT, corresponding to a simple magnetic configuration with open field lines terminating on the vessel wall. Highly reproducible plasma discharges of different gases with density and electron temperature in the range n_e~10^{16}-$10^{17}m^{-3}$ and T_e~5-10eV are driven by microwaves at f=2.45GHz (P<50kW), in the electron cyclotron (EC) range of frequencies.

The progress achieved in the period covered by this Report refines our understanding of the dynamical behaviour of macroscopic structures, plasma blobs or filaments, and their propagation (section 2.3.1); of the effects of the turbulence and related structures on the plasma transport, using newly developed diagnostic options (section 2.3.2), and of phase space dynamics of supra-thermal ions (section 2.3.3). We have also undertaken specific developments to image the plasma evolution with high temporal and spatial resolutions non-perturbatively, using a fast framing camera, discussed in section 2.3.4.

The degree of detail and the wide range of conditions achievable in such investigations provide a unique test bed for quantitative assessment and validation of specific aspects of the theoretical models and numerical codes used for predicting the plasma behaviour. The specific theory validation effort undertaken on TORPEX is discussed in section 2.3.5.

These investigations benefit from a continuously improving set of diagnostic systems and techniques, which constitute an essential part of this effort. These are described in section 2.3.6.

2.3.1 Propagation of plasma filaments in TORPEX

In the scrape-off layer of magnetic confinement devices for fusion, a large fraction of plasma particles and energy is efficiently transported across the confining magnetic field in the form of *blobs*. These are coherent structures of enhanced plasma pressure relative to the background plasma, which have a filamentary structure, as they typically extend much further along the magnetic field than perpendicular to it. Blobs are universally observed in the edge of virtually all magnetized laboratory plasmas. In the past years, their formation mechanism and their dynamical properties have been extensively studied on TORPEX. In particular, conditionally sampled time-resolved profiles of density, temperature and plasma potential have been used to reveal the dynamics of blob formation and ejection. Blobs originate from crests of ideal interchange modes, forming radially elongated structures that are sheared off by the surrounding ExB flow. In a subsequent step, blob dynamics has been investigated for the case were a plane steel limiter is inserted into the vacuum vessel. In this setup, we have interpreted blob motion within the 2D, sheath limited blob model, in which parallel currents are determined by sheath boundary conditions. We have derived an analytical expression for blob velocity, which retrieves previous theoretical scalings used in the tokamak community.

This year, blob physics studies were dedicated to further confirm our interpretation of blob motion and explore the insights gained from our previous study to actively influence blob propagation, in particular by varying the connection length and the neutral gas pressure.

In order to study the dependence of blob velocity on connection length, we installed a second limiter in TORPEX, identical to the first one and toroidally displaced by 180 degrees. We computed blob sizes and radial velocities in four different gases (H, He, Ar, Ne) using a pattern recognition technique on the 86-tip probe array (HEXTIP) data, and conditional sampling of Langmuir probe data, from which the blob temperature can be determined. The experimental results are shown in Fig. 2.3.1(left), in which we plot the measured blob radial velocity versus size for the cases with one limiter (open symbols) and two limiters (filled symbols). Over plotted is the scaling law, including the measured blob temperature, and an estimate of the ion-neutral collision frequency. The expected difference between the one limiter case (blue curve) and the two limiter case (red curve) for hydrogen and helium is mainly due to the difference in connection length. These measurements confirm the trends observed in our previous analysis. The second limiter mainly affects blob velocities in hydrogen and helium, with little effect on blobs in neon and argon. In absolute terms, the scaling law tends to underestimate blob velocity, but still provides a reasonably good estimate of blob velocity for the different plasmas.

Next, we have explored the possibility of influencing blob velocity by varying the neutral background pressure. We used four different neutral gas pressure values p_n=0.021, 0.042, 0.064, and 0.085 Pa in helium plasmas. Performing the same analysis as in the previous section, we obtain the results displayed in Fig. 2.3.1(right). The pressure scan was done during one experimental session and only discharges from this session are included in the analysis. A clear decrease of blob radial velocity with gas pressure is found, and confirmed by the conditional sampling method.

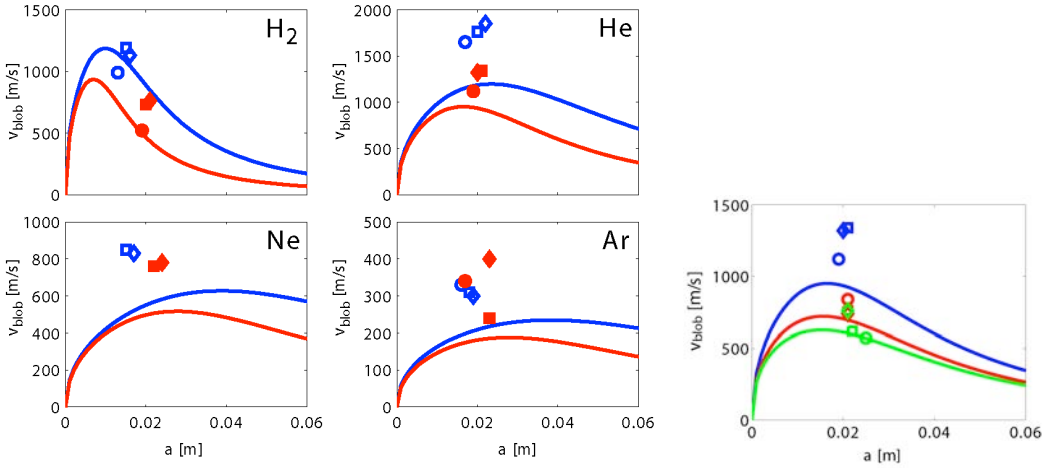

Fig. 2.3.1 *(Left) Experimental data with one limiter (open symbols) and two limiters (filled symbols) in H_2, He, Ne and Ar plasmas. Over plotted is the scaling law (one limiter in blue, two limiters in red), including the measured blob temperature, and an estimate of the ion-neutral collision frequency. (Right) In Helium plasmas, scan of the background neutral pressure P_n together with the expected scaling laws (solid lines) with increasing P_n values from blue to red to green.*

2.3.2 Triple probe studies

In TORPEX, Langmuir probes (LP) are extensively used to obtain local measurements of time-averaged plasma parameters such as density, electron temperature and plasma potential. A method to obtain local, time-dependent measurements of plasma density, electron temperature and plasma potential is the triple probe technique. In principle, this makes possible a direct evaluation of the above quantities; however, detrimental effects such as phase delay errors, ion-sheath expansion and stray capacitance can affect the measurements.

In 2010, we have conducted a detailed study of the triple probe technique in TORPEX plasmas, with a particular focus on methods to account for phase delay errors and ion-sheath expansion effects. This study has resulted in the development of compensated five-tip triple probe (shown in Fig. 2.3.2), which is equipped by a new electronic circuitry that reduces stray capacitance and improves the bandwidth of the measurements.

The probe has been extensively tested in plasmas characterized by interchange-driven turbulence in TORPEX. Time averaged and time dependent, conditionally averaged measurements of density, electron temperature and floating potential have been obtained in two ways, with the triple probe method and from applying a voltage sweep to the probe tips. Very satisfactory agreement is found between the two methods in terms of absolute values, fluctuation levels and phase shifts of the different quantities. The triple probe measurements give detailed insights on the interchange dynamics. The phase shift between density and electron temperature is close to zero over most of the radial range. Density and plasma potential are shifted by 30°-50°, less than the 90° expected from linear calculations. The fluctuation level of electron temperature is about two thirds of that in density and is important in the evaluation of plasma potential. Nevertheless, it is concluded that in the present case of weak phase shifts between density and electron temperature, the time

averaged fluctuation induced particle flux can be reliably deduced from floating potential measurements (Fig. 2.3.2, right).

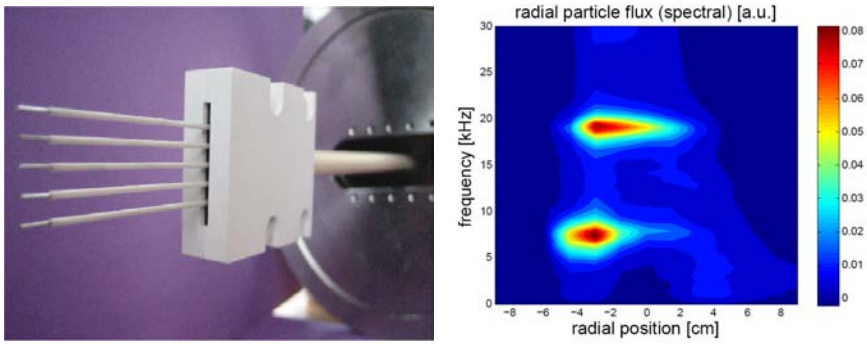

Fig. 2.3.2 *Left: Photograph of the five-tip probe. Right: Plot of the evaluated (spectral) radial particle flux, as a function of radial position and frequency.*

2.3.3 Fast ion studies

The interaction between highly energetic ions and small-scale (drift wave-like) turbulence is an open problem in fusion plasmas. As the fast ions usually have a gyroradius that is larger than the turbulence scale, their interaction with turbulence is expected to be very weak due to gyro-averaging effects. On the other hand, recent experiments indicate that significant redistribution of supra-thermal ions can be induced by turbulence. As no direct measurements of fluctuation induced fast ion transport on toroidal devices have been performed so far, there exists a strong need for experimental data with which to compare and validate the relevant theoretical and numerical models.

In previous years, we have investigated the interaction of fast ions with interchange instabilities and/or fully developed turbulence in TORPEX well established plasma scenarios, both in the mode and in the blob regions. In 2010, investigations of fast ion physics have continued on the theory side.

A fast and flexible ion tracking code has been developed. This code solves the full Lorentz equation with the TORPEX magnetic geometry and the two dimensional electric fields provided by GBS fluid simulations. The code serves two related purposes. First, it can be coupled with a synthetic diagnostic to compare simulation results directly with data from the TORPEX fast-ion source/detector pair. Second, it can be extended beyond the spatial and temporal limitations of the existing TORPEX diagnostics to find the asymptotic behaviour of the fast ions. This application leads to a deeper understanding of fast ion physics in interchange turbulence (as seen in TORPEX) and provides inspiration for future TORPEX diagnostics. As of now, the observation of radial and vertical spreading of the fast ions has been confirmed by the simulations. However, in order to obtain a more quantitative comparison with the data, it will be necessary to obtain fast ion profiles at several toroidal positions. A movable detector is now being built for this purpose. From the simulations, we have learned that fast ions in simulated two-dimensional interchange turbulence show a transition from super-diffusive to sub-diffusive radial dispersion as the injection energy of the ions is increased. This transition is explained in terms of a separable continuous time random walk model, which describes a dispersive process using trapping time and flight length distributions.

Sub-diffusion occurs for faster ions because the probability of longer trapping times becomes larger due to gyro-averaging. In the simulations we have also observed, in velocity space, an increase in the average perpendicular energy of ions, even when the parallel injection velocity is large. This energization, or heating, process is related to the occurrence of impulsive (or sudden) changes in the turbulent electric field applied to each ion along its trajectory. A change in acceleration on a timescale shorter than the Larmor frequency breaks the conservation of the magnetic moment and tends to heat the tracer ion species when the distribution is peaked near zero perpendicular velocity. We are currently investigating whether this heating mechanism can explain the bulk ion temperature observed in TORPEX and other basic plasma experiments.

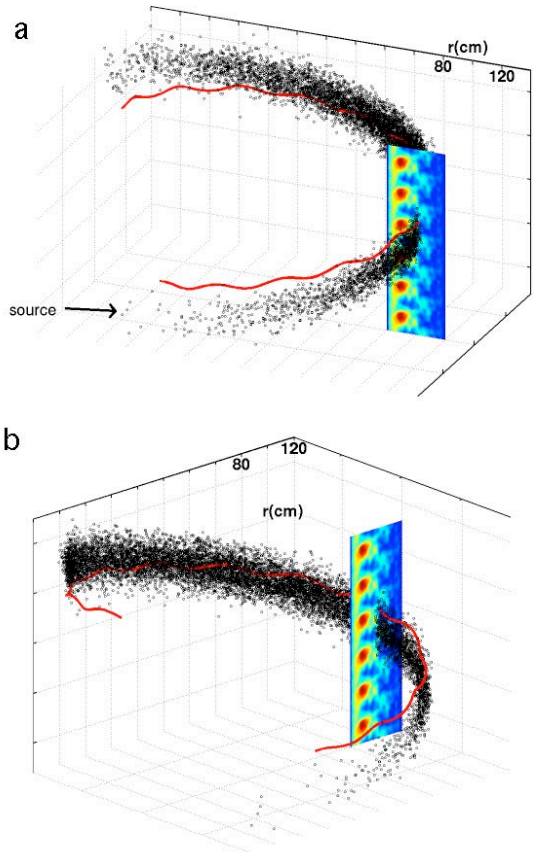

Fig. 2.3.3 *Two views of an ensemble of simulated fast ions injected parallel to the TORPEX magnetic field are shown. Plot (a) and plot (b) show the same image from two different angles. Black markers show all of the ions at a certain instant shortly after the injection. The red curve shows the motion of a single ion at many points in time. The turbulent electrostatic potential from a two dimensional Braginskii fluid simulation is shown with periodic boundary conditions in the vertical direction. The turbulent electric field changes in time but is constant along the toroidal direction. The spreading of ion positions along the field line at this early time is mostly due to the initial spread of velocity vectors, and partly due to the turbulent electric field.*

2.3.4 Fast visible imaging of TORPEX plasmas

The use of insertable probes for a full imaging of the quantities of interest for plasma turbulence studies, i.e. the field fluctuations and the particle response, suffers from two interlinked limitations, even in low temperature plasma experiments. A small number of probes only marginally perturbs the plasma dynamical behaviour, but would lead to either only local measurements or to insufficient spatial resolution to investigate the turbulence multiple scales. To obtain adequate spatial resolution, one would need to insert a large number of measuring tips, which would significantly perturb the phenomena under investigation. In recent years, to overcome these limitations, fast framing cameras have been adopted to monitor the visible light emission from magnetically confined plasmas.

In previous years, a fast imaging system, comprising a Photron Ultima APS-RX camera and a Hamamatsu image intensifier, has been installed on TORPEX. The fast camera is equipped with a 10Bit CMOS monochrome sensor, which provides extreme light sensitivity, up to 6400 ASA in the visible range. At the full chip resolution (1024x1024 pixels) the framing rate can be varied in the range 50fps-3kfps (frames per second), making possible the monitoring of average visible light profiles during a TORPEX discharge. At reduced chip size (down to 16x128 pixels) the framing rate can be increased up to 250kfps. A Hamamatsu image intensifier unit (IIU) is used together with the fast framing camera to amplify the radiation emitted by the plasma. Using this IIU the fast camera is able to acquire up to 200kfps.

In 2010, the fast imaging system has been used to investigate different plasma and turbulence features such as blobs and structures associated to the ideal interchange waves.

To investigate the modes and related structures over regions larger than their characteristic lengths, and with adequate spatial and temporal resolution, investigations were conducted in similar plasma regimes described in Section 2.3.1, with a limiter to reduce line integration effects. A tangential view of TORPEX plasmas has been used, which provides a direct view of the plasma column. A tomographic reconstruction algorithm has been developed to retrieve the plasma emissivity profile from the line-integrated images. The reconstruction is performed by solving an over-determined set of equations using singular value decomposition and a least square method.

The intensified images are compared with HEXTIP data, with which they exhibit high correlation (up to 0.8). The frequency and wavelength measured using the intensified images for the coherent plasma fluctuations associated with the drift-interchange mode agree well with those reconstructed from HEXTIP data. Measurements taken with the two diagnostics provide very similar variations of the main interchange mode characteristics, i.e. frequency, wave number, wavelength and phase velocity (referred to as speed) with the vertical magnetic field.

The emissivity fluctuations profile is obtained from the reconstructed emissivity simply by subtracting the time averaged reconstructed profile. Time Fourier analysis of the reconstructed emissivity fluctuations shows the same interchange mode (in this scenario at 3.5kHz) that is the most prominent feature in the spectrum of the electron density fluctuations measured by probes.

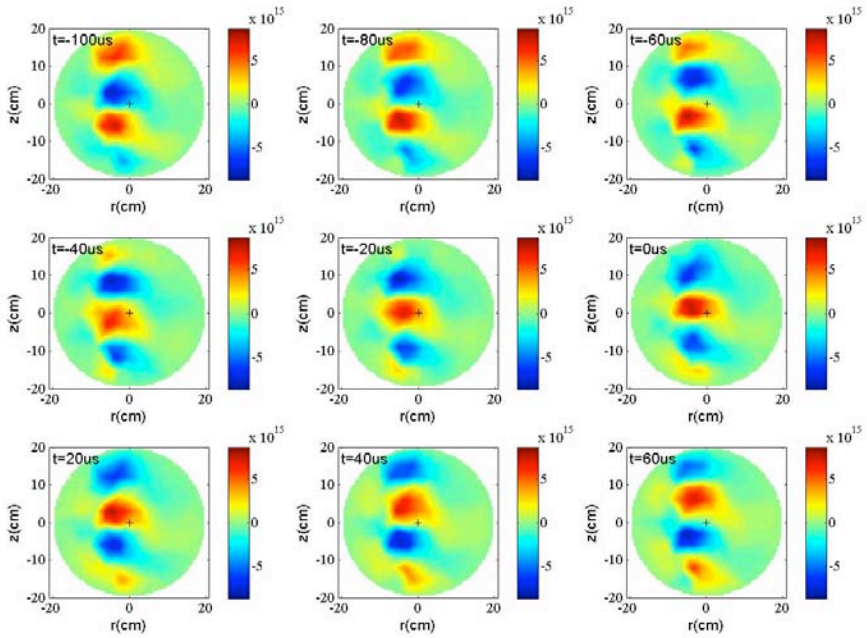

Fig. 2.3.4 *Nine consecutive frames of the CASed HEXTIP data. The cross at z=0cm, r=0cm indicates the location of the reference channel.*

Conditional average sampling (CAS) is also applied to the light and electrostatic fluctuation data, to visualize the mode and to estimate the size of the structures associated with it. For the coherent modes observed in the central part of the plasma profile and the structures that are well within the resolution capabilities of HEXTIP, a good agreement is found between the two measurements (see Figs 2.3.4 and 2.3.5).

By taking the time-resolved, 2D space Fourier spectrum of the intensified, reconstructed camera images and the HEXTIP data, one can investigate the k-spectrum of the dominant coherent modes present in both time Fourier spectra, as well as assess the spatial scales that are present in the turbulence development. A single snapshot, averaged over 40μs, is shown in Fig. 2.3.6. Although the spatial Fourier spectra evolve rather dramatically with time, these two images provide a clear idea of the k-spectrum of the dominant interchange mode in the plasma core.

In addition to a narrower k-spectrum, the much better spatial resolution of the light emission images (a factor of 3.5 in this case, from 3.5cm to 1cm), makes possible a direct observation of smaller structures. This data demonstrates that imaging with a fast framing camera, in particular in conjunction with light intensification and tomographic reconstruction, can go well beyond the limitations due to the relatively coarse resolution of probe arrays such as HEXTIP. This opens up the possibility of exploring in details the physics of small-scale structures, both in terms of the role that they have on the turbulence development (e.g. cascading effects) and dissipation, and in terms of their consequences on the plasma transport and confinement.

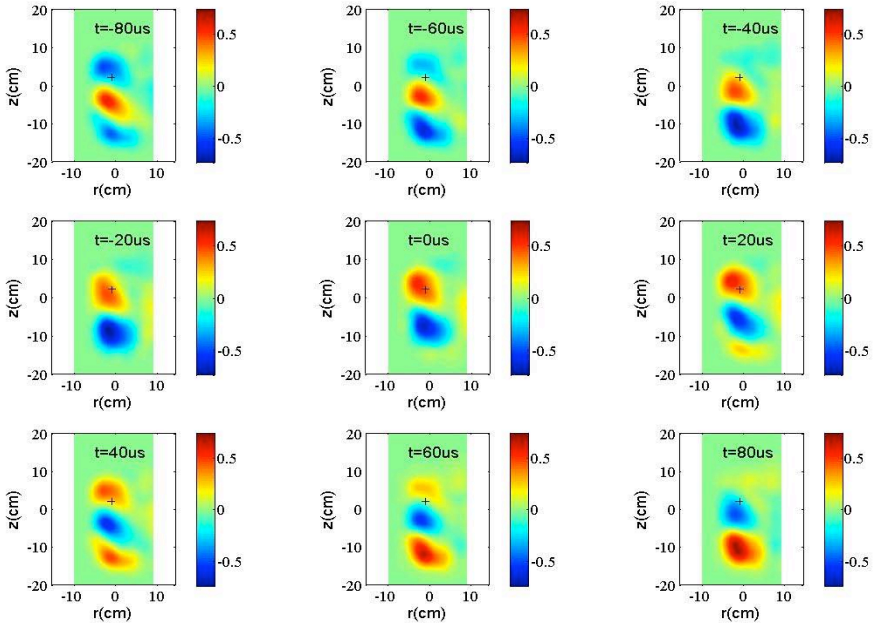

Fig. 2.3.5 *Nine consecutive frames of the reconstructed CASed emissivity profile. As in the previous figure, the cross at z=0cm, r=0cm indicates the location of the reference channel.*

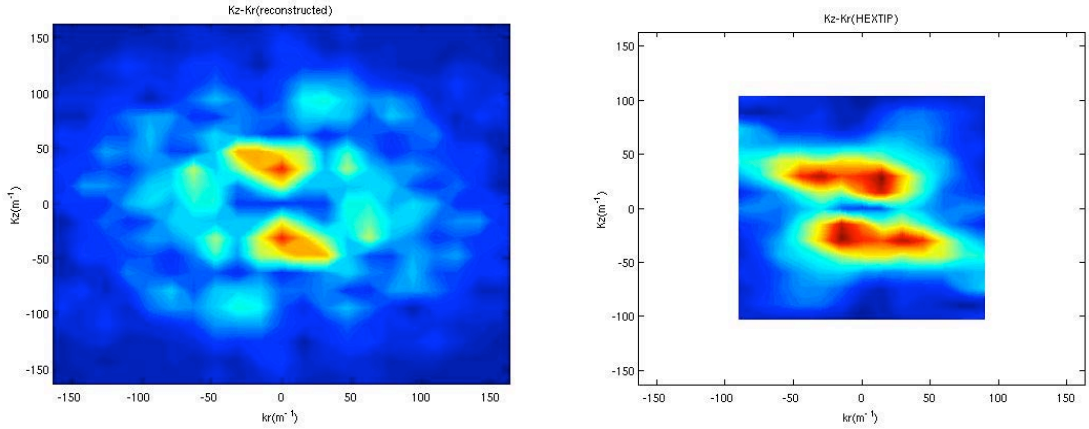

Fig. 2.3.6 *Single snapshot of the 2D spatial Fourier spectrum (k_r, horizontal axis; k_z, vertical axis) of the reconstructed intensified camera data (left) and of HEXTIP (right).*

2.3.5 The TORPEX theory validation project

TORPEX constitutes an ideal plasma environment to perform a turbulence code validation: the magnetic geometry is relatively simple and, as compared to typical fusion devices, the diagnostics provide a more complete picture of the plasma and wave dynamics that can be compared with the simulation results. In 2010, we continued the effort on the TORPEX theory validation project.

An essential aspect of this project is the determination of a methodology for the comparison, starting with the identification of a primacy hierarchy for observables that measures how stringent each observable is for the comparison. Such hierarchy quantifies how directly are the variables extracted from the fundamental data, e.g. how the measurements are combined together and what assumptions are used in the models employed to form the observables. At the lowest levels in the primacy hierarchy are the observables that require the smallest number of model assumptions and correspond to the most direct measurements. Vice versa, at the highest levels we place quantities that require the highest number of assumptions and are obtained by combining different measurements.

The quality of the agreement between simulations and experiments can be evaluated by comparing different quantities at different hierarchy levels. To quantify such an agreement, an appropriate metric should take into account all the errors associated with the model assumptions and the combinations of observables. To this aim, we have constructed a metric that casts the overall degree of agreement in the comparison into a single parameter. In this first attempt, the degree of agreement can be defined as the normalised sum over the considered set of observables of the product of three quantities: $\chi=\Sigma_i(R_iS_iH_i)/[\Sigma_i(S_i\ H_i)]$. R_i measures the individual agreement for observable i. For $R_i=1$ theory and experiment give results that are well outside the respective error bars. For $R_i=0$ the results are within the error bars. A smooth transition between the two cases is provided by an analytical function, whose value is chosen here to be 0.5 for a deviation between experiment and theory that is 1.5 the total error (of both experiment and model). S_i indicates the sensitivity, or weight, attributed to observable i, and can be calculated from the relative error bars:

$$S_i = \exp\left\{-\frac{<\Delta obs_i^{\mathrm{mod}\,el}> + <\Delta obs_i^{\exp}>}{<obs_i^{\mathrm{mod}\,el}> + <obs_i^{\exp}>}\right\}.$$

Here <Δobs> are the error bars, and <obs> the average value of a given observable over the set considered for a comparison case. Naturally, the larger the error bars, the smaller the weight attributed to the comparison of that observable. H_i quantifies the position of the variable in the primacy hierarchy: $H_i=1/[1$ + hierarchy $\mathrm{level}^{\exp}$+hierarchy $\mathrm{level}^{\mathrm{model}}]$.

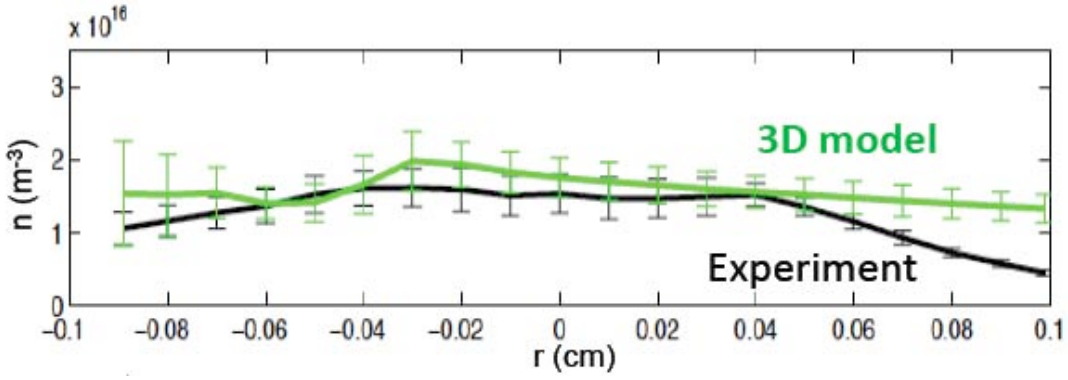

Fig. 2.3.7 *Example of comparison between probe measured (black) and 3D code calculated (green) density profiles, at z=0cm, for N=8. As expected, the region in which the two profiles are not within the respective error bars corresponds to where the model geometrical assumptions are violated.*

An example of the comparison for a single observable is shown in Fig. 2.3.7, where we represent the measured plasma density profile together with that calculated using the 3D fluid model. For the determination of the error bars in the numerical reconstruction, we performed a number of simulations using a range of values for the parameters that are only qualitatively known, such as the (anomalous) plasma resistivity and the boundary conditions for potential, temperature and flows.

The quantity χ can then be computed for different models applied to a given experimental scenario. As a first example, we have applied this method to different scenarios, starting from the turbulence regime extensively discussed throughout this paper, the one dominated by interchange dynamics and characterized by low confinement properties, and varying the vertical magnetic field value. Long 2D and 3D global simulations have been performed to provide the time series and the statistics necessary for a quantitative comparison with the data. Eleven observables have been considered: the radial profiles of density, temperature, plasma potential, ion saturation current, fluctuation amplitude, skewness and kurtosis of ion saturation current, and the fluctuation probability distribution function, power spectral density, vertical and toroidal wave numbers at the position corresponding to the largest mode amplitude. Note that all of these variables are characterised by $H_i=1/2$.

The results are displayed in Fig. 2.3.8 and they show that for high values of the vertical magnetic field (low N) only a little difference exists between the degree of agreement reached using 2D simulations and that achieved with the full 3D model. As the value of the vertical field is decreased (N increased), the 2D model leads to a very unsatisfactory degree of agreement (χ reaching values larger than 0.6, for N, the total number of field line turns from the bottom to the top of the vessel, larger than 5). On the other hand, the comparison with the 3D model provides values of χ that are below 0.5 for N up to 16. Clearly, this indicates that 3D effects play an important role in TORPEX plasma dynamics as the vertical field is decreased, which is consistent with the observation of the observed progressive departure of the profiles form a slab-like configuration, and of the transition from a turbulence dominated by zero parallel wave number modes to one in which finite parallel wave number modes play a significant role.

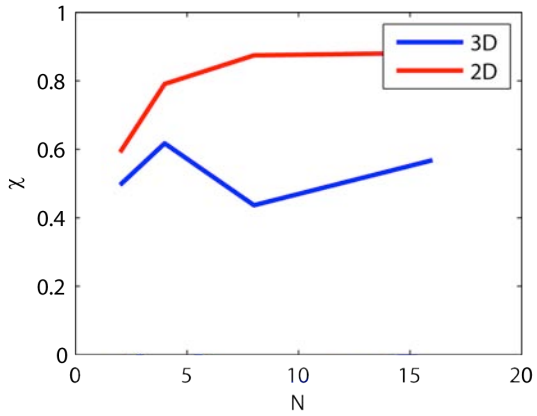

Fig. 2.3.8 *Values of the metric as a function of N for the two-dimensional (red dashed thick line) and the three dimensional simulation (solid thick blue line).*

2.3.6 Technical achievements

Magnetic probe array for current measurements

Direct local estimates of the parallel current density are very challenging in thermonuclear plasmas, in which various attempts are in progress. The use of arrays of magnetic pick-up coils allows high spatial characterization. In 2010, to this purpose, a specially designed current probe, consisting of an L-shaped array of three miniaturized three-axial pick up coils, has been developed in collaboration with Consorzio RFX in Padova (I). A picture of the probe is shown in Fig. 2.3.9. The probe is based on a simplified version of the arrangement used in the cluster mission for the measurements of magnetospheric currents. The current density probe can be oriented in such a way that the vertical and radial components of the magnetic field are measured and the parallel current can thus be computed. The probe will be used to measure parallel current filaments transported by plasma blobs and will allow us to further investigate the blob speed-versus-size scaling described above.

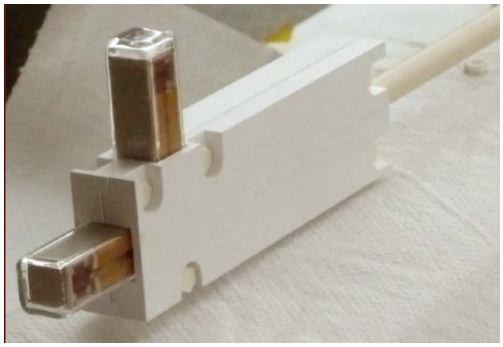

Fig. 2.3.9 *Magnetic probe array for current measurements in TORPEX plasmas.*

Chess-board biased limiter

The dynamics of blobs in fusion devices may have important consequences on the location and strength of heat and particle fluxes to the divertor or first wall, impurity screening characteristics, wall-recycling and possibly the global confinement. For these reasons, various methods to actively influence blob dynamics have been considered in fusion devices. On TORPEX, in previous years, first experiments were attempted to change the blob velocity by varying the angle between magnetic field lines and wall. For this purpose, a specially designed limiter was constructed that allows forming angles down to 10° between magnetic field and limiter. So far, we have not observed a significant dependence of the blob velocity on the tilt angle of the limiter.

In 2010, we have developed a chess-board limiter, shown in Fig. 2.3.10. This limiter consists of 24 stainless steel plates (1cm x 2cm), which can be independently biased, thus obtaining various patterns of the ExB velocity field at the blob-metal limiter interface. In Fig. 2.3.10, in different colours, examples of different biasing schemes are given. The limiter is presently installed in the TORPEX device, and preliminary tests are being conducted.

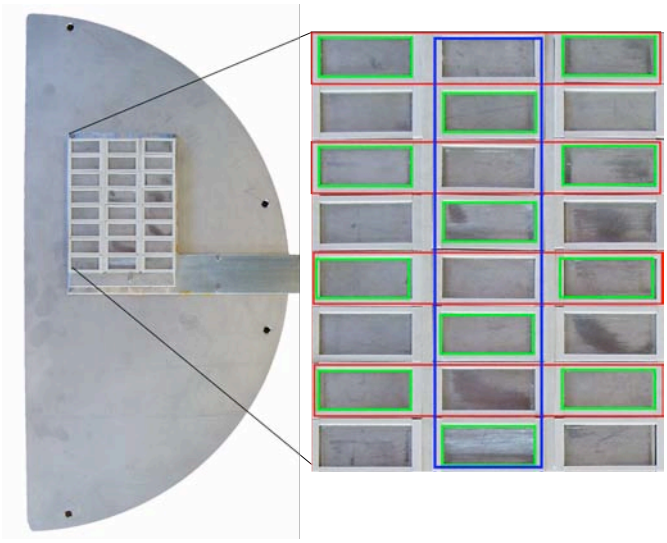

Fig. 2.3.10 *Chess board limiter for biasing experiments in TORPEX plasmas.(right) the complete limiter(left) a zoomed view of the chess-board, which allows independent biasing of each individual stainless steel plate. In different colors, three examples of biasing configurations (same color plates are at the same potential).*

Hardware development for fast ion physics

In past years, we have investigated the interaction of fast ions with interchange instabilities and/or fully developed turbulence in TORPEX well established plasma scenarios, both in the mode and in the blob regions. The relatively low energy required for the fast ions (100eV-1keV) allows us to perform these studies using a source with a very small cylindrical structure, which can be installed directly inside the TORPEX vacuum vessel. The electronics of the source makes possible a fast ion current modulation with a frequency up to 10kHz, used in connection with synchronous detection of gridded energy analyser (GEA) data. A poloidally resolved fast ion profile can be reconstructed by moving the GEA detector in between discharges in the poloidal plane. This process requires a large number of shots (~50), long time-window (3s per discharge limited by the acquisition memory), and fast acquisition frequency (250kHz) to perform an off-line analysis with increase statistics of the data. This can take several hours of experimental time. Since the expected lifetime of the fast ion source is of the order of 10-20 hours (depending on a specific sample), the detection scheme was a limiting factor to perform measurements using a single source.

In 2010, we have designed, built and installed a lock-in amplifier circuit, which makes possible to perform a hardware synchronous detection of the GEA data, thus allowing acquiring time traces with a reduced acquisition frequency (1kHz). The system has been tested and reliable measurements of the fast ion current can be obtained over 30s of plasma discharges, thus avoiding running out of acquisition memory. At the same time, a new software routine that controls the movement of the GEA positioning system has been developed. This new control software allows moving the GEA in real time during a plasma discharge. The combination of the two upgrades (the hardware lock-in detector, and the new position control system) makes possible the reconstruction of the profile of the fast ion source in a single plasma discharge that takes approximately 10 minutes. Therefore, the experimental time is now compatible with the expected lifetime of the fast ion source.

2.4 Materials research

R&D activities on fusion reactor materials in Switzerland are being performed within the Fusion Technology Materials (FTM) group of the Centre of Research in Plasma Physics (CRPP, EPFL). This group is located at the Paul Scherrer Institute (PSI) in Villigen. R&D activities of the FTM group focus on (1) the development of advanced metallic materials for structural applications in plasma facing (first wall, divertor) and breeding blanket components of the future fusion power reactors, in particular oxide dispersion strengthened (ODS) reduced activation ferritic (RAF) steels and tungsten-base materials, (2) the modelling of radiation damage and radiation effects, (3) small specimen test technology for the future International Fusion Materials Irradiation Facility (IFMIF), and (4) the qualification of metallic materials for the International Thermonuclear Experimental Reactor (ITER). The scientific approach being used is based on investigating the structure/mechanics relationships at different length scales (nano-, micro-, meso-, and macroscopic), before and after irradiation, by using a wide range of experimental and numerical tools. For simulating experimentally the effects of 14 MeV neutrons, irradiations are being performed with a mixed spectrum of high-energy protons and spallation neutrons in the Swiss Spallation Neutron Source (SINQ) located at the PSI, as well as with ions in the Joint Accelerators for Nano-science and Nuclear Simulation (JANNuS) facility located at Orsay/Saclay (France) and with fission neutrons in reactors in Belgium, Hungary and the Netherlands.

2.4.1 Emerging technologies

Development of material science and advanced materials for DEMO

Development of ODS ferritic steels

Development of the present generation of ODS RAF steels

Recent activities have been focused on the ODS RAF steel Fe-14Cr-2W-0.3Ti-$0.3Y_2O_3$ (in weight percent). (1) A batch of about 500 grams of steel powder had been previously sent to the CEA (France) for compaction by hot extrusion using a cylindrical shape die. The microstructure and mechanical properties of the compacted rod have been characterized at the CRPP. The material was found relatively brittle. Therefore, a new batch of about 500 grams of steel powder, prepared by mechanically alloying elemental Fe, Cr, W and Ti powder particles with $0.3Y_2O_3$ powder particles in hydrogen using a planetary ball mill, has been sent to the CEA for compaction by hot extrusion using a cylindrical shape die and subsequent hot rolling in the aim to improve the fracture properties. (2) Small amounts of steel powder prepared by mechanically alloying elemental Fe, Cr, W and Ti powder particles with either $0.3Y_2O_3$ or $0.5Fe_2Y$ powder particles in hydrogen using a planetary ball mill, have been sent to Oxford University (England) for short-term annealing experiments and further analysis of the nanoclusters by atom probe tomography and transmission electron microscopy (TEM). Results will be compared to those previously obtained for steel ingots produced by hot isostatic pressing (HIPping). (3) An attritor, allowing for mechanical alloying of powder batches up to 15kg, has been purchased, and optimal mechanical alloying parameters have been defined. (4) A new collaboration with ENEA-Casaccia (Italy) has been initiated, in the aim to develop adequate thermo-mechanical treatment for ODS RAF steels. A

small steel ingot produced by mechanically alloying elemental Fe, Cr, W and Ti powder particles with $0.3Y_2O_3$ powder particles in hydrogen using the attritor and subsequent HIPping was sent to ENEA-Casaccia for first trials. As soon as the adequate thermo-mechanical treatment will be defined, it will be applied to a 1kg steel ingot previously produced by mechanically alloying pre-alloyed Fe-14Cr-2W-0.3Ti powder particles with $0.3Y_2O_3$ powder particles in hydrogen using a planetary ball mill and subsequent HIPping. (5) Small steel ingots have been produced by mechanically alloying elemental Fe, Cr, W and Ti powder particles with either $0.3Y_2O_3$ or $0.5Fe_2Y$ powder particles in hydrogen using a planetary ball mill and subsequent HIPping. Various types of specimen have been cut out from the ingots for further aging experiments. (6) Previous investigations had shown that using Fe_2Y powder particles instead of Y_2O_3 powder particles during mechanical alloying helps reducing the oxygen content in ODS RAF steels, but recent TEM observations revealed that the nanoclusters that form during HIPping are then larger and less densely distributed than those in the Y_2O_3 steel (Fig. 2.4.1, middle and right). Moreover, annealing of the ODS Fe_2Y material at 1350°C for 1 hour revealed significant grain growth and nanocluster coarsening. TEM investigations of the coarser nanoclusters in the annealed Fe_2Y steel showed that they have an austenitic face centred cubic (fcc) structure. The Fe_2Y material exhibits significantly better Charpy impact properties, with a ductile-to-brittle transition temperature (DBTT) of about -24°C and an upper shelf energy (USE) of about 8.8J, than the Y_2O_3 material that exhibits a high DBTT of about 80°C and a very low USE of about 2.4J (Fig. 2.4.1, left). Thus, using Fe_2Y intermetallic powder particles instead of Y_2O_3 oxide powder particles can be an effective approach for producing a softer material with improved impact fracture properties. However, stability of the nanoclusters in the Fe_2Y steel upon aging and irradiation as well as high-temperature creep behaviour of the material are also important concerns.

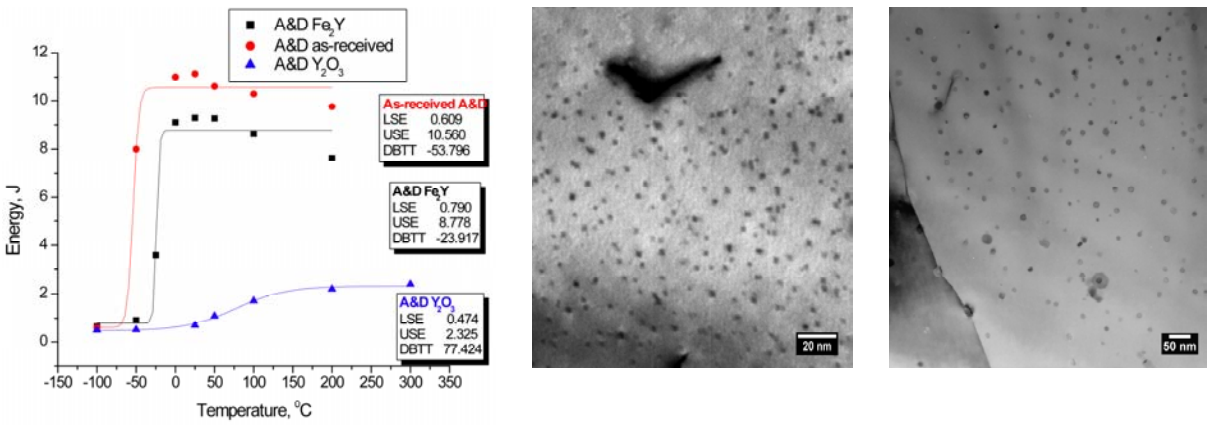

Fig. 2.4.1 *(Left) Charpy impact behaviour of Fe-14Cr-2W-0.3Ti-$0.3Y_2O_3$ ODS RAF steels manufactured by mechanically alloying a pre-alloyed Fe-Cr-W-Ti powder (A&D) with either $0.3Y_2O_3$ particles or $0.5Fe_2Y$ particles and HIPping. (Middle) TEM image of nanoclusters in the $0.3Y_2O_3$ material, (Right) TEM image of nanoclusters in the $0.5Fe_2Y$ material.*

<u>Development of an optimised generation of ODS RAF steels</u>

Two 250 grams ingots of the ODS RAF steel Fe-14Cr-2W-0.3Ti-$0.3Y_2O_3$ have been produced by mechanically alloying elemental Fe, Cr, W and Ti powder particles with either $0.3Y_2O_3$ or $0.5Fe_2Y$ powder particles in hydrogen using a planetary ball mill and subsequent HIPping. The ingots were sent to IPPLM (Poland) for subsequent thermo-mechanical treatment by high-speed hot extrusion in the aim to refine the

size of the grains and, therefore, to improve the ductility and the fracture properties.

Stability of ODS RAF steels under irradiation

(1) TEM specimens have been prepared from ingots of the ODS RAF steel Fe-14Cr-2W-0.3Ti-0.3Y_2O_3 which were produced by mechanically alloying elemental Fe, Cr, W and Ti powder particles with either 0.3Y_2O_3 or 0.5Fe_2Y powder particles in hydrogen using a planetary ball mill and subsequent HIPping. They are destined to be ion irradiated/implanted in the JANNuS facility under various conditions of dose, temperature and He content. (2) TEM specimens, tensile specimens, Charpy impact specimens and mini-bend bars have been prepared from steel ingots produced by mechanically alloying elemental Fe, Cr, W and Ti powder particles with 0.3Y_2O_3 powder particles in hydrogen using the attritor and subsequent HIPping. They will be irradiated with a mixed spectrum of high-energy protons and spallation neutrons in the SINQ facility under various conditions of dose, temperature and He content.

Development of tungsten-base materials

Optimization of armour materials

Recent activities have been focused on the development of a W-2Y material (in weight percent) by mechanically alloying elemental W and Y powder particles in argon in a planetary ball mill and subsequent HIPping. (1) A series of small ingots have been produced. Charpy impact specimens, tensile specimens and mini-bend bars were cut out from the ingots. The Charpy impact and tensile specimens were tested at high temperatures at Karlsruhe Institute of Technology (Germany) and the mini-bend bars were tested at the CRPP. TEM observations showed that yttrium transformed into yttria during the manufacturing process, yielding the formation of nano-sized particles, with sizes in the range of 2-20nm, located inside the grains and at the grain boundaries. In spite of the small size of the grains, in the range of 50-150nm (Fig. 2.4.2, left), the material appears very brittle in tensile and fracture tests. Non-standard three-point bend tests showed that the specimens failed in a brittle manner up to the maximum investigated temperature of 1000°C (Fig. 2.4.2, middle). Although some plastic deformation seems to have occurred at 1000°C, fracture surface analyses showed that the material fractured in a purely brittle manner even at that high temperature. Therefore, the shape of that curve most probably reflects some unstable crack propagation. The bending stress was found to decrease with increasing the test temperature from about 800MPa at 500°C down to about 600MPa at 1100°C, reflecting the decrease of elastic modulus with increasing temperature (Fig. 2.4.2, right). Charpy impact tests revealed that the material is brittle at the highest investigated temperature of 1000°C. Tensile tests confirmed that the material is brittle at 1000 C but ductile at 1300°C with a yield strength of about 100MPa, an ultimate tensile strength of about 140MPa, a uniform elongation of about 3% and a total elongation of about 11%. Therefore, the ductile-to-brittle transition temperature should lie between 1100 and 1200°C. (2) A powder batch of about 5kg of W-2Y was prepared and sent to the Plansee company (Austria) for further compaction and thermo-mechanical treatment. The treated ingot was received back from the Plansee company. Charpy impact specimens, tensile specimens and mini-bend bars are being cut out from the ingot. The Charpy impact and tensile specimens will be tested at high temperatures at KIT and the mini-bend bars are being tested at the CRPP. (3) An ingot of about 5kg of W-2Y_2O_3 was ordered and received from the Plansee company.

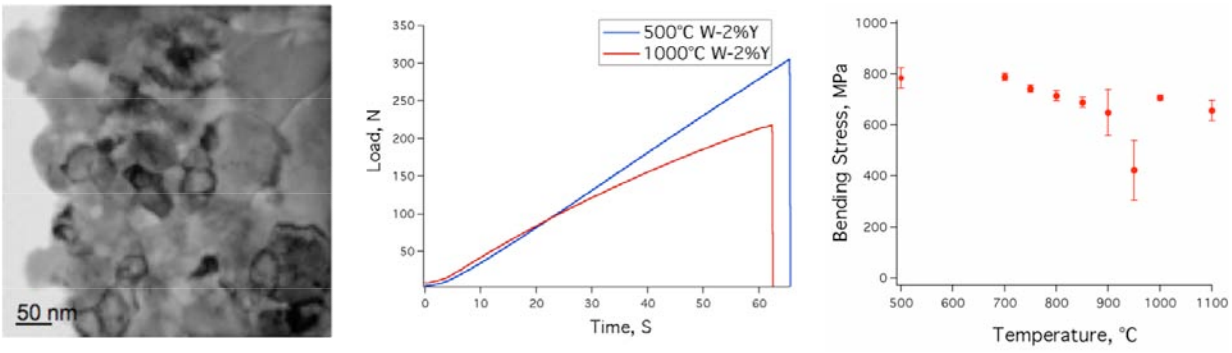

Fig. 2.4.2 *(Left) TEM image of the overall microstructure of a W-2Y material manufactured by mechanical alloying and HIPping. (Middle) Applied bending load versus time at two different test temperatures of 500°C and 1000°C. (Right) Bending stress versus test temperature.*

Irradiation performance testing

(1) Preliminary dual beam (with Fe and He ions) irradiations/implantations of TEM specimens of W-2Y and W-1.7TiC materials (in weight percent) were performed in the JANNuS facility under various conditions of temperature (room temperature or 500°C), dose (1 or 5dpa) and He content (0 or 75appm). It was attempted to measure the irradiation-induced hardening by means of nano-indentation tests, but unfortunately the surface of irradiated specimens was too oxidized for allowing such measurements. Following irradiation the microstructure was analysed by means of TEM observations. No irradiation-induced defects were observed, whatever the irradiation condition. (2) Nano-indentation tests are being performed on specimens of pure W which were neutron-irradiated in the High Flux Reactor at NRG (Petten) either at 600°C or at 800°C to a dose of a few dpa.

Materials modelling

Plasticity and fracture: experimental validation of dislocation dynamics properties, MD simulations of the hardening due to irradiation-induced defect clusters

Large-scale molecular dynamics (MD) simulations using the MOLDY-CRPP code implemented in the high power computer for fusion (HPC-FF) have been performed in order to understand the discrepancy observed between the dispersed barrier hardening (DBH) model and MD simulations. Indeed, according to MD simulations, the hardening induced by voids in Fe, calculated by measuring the shear stress response of a 0.5 million-atoms specimen ($14x20x2nm^3$) containing an edge dislocation and a 2nm void, gives an obstacle strength, α, of 2, which is out of the bounds defined by a weak obstacle (α=0) and an unshearable obstacle (α=1). Until now the strain rate was typically $3x10^{-8}fs^{-1}$ for all MD calculations the access to the HPC-FF allows us to perform massively parallel runs and thus to simulate much smaller strain rates. Fig. 2.4.3 shows the flow stress response to various strain rates for a Fe specimen containing an edge dislocation interacting with a 2nm void at 10K. The lower strain rate of $3.0x10^{-10}fs^{-1}$ corresponds to a macroscopic strain rate of $3.0x10^{-5}s^{-1}$, which is reachable experimentally in special facilities, e.g. at the University of Applied Sciences of Southern Switzerland (SUPSI). It can be seen in Fig. 2.4.3 that the stress response is basically the same as the one obtained at 100 times higher deformation speed, confirming past results. The inferred obstacle strength for the 2nm void of about 550MPa does not depend significantly on the

strain rate. The independence of the obstacle strength on the strain rate implies that the discrepancy observed between the DBH model and MD simulations remains unresolved. Besides, calculations are in progress to study the temperature dependence of the flow stress response as a function of the strain rate.

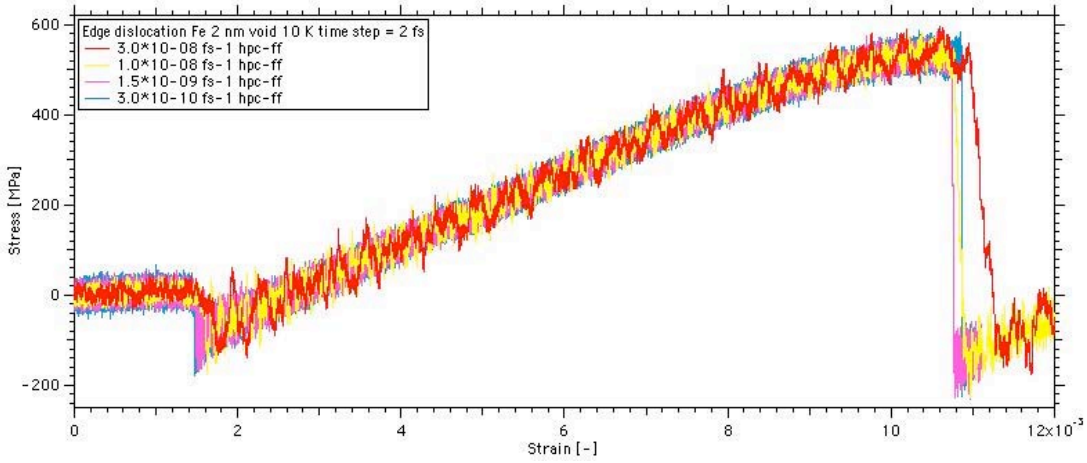

Fig. 2.4.3 *Stress-strain response of Fe containing an edge dislocation interacting with a 2nm void at 10K as a function of strain rate. The sample size is 25x14x20nm^3. The interatomic potential for the Fe-Fe interactions is from Ackland et al. (1997).*

Plasticity and fracture: screw dislocation mobility in presence of nanometric obstacles observed in TEM

Tungsten-based materials have a body centred cubic (bcc) structure and exhibit a low ductility, a low fracture toughness and a high Ductile-Brittle Transition Temperature (DBTT), because of the peculiar core structure of the screw dislocations. Properties of the core and mobility of a screw dislocation with a Burgers vector of the type b=½a_0<111> have been studied by means of MD simulations using the MOLDY-CRPP code. The dislocation moves between two adjacent Peierls valleys by the formation of a pair of kinks moving along the dislocation, which can have different types (Fig. 2.4.4). We artificially created all four possible kinks and studied their formation energy as well as their response to the strain using available empirical potentials, namely the ones of Ackland et al. (1987) and Derlet et al. (2007).

A new method for studying the kink along a screw dislocation has been developed. In this method the screw dislocation is placed in the central axis of a cylinder, thus benefiting from a stress field with cylindrical symmetry around it, as opposed to the non-symmetrical geometry of the classical shoe-box type specimen geometry. The cylinder has a free surface and the two ends can be free or with periodic boundary conditions. Thanks to this axisymmetry the artefacts related to boundary conditions are minimized. The screw dislocation line is decomposed into two segments of equal length, A and B, separated by two short kinks. The axis of the cylinder is parallel to the A-B direction. The cylinder contains 10^6 atoms. MD calculations consist in relaxing the structure. The formation energy of the pair of kinks is then deduced. In addition, quasistatic MD simulations were run to study the stress needed to move the dislocation with or without the kink pair. In this simulation the cylinder is sheared by applying a displacement on the atoms of the skin of the cylinder along the dislocation line. The displacement is made with a linear gradient along the cylinder diameter, passing through zero when crossing the centre. The diameter

direction is chosen to promote the glide of the dislocation in a specific glide plane, either {110} or {112}. It was found that the kink pair 1/3<112> has a formation energy of 2.13eV, the second closest to the experimental value of 1.75eV. Besides, it significantly decreases the critical stress to move the dislocation. The shorter kink pair 1/3<110> has an even lower formation energy of 2.07eV, the closest to the experimental value, but does not decrease the critical stress as much.

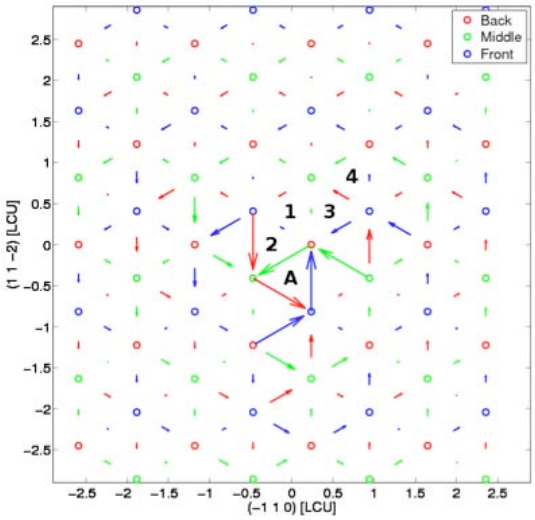

Kink id	Burgers vector	Type
1	1/3<112>	left
2	1/3<110>	right
3	2/3<110>	right
4	<110>	left

Fig. 2.4.4 *(Left) Differential displacement map in bcc tungsten showing the four crystallographically possible kink types in the screw dislocation core, 1, 2, 3 and 4, as described on the (right).*

Experiments: development and user's facilities: primary damage in pure Fe and Fe-Cr alloys

Helium is produced in metals as a result of nuclear transmutation reactions engendered by the high-energy fusion neutrons. The resulting nanometric He bubbles degrade the mechanical properties. It is thus important to understand the behaviour of He in those materials. It is typically characterized by the pressure and atomic configuration of the He inside the bubbles, but also at interfaces and grain boundaries. A simulation study was performed in order to understand the limits in this characterization using electron energy loss spectroscopy (EELS) in TEM. The structure of He in pure bcc Fe (ferrite) was obtained by MD simulations. The many body potential derived by Ackland et al. (1997) for the Fe-Fe interactions, and the pair potentials derived by Wilson-Johnson (1975) and Beck (1968) for Fe-He and He-He interactions, respectively, were used. This type of simulation is suitable to describe nanometric pressurized He bubbles in Fe (Fig. 2.4.5).

EELS is a very sensitive method able to detect light elements. The dependence of the He-K edge onset on the lattice parameter of idealized bcc and fcc He crystals was calculated within the random phase approximation (RPA) using the OPTIC package of the WIEN2k code and two different ab initio techniques: generalized gradient approximation (GGA) and local density approximation (LDA). Calculations showed a weak dependence of both the He-K edge onset and fine structures on the ordering of the He atoms and a strong dependence on the density or lattice parameter.

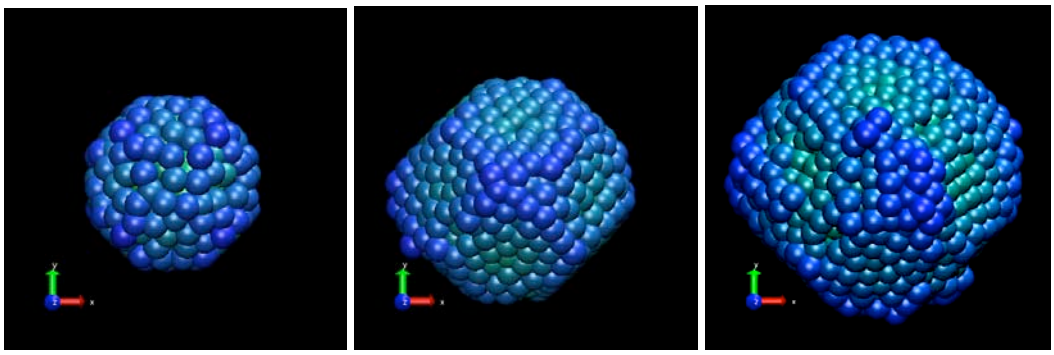

Fig. 2.4.5 *Results of MD simulations of the atomic configuration of a nanometric He bubble in Fe lattice at 10K, containing (left) 1 He atom, (middle) 3 He atoms, and (right) 5 He atoms per Fe lattice site, corresponding to a density of respectively 84, 255 and 424He/nm^3 before relaxation. The axes correspond to <100> directions.*

Experiments: development and user's facilities: kinetic modelling validation

Single and dual beam irradiation/implantation experiments have been conducted in the JANNuS facility on specimens of ultra high purity (UHP) Fe and Fe-5Cr, Fe-10Cr and Fe-14Cr alloys, at room temperature and LN_2 temperature to 1dpa with or without He at levels up to 1000appm. Two irradiations campaigns were conducted in December 2009 and September 2010, respectively. Irradiation conditions are provided in Fig. 2.4.6. Analysis by TEM of the irradiation-induced defects is in progress. The TEM technique was further developed. The main problem when quantifying irradiation-induced defects in TEM images is that the diffraction contrast strongly depends on two parameters, namely the diffraction condition and the beam convergence. In order to circumvent this difficulty the convergent weak beam technique (CWBT) was further developed and applied successfully.

Specimen	Actual dose [dpa] / He content [appm]
Fe-14Cr (n1)	0.45 dpa 988 appm
Fe-14Cr (n2)	0.45 dpa
Fe-14Cr (n3)	0.45 dpa 176 appm
Fe-5Cr (n4)	0.45 dpa 1000 appm
Fe-5Cr (n5)	0.45 dpa
Fe-5Cr (n6)	0.45 dpa

Specimen	Actual dose [dpa]/ He content [appm]
Fe-10Cr (n7)	0.45 dpa 880 appm
Fe-10Cr (n8)	0.45 dpa
Fe-14Cr (n9)	0.45 dpa 790 appm
Fe-14Cr (n11)	0.45 dpa
Fe-5Cr (n12)	0.45 dpa 790 appm
Fe-5Cr (n13)	0.45 dpa
UHP Fe (n14)	0.45 dpa 790 appm
UHP Fer (n15)	0.45 dpa

Fig. 2.4.6 *JANNuS irradiation conditions for UHP Fe and Fe-Cr alloys: (Left) campaign of December 2009, and (right) campaign of September 2010.*

2.4.2 Collaborative activities

Participation in FEMaS-CA (Fusion Energy Materials Science – Coordination Action)

Participation in the work package 4 (WP4) entitled 'TEM-based methods'

This work package aims at (1) building a network of TEM competences of interest to fusion material development in order to expand our knowledge on irradiation-induced defects, and (2) improving TEM techniques and related modelling tools for that purpose, in synergy with modelling of related micro-structural phenomena in fusion relevant materials. The CRPP acts as a coordinator of WP4 and listed all electron microscope equipments available in the FEMaS network as well as outside of the network in Europe, in order to provide efficient coordination and use of the best available equipments for characterizing fusion materials. The list is now available on the FEMaS server. In addition, the CRPP organized an international conference entitled 'Electron Microscopy and Multiscale Modelling' (EMMM09), which was held in Zürich (Switzerland) and attended by 66 persons of 22 nationalities and sponsored by major electron microscope suppliers (JEOL, Zeiss and FEI).

Participation in the work package 5 (WP5) entitled 'Advanced mechanical testing and characterisation methods'

This work package aims at establishing advanced mechanical testing and characterisation methods in the field of fusion materials research. Scientists of the CRPP visited the University of Applied Sciences and Arts of Southern Switzerland (SUPSI) for performing high strain rate tensile and fracture tests on steels for fusion reactor application and the University Carlos III in Madrid (UC3M) for discussing the manufacturing of tungsten-base materials for fusion reactor application.

2.4.3 EFDA Technology Tasks

A. Tasks Long Term

TW3-TTMS-005 deliverable 2 : Investigation of irradiated fracture mechanics samples by indentation/punch tests

Finite element simulations of the shear punch test were performed. Small disks with a diameter of 3mm and a thickness of 0.25mm and deformed with a flat punch were considered. In order to investigate the effect of the true stress-strain constitutive law on the resulting load-displacement curve provided by the puncher, a series of constitutive behaviours were used as input for the finite element simulations. The constitutive behaviour of reference was that of the tempered martensitic steel EUROFER 97, while the others were arbitrarily constructed to simulate different radiation hardening conditions. The relative values of the stress tensor components in the plastic zone of the deformed disk were studied, which revealed that the dominating components are the normal ones, are compressive, and none of them scales with the load. They depend in a complex manner on the

specific constitutive behaviour used. However, it was shown that the general yield load of the punch disk corresponds to the spreading of a very narrow nascent plastic zone. The general yield load was found to follow a simple correlation with the elastic limit of the true stress-strain curve, independently of the constitutive behaviour. With compression tests performed on EUROFER 97 micro-pillars machined with a focused ion beam (FIB), it was possible to measure reasonably well the overall shape of the true stress-strain curve, which was compared with that of the standard tensile test. Hence, the combination of these two small specimen test techniques makes possible the access with rather good precision the overall constitutive behaviour of a material.

TW6-TTMS-001/D4 : PIE SINQ irradiation

The irradiation rig containing specimens of the tempered martensitic steel EUROFER 97 and the ODS EUROFER material, which had been irradiated in the SINQ facility in 2004/2005, has been transported to the Hot Laboratory of the PSI in Spring 2007. Unfortunately, due to a lack of technical manpower at the PSI, the irradiated specimens have been extracted from the rig only in spring 2008. They were decontaminated in a hot cell in 2009. Charpy impact testing of irradiated specimens of EUROFER 97 has been recently completed. Tensile testing and TEM observations of irradiated specimens should be performed in 2011.

B. Tasks Next Step

TW4-TVM-CUSSPIT : Testing of irradiated CuCrZr/SS joints produced under different blanket manufacturing conditions

CuCrZr/SS joints, where CuCrZr refers to a precipitation strengthened Cu-base alloy and SS to the 316LN austenitic stainless steel, are part of the current ITER design. Their final applicability in ITER will depend on their mechanical properties before and after neutron irradiation, with respect to those of the base materials. This work is aimed at investigating the effects of two different heat treatments on the mechanical properties of the unirradiated and neutron-irradiated CuCrZr base material. Two series of six specimens of the CuCrZr base material, having withstood two different heat treatments, have been irradiated with neutrons at SCK-CEN (Belgium) at 150 C to three different doses of 0.001, 0.01 and 0.1dpa, which means that two specimens were irradiated to a given dose. The shape and geometry of the specimens have been investigated. As the specimens were apparently not pre-cracked before irradiation, it was decided to test them by means of 3-point bend tests at room temperature and at the irradiation temperature and hardness measurements at room temperature by the end of 2010.

*2.4.4 Broader approach activities**

International Fusion Materials Irradiation Facility – Engineering Validation Engineering Design Activities (IFMIF-EVEDA): Design of a test module for in-situ creep-fatigue tests to be performed in the IFMIF facility and construction of a mock-up of the test module

A test module for performing in-situ creep-fatigue tests, under intense neutron irradiation, in the medium flux test module of IFMIF has been conceived and designed (Fig. 2.4.7). This module is referred to as the creep-fatigue test module (CFTM). The information obtained in these experiments will be of special relevance for structural materials to be used in DEMO-type reactors and beyond. The CFTM consists of three parallel testing machines, mounted on a frame, which will be operated independently. Each testing machine includes an actuator, a specimen, a specimen holder, a load cell, a strain measurement system, a frame, and a temperature controlling system. The CFTM will be exposed to intense radiation fields, including both neutron and gamma fields, and will be thus made of temperature and radiation resistant elements. Part of the radiation heat will be used for heating the specimens. The rest of the heat, absorbed by the various parts of the CFTM, will be extracted by means of a helium gas (coolant) passing through independent cooling channels. The design has been validated by means of thermo-hydraulic calculations. For the time being, a single testing machine has been constructed and successfully tested at room temperature. It will be further tested at various higher temperatures up to 550 C. Thermo-hydraulics calculations showed that additional electrical heaters are not needed for reaching such specimen temperatures. The targeted specimen temperatures can be reached and maintained by varying the helium flow rate and by using tungsten blocks as heating bodies. New calculations of neutron and gamma radiation effects will be performed in order to get information on the eventual need of an additional shielding for the most radiation sensitive elements.

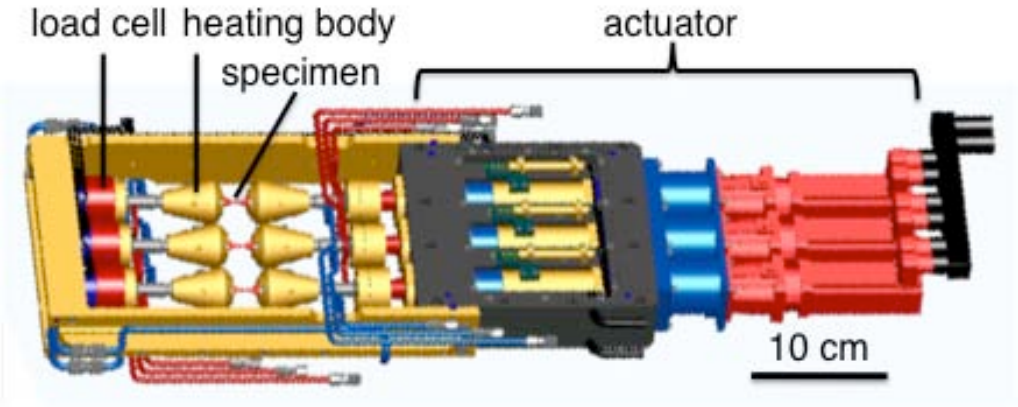

Fig. 2.4.7 *Schematics of the whole CFTM for IFMIF.*

* Work not belonging to the Euratom Association Work Programme

International Fusion Energy Research Center (IFERC): Contribution to the definition of irradiation matrices for IFMIF by means of development of new methods for testing and analysing subsized specimens

Neutron irradiation effect on the EUROFER 97 steel fracture properties:

Characterization of the fracture toughness behaviour in the ductile-to-brittle regime of the tempered martensitic steel EUROFER 97 after neutron irradiations was performed. The irradiations were realized in the experimental reactor at AEKI-KFKI in Budapest (Hungary). Two irradiation temperatures were chosen: 150 C and 350 C at a nominal dose of 0.35dpa. These irradiation conditions are well known to lead to radiation hardening (increase in the flow stress) that in turn induces a degradation of the fracture properties, reflected in an upper temperature shift of the fracture toughness-temperature curve. The irradiation capsules were filled with subsized pre-cracked compact tension (C(T)) fracture specimens, 0.18T C(T). The standard 1T C(T) specimens to characterize the fracture toughness in the ductile-to-brittle transition region have a thickness of 25.4mm. In order to account for the specimen thickness effect on the measured toughness, the data obtained from the subsized 0.18T C(T) specimens were adjusted to 1T data following the procedure recommended in the ASTM-E1921 standard. The test temperatures were targeted so that to be able to estimate the reference temperature T_o at which the median fracture toughness value is 100MPa.m$^{1/2}$.

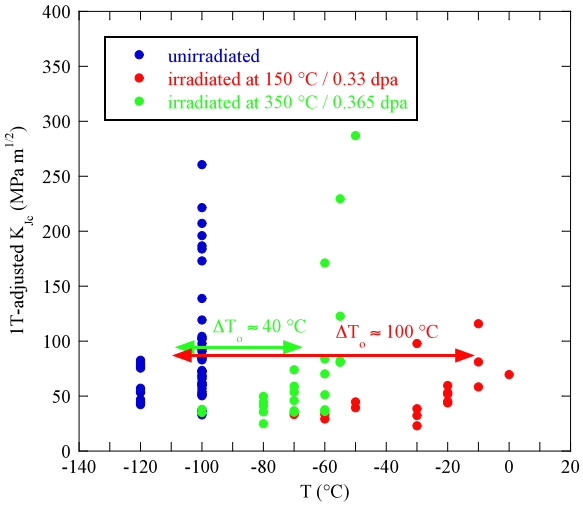

Fig. 2.4.8 *1T-adjusted fracture toughness (K_{JC}) versus temperature for the EUROFER 97 steel, unirradiated and irradiated at 150 C or 350 C to about 0.3dpa.*

In Fig. 2.4.8, the 1T-adjusted data obtained for all the 0.18T C(T) specimens tested in the transition region are reported as a function of temperature for the unirradiated EUROFER 97 steel as well as for the two irradiation conditions. Two series of tests on the unirradiated EUROFER 97 steel were carried out at -120 C and -100 C, which made possible to estimate T_o around -110 C. From eyeball fitting, reasonable estimates of the irradiation-induced reference temperature T_o, albeit rough, were done from the irradiated specimen data. As expected, a significant larger shift was determined for EUROFER 97 irradiated at 150 C than at 350 C. This observation reflects the difference in the irradiation-induced hardening

resulting from those two irradiation experiments. Indeed, a T_o shift of 100 C was found for the 150 C irradiation while only 40 C was measured for the 350 C one, as illustrated in Fig. 2.4.8. Note that a rigorous determination of T_o could be done by using the procedure of ASTM-E1921 standard, assuming that this procedure remains valid for the tempered martensitic steels after irradiation.

For the time being, the irradiation-induced hardening was quantified with Vickers hardness tests realized on a few broken parts of 0.18T C(T) specimens from each irradiation. A 10kg load was employed to realize deep indents in order to make sure that the hardness data, HV10, represent the response of the bulk material and to minimize surface effects (such as oxidation layer), if any, because the specimens have not been re-polished after irradiation. The hardness tester as set up in a hot cell is shown in Fig. 2.4.9 (left). The change in the Vickers hardness with the irradiation condition is shown in Fig. 2.4.9 (right), where one can see a clear increase of HV10 after the 150 C irradiation, from 216 up to 241. On the contrary, no increase in hardness could be detected after the 350 C irradiation. It is remarkable that, despite that observed lack of hardness increase, a 40 C shift of the toughness-temperature curve was found. The underlying reason of this apparent contradiction is not well established. However, hardness is a quantity that represents an average flow stress (averaged over about 10% of plastic strain). So, it is quite plausible that the irradiation at 350 C induces a moderate yield stress increase together with a moderate decrease of strain-hardening capacity, so that the effect of these two conjugate modifications of the flow stress is such that the average flow stress remains essentially constant. Work is in progress to gain insight into that issue.

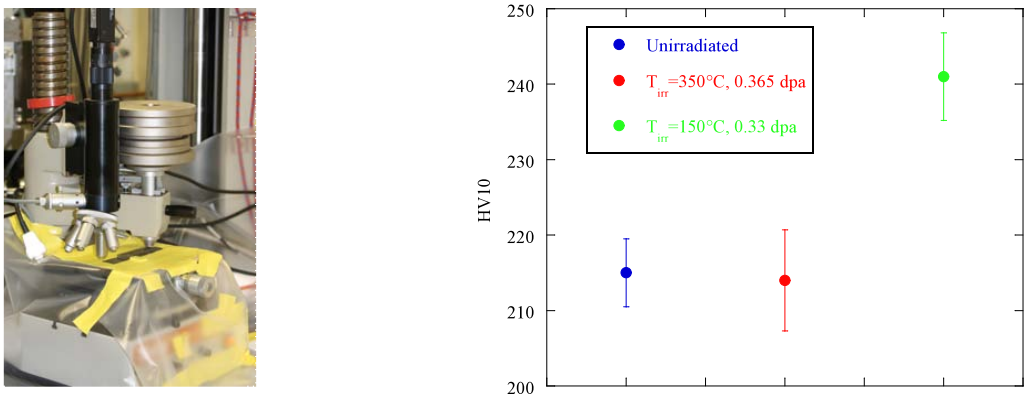

Fig. 2.4.9 *(Left) Hardness tester in a hot cell, and (right) Vickers hardness HV10 before and after neutron irradiation, EUROFER 97 steel.*

Preparation of a cold-deformed EUROFER 97 steel plate for fracture toughness study

Small plates of the EUROFER 97 steel were cold deformed to harden the material. The objective is to produce large plates in such a strain-hardened state that it is susceptible to represent an irradiated state in terms of the increase in the yield stress and decrease of strain-hardening capacity. One critical issue is to get large plates that are deformed homogeneously to cut out enough fracture specimens to characterize the fracture behaviour in the transition region and to follow the temperature dependence of the fracture toughness in more details. Two types of cold deformation were applied: cross cold rolling with a total reduction in the plate thickness of about 10%, and cold forging by compression of about 10% too. The

homogeneity of the deformation was evaluated with Vickers micro-hardness tests (applied load =0.1kg) at different positions in the plates. The results are reported in Fig. 2.4.10 (right) where the micro-hardness tests are plotted as a function of the position in the cold-rolled plate; the positions in the plate are indicated in Fig. 2.4.10 (left). On can see that, in the middle of the plate (positions D, E, F), the Vickers micro-hardness is not constant but varies from about 225 to 235. Such a variation is quite large and corresponds to a difference in plastic deformation of more than 10%. This deformation gradient in the plate is of course not adequate to perform fracture tests, as it would broaden the already intrinsic scatter band of the fracture toughness data in the transition region.

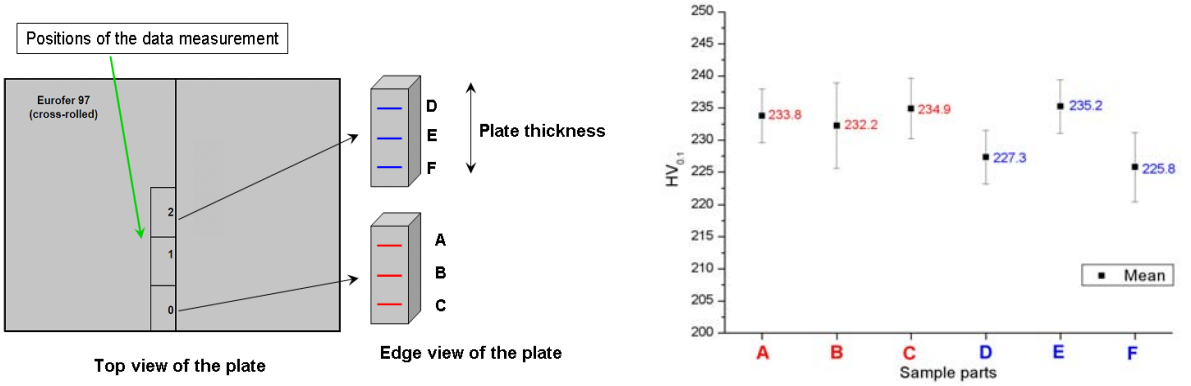

Fig. 2.4.10 *Evaluation of the deformation homogeneity of the cold-rolled plate with Vickers micro-hardness tests HV0.1, EUROFER 97 steel.*

It was then decided to apply another cold-deformation process to produce a more homogeneous deformation than by cold rolling. A few plates were cold forged by 10% in compression. Vickers micro-hardness tests were also carried out through the plate thickness, and it was found that the through-thickness dependence of the Vickers micro-hardness is practically constant (Fig. 2.4.11). Some compression tests were realized to determine the real change in the true stress-strain curve with respect to that of the as-received EUROFER 97 steel. An increase in the yield stress of more than 200MPa accompanied by a strong reduction of the strain hardening was evidenced. This deformed state is believed to 'simulate' some irradiation conditions properly, and a detailed study of the toughness-temperature dependence and overall characterization of the fracture behaviour will be done. We emphasize here that a precise determination of the toughness-temperature dependence with irradiated specimens cannot be conducted without many assumptions, which cannot be firmly verified. This is due primarily to the limited number of specimens that can be irradiated in a given condition but also to the unavoidable irradiation and temperature gradients in the irradiation capsules. Hence, having a large plate strain hardened by cold forging at disposal will help to assess the fracture behaviour in conditions similar to those resulting from irradiation without any limitation in the specimen quantity.

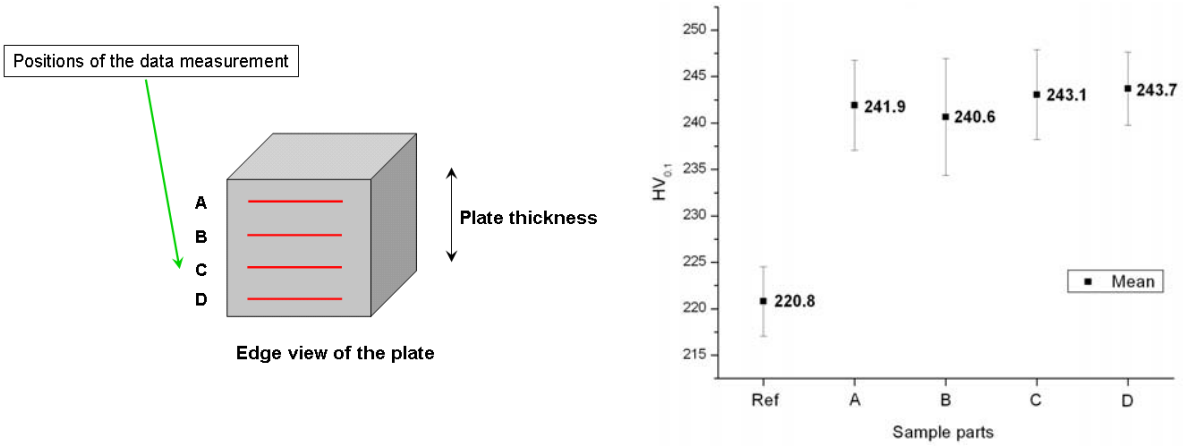

Fig. 2.4.11 *Evaluation of the deformation homogeneity of the cold-forged plate with Vickers micro-hardness tests, EUROFER 97 steel.*

*2.4.5 Supporting research**

Development of a material resistant to high-pressure aluminium and magnesium die casting

The cylinder used to inject liquid Al into moulds, the so-called shot sleeve, suffers an important degradation during operation and needs to be replaced frequently. Through experimental testing, microscopic observations and modelling, the present research aims at understanding the fundamental phenomena occurring at the interface between the molten Al and the shot sleeve material, which is steel, and eventually provide a solution to the shot sleeve wear. It is proposed to perform a systematic study of the influence on the degradation of the steel of the various intervening parameters, such as the liquid Al temperature, speed, exposure time and thermal cycle characteristics. A testing facility, reproducing the conditions of operation of an industrial shot sleeve, is being developed, which allows for such a parametric study. It will provide a tool that is unique for its ability to decouple the phenomena at the origin of the shot sleeve wear. The liquid metal immersion facility (LMIF) located at the CRPP has been refurbished and is being further developed for the present project. More precisely, part of this facility is being redesigned to simulate the thermal cycling due to the iterative Al injections. The LMIF is located in a glove box, making possible experiments in an argon atmosphere that limits oxidation, and consists in several instrumented crucibles. Six units are now operational. Two additional ones will allow for thermal cycling.

Iron and steel samples have been prepared as 50mm long cylinders of 10mm diameter and dipped in Al at 700 C for 15', 30', 45', 60', 75' and 90'. After air-cooling, they have been cut radially and axially, and polished with 1μm diamond paste for scanning electron microscopy (SEM) observations. Secondary electron (SE) and backscattered electron (BSE) detectors were used to form the images. BSE images were mainly used for intermetallic phases thickness measurements. The electron backscattered diffraction (EBSD) method was also used to determine the crystallographic orientations and the grain structure. Three types of material have been tested: pure Fe (ARMCO, 99.98%), 1.2343 and centrifuged 1.2367 (C-31) steels. Results are presented in Fig. 2.4.12. One can see that intermetallic

* Work not belonging to the Euratom Association Work Programme

compounds grow faster in the case of Fe than for steels. Furthermore, interfaces are flatter in both steels relative to Fe. The presence of Si and C in the composition of steels can partly explain this feature, as reported in the literature. The effect on the growth rate of graphite lamellas (the dark lines in the images), which act as diffusion barriers, was also evidenced.

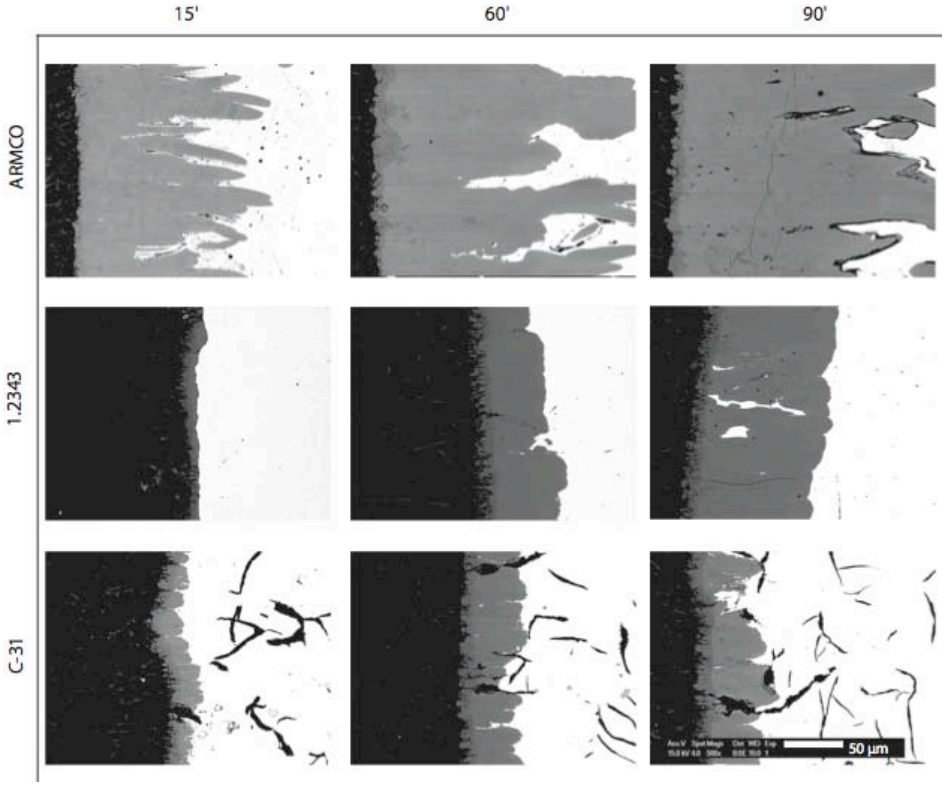

Fig. 2.4.12 *SEM images of cross sections of Fe, 1.2343 and 1.2367 (C-31) steels after 15', 60' and 90' dipping in Al at 700 C. Left dark contrast: solidified Al, narrow dark grey: $FeAl_3$, wide light grey: Fe_2Al_5, and white: Fe/steel.*

2.5 Superconductivity

The bulk of the activities of the Superconductivity section in 2010 are shared between SULTAN (test of ITER conductors) and EDIPO (preparation of the test facility). Other activities include the high temperature superconductors (HTS) in the scope of various collaborations / contracts.

The SULTAN test operation has suffered in the first four months of the lack of samples due to delays in the deliveries of the ITER Domestic Agencies. Between May and August two failures of the compressor motor caused a disruption of the operation. From mid August to the end of 2010, the test activity resumed at very high rate to attempt a recovery of the forced shut-down. At the end of 2010, the queue of samples accumulated in summer has eventually disappeared.

The preparation work for the EDIPO test facility at CRPP was boosted in the first quarter of 2010, when the stand-by of SULTAN allowed full access to the SULTAN hall for installation of the power supply, transfer lines, vacuum vessel, thermal

shield, as well as the full test of the assembled HTS current leads. The expected delivery of the EDIPO windings has been shifted from December 2010 to May 2011.

ITER studies are reported in Chapter 4, Section 4.5 and technical developments in Chapter 3, Section 3.6.

2.5.1 The Preparation of the EDIPO Test Facility

The operation break of the SULTAN test facility allowed intensive assembly work for EDIPO in the SULTAN hall from mid December 2009 to April 2010.

- All the drawings and the procurement of the large components are completed. The hardware for the quench detection (QD) is procured and the software has been programmed. The functional test of the QD must wait for the coil commissioning. The specification for the control system for the EDIPO test facility has been drafted, three offers have been obtained and the order for the control system is being placed at the end of 2010 (the acceptance of the control system can only be done at the commissioning of the facility).
- The vacuum vessel, thermal shield and vacuum pumps have been installed and commissioned in January 2010. The new transfer lines from the refrigerator to the vacuum vessel and from the refrigerator to the transformer are installed and commissioned in March 2010, including also the required modification of the existing transfer lines, see Fig. 2.5.1.

Fig. 2.5.1 *Left, the EDIPO vacuum vessel and access frame (pink) erected in the SULTAN hall next to the SULTAN test facility, March 2010. Right, one of the 17kA HTS leads after the test.*

- A trial assembly of the High Temperature Superconductor (HTS) current leads, with only four HTS stacks, was carried out in January 2010, with test at liquid nitrogen, 2.5kA. The assembly of the two 18kA leads was completed in March 2010, including instrumentation and temporary installation in the EDIPO vacuum vessel.
- The final assembly work of the new 100kA *Transformer and Sample Holder* at CRPP continued at low priority during 2010 (heat exchanger, termination of the secondary coil, etc.). The installation and commissioning of the transformer unit can only start after completion of the EDIPO commissioning.

Test of the 18kA HTS current leads

The two 18kA HTS current leads were tested at different combinations of current and 75K helium mass flow rate through the heat exchanger. The HTS module was cooled only by heat conduction from the cold end. During the test of the current leads the helium inlet temperature varied between 72K and 78K. The results of steady state operation are presented in Fig. 2.5.2. At a fixed current the difference of the helium inlet and the warm end HTS temperature (T_{HTS}^{w}-T_{He}^{in}) decreases with increasing mass flow rate. In addition, the helium outlet temperature is reduced at enlarged mass flow rates. The data in Fig. 2.5.2 are average values of several runs. The mass flow rates required to achieve a helium outlet temperature in the range of 261K to 276K varied between 0.6g/s at 8kA and 2.1g/s at 18kA. The corresponding values of T_{HTS}^{w}-T_{He}^{in} are in the range of 11.9K at 8kA and 6.5K at 18kA. The minimum and the maximum values of this difference at 17kA are also indicated in Fig. 2.5.2.

The contact voltages were measured on 4 out of 65 superconducting stacks. In a measurement at 17kA, the voltage at the cold end varied between 49μV and 62μV, while values in the range of 168μV to 182μV were found for the warm end. Supposing a uniform current distribution among the HTS stacks we find total resistances of 3.3nΩ at the cold end and 10.5nΩ (84K) at the warm end.

Furthermore, the current sharing temperature T_{cs}, defined by a voltage of 10μV along the whole HTS module, was measured. The results are illustrated in Fig. 2.5.3. The current sharing temperature at 17kA is as high as 95K. Due to the fact that in the test of the current leads the EDIPO magnet was not installed the calculated average magnetic field component perpendicular to the broad face of the HTS stacks was only 10mT (self field). For later EDIPO operation, the stray field of the main coil adds up to ≈30mT. As a consequence, T_{cs} in EDIPO operation is expected to be 5K lower than in the present tests. To reach the fully superconducting state (zero voltage) it would be necessary to operate at a temperature 2K below T_{cs}. Even the zero voltage line for EDIPO operation in Fig. 2.5.3 is well above the highest warm end HTS temperature found at 18kA and the highest possible mass flow rate of 2.1g/s. Thus the temperature margin of the HTS current leads is sufficiently large for later EDIPO operation.

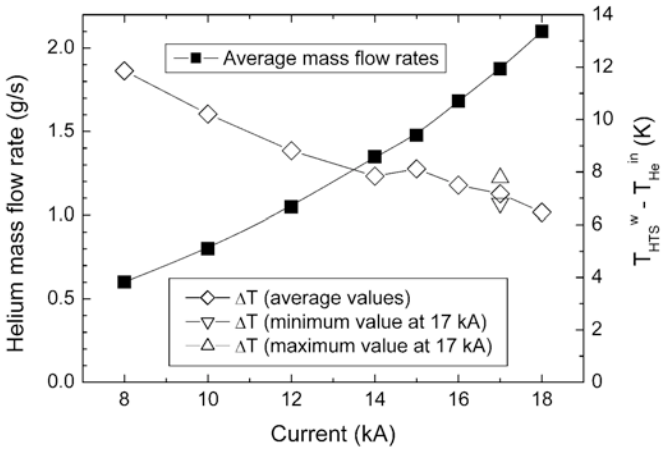

Fig. 2.5.2 *Mass flow rate required to achieve a helium outlet temperature in the range of 261K to 276K. The corresponding values of T_{HTS}^{w}-T_{He}^{in} are also shown.*

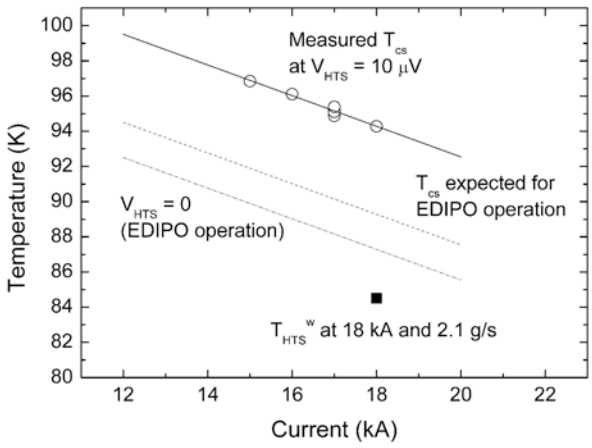

Fig. 2.5.3 *Measured current sharing temperature (T_{cs}) versus current and estimated operational limits for EDIPO operation.*

The behavior of the HTS current leads in the case of a loss of flow was also experimentally investigated. The current sharing temperature was reached 180s after switching off of the helium mass flow rate at a current of 17kA. During the considered loss of flow test the HTS reached a maximum temperature of 110K. The maximum temperature close to the warm end of the heat exchanger part reached a value of ≈450K within 240s. Due to this hot spot close to the warm end the voltage along the heat exchanger increased from ≈95mV to 280mV. This voltage can be used to protect the heat exchanger against an excessive temperature rise.

Taking into consideration a very short time constant of less than 2s for the safety discharge of the EDIPO magnet the times before T_{cs} is reached or a burn-out of the heat exchanger will occur are sufficient to de-energize the EDIPO magnet in the case of a loss of flow.

2.5.2 High Temperature Superconductors

The scope of an EFDA project aimed to develop HTS conductor and technology for DEMO was agreed in 2009 by a dedicated task ("*Elaboration of a project for the preparation and execution of the qualification tests*"). The actual project was not launched in 2010, waiting for an assessment of the overall DEMO planning. Recent information indicates that the EFDA HTS project may start in 2011. Despite the absence of the EFDA coordination, some of the planned activities have started anyway at CRPP and the results will be used in the coming EFDA project.

Quench analysis of a high-current forced-flow HTS conductor model for fusion magnets

High Temperature Superconductors (HTS) are considered a serious alternative to Low Temperature Superconductors (LTS) for magnets of future fusion devices because of several potential advantages, e.g. high operation temperature, high temperature margin, high magnetic field properties, cryogenic power saving, etc. For these applications (RE)BCO (Rare-Earth Barium Copper Oxide) coated conductors are preferred to other HTS conductors because of their high critical current density in high magnetic fields and the potential of lower cost. Studies and experiments of quench propagation in HTS tapes have shown that because of the high temperature margin and the rapidly increasing specific heat with increasing temperatures, HTS coils can have low propagation velocity of the normal zone making the quench detection and protection a difficult task. Therefore a fundamental understanding of the quench phenomenon is particularly important in the design and operation of magnets using HTS.

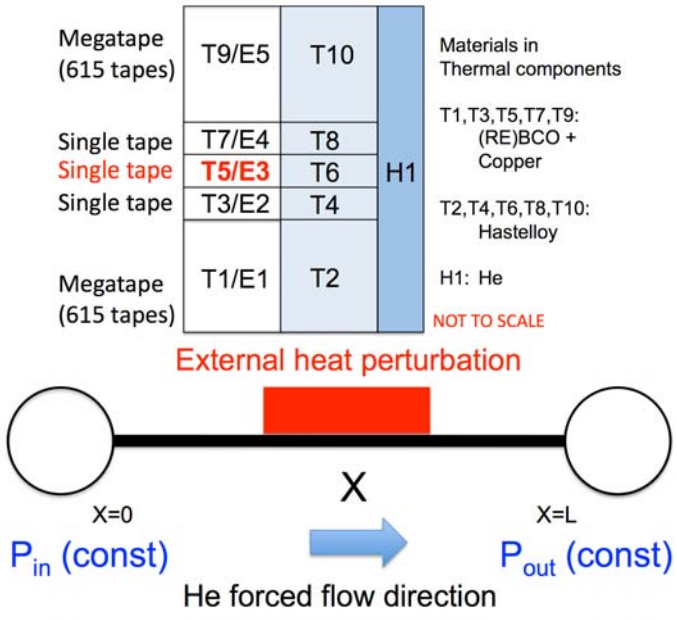

Fig. 2.5.4 *Model cross section (left) and along the conductor length (right).*

The quench behavior of a full size high current conductor, i.e. a stack of 1233 (RE)BCO tapes cooled by forced flow of gaseous helium, is studied using the CryoSofty™ code THEA. The operating conditions (B=10T, I=16.5kA, T=50K) are

similar to those used for the development of a coated conductor cable by the Roebel technique at the Karlsruhe Institute of Technology. The model, consisting of 5 parallel tapes (Fig. 2.5.4), is used to study the transverse (tape to tape) and longitudinal (along the conductor length) quench propagation.

The analysis confirms that if the helium is stagnant, the normal zone is practically confined to its initial position, with an extremely low longitudinal propagation. On the other hand, the helium flow is beneficial for moving the normal zone downstream, thus reducing the peak temperature in the heated zone (Fig. 2.5.5). These preliminary results are encouraging as there is a margin to optimize this effect, e.g. by selection of the channel size and mass flow rate.

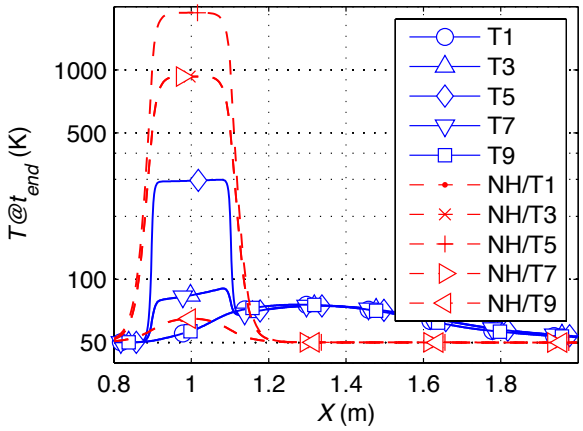

Fig. 2.5.5 *Distribution of the conductor temperature along its length in the thermal components. Comparison between Reference Case (blue) and the case with stagnant helium (red, NH).*

*2.5.3 Technology transfer on HTS current leads**

Within the framework of the project "*Hoch-Tc-Supraleiter Stromzuführungen für supraleitende Magnete*", funded by the "Förderagentur für Innovation KTI", CRPP and WEKA AG (Bäretswil) have started to develop high temperature superconductor current leads for currents above 10kA. The main goal of the project is the standardization of the current lead design to a degree, which allows the industrial manufacture of high current HTS current leads.

In the first phase of the project, model calculations for different cooling options have been performed. In most high temperature superconductor (HTS) current leads the HTS module is cooled only by heat conduction from the cold end, while the copper part operated between an intermediate temperature (typically in the 50K to 70K range) and room temperature is cooled by helium gas. The use of two helium circuits for the copper part of the current lead provides the possibility to have a large mass flow through the cold end of the copper part of the lead. This helium mass flow can also be used to cool the thermal shields of the magnet in question. Most of the length of the copper part up to the warm end is cooled by a second smaller helium mass flow. This alternative cooling option would reduce the necessary difference of the helium inlet temperature and the warm end HTS

* Work not belonging to the Euratom Association Workprogramme

temperature (leads to a slightly reduced temperature at the warm end of the HTS) at moderately improved cryogenic performance.

The HTS stacks need to be soldered into the milled grooves of a stainless steel support structure. Soldering trials in air led to high and strongly varying resistances between superconducting stacks and copper end caps. These results confirmed that a dedicated furnace is required for soldering under vacuum or protective atmosphere. The design of such a furnace has been started.

From a manufacturing point of view the connection of copper and stainless steel parts by electron beam welding instead of brazing would be advantageous. Welding trials, performed at CRPP, suggest that it is feasible to connect the stainless steel and copper parts of HTS current leads by electron beam welding.

An alternative design of the heat exchanger (copper) part of the current lead has been proposed by WEKA AG. To investigate the performance of this heat exchanger a 10kA prototype HTS current lead needs to be tested at CRPP. A first draft of the outline design of the prototype current lead has been already prepared.

*2.5.4 Use of HTS for High Magnetic Field Generation**

In the framework of the project *"Use of HTS for High Magnetic Field Generation"*, funded by the Swiss National Science Foundation, we intend to enhance the magnetic field of a 12T Nb_3Sn laboratory magnet by means of an HTS insert coil. In a first step, the expected gain in magnetic field provided by HTS insert coils based on the use of steel-laminated Ag/Bi-2223 tapes and REBCO coated conductors has been compared. For both HTS materials, the critical currents at 4.2K and 15T are well above 250A, which is much larger than the operation current of 82A of the Nb_3Sn magnet. In order to make a full use of the current carrying capacity of the HTS tapes it would be necessary to charge the insert coil by means of a second power supply.

The envisaged inner and outer radii of the insert coil are 22mm and ≤38mm. In case of the Bi-2223 tapes bending radii of less than 30mm are not feasible, and hence the space available for the insert coil can not be fully used. Due to this problem the maximum enhancement of the magnetic field is limited to approximately 2T leading to a maximum field of 14T.

On the other hand, bending radii down to 11mm can be achieved using REBCO coated conductors. The maximum achievable gain in magnet field depends on the required amount of copper to ensure quench protection and the thickness of the tape insulation. First quench calculations suggest that the copper cross-section of the commercially available standard tapes of SuperPower may be sufficient for safe operation of the insert coil. Supposing a tape thickness of 0.25mm including electrical insulation the magnetic field can be increased by 3.6T. In case of a thin electrical insulation (total tape thickness of 0.15mm) the field could be enhanced by up to 4T leading to a maximum field of 16T. The quoted values are based on an operation current of 250A and a total conductor length of 300m. Presently winding (layer wound versus pancake coil) and insulation trials are in preparation. The results of these trials will provide the basis for the final design of the insert coil.

* Work not belonging to the Euratom Association Workprogramme

*2.5.5 Collaboration with Helmholtz Centre Berlin (HZB)**

In the scope of a collaboration between Institutes, CRPP is developing a set of 20kA HTS current leads for the High Field Hybrid. In 2010, also using the experience accumulated with the EDIPO current leads, the design of the 20kA leads for HZB was finalized.

The main difference compared to EDIPO is the temperature of the coolant. In EDIPO the coolant of the thermal shield is at 73K, in the HZB it is only 44K. The lower temperature allows a more effective use of the HTS stacks, which are 28/lead for 20kA, compared to 65/lead for 18kA in EDIPO.

The HTS stacks, with the same specification as for EDIPO, have been procured in 2010 by HZB. The manufacturing drawings for the HZB leads are completed. A comparison between EDIPO and HZB leads is shown in Fig. 2.5.6. The manufacture of the parts will be released in the beginning of 2011, after final agreement on the assembly interfaces with the partners of HZB responsible for the coil and cryostat manufacture. The assembly of the leads at CRPP and their installation at HZB are scheduled at the end of 2011.

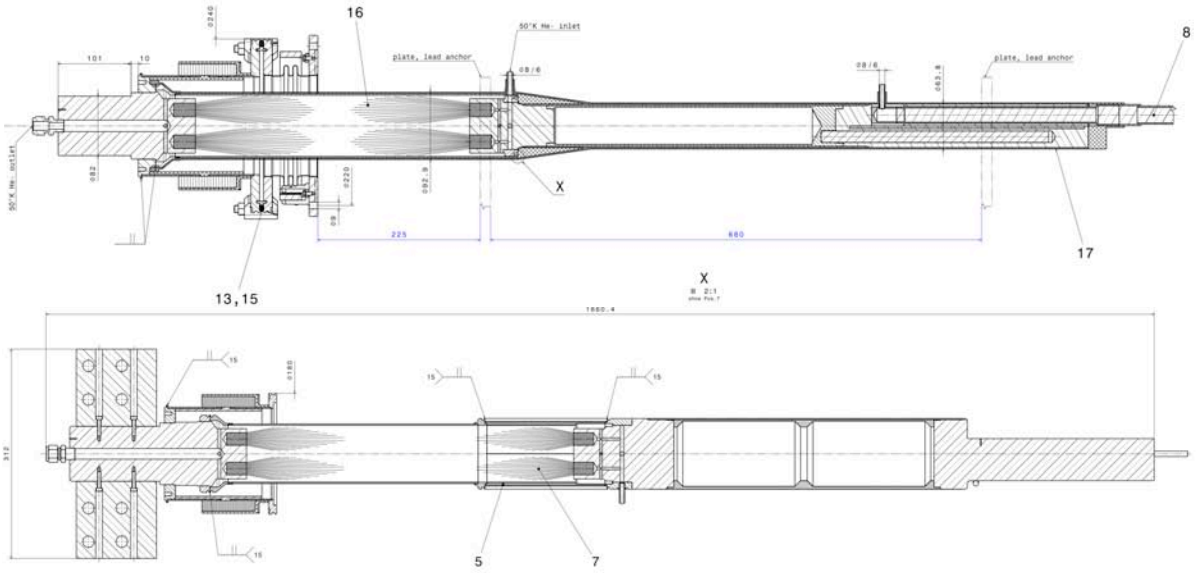

Fig. 2.5.6 *Comparison between the HTS current leads for HZB (20kA/44K, top) and EDIPO (17kA/73K, bottom)*

*2.6 Industrial process plasmas**

The ongoing projects concern the development of plasma sources for high rate deposition processes. New high deposition rate plasma sources have to be developed, novel plasma reactors have to be designed and process development is necessary before introduction in industry. These important topics are investigated in the frame of several CTI projects in collaboration with Sulzer-Metco, TetraPak and Helyssen. In addition the group worked intensively on a CTI project in collaboration with OC Oerlikon Solar concerning the development of a novel

* Work not belonging to the EURATOM Association workprogramme.

capacitively coupled RF plasma reactor designed for the specific demands of the amorphous/microcrystalline deposition for the thin film solar cell production.

During the year a new CTI project could be started studying the properties of RF and DC plasma sources for the deposition of semiconductor GaN layers for the production of LEDs. This project, also in collaboration with Sulzer-Metco, has been launched with the help from seed money obtained from the faculty SB.

Discharge physics remains a key issue in the world of industrial plasmas, in particular the arcing phenomena. One of the main problems for high deposition rate plasma sources where high AC/DC powers are applied is the occurrence of arcing and parasitic discharges. This problem has been investigated in previous years. At present in collaboration with RUAG Aerospace funded by ESA the origin of arcing occurring in so-called slip-rings used in spacecraft is studied. Research and development of Electrical Discharge Machining (EDM) is an other important point in the research of the industrial plasma group. The currently running CTI project on dry EDM is grouped around Inspire SA at the ETHZ and Charmilles-Agie Technologies SA.

The industrial plasma group participates in collaboration with the Laboratoire de Thermique Applique et de Turbomachines (LTT) and the Laboratoire d'Ingénierie Numérique (LIN) of the Energy Institute (ISE) from the Faculty of Engineering (STI) in the European PLASMAERO project. The main goal of this project is the application of plasma in aerodynamics.

To summarize: a particular weight is given to discharge physics, arcing under various conditions and the development of novel high deposition rate plasma source and its processing procedures. During the year meetings and discussions with various industries on other new plasma processing issues have been made and will give interesting R&D topics and interesting science for the industrial plasma group of the CRPP.

Furthermore the industrial plasma group ensured the education of master and TP students at the CRPP and participated in lecturing in the frame of the Doctorate School.

2.6.1 Thin and thick film coating using liquid and gaseous precursors with low pressure plasma spraying (LPPS) equipment

Conventional plasma spraying provides rapid coating due to the high enthalpy of the plasma jet. In this technique metal and also ceramic powder material can be melted and deposited in the form of splats which produce thick and porous coatings. Previously we showed that it is possible to deposit thin and dense layers from liquid or gaseous precursors at very high deposition rates using conventional plasma spraying equipment operated at low pressure. With this approach it is possible to combine the conventional thermal spray coating with the newly-developed thin film deposition using the same equipment to obtain multilayer deposits with special functionalities and properties. In the last year we focused on processing of possible future applications and on investigations exploring the limits of the novel process and the necessary equipment.

The production of metal based coatings (Transparent Conductive Oxide and metallic layers) has been identified to be a potentially very interesting application. The main

difficulty in these processes lies in the injection of the metallic precursor into plasma jet. A possible approach is to evaporate the metal by means of a effusion cell or to use the high enthalpy of the plasma jet to heat a crucible containing the evaporating metal.

Using these techniques, metal based coatings and different metal oxides (such as SnO_2 and ZnO) have been produced. The metal coatings obtained were homogeneous and very conductive, whereas the metal oxide layers were transparent as desired and for preliminary tests already show reasonable conductivity. The experiments showed that a very good control of the metal gas influx into the plasma jet is necessary to produce high quality metal (oxide) layers.

In addition to these metallic layers also some SiOx layers were deposited on various substrates metallic foils and different hard alloys, using Hexamethyldisiloxane (HMDSO) and oxygen injection into the plasma jet. External tests in view of an anticorrosion application showed that the deposited layers have interesting barrier properties.

One of the most interesting topics within this project is the interaction between the plasma jet and the substrate during low pressure plasma spraying of dense thin films. In order to interpret the deposition profiles obtained, temperature and enthalpy probe measurements, interferometry and mass spectroscopy measurements were made. 2D finite elements calculations using the commercial software Comsol have been used to simulate the deposition and its profile. The study is still on-going and the first interesting conclusions concerning plasma jet-substrate interaction have emerged.

2.6.2 A new low ion energy bombardment Plasma Enhanced Chemical Vapour Deposition (PECVD) reactor for the deposition of thin film silicon for solar cell applications

A novel electrode configuration is being studied for improved plasma-enhanced chemical vapour deposition of films such as amorphous silicon and micro-crystalline silicon. The new electrodes are designed to protect the growing film from damage by plasma ion bombardment which is crucial for the manufacture of high-performance photovoltaic material. The new plasma reactor concept is being optimised in laboratory tests and in a R&D industrial reactor. A feasibility study will be carried out to evaluate the usefulness and cost-of-ownership for production of next-generation thin film equipment.

Experiments in the laboratory reactors at CRPP include an RF-pulsed ion flux probe and a retarded-field ion energy analyser to measure ion flux and ion bombardment energy distribution on the substrate. Since ion bombardment is known to cause defects in the growing film sub-surface, the ion energy measurements will be correlated with film defect density and Raman crystallinity measurements. The minimum obtainable ion energy occurs across an electrically-floating sheath, and this will be investigated by incorporating the ion energy analyser and its electronics into a floating substrate arrangement. Optical emission spectroscopy was used to estimate the efficiency of hydrogen dissociation. The emission intensity ratio of atomic hydrogen to molecular hydrogen (Fulcher lines) is not directly related to the species number density ratio: Fulcher emission comes exclusively from electronic impact excitation of the (H_2) ground state, whereas H-alpha emission also includes dissociative excitation. It is further complicated by the de-excitation branching ratio to various excitation levels and collisional quenching. The required rate constant

values depend strongly on the electron temperature for which only numerical simulation estimations are currently available. CCD camera 2D imaging of the hydrogen plasma emission through a selectable pass band filter confirms that the fastest dissociation rate occurs at the intense plasma near to the electrode structure, whereas the deduced highest degree of dissociation appears to be in the volume between the electrodes. These seemingly contradictory observations can be reconciled by recognising that surface recombination losses of atomic hydrogen are much higher in the narrow grid gap. This is a reminder that reactor design plays a role in radical transmission efficiency to the substrate. Nevertheless, in this project the primary issue concerns material quality, not high deposition rate.

Parameter scans using structured electrodes are interpreted by means of numerical fluid plasma simulation, including the influence of electrode structure on gas breakdown RF voltage. An analytical model and numerical fluid dynamics show the necessary and sufficient properties of a gas showerhead system for uniform plasma processing. Film deposition and characterisation continues in parallel in the R&D industrial reactor.

2.6.3 Plasma diagnostics for dry Electrical Discharge Machining (EDM)

Electrical Discharge Machining (EDM) is a widely-used machining technique. The process consists in successively removing small volumes of work piece material, molten or vaporized during a discharge. The sparks are usually created in a flowing dielectric, generally water or oil. In the project the physical basics of dry EDM are investigated. In dry EDM the oil or water dielectric is replaced by air or some reactive or inert gases. Dry EDM is quite a difficult process and its industrialization is still far from being achieved.

The CTI project is in collaboration with Charmilles-Agie Technologies SA, Inspire AG at the ETHZ, Balzer Technik and Carbagas.

Extensive optical emission spectroscopy has been used in order to investigate the resulting spark in dry EDM. Very small electrode-substrate gaps are indicated in the case of dry EDM. In this case many short circuits between electrode and substrate might occur. A way to decrease the very small gap is to increase the spark voltage. Experiments with increased voltages show the difficulty to control the discharge. At very high electrode voltages uncontrollable discharges probably also due to oxidizing reactions in the air could be observed. Therefore inert gas protection of the working area during machining is the way to go in future in dry electrical machining.

Emission spectroscopy has been introduced to Inspire AG in order to perform real-time measurements during EDM machining.

2.6.4 Very fast SiOx barrier deposition on polymers by plasma-enhanced chemical vapour deposition (PECVD) process with a helicon plasma source

The principal objective of the present project is to increase the deposition rate in the PECVD process producing SiO_x barrier coatings by using the novel high density

Helyssen source and to optimize the use of monomers while keeping excellent barrier characteristics of the coating. High deposition rates of SiO_x for barrier application can only be achieved if the monomer is dissociated as much as possible. To achieve high dissociation degrees new more powerful plasma sources must be applied. The main goal of this project is to design and to test a novel planar RF plasma source developed by Helyssen S.a.r.l. A large part of the physical concepts and capabilities of this source is still only theoretical and has to be concretized by basic experiments at the CRPP. The first investigations clearly demonstrated that with a tubular Helicon RF plasma source interesting oxygen barriers on polymer substrates with elevated deposition rates can be obtained. In the meantime a first version of a planar RF plasma antenna has been designed and finally constructed at the CRPP. The planar antenna has been installed in a vacuum vessel in order to perform electrical tests and plasma diagnostics. For plasma diagnostics in particular Langmuir probes, optical emission spectroscopy and visualisation using a CCD camera are used, whereas the plasma wave diagnostics is mainly performed using 2D magnetic (B-dot) probes. At present a master work is being performed on the characterisation of the planar RF antenna and plasma which will be installed at the end of the masters period in a semi-industrial coater at TetraPak at Romont. With this roll-to-roll coater at TetraPak the coating performances of the planar antenna will be evaluated in view of packaging applications.

2.6.5 European FP7 project: PLASMAERO

The consortium of the FP7 project PLASMAERO is composed of 12 partners from 8 countries (Arttic (F), ONERA (F), CNRS (F), EPFL (CH), CIRA (I), Technische Universitaet Darmstadt(D), University of Nottingham (GB), NLR (NL), University of Southampton (GB), TRINITI RU), SNECMA (F) IMP (PL)). It gathers the key players from the plasma and aerodynamic scientific community of Europe. The PLASMAERO project was officially started at the end of 2009 and will last three years.

The CRPP participates together with the Laboratoire de Thermique Appliquée et de Turbomachines (LTT) and the Laboratoire d'Ingénierie Numérique (LIN) of the Energy Institute (ISE) from the Faculty of Engineering (STI) in this project. In addition the CRPP is work-package 1 leader (“Plasma devices, investigation, development and improvement” and task leader 3.5 (Shock/Boundary layer interaction).

The different partners from the EPFL will perform experiments at transonic flow speed in their research wind tunnel facility on basic configurations of a flat surface dielectric barrier discharge (DBD) and on 2D profiles with curved DBD in order to obtain results on the modifications of flow and plasma characteristics. One part of the wind tunnel testing shall be performed at CIRA which possesses a large wind tunnel.

A new high voltage switching unit has been developed at the CRPP which can provide voltage pulses with rise times of 20ns at 10kV and a pulse width of about 200ns (Fig. 2.6.1). Maximum currents up to 30-40A could be obtained with this device. This fast pulsed 10kV pulser is lightweight and small enough so that it can be incorporated in the planned unmanned aerial vehicle (UAV) to fly a fast pulse DBD aerodynamic actuator towards the end of the PLASMAERO project. The newly developed equipment might also find application with other partners.

As well as the electrical characterization, measurements of the spatial and temporal plasma light emission were conducted using a photomultiplier tube, a fast imaging ICCD camera and time-resolved optical emission spectroscopy. Different discharge types were observed at the rising and falling edge of the voltage pulse. The emission intensity and duration was found to depend on the voltage rise time and on the magnitude of the current pulse. Furthermore, the evaluation of the discharge has been investigated with the fast ICCD camera. It was found that a shorter voltage rise and fall time leads to higher light emission intensity and faster discharge propagation along the surface of the dielectric (Fig. 2.6.2 and Fig. 2.6.3). A first group features a continuous, homogeneous propagation of the discharge from the edge of the exposed electrode along the surface of the dielectric. The second group is characterised by sudden, explosive discharge propagation. For this kind of discharge, the intensity distribution was found to be very inhomogeneous with maxima at the edge of the exposed electrode and the propagating discharge front.

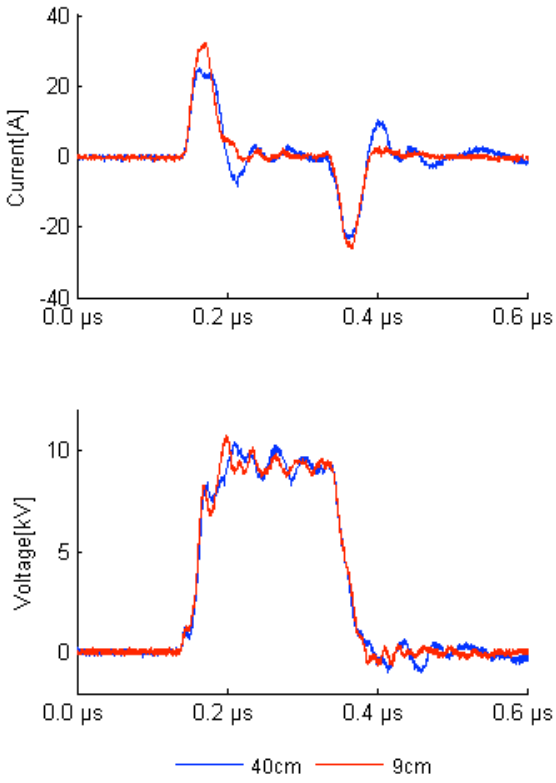

Fig. 2.6.1 *Comparison of current and voltage waveforms for DBD actuators with 9cm and 40cm electrode length.*

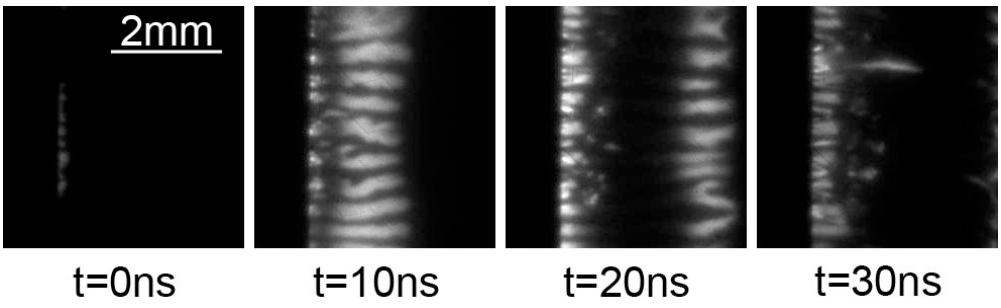

Fig. 2.6.2 *Temporal-spatial plasma development at voltage rise. (U_{out}=10kV)*

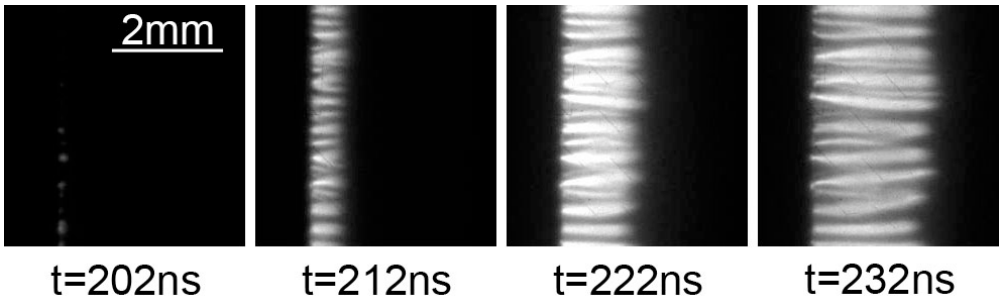

Fig. 2.6.3 *Temporal-spatial plasma development at voltage decay. (U_{out}=10kV)*

Synthetic Schlieren was applied to visualize the interaction of FRP DBD plasma with the ambient air. The experiments were performed with a two electrode DBD actuator in asymmetric configuration in the absence of flow at atmospheric pressure. Although the experimental setup has to be improved to enhance the picture quality, the propagating micro shock wave produced by the discharge was observed (Fig. 2.6.4). This observation is in agreement with simulations at the EPFL and at LAPLACE in Toulouse. Classic Schlieren visualisation gives a more clear picture of the propagating micro shock (Fig. 2.6.5) .

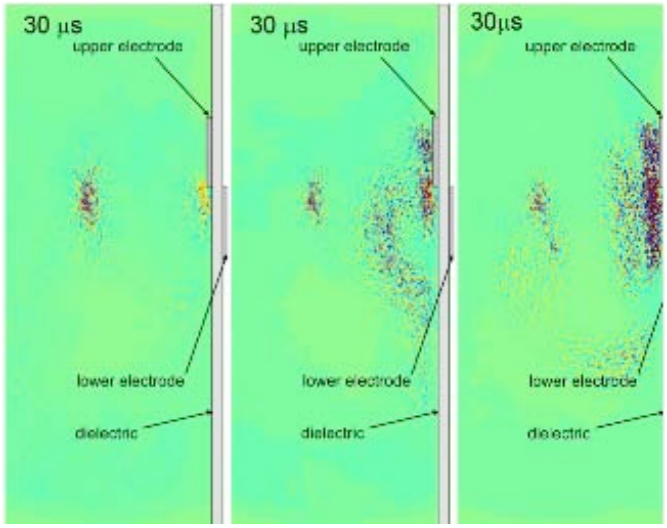

Fig. 2.6.4 *Micro-shock produced by DBD discharge for different pulse repetition frequencies (133Hz, 400Hz, 1000Hz)*

The first series of wind tunnel tests (low velocity wind tunnel; 0-30m/s) with a FRP DBD actuator was prepared and initial experiments were conducted. A DBD actuator that covers the full span of the future WT model (~45cm) in order to prepare a DBD actuator for the larger wind tunnel at CIRA(Italy) was manufactured. The fast imaging camera was installed to investigate the spatial temporal development of the plasma. First results of both experiments at flow speeds of 20 m/s indicate that the structure of the plasma as well as the propagation of the micro shock wave is not significantly different to those observed in the absence of flow.

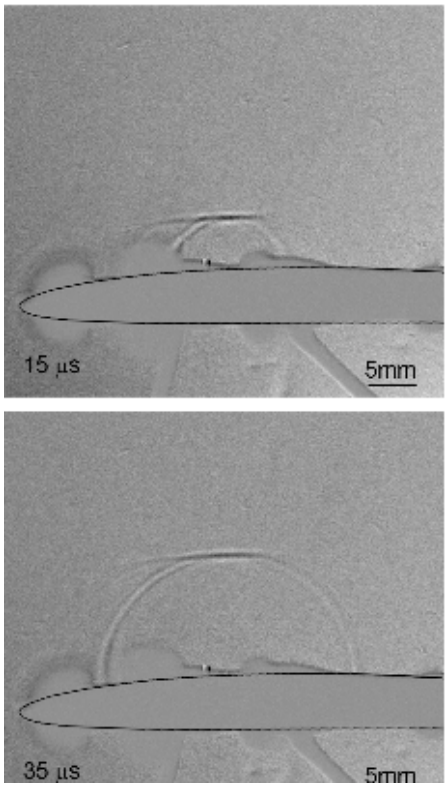

Fig. 2.6.5 *Schlieren visualisation of the discharge produced micro-shock on an airfoil (NACA 3506) for wind tunnel tests*

2.6.6 Arc Phenomena in Space Environment and Equipment (Project RETS)

Arcing is again a key issue in the application of plasma in industry and also, as in the present case, in space environment and space equipment. Modern satellites, in particular transmission satellites are being equipped with larger and larger power systems. Since also the weight aspect is very important the dimensions of the conducting paths for instance, in slide rings, are small. Therefore arcing is also considered to be a limiting factor in several other applications of plasmas, thus triggering intense research and development on this topic.

In the present work for the European Space Agency (ESA) in collaboration with RUAG Aerospace in Nyon and the Haute Ecole d'Ingénierie et de Gestion du Canton de Vaud (HEIG/VD-IESE) laboratory, the necessary fundamentals of the arcing shall be established and be applied to the space equipment in order to reduce or suppress arcing in space environment and equipment.

The aim of the work at CRPP is to conduct arc ignition, propagation and stability experiments in space environment and to define and conduct elementary experiments. Electrical simulations of the whole solar cell circuit will be conducted by the HEIG/VD-IESE laboratory at Yverdon.

After a long administrative preparation the project started in summer time 2010. The test facilities proposed at the present time consist of metal and insulation rings arranged as in a real slip-ring device connected to a high power DC (high voltage) power supply. The first series of foreseen tests evaluate the extreme limits of a small test ring assembly as a function of the environment gas pressure and different gases. Figure 2.6.6 shows the inside of the vacuum chamber. Teflon® pieces and a

Nylon® cylinder support the preliminary small test ring assembly: 2 conductors and 1 insulator. To simulate a brush on each ring the HV and grounded wires were bare from their connection with the ring. The main phenomena when a DC high voltage up to 30 kV has been applied were vacuum arcs, corona and glow. Two different zones depending on the applied high voltage are observed. The high pressure side where the breakdown voltage is clearly dominated by gas effect, whereas on the low pressure side breakdown leads to vacuum arcing.

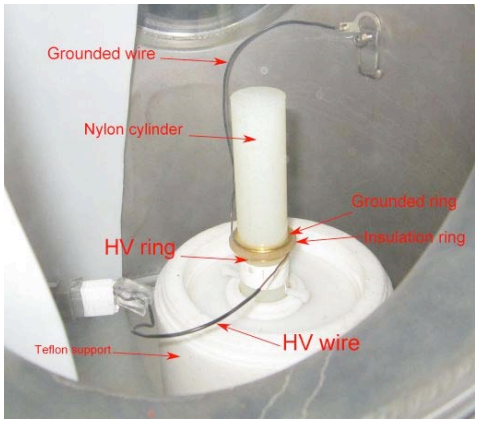

Fig. 2.6.6 *Test arrangement for arcing limit testing*

Multiple phenomena occur according to pressure and voltage have been observed. Figure 2.6.7 shows some of the different discharge forms which can be observed at higher gas pressures.

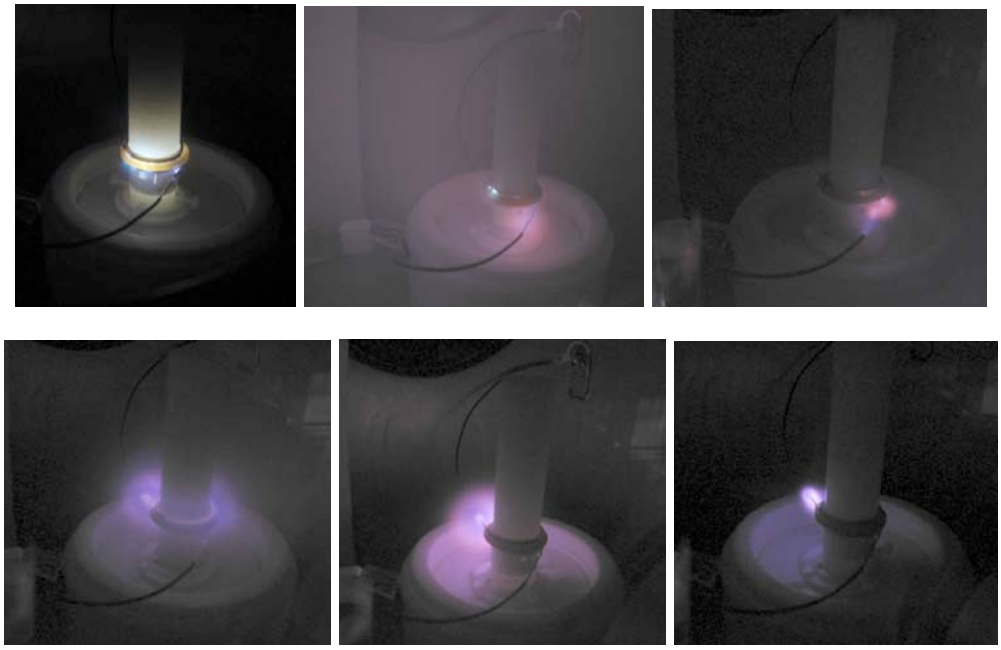

Fig. 2.6.7 *Different discharges during high voltage testing*

2.6.7 Helyssen SARL, a start-up company in the CRPP

Helyssen SARL (www.helyssen.com), a start-up company, has for several years used a test bed at the laboratories of the industrial plasma group to evaluate the performances of different novel antennae for high deposition rate sources. The

magnets and the necessary equipment for benchmarking and infrastructure have been lent to Helyssen SARL by the CRPP. This includes equipment also for plasma diagnostics and know-how in order to quantify the performance of high power RF plasma sources.

In collaboration with TetraPak Romont and the CRPP a CTI project has been started to investigate the application a planar Helicon RF Plasma source developed by Helyssen SARL in the packaging industry.

3 TECHNICAL ACHIEVEMENTS

3.1 TCV operation

The TCV tokamak facility was operated at a high duty cycle during 2010, with approximately 150 experimental sessions (half-days) until 8 October. Other than a four-week summer break, the only other major interruption was a six-week intervention in January-February to reinforce the severely worn-out polyurethane shock absorber pads on the supports of two horizontal coils in the Ohmic coil circuit. This was combined with an already planned vessel opening for maintenance and minor replacements.

3.2 TCV ECH systems

During 2010 the X2 system continued a successful operation using 5 gyrotrons. The non-working gyrotron magnet was sent to a magnet supplier and a quote for reparation was requested. The decision to repair the magnet is to be made. The gyrotron that was providing only half the nominal power was replaced with the one in the non-working magnet. This operation took 4 weeks and was accomplished during the TCV shutdown. Free-space beam measurements with phase reconstruction were made for the first time to aid in the alignment of the associated Matching Optics Unit (MOU). These measurements did not lead to an improvement of the alignment (power coupling to the waveguide) and, due to time constraints, the previous alignment method using fax paper was used in the end.

The X3 system was limited to a total power of ~1MW (2 gyrotrons). In the meantime a decision was made to repair the 3rd gyrotron, which has a faulty window. This gyrotron has been disconnected and is ready to be sent to the supplier (Thales). Repairs should take a minimum of 8 months. One of the other working gyrotrons has been displaced to the position of the faulty gyrotron because non-absorbed power launched from this transmission line is expected to minimize the perturbation of TCV operation.

The upgrade of the X3 electron cyclotron heating system with three additional 1MW gyrotrons in top-launch configuration has been studied in detail from the physics and technology points of view and is described in this report in the section devoted to the TCV upgrades.

3.2.1 ECH security

The present EC protection system (incorporating procedural measures so that 1) an 'ECRH standard shot' is required before the start of any operational day needing EC power – to test the full functionality of the EC protection system – and 2) the EC power injection configurations with large toroidal angles are not permitted) has proven to be sufficient. On the other end it does not give an exhaustive protection of all components in the TCV vacuum vessel. More importantly, it over constrains the potential of the EC system. The new EC protection system (section 3.3.8) is expected to restore flexibility while increasing protection of all windows.

3.2.2 ECH Real-time control

The new distributed real-time plasma control system has been successfully integrated into the EC systems. Commissioning experiments to control the TCV plasma, including the coil currents, gas valve and ECRH power and launcher systems are well underway. The system has been used in experiments to maximise the sawtooth period, control the plasma soft x-ray profile and set the plasma central temperature. Additional control of the plasma beta, height of the eITB and the first experiments to stabilise NTMs using event based controllers have been carried out. Algorithms to optimise the plasma control are now being developed and tested. Experiments to track the NTM phase and modulate the gyrotron power accordingly have been carried out successfully. Finally, maximizing the X3 absorption in the plasma by controlling the X3 launcher has been tested with the new system (replicating earlier analog-control results).

The fast polarizers purchased for one X2 transmission line have first been installed in the oblique ECE diagnostic (see section 3.3.7). Later they will be installed in the X2-4 transmission line.

3.3 Diagnostics

3.3.1 Thomson Scattering and FIR Interferometery

The Thomson scattering system was regularly operated over 2010. The effect of a misalignment drift was partially compensated by more regular beam alignment monitoring with an array of IR sensitive webcams. One of the most likely optical elements responsible for the alignment drift was identified and a modified optical holder is in design and construction for 2011.

The FIR detector's cryostat's performance has worsened over the last years. The intervention of a cryostat expert found that one of the rubber liquid Helium feed-throughs had been dislodged. Following this relatively minor intervention whereby the feed-through was restored, the original performance was restored with the cryostat again able to keep operational temperature for ~2weeks before requiring refilling.

3.3.2 Diagnostic Neutral Beam Injector (DNBI)

The 50keV, 3A hydrogen diagnostic neutral beam (H^+ fraction 85%) has been intensively used in the TCV for active CXRS measurement of the plasma ion temperature, impurity (carbon) density, toroidal and poloidal C^{VI} ion velocity. The beam availability was ~93% and the DNBI was operated for 909 plasma tokamak discharges. The statistics of the DNB faults is shown in Fig. 3.3.1. The main faults, not always essential for the CXRS diagnostic operation, were electrical breakdowns (11% of beam shots) in the injector ion optical system, mainly caused by non sufficient vacuum conditions in the beam extraction and acceleration region.

The DNBI has operated with an arc-discharge plasma source since October 2006 and source inspections in December 2008 and October 2009 were used to verify the resource of key elements of the arc-discharge channel. It was found the integral resource time for arc discharge cathode, anode and channel washers expected to be in the range of 3000-5000sec (corresponding to 2000-3000 TCV plasma discharges). A "fresh" arc discharge plasma source delivered in a contract with Budker Institute (Novosibirsk, Russia) and was installed on the DNBI-TCV in February 2010. This recovered the beam extracted ion current from 2.2-2.4A to the nominal 2.7-3.0A.

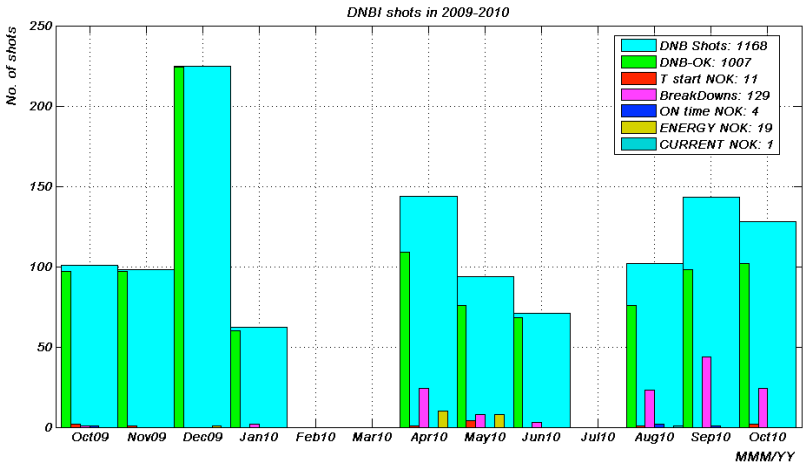

Fig. 3.3.1 *Statistics of DNBI-TCV operation in October 2009 – October 2010*

Fig. 3.3.2 *New Capacitor Bank of DNBI-TCV High Voltage Power Supply*

The lifetime degradation of super-capacitors ESCap 90kJ/300V and 2F/0.3Ω (10 units) of the 600V capacitor bank of the DNBI high voltage power supply since December 2005 resulted in a limitation of the maximal beam energy to 46-47keV.

The capacitors were replaced in May 2010 by 8 265kJ/75V/94F/15mOhm Ultracapacitor Modules from Maxwell Technologies Inc. (Fig. 3.3.2). The capacitance and stored energy of the bank were increased from 5F/900kJ to 12F/ 2.16MJ.

This permitted an increase of the beam energy to the optimal for CXRS measurement 49-51keV (Fig. 3.3.3).

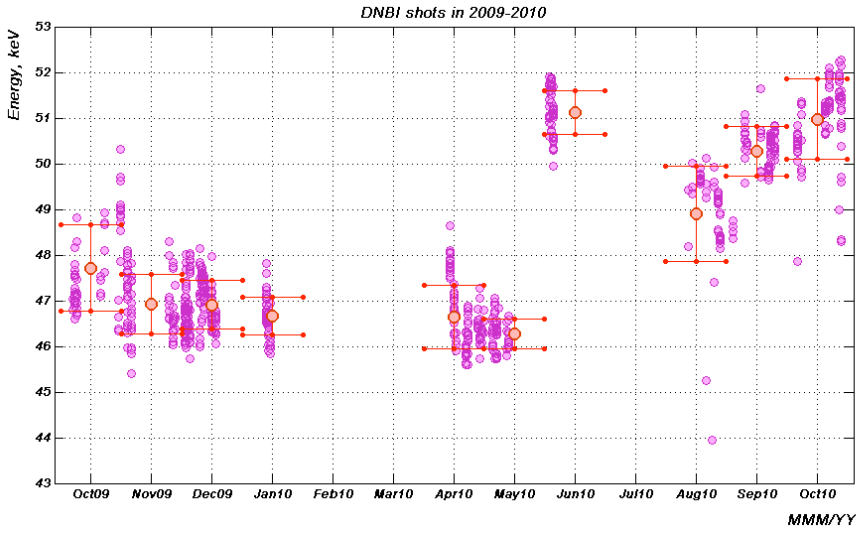

Fig. 3.3.3 *The energy of DNB-TCV before and after upgrade of the high voltage power supplies (March 2010)*

3.3.3 Charge Exchange Recombination Spectroscopy (CXRS)

During the second semester of 2010 the CXRS system was upgraded by the installation of two highly sensitive and time resolved CCD cameras featuring on-chip gain (Andor iXon EM+ DU897). A new water cooling system was also purchased that, in combination with the camera's Peltier coolers, permits continued CCD operation down to -80°C.

The installation of the new cameras was optimised to work with the present spectrometers (SPEX 750) in order to eliminate parasitic light or signal attenuation to obtain well focussed spectra from the double entrance slit (see Fig. 3.3.4 for the new CXRS set up).

The new on-chip electronic gain can be used to greatly improve the signal to noise ratio in situations where the light level is low and/or a fast readout speed is required.

Recent experiments proved the new cameras' improved the signal to noise ratio and permitting integration times down to 2ms with active signal increased by an effective factor of ~8 for the complete CXRS observation array.

Finally, the new cameras were integrated into the TCV control cycle where they may be operated automatically and synchronously with the plasma discharge and then automatically acquired.

Furthermore, the analysis routines providing the temperature, velocity and density profiles have been updated in order to be able to analyse future plasmas with the new CXRS cameras.

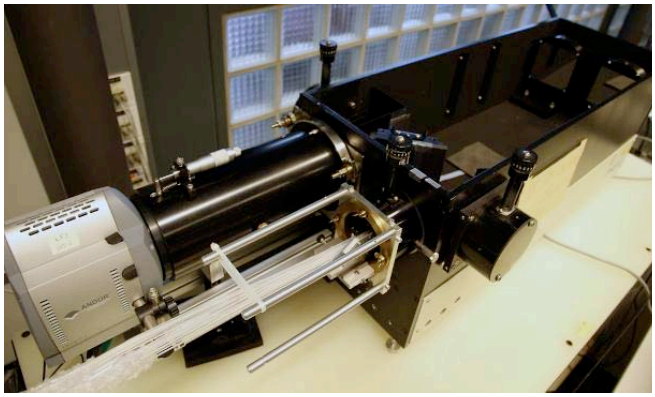

Fig 3.3.4 *Photograph of new camera (bottom left) installed on one of the CXRS spectrometers.*

The much higher sensitivity of these Andor cameras will be especially exploited to resolve variations in plasma rotation on times scales of 1-2ms. Firstly, experiments will be performed to deepen existing momentum transport studies across sawteeth events and to assess the role of rotation and EXB shearing rate in eITBs plasmas.

In a first campaign, previous results showed the existence of a co-current acceleration in the plasma core at the sawteeth crash. These experiments were previously limited to a reduced radial resolution (5 positions) and spectral range (200 pixels) and even then obtained poor active signal quantity. With the new cameras it is possible to acquire the entire array (20 radial positions with a 512x16um pixel CCD width) with the same 2ms resolution with the on-chip gain compensating for the fast readout rates. These “state of the art” detectors have thus increased the whole system’s performance considerably.

3.3.4 X-Ray Tomography

Since the upgrade of the system done in 2007, the dynamic range of the diagnostic has been increased (acquisition frequency up to 500kHz). Consequently, high frequency noise associated with grounding loops between the torus and the acquisition rack is detected, strongly polluting the physical signals. To solve this problem, the entire system (amplification and acquisition) was moved to a rack in the basement that lies at the same earth grounding as the torus. The noise level was significantly reduced as illustrated in Fig. 3.3.5 where the signal, measured by a diode with its line-of-sight looking at the plasma centre (left plot), is shown for a TCV standard shot before (blue) and after (red) the system displacement.

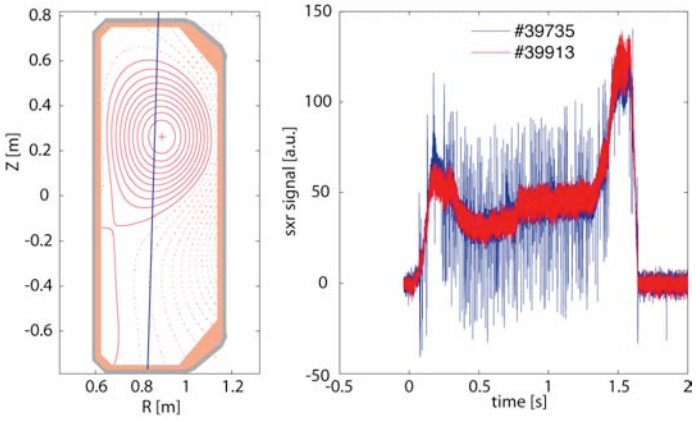

Fig. 3.3.5 *Shape of TCV standard plasmas with one of the 200 lines-of-sight of the X-Ray tomography system (left); Measured signals before (blue) and after (red) resolving the ground loop problem.*

3.3.6 One-millimeter interferometer

A far-infrared (FIR) interferometer is used as the standard tool for measuring line integrated electron density on TCV. It is a reliable device and provides data systematically. However, at low density (n_e<2•$10^{19}m^{-3}$) the phase resolution becomes poor and the device's sensitivity to mechanical vibration of the machine limits the usefulness of the instrument.

With a view to providing a means to correct the FIR data against mechanical vibration and to provide data at very low densities a one-millimeter wavelength (1mm) interferometer has been installed and commissioned on TCV.

The 1mm interferometer is now used systematically for TCV discharges and provides a measurement of line integrated density along a single vertical line of sight. The instrument functions reliably, even in the presence of electron cyclotron resonance heating, and is considerably less sensitive to mechanical perturbations that the FIR.

Signals from the 1mm interferometer will be connected to the Real Time control system for plasma density control that should be particularly useful for low density discharges.

3.3.7 Vertical ECE

The CRPP has purchased a pair of fast rotating polarizers, for installation either in the ECW system transmission line or in the front-end of the oblique ECE antenna. Installation in the ECE system was performed after laboratory tests with the fast polarizers were completed. Testing results for rotation rate and controllability are in agreement with the system requirements in view of the foreseen studies. Development and tests for data acquisition as well as of integration in TCV system control will be carried out in the near future.

These polarizers may be controlled in real-time to track polarisation changes due to shape and plasma refraction during the plasma discharge. By changing the

polarisation dynamically, optimal heating may be obtained over a wide range of plasma evolution either by pre-programming or, eventually, under real-time control. The polarizer positions and tracking tests are shown in Figs 3.3.6a-d)

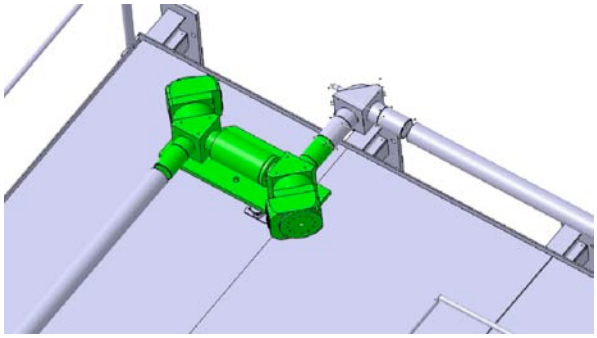

Fig. 3.3.6 *a) Drawing of the fast polarizers assembly (green) at the foreseen position in the transmission line number 4 of the ECW system for plasma heating.*

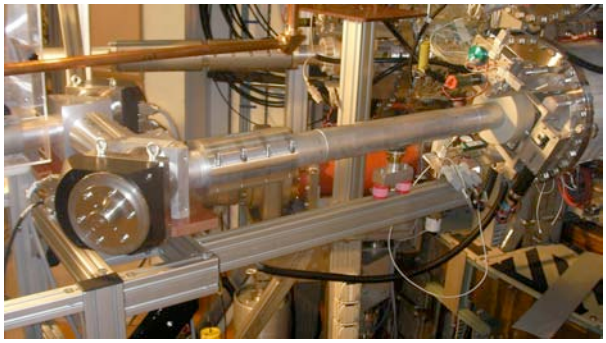

Fig. 3.3.6 *b) Photograph of the fast polarizers installed in the ECE diagnostic system.*

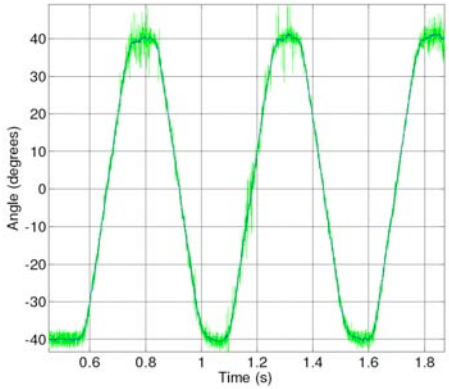

Fig. 3.3.6 *c) Traces of measured polarizer position for a 40° amplitude. Obtained results varied in the 2-3 Hz range, depending on controller configuration parameters.*

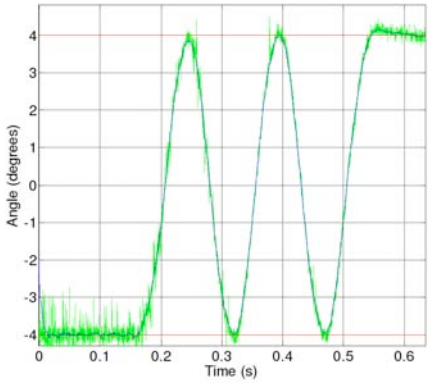

Fig. 3.3.6 *d) Traces of measured polarizer position for a 4° amplitude. Obtained results varied in the 6-8 Hz range, depending on controller configuration parameters.*

3.3.8 TCV Protection

Following window damage due to EC power interacting with diagnostic windows, it was decided to equip TCV with a full array of stray power detectors. In order to cover the complete machine, this system is better earthed to the machine vessel.

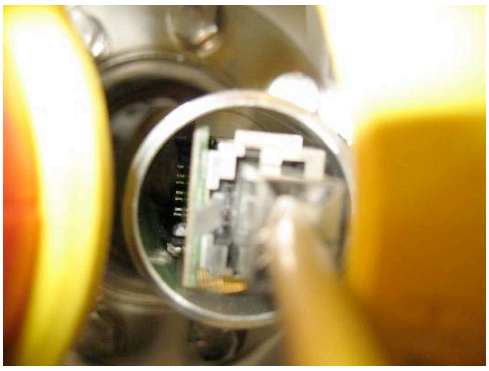

Fig. 3.3.7 *Backview of detector assembly. The PyroElectric detector is equipped with a high gain logarithmic amplifier with a bandwidth ~1kHz*

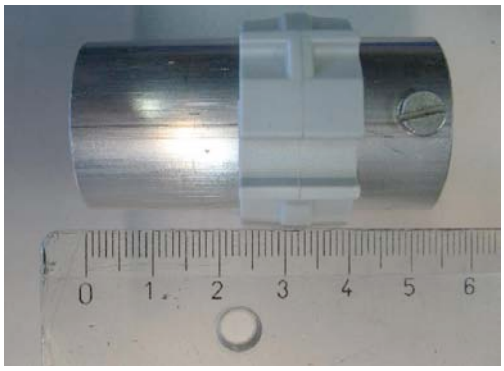

Fig. 3.3.8 *Plan view of a detector assembly. The standard plastic clip shows one of the mounting possibilities.*

The present status is that 50 pyroelectric based detector modules have been built, Figs 3.3.7 and 3.3.8 and the signals are divided into two clusters that are fed to a controller unit, Fig. 3.3.9. If any of the detector units exceeds a pre-set threshold, the controller unit stops the ECH power entering TCV, thus protecting the machine. The thresholds for tripping the EC power may be set independently for each detector and function independently of the TCV control software in order to assure machine protection even during computer software fault situations.

Fig. 3.3.9 *Front panel of controller chassis. Each detector connects with a standard EtherNet-type cable and the large connectors on the Left Hand Side may be connected to acquisition modules for post-discharge analysis.*

3.3.9 Hard X-ray tomography

A spectroscopic hard X-ray tomography diagnostic for TCV is currently in the final construction phase. This system comprises 4 cameras of 24 detectors each, distributed around the poloidal plane to provide the possibility of tomographic inversion (Fig. 3.3.10). The primary goal is to study for the first time the full 2D

distribution of bremsstrahlung emission from suprathermal electrons, and compare its poloidal dependence with theoretical predictions. This is particularly important in the presence of electron cyclotron heating and current drive, which at high power levels generates a significant suprathermal population. The dynamics of this population is thus a crucial element in the physics of wave-plasma coupling. Two of the cameras are also rotatable by 90 degrees, to view the plasma tangentially when desired. Tangential emission is expected the case of electrons travelling preferentially along the field lines; this occurs in particular when strong parallel electric fields are generated, such as during the formation of magnetic islands. This geometry thus complements the existing Tangential X-ray Detector Array (TXDA) diagnostic, which has more extreme tangential views but no spectroscopic resolution.

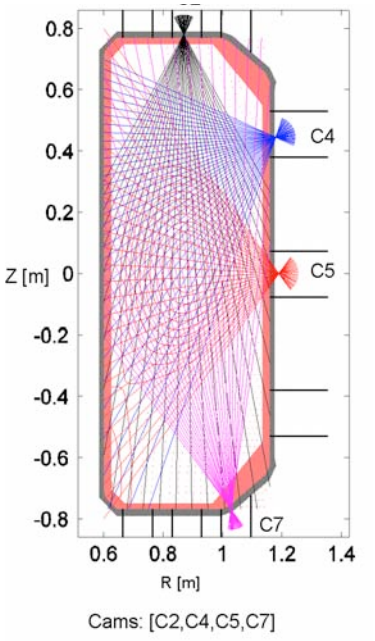

Fig. 3.3.10 *Four-camera hard X-ray spectroscopy arrangement on TCV*

The design relies on CdTe detector technology, with typically 7-8keV resolution in the 5-200keV energy range, and on a novel radial Soller collimator concept to maximize étendue uniformity across the arrays (Fig. 3.3.11). The procurement is in two phases. In phase 1, all the high vacuum components (the vacuum interfaces being Beryllium windows) have been purchased together with a first set of 36 detectors, to be distributed over two cameras for a preliminary tomographic study. The Soller collimators for these two cameras have also been fabricated. A prototype electronic card, comprising a high-gain, low-noise charge preamplifier and a current driver, has been developed in-house and is currently being tested in the tokamak environment. All the detectors and electronics are kept in a differentially pumped chamber which is water-cooled to prevent overheating during torus baking. All the mechanical support and housing components have been designed and the parts for the two initial ports are ready for a scheduled mid-November installation. Data treatment will rely, at first, on high-speed (10 MHz) digitisation of the integrated charge pulses, and all data reduction will be performed digitally in post-processing. The acquisition modules for the initial commissioning are two existing 16-channel D-Tacq ADCs.

The second and final commissioning phase requires primarily the purchase of the remaining 60 detectors and of the additional data acquisition modules, and is planned for early 2011.

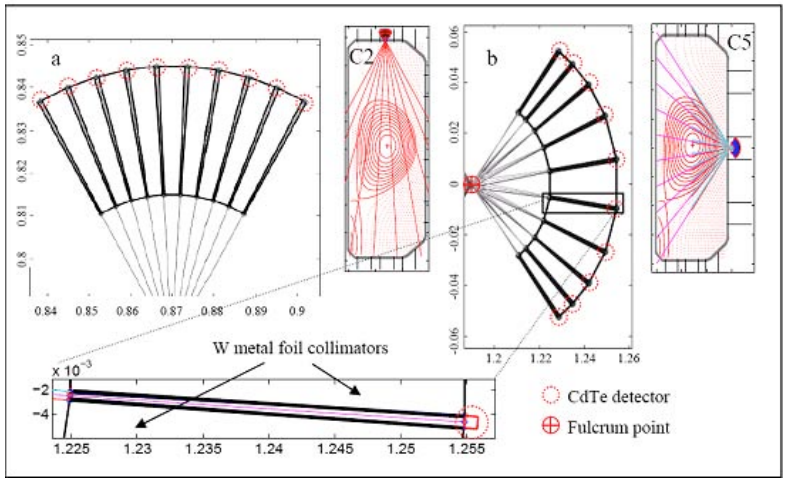

Fig. 3.3.11 *Soller collimator arrangements together with detail of tungsten components up to CdTe detector*

3.3.10 Tangential phase contrast imaging

A laser imaging apparatus has been installed on TCV to study core density fluctuations with very high spatial localization (down to 1% of the minor radius), thanks to a tangential arrangement. All components have been procured and the system is awaiting final alignment and initial testing. The project was put on hold approximately for one year for lack of available manpower, but has been restarted in August 2010 and first data are expected for the beginning of 2011.

3.3.11 FastCam

The optical system of the FastCam (fast visible camera) has been completely redesigned. The relay optics concept was kept, however the angle of view was increased from about 40 degrees to 70 degrees. With the new optics almost the full plasma is visible i.e. for a standard diverted configuration the top edge as well as the bottom divertor legs can now be observed (see Fig. 3.3.12).

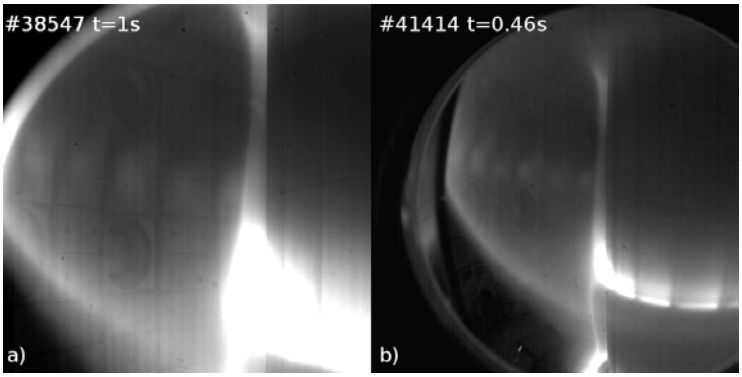

Fig. 3.3.12 *Comparison of images from the FastCam with the two relay optics with different angles of view: a) 40 degrees, b) 70 degrees.*

3.3.12 DMV (Disruption Mitigation Valve)

The fast gas injection valve originally designed for massive gas injection for disruption mitigation studies has been modified and converted into a multi-purpose gas injection valve: the system is capable of delivering small amount of gaseous impurities (Ar, Ne, He, etc.) into the plasma in a non-perturbative way (Fig. 3.3.13). The new system is to be exploited in the next experimental campaign.

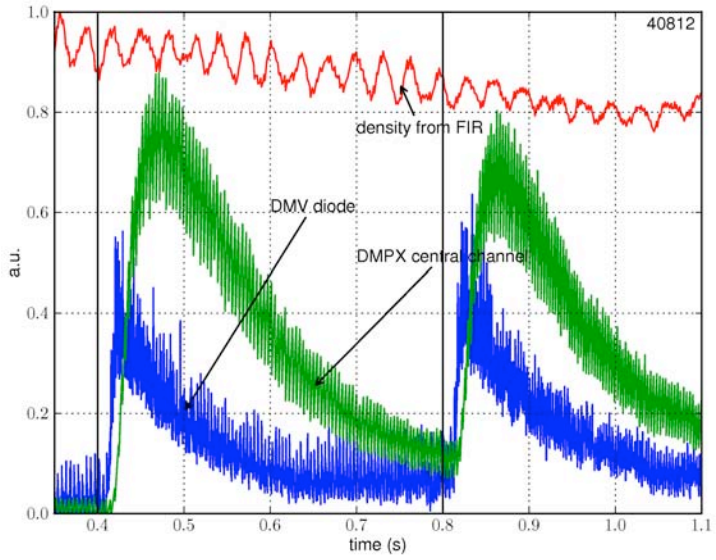

Fig. 3.3.13 *Ar injection as seen by different diagnostics: soft X-ray intensity on a DMPX central coord (green), a photodiode equipped with a 420nm filter (blue) and the density from the interferometer (red). The transport properties of Ar can be deduced for instance from the temporal evolution of the DMPX signals, and that of some spectral lines. Note that the main plasma properties such as density, current, etc. remain unchanged (only the density is shown). Injections are at t=0.4s and 0.8s with a length of 1 ms.*

3.3.13 AXUV (Absolute eXtreme Ultra Violet) Bolometers

Following the conclusion that the AXUV bolometer diode were ageing too quickly to be used in a tomographic arrangement, a full upgrade was performed in collaboration with the KFK group in Hungary. All 7 camera modules were modified to include a shutter that can shield none, one or both of the detector arrays that are now identically filtered. The new operational regime involves exposing only one bolometer array to the plasma and then, only upon request and very occasionally, exposing both bolometer arrays to the plasma to measure the first array's ageing. Furthermore, by shielding the diode arrays from boronisation and Helium cleaning discharges, the ageing process should be considerably slowed.

Fig. 3.3.14 *Front (vacuum side) view of modified camera showing the three mask positions*

3.4 TCV control and acquisition

During 2010, the first stage of the new TCV digital control system was completed. The final system consists of 4 separate computer nodes connected by their internet and fibre-optic linked reflective memory cards. This approach is particularly symmetrical with all nodes that acquire data, posting it onto the reflective memory bus. All nodes that use the Real Time (RT) data take their information from the reflective memory bus and, again, post their results back to the reflective memory bus, Fig. 3.4.1. Clearly, as long as the reflective memory bus performance is sufficient, this system is designed to be readily extendable to include further nodes and newer technologies as long as a reflective bus transducer card may be included- (Note: the reflective bus functions autonomously with its own fibre optic links and is able to reproduce any data written to it on a local node to the other nodes without external intervention).

In order to preserve TCV's historical plasma parameter and shape possibilities whilst introducing the digital control system, the RT system was first programmed to emulate the legacy system. Furthermore, the system was also integrated in the TCV control system in which all the machine components are formalised as state machines that interact to execute a TCV discharge and acquisition design. The graphic SIMULINK™ package within Matlab™, already extensively used on TCV, was chosen to manipulate the 4 node RT system. The programmer visualises, programs and tests control algorithms in SIMULINK™ language offline to TCV operations. The RT state machine, when selected, takes this code, translates it into the C language, compiles, links and uploads the resulting executable code to each RT node and prepares the RT system for the TCV discharge. The system also provides extensive capabilities for testing algorithmic performance and efficiency using recorded data from previous discharges thus strongly decreasing the time from conception to operation.

Following the TCV discharge, all the control data and the recorded parameters are stored for post shot analysis and evaluation. The complete process from algorithm design to TCV operation is completely automatic opening up this technology to the non computer-expert. All four of the RT nodes can be programmed with separate algorithms and the data blocks transferred by the reflective memory loop are directly available to the algorithm designer. For the development phase, the RT system could be switched in and out of the legacy control system at an extremely detailed level. It is entirely possible to allow the legacy system to control any of the control feedback loops whilst the RT system controls the others. The resulting

hybrid system can thus always be compared to the legacy system and then completely take over the TCV RT control, Fig. 3.4.2.

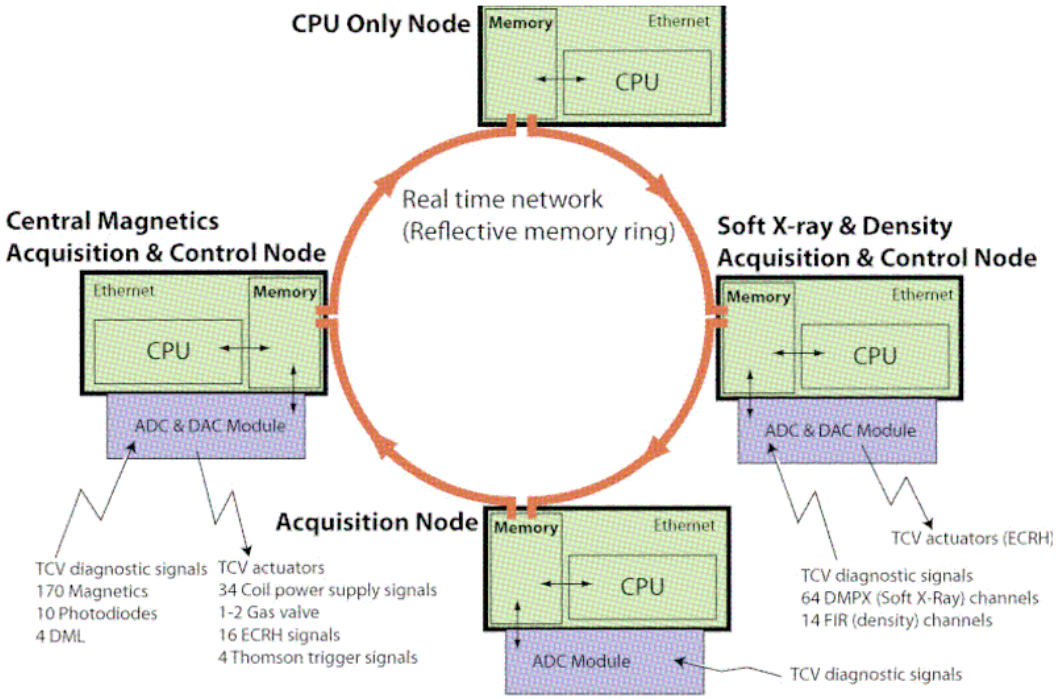

Fig. 3.4.1 *Final version of the first TCV Real Time control computer system. Four nodes, linked by reflective memory cards, share acquired and calculated results symmetrically. Here four of the nodes include data acquisition, two nodes are able to output data (DAC) to control TCV actuators and a CPU Only Node receives information uniquely from the data bus and only performs calculation.*

Since the control algorithm is re-compiled during each shot cycle, the algorithms and their dependent parameters may be modified between discharges. The system is thus an extremely powerful tool for everyday TCV experimental operation. Although still in its early days, the system has already been used in a wide range of control algorithms from intelligent triggering of diagnostic systems to control of the high power EC injection system to optimise the plasma performance for a particular experimental campaign.

In the example shown in Fig. 3.4.4, the possibilities of the RT control system become apparent. On one RT node, the soft X-ray radiation profile from the DMPX multi-wire detector is taken together with the full interferometer density profile measurements. Both diagnostics provide line integrated plasma measurements, (often the case for measurements in Tokamaks). This is then combined with a core electron temperature measurement from an array of differentially filtered X-ray sensitive diodes. Together, with the aid of a trained Neural Network, the calculation labelled “TENEX” deduces real-time electron temperature and density profiles. This information is then numerically fed to the “RAPTOR” section. This solves the partial differential equation describing the physics of poloidal flux profile diffusion. The model is sufficiently efficient to run in real-time, yet sufficiently complex to include important nonlinear physics allowing simulation of advanced (ITB) and hybrid scenarios with significant non-inductive current drive fractions. Following these calculations, the control system can use the permitted actuators, such as EC power

and/or aiming angle, to control one or more of the deduced plasma parameters, (in this case the plasma inductance is tracked and controlled).

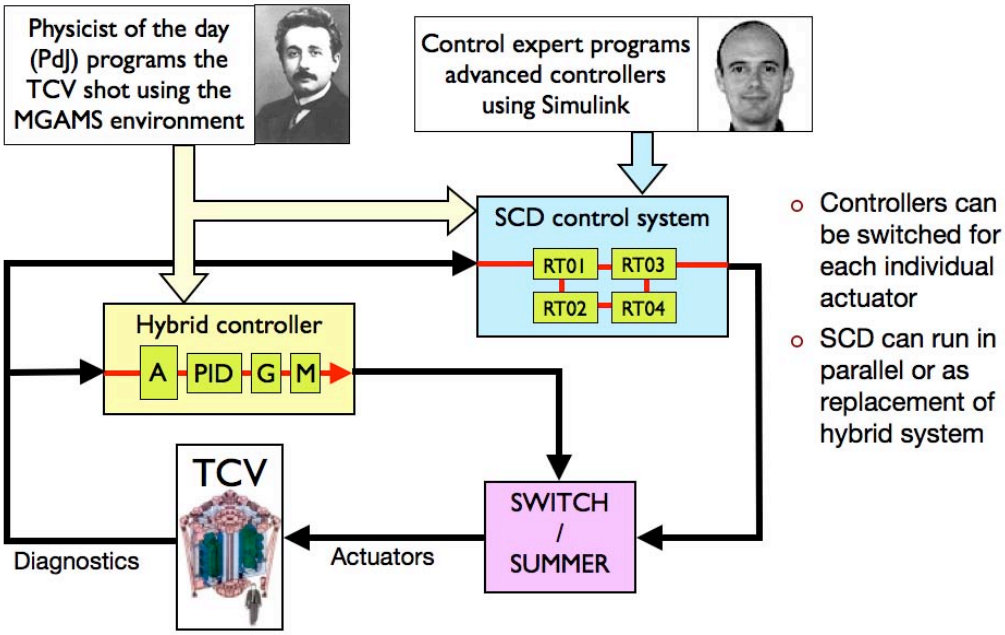

Fig. 3.4.2 *Schematic of the complete control system showing the legacy Hybrid Controller and the new SCD RT control system. Using the Switch/Summer, a complex combination of both controllers can be used to monitor and adjust the TCV control based on the original linear and/or new non-linear control algorithms.*

In the example shown in Fig. 3.4.3, Neoclassical Tearing Modes (NTMs) are stabilised by the application of EC power just outside the rational q=2 surface. The RT system recognises the existence of a strong NTM mode, displaces the EC beam mirror to aim just outside the q=2 surface, turns up the EC power and slowly scans the power resonance inwards until the NTM mode is stabilised whereupon the scan ceases and the mode is stabilised until the discharge end.

The less complex algorithms take RT measurements from TCV's diagnostic array and, following the control algorithms, react upon the TCV actuators. The availability of only calculating nodes can also be enhance the control algorithms by solve plasma equilibria or other physics equations.

In its present incarnation, all the RT nodes are synchronized to a system clock cycle, often in the range 50μs to 1ms. Since some of the required calculations will become longer than the reaction time required for the whole system, each node can choose to provide its result in a multiple of the base clock. i.e. if the simulated hybrid controller has a 100μs cycle time, the calculations may take 100, 200, 300μs etc. allowing extremely complex calculations to be integrated into the control system. On another front, data is presently acquired in an almost "raw" form from the diagnostics. The rapid evolution of high power dedicated calculation computer chips such as DSPs and more recent FPGAs may be harnessed. The acquisition cards in the RT nodes may be equipped with "daughter" co-processor cards that can take the raw data at high rates and provide pre-calculated data to the control system. To provide an example, instead of the control system acquiring raw data and calculating a Fast Fourier Transform (FFT) to monitor the oscillatory signal

properties, an FPGA could take the raw data, here at possible quite high data rates, and send the resulting FFT to the control system directly. The control algorithms can thus access extracted real-time parameters without necessarily performing the calculations themselves freeing the control algorithm to perform more complex control algorithms. Furthermore, since these co-processes are not limited to accessing data at the system clock cycle rate, they may access parameters requiring higher frequency data rates without complicating the main control cycle itself. This high speed data pre-processing is the subject of an ongoing project with the company that provided our acquisition modules.

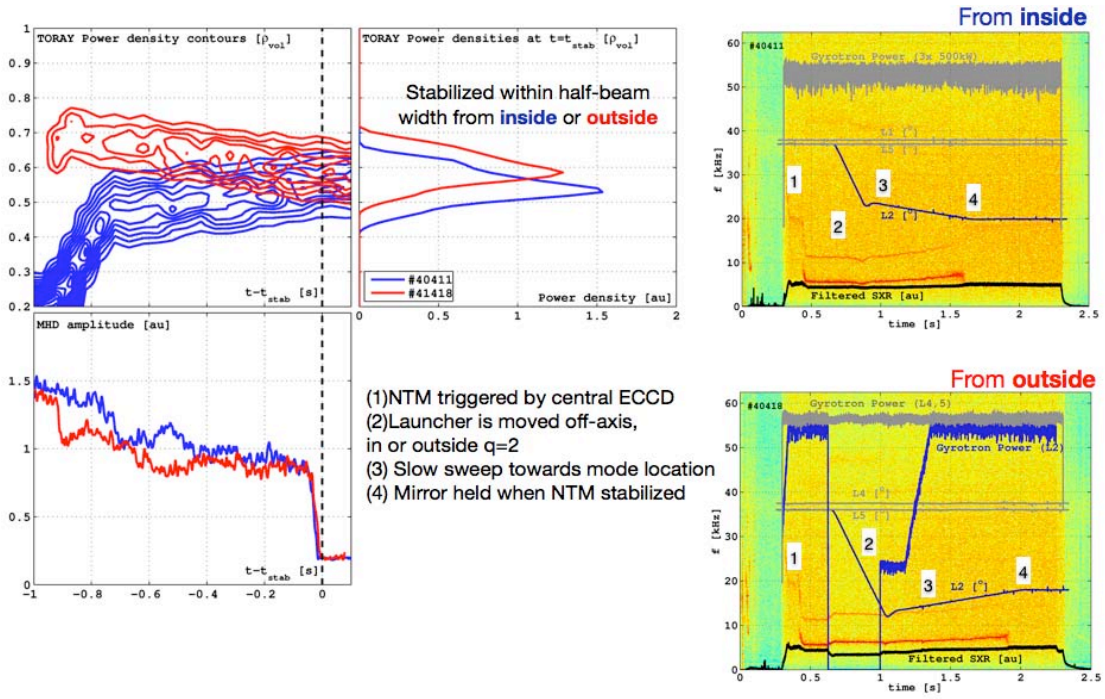

Fig. 3.4.3 *The EC power deposition contours as a function of normalised plasma radius. On the Right are the time histories corresponding to the stabilisation of two discharges with NTM instabilities and the RT system's reaction that results in mode stabilisation.*

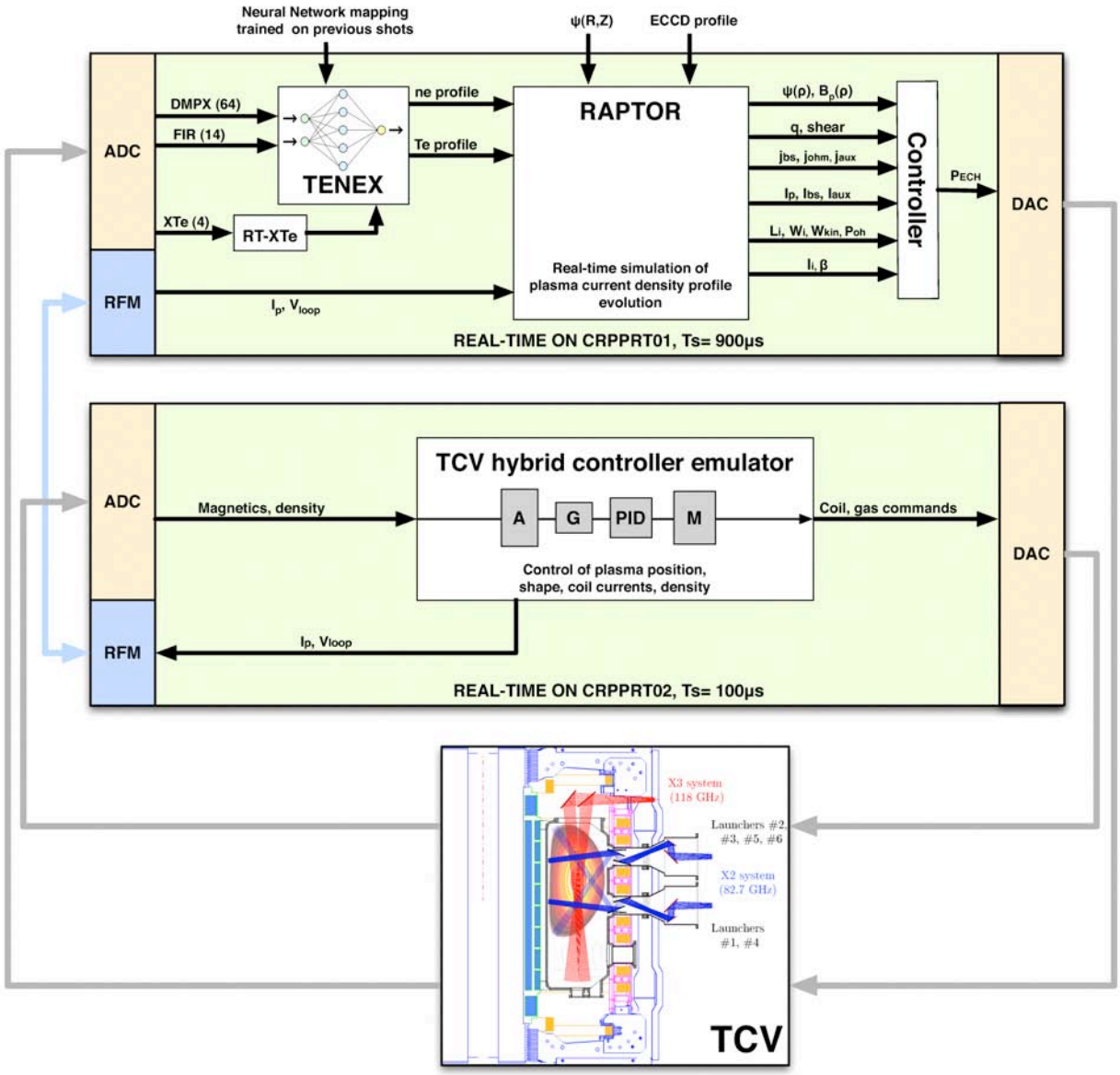

Fig. 3.4.4 *In this complex control loop, the first RT node acquires data and deduces the Electron temperature and density profiles that are used in the "RAPTOR" section to solve a relatively complete poloidal flux profile diffusion equation that calculate several complex plasma parameters. A further control algorithm provides feedback to the TCV actuators to control these parameters. The second node simultaneously emulates the legacy TCV Hybrid control system. These nodes combine to control the TCV plasma discharge and control the poloidal flux. Using the reflective memory, the nodes share both their measurement, calculated and actuator values during the discharge.*

3.5 TCV upgrades

3.5.1 Introduction

TCV results in the past decade and advances in the field of fusion research in general suggest that a number of upgrades should be implemented on TCV, with the aim of extending the operational domain of TCV towards an increased relevance to the ITER and DEMO burning plasma regimes. This implies accessing plasma parameters with relatively high density, comparable ion and electron temperatures, and with significant populations of fast ions, as well as exploring new configurations. In terms of physics parameters in particular, one should aim for higher normalised pressure β_N, a wider range of accessible temperature ratios (T_i/T_e) and lower collisionality, as will prevail in a reactor. It is possible to achieve these conditions on TCV by:

- Increasing the ability to heat electrons at higher density. For this, the power of the 3rd harmonic (X3) EC system should be increased by about 3MW;
- Directly heating the ion population. For this, a Neutral Beam Injection (NBI) heating system, with a power of about 3MW, is needed;
- Learning how to control the most deleterious instabilities (viz. edge localised modes, ELMs) in these regimes, by installing the hardware necessary for the test of the most promising control techniques;
- Adding or modifying in-vessel components to combine the shape capabilities of TCV with the increase in additional heating power in the most reactor relevant plasma scenarios.

With the proposed upgrades, TCV would become the only tokamak to perform physics experiments, including ELM control and shape studies, in ELMy H-mode, which is the Q_{DT}=10 ITER reference scenario, with β_N values in the same range of ITER or higher, with dominant electron heating generating little or no momentum input, and with T_e/T_i covering a wide range including the ITER, DEMO and reactor relevant value of T_e/T_i =1.

In the following we summarise the activities undertaken in 2010 on the three main upgrade projects, for which engineering design studies are now in a fairly advanced development stage: the saddle coil system, the Neutral Beam system, and the EC power upgrade.

3.5.2 Saddle coil system

No significant activities were undertaken in 2010, after the preliminary design and the feasibility studies completed in the previous years, except a 0D calculation of the coil cooling.

3.5.3 Neutral beam heating for TCV

The implementation of direct ion heating on TCV by the installation of a 20-35keV neutral beam injection (NBI) with a total power of 1-3 MW would permit an

extension of the accessible range of ion to electron temperatures to well beyond unity, depending on the NBI/ECH mix and the plasma density. A NBI system would provide TCV with a tool for studying plasmas at reactor relevant T_i/T_e ratios ~1 and for investigating fast ion and MHD physics together with the effects of plasma rotation and high plasma β scenarios. The ion to electron temperature ratio is of particular interest in the projection of the transport mechanisms from existing experiments to burning plasma, and plays a key role in the transition between ion temperature gradient (ITG) and trapped electron (TEM) mode dominated turbulence and transport. The behaviour of toroidal rotation in the vicinity of an ITB is of interest because of its influence on triggering and/or sustaining the barrier.

The proposed NBI system would also provide TCV with a tool to investigate fast ion and related MHD physics. Target plasmas could include ITER-like H-mode shapes together with advanced shapes, recently accessible only in Ohmic regimes.

The feasibility studies for a NBI heating on TCV presented in this section were undertaken to construct a specification for the neutral beam injectors, together with an experimental geometry for possible operational scenarios.

Scenarios of NBI heating experiments

Experimental scenarios for the NBI experiments on TCV are strongly linked to limitations imposed by ECH and ECCD. For the eITBs and fully non-inductive scenarios on TCV, the accessible plasma density is limited by the X2 cut-off ($n_e<4\times10^{19}m^{-3}$). Conversely, efficient X3 deposition is obtained for electron density in the range of $5.0\text{-}7.5\times10^{19}m^{-3}$ and $T_e>2keV$.

The ASTRA code was used to simulate the plasma response to NBI. The code solves equations for plasma current density, electron and ion temperatures, with the electron density profile and total plasma current taken from the experiments. Neoclassical ion heat conductivity (χ_i) gives T_i profiles that match the CXRS measurements. The experimental electron heat conductivity (χ_e) was normalised to obtain the energy confinement time predicted by power law scaling: IPB98(y,2) for ELMy H-mode and standard power law regression for L-mode. The EC power deposition profile was calculated using the TORAY ray-tracing code.

High density ELMy H-mode regime

The target parameters for modelling were taken from Ohmic and X3 heated stationary ELMy H-mode phases of TCV discharge. About 95% of injected 25keV deuterium NB power can be absorbed by the plasma for a tangentially injected beam. The simulations show that $T_i(0)=T_e(0)\cong2.2keV$ can be achieved with ~0.8MW of NBI and 1.3MW X3-ECH (Fig. 3.5.1). Access to $T_i/T_e>2$ should be possible at increased NB power (≥2MW) or reduced X2-ECH power. The fast ion charge-exchange (CX) losses on background neutrals strongly depend on the first wall recycling conditions. The density of background atoms $n_0^D(LCS)=5\times10^{15}m^{-3}$, obtained from EIRENE modelling, reduces the NB heating efficiency by ~15%, while CX losses on beam neutrals (≤2%) are negligible.

At high plasma density and current, neutral beam injection could result in an increase of the thermal β_N from 2.0 (pure 1.5MW X3-ECH) to 2.6 (2MW NBI), and could even lead to a total β_N exceeding the ideal MHD β limit (~3). Fast ion slowing down times in such regimes are of the order of 10ms, i.e. shorter than or

comparable to the bulk plasma energy confinement time (τ_E, 10-50ms). Perturbations to the ion energy Maxwellian distribution by fast ions are therefore expected to be small, as in a reactor.

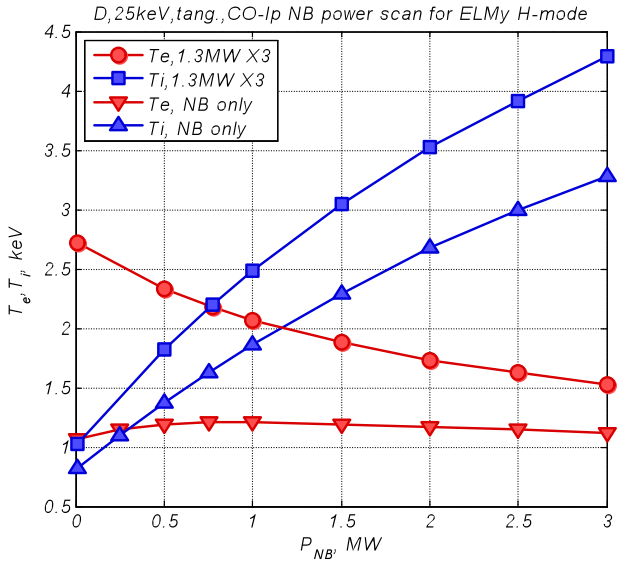

Fig. 3.5.1 *Electron and ion temperatures vs. NB power for ELMy H-mode without and with 1.3MW X3-EC heating.*

X2-EC and NBI heating

The NB heating was modelled in low density regimes for a 2MW X2-EC heated L-mode reference discharge. Such level in the NB deposited power per ion at low density results in a value of the NBI power necessary to access a central ion temperature of 2-3keV that is ~2 times lower (0.5MW) than in high density regime (Fig. 3.5.2). Near-normal NB injection (E_{NB} 15keV) cannot be considered here due to higher (>20%) shine-through losses, resulting in first wall overheat of the TCV central column. ASTRA simulations confirm earlier experimental and numerical studies of fast ion orbit losses on the TCV. At low plasma current, fast ion orbit losses are extremely important and become substantial for counter-Ip NB injection (Fig. 3.5.3); losses increases at high ion energy (32% for 25keV D-NB and 59% for 50keV) and for higher NB atomic mass.

NB injection at low plasma density and current provides the possibility to study fast ion and MHD physics. In the unfavourable scenario, the 200-300kW delivered to the plasma NB power leads to the creation of a strong fast ion population with a stored energy of few tens kJ that, at low current, significantly contributes to the ideal MHD β limit. Fast particle instabilities would dominate the plasma behaviour under these conditions.

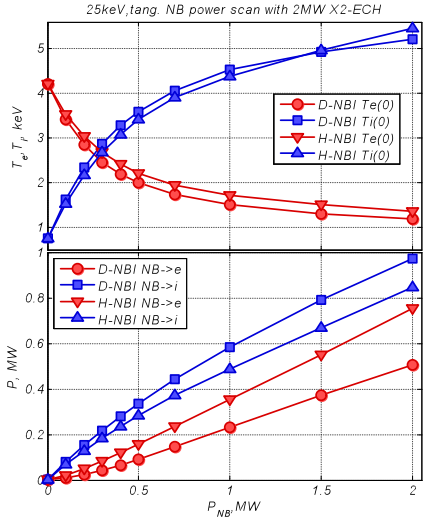

Fig. 3.5.2 *Deuterium and hydrogen NB heating for L-mode with 2MW X2-EC heating.*

Neutral beam injection layout

TCV was not originally designed for neutral beam heating, although several relatively wide machine midplane lateral ports were implemented for flexible diagnostic access. The location of magnetic field coils and the existing support structures provide major challenges for NBI plasma access, in particular for tangential injection. Two schemes for NB injection through 15cm diameter ports at near normal angle (tangency radius R_{tan} 23cm) and through a single Ø10cm aperture nearly tangentially, have been analysed. Shine through for $R_{tan} \cong 23$cm is acceptable at the high densities, while NB usage at low densities is severely limited by excessive shine-through and high inner wall power loads. The maximal acceptable power load of 7.6MW/m^2 for a 1sec duration leads to temperature rise of graphite inner wall tiles of 1000K corresponding to ~10% shine-through of the 1MW beam with the 15cm foot-print size.

A model of a neutral beam with geometric focussing and angular divergence was developed to calculate the beam transmission and power load on the critical scrapers in the NBI duct. The acceptable ~80% beam power transmitted into the tokamak for 1MW, 25keV, 1sec beam with 200mA/cm^2 extraction current from the ion optical system is feasible only with low beam divergence: 0.7/0.8° for Ø10/15cm duct apertures respectively. The transmission of the high power (0.6-1.0MW) NB through narrow ports demands high current density, low divergence neutral beam injector only reachable, at present, by lower current diagnostic neutral beams.

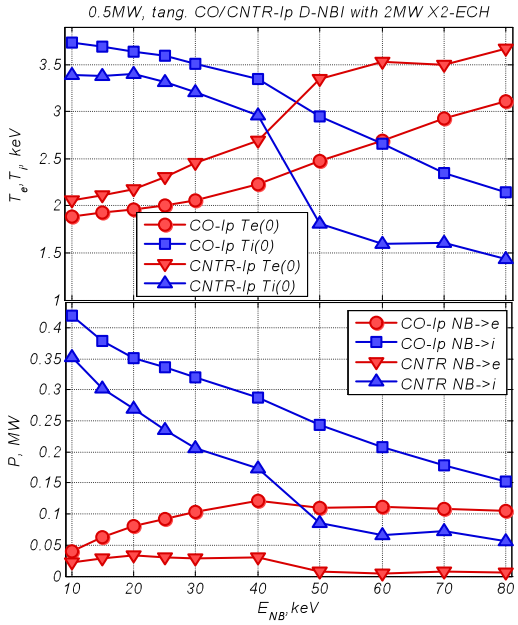

Fig. 3.5.3 *Co- and counter-Ip NB heating vs E_{NB} in L-mode.*

To alleviate these requirements on beam divergence and current density, a modification the TCV vacuum vessel to create new port(s), specifically designed for NBI and fitted between magnetic field coils, is considered. The available gaps between toroidal and poloidal magnetic field coils at the TCV midplane are 22cm vertically and 38cm toroidally. The design of a duct with inner minimal aperture of 20cm, wall thickness 1cm and 3cm gaps to toroidal field coils, beam axis tangency radius of 74cm, (Fig. 3.5.4) was found to be feasible and permits to transmit >90% of the NB power to the plasma for 1MW, 25keV deuterium beam with divergence ≤1.2°.

This geometry could accomodate two NB injectors (aiming in co– and counter-current directions) on the same port. With proper power adjustment, one could obtain scenarios with balanced momentum transfer to the plasma.

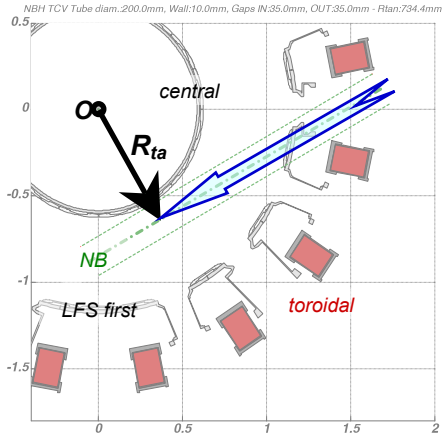

Fig. 3.5.4 *Tangential injection arrangement with modified vacuum vessel.*

Conclusion

The installation of a 1MW, 25keV, deuterium, tangential neutral beam injector would significantly increase the experimental capabilities of TCV by extending the operational domain at higher T_i/T_e ratio and plasma β, and by widening the H-mode operational domain. An injected power of 1MW would be sufficient to access $T_i=T_e$ 2keV, taking into account 20% CX fast ion losses on background neutrals. Two balanced co- and counter-I_p orientated injectors with total power of 2MW would permit at once the investigation of the effects of NB induced plasma rotation, to reach T_i/T_e ratio 2 and studies of fast ion behaviour and MHD physics in scenarios such as stationary ELM free H-modes and fully non-inductive electron internal transport barriers. Lowering the beam energy results in a decrease of the on-axis ion heating power density. It is easy to access low neutral beam divergence at high beam energy, though at higher beam energies fast ion orbit losses strongly reduce the heating efficiency, especially for CNTR-Ip beam alignment (Fig. 3.5.3).

For a given injection energy and target plasma parameters, the fraction of NB power delivered to bulk ions is higher and shine-trough losses are lower for deuterium beam than for hydrogen. Due to unacceptable shine-through power load on the central column, only double-path tangential NB injection is acceptable for intermediate and low plasma densities (<4×$10^{19}$$m^{-3}$, for 25keV deuterium beam).

The capability of the NBI system to use hydrogen ions is essential for heating high ion densities ($10^{20}$$m^{-3}$) on-axis and reducing orbit losses of CNTR-Ip injected fast ions at low plasma currents (<200kA).

3.5.4 EC-system upgrade

Extensive simulations with the ASTRA transport code also supported by experimental results obtained with the existing system have demonstrated that an upgrade with 3MW in top-launch will allow us to study H-mode plasmas in TCV at ITER relevant conditions, as shown in Fig. 3.5.5.

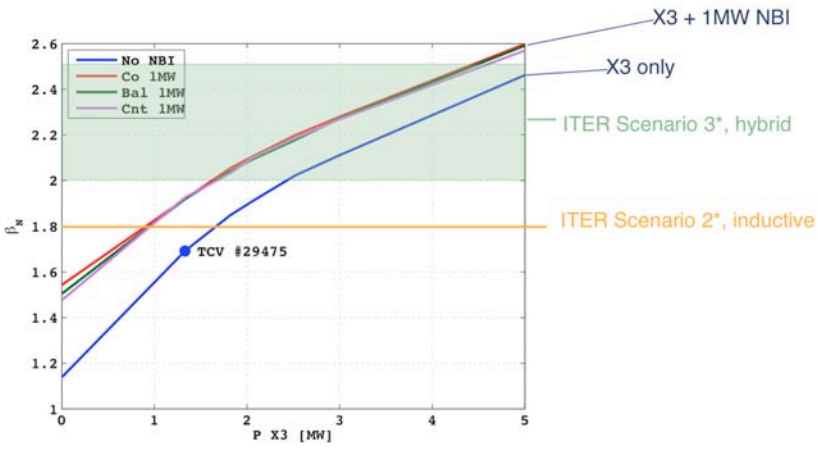

Fig. 3.5.5 *Normalized beta, β_N, calculated with the ASTRA transport code, versus X3 absorbed power for two different situations: a) 3MWX3 heating only (blue curve), b) 3MWX3 heating and 1MW of NBI (red, green and violet curves). The red, green and violet correspond to co, perpendicular and counter injection for the NBI, respectively. The orange line and green surface represent the values of β_N for two different ITER scenarios.*

In addition, by using the three existing 118GHz/0.5MW/2s gyrotrons in Low-Field-Side injection, one can take full advantage of the localized deposition features essential for controlling crucial MHD instabilities for ITER such as sawteeth and NTMs. This upgrade would also significantly widen the TCV operational space for basic studies such as H-modes in advanced divertor concepts such as, for instance, the snowflake divertor.

Figure 3.5.6, shows the EC/RF-beams launching configuration planned for the TCV-upgrade. The new 3 gyrotrons (1MW each at 126GHz) would be injected in top-launch, whereas the existing 118GHz gyrotrons would be moved from top-launch and connected to the existing X2 launchers injecting the RF from the low-field side.

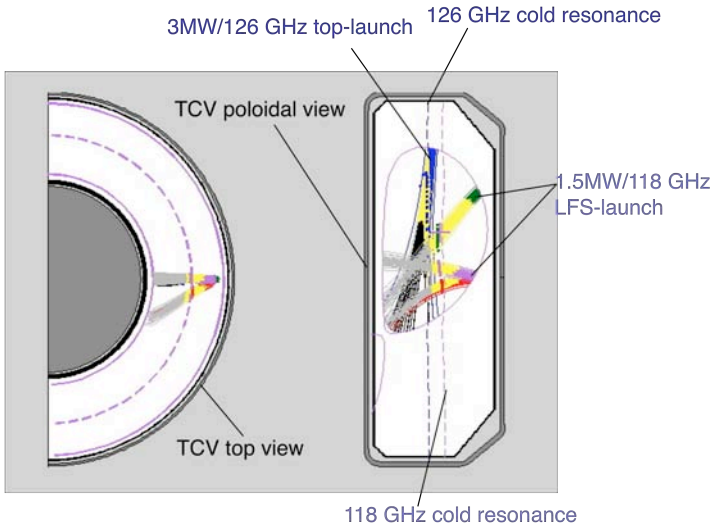

Fig. 3.5.6 *Ray tracing (TORAY) in TCV plasma for top-launch (3MW @ 126GHz) and low-field-side launch (1.35MW @ 118GHz). For a plasma central density and temperature of, $n_{e0}=8*10^{19}[m^{-3}]$ and $T_{e0}=3.4keV$, respectively, the TORAY simulated top-launch and central LFS-launch single-pass absorptions are 90% and 76%, respectively.*

For the additional 3MW at 126GHz, the proposed solution envisages to consider as a starting reference the 140 GHz gyrotron developed within the European development programme for W7-X and implement a minimum redesign. The redesigned gyrotron would operate in the $TE_{26,7}$, cavity mode compatible with an operation at 126GHz. In addition, it has been shown that by redesigning the electron gun from a diode to a triode configuration and using the same magnetic field profile, one not only meets the TCV requirements but also opens the possibility of operating this gyrotron/magnet system at the ITER/FAST relevant frequency, 168GHz, and power, 1MW.

Figure 3.5.7 shows the RF power as a function of the accelerating voltage, V_b, for the two cavity modes corresponding to 126 and 168GHz. It is important to notice that the only elements in the gyrotron that need to be modified are the electron gun and the diamond window thickness. All other subsystems are exactly the same as for the 140GHz gyrotron.

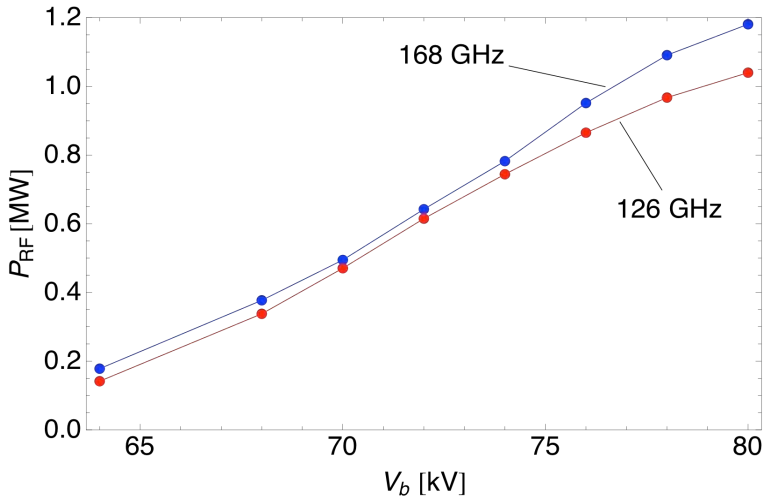

Fig. 3.5.7 *Radiated RF power versus beam energy for the two frequencies (126GHz, $TE_{26,6}$ and 168GHz, $TE_{35,9}$) calculated with the self-consistent mono-mode time-dependent code TWANG developed at CRPP. The electron beam parameters are I_b=40A, $\langle\alpha\rangle$=1.3, $\delta\alpha$=5% and the magnetic fields are 5.02T and 6.7T respectively.*

From the technical and implementation point of view, this upgrade minimizes the intervention on TCV itself, thus maintaining the operational capabilities while the technical part of the X3 upgrade would be carried out. The existing EC system is fully compatible with the foreseen X3 upgrade, which, with the implementation of 1MW gyrotrons, will be operated in ITER relevant conditions.

3.6 Superconductivity

3.6.1 Failures of the electric motor of the compressor of the SULTAN refrigerator

In 2009, the 750kW motor of the main compressor of the SULTAN cryo-plant failed after 25 years of operation and was repaired by replacing the full winding. The interruption of the test operation in SULTAN lasted about 11 weeks, including the re-cooling of facility after re-start of the refrigerator.

On May 21st 2010, the motor failed again, with a short in the winding. The winding was replaced and the motor was re-started on June 24th 2010. On the same day, another failure (short circuit inside the winding) destroyed once more the motor, see fig. 3.5.1. The reason of both failures could not be clearly identified, but the company took responsibility for both repairs. Eventually, the motor was delivered to CRPP on August 9th 2010 and the re-cooling of SULTAN was completed on August 20th, exactly three months after the initial failure.

Since August 11th, the motor runs without disturbances. Additional temperature sensors in the winding and interlocks in the control system have been built to prevent any overheating. A spare motor is procured under contract with ITER Organization at the end of 2010 in the scope of protective investments to improve the reliability of the test operation in SULTAN, see section 4.5.

Fig. 3.6.1 *Damage of the motor winding: May 2010 (left) and June 2010 (right)*

3.7 Gyrotron for Dynamic Nuclear Polarization Enhanced Magic Angle Spinning (MAS) Nuclear Magnetic Resonance (NMR) Spectroscopy[*]

The delivery and commissioning of the He-free 10Tesla/75mm warm-bore superconducting (SC) magnet to be used with the gyrotron has been successfully completed in March 2010. It is worth mentioning that, to our knowledge, this is the first SC-magnet installed at EPFL making use of this advanced technology allowing to operate a SC system without any liquid helium. In addition, a NbTi SC has been used to fulfill the requirements on magnetic field profile precision. With this type of SC-wire, only the He-free technology allows to operate this magnet at 10Tesla since the operating temperature is at 3.5-3.6K, therefore giving sufficient safety margin in terms of critical magnetic field and current density.

Due to administrative issues associated to the gyrotron manufacturer, the gyrotron delivery has been significantly delayed and is presently foreseen for the first-half of 2011.

Using the low-power microwave equipment procured within the “SNSF Requip-grant”, an optical table has been set-up for detailed studies of the μwave magnetic field spatial distribution inside the sample located in the NMR-probe. This is relevant for assessing the global enhancement associated to DNP. In parallel to this experimental activity, detailed simulations with the commercial finite element software COMSOL multi-physics has been initiated. From the modeling point of view the main difficulty is associated to the fact that a MAS-NMR probe is a highly heterogeneous electromagnetic system and that it is a highly overmoded system since the wavelength of the μwave is significantly smaller than the characteristic probe-size.

[*] Work not belonging to the EURATOM Association's work programme.

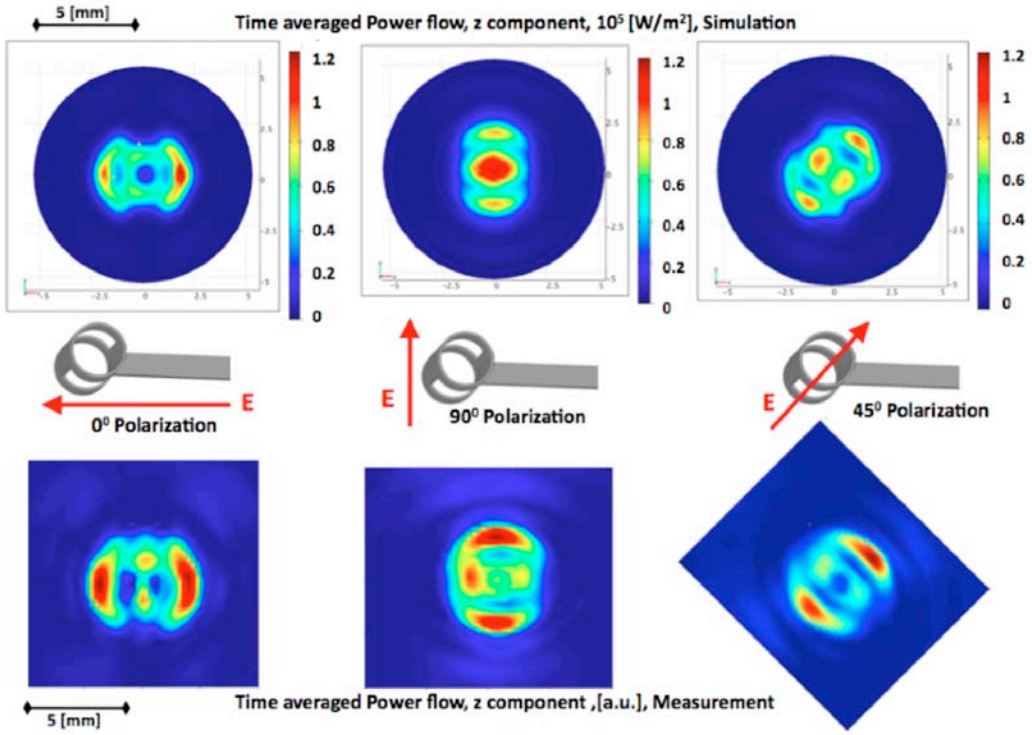

Fig. 3.7.1 *Comparison between the simulated (top row) and measurements (bottom row) of the z-component of the time-averaged Poynting vector at the output of the NMR saddle-coil. The 263.5GHz gaussian beam injected into the saddle coil has a waist of 1.67 [mm] and is located at the saddle-coil entrance. This study is performed for three linear polarizations of the incoming gaussian beam.*

As shown in Fig. 3.7.1, a good agreement is found between the simulated and measured quantities. This validation is extremely important because the field inhomogeneity in the sample will be only calculated via simulations since it cannot be measured experimentally.

A novel technology to manufacture a HE_{11} corrugated waveguide for efficiently transmitting the μwave from the gyrotron to the NMR sample has been developed. A prototype 80cm long section has been designed, manufactured and is presently being characterized with respect to its μwave properties. This design is compatible for transmitting μwave in the THz domain and its patenting is presently underway.

4 ACTIVITIES IN SUPPORT OF ITER

4.1 Introduction

Most of the research programme of CRPP is related to fusion development in general and to ITER in particular. In this chapter we assemble the more specific activities directly linked to the ITER project. They are covered by IO, F4E or Domestic Agencies grants and contracts.

4.2 ITER 170GHZ gyrotron and its test facility

4.2.1 Coaxial Cavity Gyrotron refurbished First Prototype

Summary of the activities

A contract for the refurbishment was signed between F4E and Thales by end of July 2009. The refurbished tube delivery was expected by mid of October 2010.

At the end of the manufacture, during the bake-out cycle, a leak developed at the interface between the collector and the insulator ceramic. A careful inspection revealed that 2 other leaks, located at the CVD window and on one of the internal water loads, are present. The tube delivery is postponed to end of March 2011.

In parallel, the gyrotron development activities covered by F4E Grants continued.

Refurbishment (contract F4E-2008-OPE-09)

In parallel to the procurement of long lead replacement items (approximately 14 weeks for the ceramic insulator), investigations are pursued in order to find the cause of the problem and to assess whether the diamond disk should be replaced (a spare item is available).

In case of necessity to replace all the internal water loads, the tube should be taken apart at a deeper level and this could cause an additional delay in the delivery. The optimistic option (no change of the water loads) foresees a delivery by end of March 2011.

As a consequence, no recommendation about the decision between the 2MW/Coaxial and the 1MW/Conventional options could be made in March 2011 as was initially foreseen. However, the European strategy remains in line with the Coaxial Tube development.

Mock-up tests

The first item delivered to CRPP in the frame of the refurbishment contract (OPE-09) was a maquette of the new gun. It reproduces the geometry of the gun, the beam-tunnel, the cavity and the launcher of the tube, but has no emitter. An

additional design criterion, consisting in avoiding the presence of any potential well, yielding to trapping of secondary electrons, was applied.

The new gun voltage stand-off was successfully checked with and without magnetic field. By changing the magnetic field configuration, it was confirmed that the stand-off properties would dramatically be affected by the presence of a potential well, confirming their dominant role in the poor behavior of the first prototype tube.

This, along with a much more robust electron beam design (the perpendicular velocity spread has been minimized), gives a very positive and encouraging sign about the possibility for the refurbished tube to reproduce the excellent results obtained at KIT with the short pulse prototype.

On-going activities

Even in the absence of running high power experiment at CRPP, development activities related to the ITER gyrotron are continued under the following F4E Grants and supply contracts:

Grant GRT-08, Development of the European Gyrotron ("CCGDS6"), managed by CRPP

The ending date of this grant was June 30st, 2010. All the activities are closed and the final ADP (Acceptance Data Package) is under preparation.

Grants GRT-034: Analysis of design issues, Interfaces and preparation of the Procurement Arrangement for the ITER gyrotron, managed by KIT

An analysis of the gyrotron operation in the environment of ITER is performed under this grant. It involves taking into account the ITER stray magnetic field, the field of the other gyrotron magnets, and the building structure considered as a ferromagnetic material. For this study, an extended version of the 3D ARIADNE code and the commercial software COMSOL Multiphysics were used.

The gyrotron Procurement Arrangement description is also covered by this grant.

Grant GRT-049, Design and Development of the European Gyrotron ("CCGDS7"), managed by KIT

The CRPP is involved in the continuation of electron gun studies, in experimental and theoretical investigations on the causes and consequences of RF parasitic oscillations.

In this frame a new self-consistent time-dependent monomode code, TWANG, was developed for modeling the wave-particle interaction in the gyrotron cavity. One specificity of this code is the finite element numerical technique used for solving the wave equation. This code has been benchmarked and validated against other codes based on a finite difference solution (EURIDICE and SELFT) of the wave equation. Preliminary theoretical studies showed that the TWANG code is adequate for studying parasitic instability potentially occurring in the launcher section and called After Cavity Interaction (ACI).

Within this Grant, CRPP is also responsible for the follow-up of the gyrotron refurbishment. The design review for the technical specifications of the second prototype gyrotron is also covered by this grant, as well as the scientific participation to the tests with the refurbished tube.

Grant GRT-054, Tests with the refurbished 2MW First Prototype Gyrotron, Managed by CRPP

This grant mainly covers the technical operation of the test stand. Some improvements of the data and control acquisition system are being implemented. The superconducting magnet power supplies have been changed to gain stability, and the purchase of a new diagnostic to detect possible parasitic oscillations is necessary.

OPE-094 Supply of Mirrors for the RF-Conditioning Unit (RFCU)

A supply contract between F4E and CRPP has been signed for the procurement of new mirrors for the RFCU. This is necessary because of the updated, and improved radiation pattern of the refurbished tube.

Prospects

Due to the bake-out problem, the tube is now expected to be delivered by the end of the first quarter 2011 (optimistic estimate).

Deeper investigation of the physical mechanisms involved in the formation and saturation of potential wells will be carried out on the mock-up gun. This will be the subject of a newly started PhD thesis.

4.3 C-GT170 Test facility

The MHVPS (Main High Voltage PS) supplying the cathode of the gyrotron at the rated DC output values of -60 kV, 80A, CW has been further tested. CRPP operated the MHVPS on dummy load in order to:

- Apply repetitive pulses during several days to heat up the components with higher thermal constant, like the transformers. These tests allow also verifying the correct operation of the cooling system regulating the room temperature.
- Integrate the control system into the ITER gyrotron test facility control system.
- Implement the possibility to control synchronously both power supplies (MHVPS and BPS) mandatory for the future gyrotron operation.

Improvements to be brought to the MHVPS installation, as to the other test facility equipment, have been identified and agreed in view of the next tests campaign of the 2MW EU gyrotron. Among them, the most important are:

- The exchange of the flow detectors on the MHVPS parallel water cooling circuits which were not adapted to the flow and pressure available on-site,

and which were influenced by electrical transients (EMC) during fast modulation tests.
- The improvement of the synthetic material layer placed under the MHVPS transformers support structure to damp the low frequency resonance transferred from the active parts to the building structure.
- The installation and testing of new power supplies to be connected to the SCM (Superconducting Magnet) coils to improve the operation robustness in case of fast transients like arcs.
- The modification of control logic driving the cathode heating power supply to offer the possibility to the Test Facility operator to promptly restart the cathode heating current in case of shutdown due to short vacuum perturbations.
- The adaptation of the acquisition system to implement an easiest way of acquiring data during repetitive pulses, e.g. during gyrotron conditioning.

By the end of the year still minor improvements will be brought to the Test Facility installation and control before the refurbished gyrotron will be delivered for testing in 2011.

4.4 The ITER Upper Launcher for Electron Cyclotron Waves

4.4.1 Completion of the preliminary optical design and preparation of technical documentation (mm-wave design & components) for the ITER Upper Launcher Preliminary Design Review (Contract F4E-2009-0PE-050-01)

This service contract covered the work to deliver and present the design, analysis and documentation on the mechanical and optical design of the ITER Electron Cyclotron Upper Launcher at the Preliminary Design Review (PDR) that took take place from the 16th to the 20th of November 2009 at ITER IO in Cadarache, France. The design presented was the outcome of the previous ECH-UL contract EFDA/06-1404, established in 2006 and finished 2008. The work received a very positive evaluation by the international ITER IO expert panel and the other Domestic Agencies participating to the PDR, resulting in the formal acceptance of the mm-wave optical system (UL-OS) designed by CRPP. Among the conclusions of the PDR was the compilation of issues related to technical and physics aspects of the UL-OS. These issues will be addressed within the framework of an impending call for tender, expected by the end of 2010, for the final design and prototyping in preparation of the procurement of the four Upper Launchers.

4.4.2 Service for the EC UL Prototype and test Program Review of the Optical System (Contract CT-10/4300000187)

This small service contract covered the work to assist IO in evaluating a preliminary prototype test plan for the structural and mm-wave components of the EC Upper Launcher. These tests are to be used to validate the optical design, critical components and assemblies of the UL optical system (UL-OS) prior to the final design review (scheduled in January 2013) and evaluate the prototype test plan in terms of scope, schedule, costs and quality. The results of this work are used by

both ITER IO and F4E to establish the procurement planning for the four Upper Launchers and the impending call for tender, expected by the end of 2010, for the final design and prototyping.

4.5 Superconductivity ITER studies

4.5.1 Tests in SULTAN

The activities in support of ITER are focused on the test in SULTAN of the ITER conductors, carried out under bilateral contract with the Domestic Agencies. In 2010, following samples have been tested:

1. PF234, qualification sample for the poloidal field conductor of coils PF2/PF3/PF4, under contract with ASIPP, in May 2010.
2. KOTF3, process qualification sample for the Korean Toroidal Field conductor, under contract with KO-DA, including sample assembly, August 2010.
3. PF1/6, qualification sample for the poloidal field conductor of coils PF1/PF6, under contract with F4E, in September 2010.
4. CNTF2, qualification sample for the Chinese Toroidal Field conductor using internal Sn strand, under contract with ASIPP, including sample assembly, September-October 2010.
5. JACS1, qualification sample for the Japanese Central Solenoid conductor, under contract with JA-DA, October-November 2010.
6. CNTF3, qualification sample for the Chinese Toroidal Field conductor using bronze strand, under contract with WST, including sample assembly, November 2010.
7. Trasek, conductor sample for the secondary winding of the EDIPO transformer, under contract with F4E, December 2010.
8. JATF5 and JATF6, qualification and process qualification sample for the Japanese Toroidal field conductors, under contract with JADA. Sample assembly October-December 2010, test in SULTAN will be carried out in 2011.

For each test in SULTAN, a detailed report including results assessment is handed to the respective Domestic Agency.

The six ITER conductor samples (3 for Toroidal coils, 2 for Poloidal coils and 1 for Central Solenoid) belong to the ITER Conductor Qualification phase. The Trasek sample is made from a left section of the conductor developed at CRPP for the superconducting transformer of the EDIPO facility. It is tested in SULTAN for full characterization over a broad operating range up to 100kA. The T_c test on one single section of TF conductor is carried out in the scope of a PhD thesis aimed at deducing the strain state, ε, of the Nb_3Sn filaments inside a Cable-in-Conduit Conductor (CICC) through the in-situ measurement of the critical temperature, which is a known function of the strain, $T_c(\varepsilon)$.

The sample preparation at CRPP for the three TF samples was identical as in 2009, with solder filled joints. A typical test campaign for ITER TF samples lasts three weeks including cool-down and warm-up, with a target of 1000 load cycles. An intermediate warm-up is done before the final test. The performance of the conductors in terms of current sharing temperature, T_{cs} at a background field of 10.78T and 68kA (nominal ITER operation), is gathered in the three plots of

Fig. 4.5.1. The results assessment is done straight from the raw data, as the baseline of the V-T plot has no significant slope. At large, the performance degradation upon cyclic load is similar to the former ITER TF samples, with a drop of T_{cs} in the range of 0.3K-0.5K. For all the three samples, the two conductor legs are identical. However, some performance difference, up to 0.3K is observed between right and left conductor in the same sample. All the TF samples fulfill the ITER criterion of 5.7K for T_{cs} after 1000 load cycles and one thermal cycle.

The left conductor of the CNTF3 sample was subjected to 15 thermal cycles from room temperature to liquid nitrogen prior to the SULTAN test. The final test results suggest that the thermal cycles before the SULTAN test have no impact on the performance.

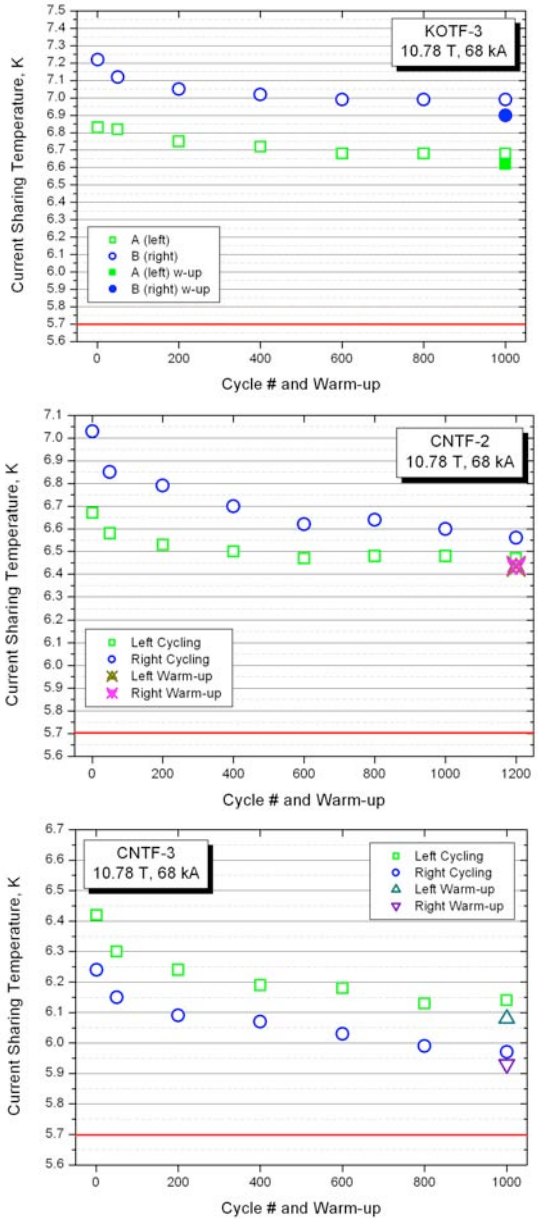

Fig. 4.5.1 *Summary of the T_{cs} results of the three ITER TF conductor samples tested in SULTAN in 2010. From top to bottom, the KOTF3, the CNTF2 and the CNTF3 sample.*

The two ITER PF conductor samples are designed for use in the PF1 and PF6 coils (EUPF1/6, also named SSPF1) and in the PF2, PF3 and PF4 coils (CNPF1, also named SSPF2). The DC performance of the two NbTi CICC is consistent with the strand performance, as in all NbTi conductors previously tested. The AC loss was measured in both samples at the background field of 2T and 5T, see Fig. 4.5.2. In both conductors, the power generated by the 5Hz AC loss under realistic operating conditions was sufficient to raise the temperature above the current sharing temperature and drive a quench.

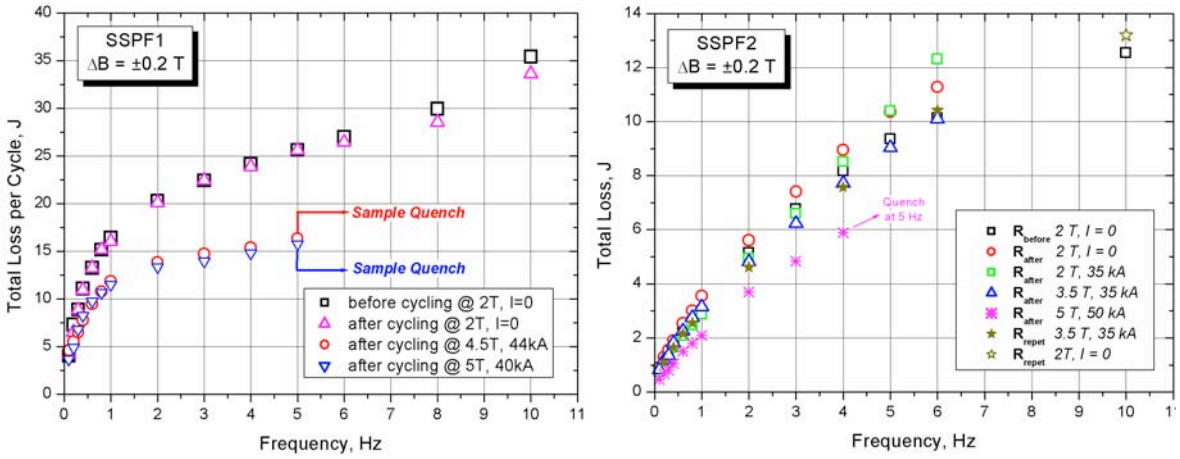

Fig. 4.5.2 *The AC loss curves under various operating conditions for the two ITER PF conductor samples*

In both PF conductor samples, the take-off electric field in the DC test was very low. At the nominal operating current (44kA for PF1/6 and 35kA for PF234), the take-off was lower than the 10μV/m criterion for T_{cs}, see Fig. 4.2.3.

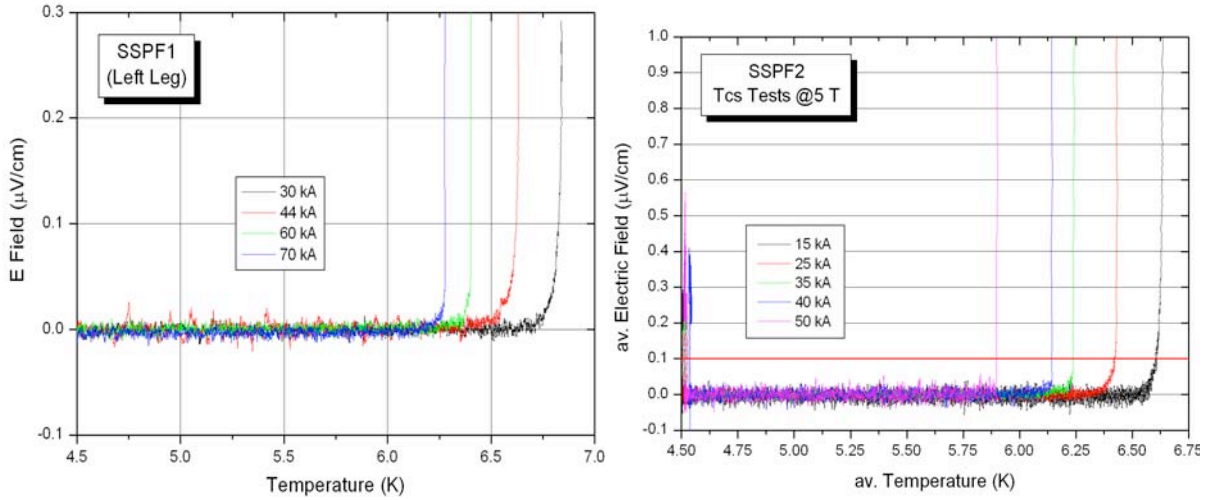

Fig. 4.5.3 *DC transition, with take-off electric field, vs. operating current for the two ITER PF conductor samples.*

The JACS1 sample, assembled in Japan, is the first ITER sample relevant for the Central Solenoid conductor, which must endure over 50000 load cycles over its lifetime. The test program has foreseen 10000 load cycles in SULTAN, with the

expectation that the performance degradation stabilizes after few hundred cycles. In fact, the performance initially improved after few cycles, possibly due to a slippage of the cable inside the jacket, causing a relaxation of the axial compressive strain. With increasing number of cycles, the performance dropped continuously. After 6000 cycles, the T_{cs} was already below the acceptance level and the thermal cycle, planned after 10000 cycles, was anticipated. After the thermal cycle, the performance was so poor that no more test was possible at the operating conditions, see Fig. 4.5.4.

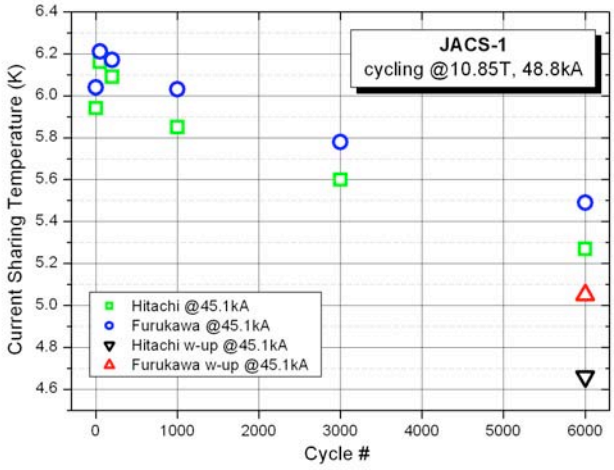

Fig. 4.5.4 *Summary of the T_{cs} measurements on JACS1 along the cyclic loadings and after final warm-up/cool-down.*

The Trasek sample is made from a left section of a NbTi CICC designed and procured by CRPP for the secondary winding of the superconducting transformer (flux pump) for the EDIPO test facility. The conductor must carry DC current up to 100 kA in low magnetic. In the conductor design, high Cu:non-Cu ratio in the strand (no copper segregation), low void fraction and Sn coating of the strand surface are selected to allow smooth current redistribution and enhance the take-off voltage even at high current. The behaviour of the take-off electric field versus the cable current density is the main object of the DC test to assess the impact of self-field instability. For operating current up to 80kA, a smooth transition is observed, see Fig. 4.5.5.

In normal operation, the secondary coil of the transformer is not exposed to significant magnetic field sweeps. The AC loss is expected to be large according to the design choices (tin coating, low void fraction). The AC loss test in SULTAN, see Fig. 4.5.6, clearly show a shift of the peak of the loss curve and hence of the time constant of the coupling currents from about 200ms initially to about 100ms after 200 load cycles.

The pressure drop of the TRASEK conductor is not critical because of the short hydraulic length of the secondary coil, but it is measured in SULTAN to complement the data base for friction factor of CICC's, see Fig. 4.5.7.

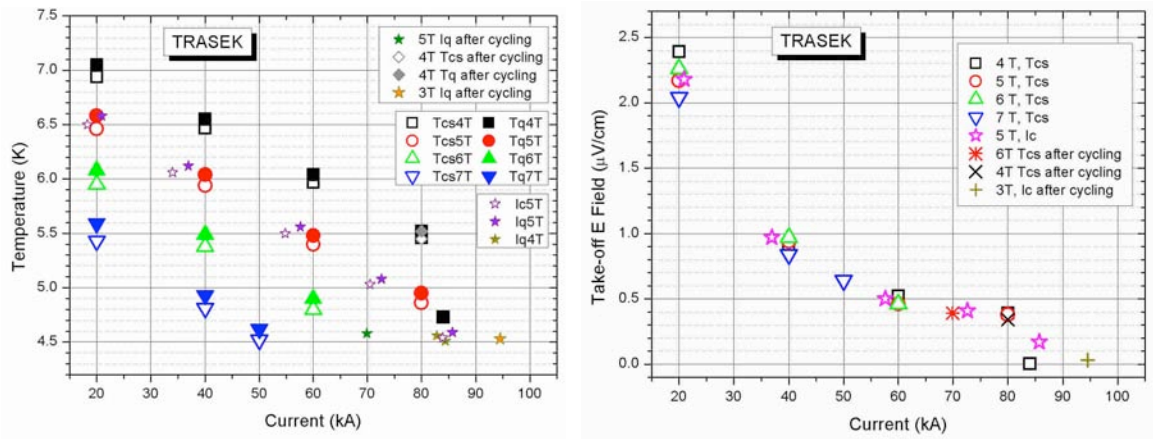

Fig. 4.5.5 *Summary of DC performance and take-off electric field of the Trasek sample*

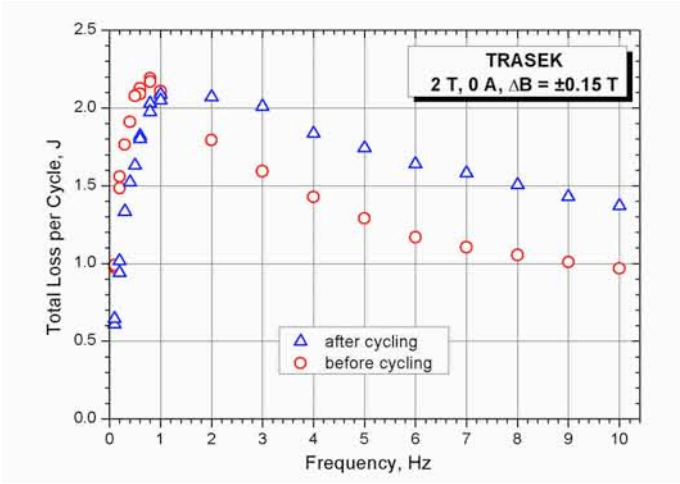

Fig. 4.5.6 *Summary of the AC loss measurements on Trasek sample before and after cyclic loading*

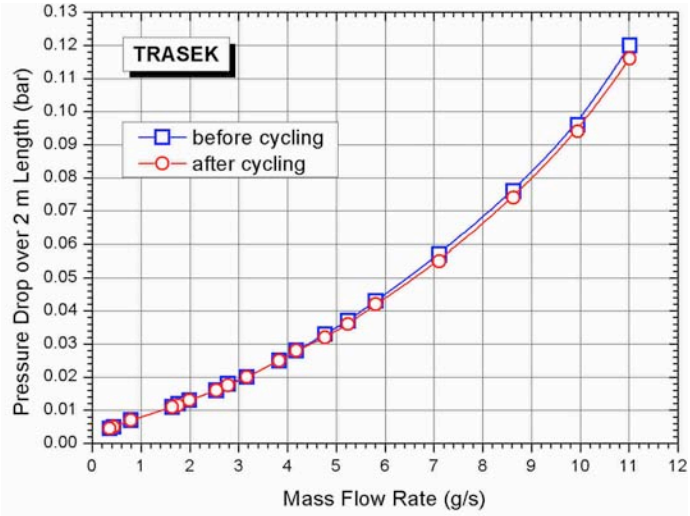

Fig. 4.5.7 *Pressure drop results on Trasek sample*

4.5.2 Protective Investments

A contract was placed in October 2010 by the ITER Organization to procure a spare motor for the SULTAN refrigerator (see also 3.5), a second vacuum furnace to support the intensified preparation of the Nb_3Sn ITER conductors and a new set of instrumentation cables. The procurement actions just started at the end of 2010.

4.5.3 Critical Temperature Measurements

A contract was placed in October 2010 by the ITER Organization to carry out critical temperature (T_c) measurements on a TF conductor section and on free-standing strands used for the same conductor. The selected conductor is from the KOTF3 sample, tested in August 2010. The T_c test for the free-standing strand is carried out in a small solenoid, for the TF conductor section in SULTAN. In both cases an inductive method for T_c is applied. The tests have been completed by the end of 2010.

4.5.4 Thermal cycles of a TF conductor section

In the scope of a supplementary agreement (2010) of the contract placed by the ITER Organization in 2009, CRPP has carried out thermal cycles (cool-down/warm-up from room temperature to liquid nitrogen) for one section of heat treated TF conductor for CNTF3. A total of 15 cycles were applied during one week in October 2010 into an evacuated pipe with heaters and temperature sensors set-up for this purpose. The performance of the conductor section will be compared with the other section of CNTF3, which did not undergo thermal cycles.

4.6 The development of the ITER magnetic diagnostics

During the last week of 2009 an F4E grant was signed, F4E-2008-GRT-012 (PMS-DG), entitled “R&D on ex-vessel magnetics and construction of a magnetics test facility”. The suppliers are CRPP, CEA-Cadarache and RFX, with the CRPP as Lead Member and CEA providing the largest fraction of the manpower. A Kick-Off-Meeting was held early April 2010 and the work should complete by early 2011. The principal components of the Task are threefold, namely: the development of requirements for qualifying and calibrating the full set of magnetic diagnostics for ITER, the production of prototypes of the ex-vessel inductive sensors and variants of TF coil Rogowski cable for measuring the toroidal current and finally the qualification of those prototype components. The work has progressed with little delay and the prototypes are expected within 2 weeks of the time of writing. The qualification tests will be shared between CEA and CRPP and the test rigs are already under assembly.

During 2010 a call for a larger F4E grant was made and a proposal was developed between CRPP, CEA-Cadarache, RFX, CIEMAT, SCK-CEN, CCFE and an industrial supplier of electromagnetic modelling. Regrettably, this proposal was not accepted

and the staff who were expecting to work on the ITER magnetics have been redeployed.

Work continued on prototyping novel high frequency sensors using Low-Temperature Co-fired Ceramics in different configurations, work carried out in collaboration with the EPFL Laboratoire de Production en Microtechnique. The solutions have been proposed to ITER. CRPP has participated in the magnetics Conceptual Design Review held in November 2010.

CRPP has led a working group on the diagnostic requirements for MHD stability control in ITER, assembling the ITPA expertise and opinions. This work has nearly completed. CRPP has led a revision of the specific detection amplitude requirements for Alfvén Eigenmodes, based on our experience at JET, and this revision has now been taken on board by ITER, albeit with difficulty. The requirements on mode identification have been examined in great detail by CRPP and we are proposing an increase in the number of sensors, to expand the range of mode identification, although this will increase cost somewhat, we are simultaneously proposing to reduce the data acquisition speeds, which will save money to compensate

4.7 ITER discharge simulation

At the end of 2009 an ITER IPT (Internal Project Team) was created with representation from all partners. A second meeting was held in summer 2010. CRPP is active in this group which is assisting ITER in the development of the highest level requirements for controlling the pulses.

Within the context of plasma control simulation, two ITER calls were responded to in 2010. The first provides conceptual and engineering design support to the ITER Fusion Science and Technology department for the development of integrated tokamak modelling. A consortium between CEA (as lead member), CRPP, Chalmers and Corys is in the phase of final negotiations on this framework service contract, which should last for 3 years. The second provides support for developing Error and Exception handling within the plasma control system. A consortium between Sopra Group as lead member and CRPP was assembled but the proposal was not accepted.

Currently, a consortium is being assembled with a view to providing full tokamak modelling services to ITER through an F4E grant, GRT-255, with CCFE (as lead member), CREATE, CRPP, CEA-Cadarache and TU Wien. This proposal is under examination at present, but if awarded would place CRPP and CEA-Cadarache as partners in the modelling of the ITER hybrid scenarios, using the DINA-CH & CRONOS suite developed in 2007-2009.

A research activity has recently started as a PhD project to develop scenario optimisation and limit avoidance and small exception handling, as proposed at the IPT plasma control meeting in December 2009. In order to carry out this work, the structuring of the DINA-CH simulator has been modified to correspond more closely to the architecture of the ITER CODAC and Plasma Control System, and to provide a clearer location for the limit avoidance and optimisation functions. At the same time, we are attempting to align the data handling with the ITM concepts, where this is possible and reasonable.

4.8 F4E and IO committees

CRPP staff contributed to F4E Technical Advisory Panel and ITER Council Science and Technical Advisory Committees.

5 INTERNATIONAL AND NATIONAL COLLABORATIONS

5.1 Exploitation of the JET facilities

5.1.1 Control of MHD instabilities

As reported in the 2009 annual report, experiments have been carried out under the JET Task Force MHD to investigate the mechanism for sawtooth control using toroidally propagating ion cyclotron resonance heating (ICCD). New experiments, exploiting the lessons learned from both theory and dedicated experiments, were devised employing higher power ICRH with the aim of controlling monster sawteeth. NBI ions, injected at higher power, played the role of alpha particles in ITER, and the trapped fraction of the NBI ions initially created monster sawteeth. The application of -90° phased ICRH with minority He^3, and resonance close to the q=1 surface on the high field side, greatly reduced the sawtooth period. This was undertaken also in H-mode, and as a result, improves the prospect of sawtooth control via ICRH in ITER. Finally, new experiments have been designed, and experiments proposed at JET in order to improve real time control techniques, and to attempt sawtooth control employing He^3 minority with resonance on the low field side. This will require a very high toroidal magnetic field (B>3.45T).

5.1.2 Collaboration on Alfvén waves and fast particles studies

The study of Alfvén waves and their interaction with fast particles is an important topic in the JET programme. This work is undertaken using passive measurements of fast-ion driven instabilities, and active measurement of antenna-driven modes, obtained using the KC1T diagnostic system, which was designed, built, commissioned and routinely operated by CRPP staff.

During the period covered in this report, JET has been in a major shutdown for the installation of the ITER-like wall, hence our activities have mainly focused on the analysis of the data collected during the C20-C27 experimental campaigns, and on the preparation of the documentation and public data analysis package for the handover of the KC1T diagnostic system to the JET operator.

During the C20-C27 JET experimental campaigns, measurements have been taken routinely of the frequency and damping rate of Toroidal Alfvén Eigenmodes (TAEs) with toroidal mode number (n) in the range $|n|<20$, making full use of the new Alfvén Eigenmodes Diagnostic system (KC1T) in support of JET operation. The analysis of the data collected during these experimental campaigns has taken advantage of the real-time and post-pulse implementation of an algorithm based on the Sparse Representation of Signals and the SparSpec code. An example of this analysis is shown in Fig. 5.1.1(a-c) for the JET shot #77788, where the KC1T system was configured to predominantly drive an odd-n spectrum, peaked towards the lower mode numbers $|n|=3,5,7$, with a negligible drive for components with $|n|>10$.

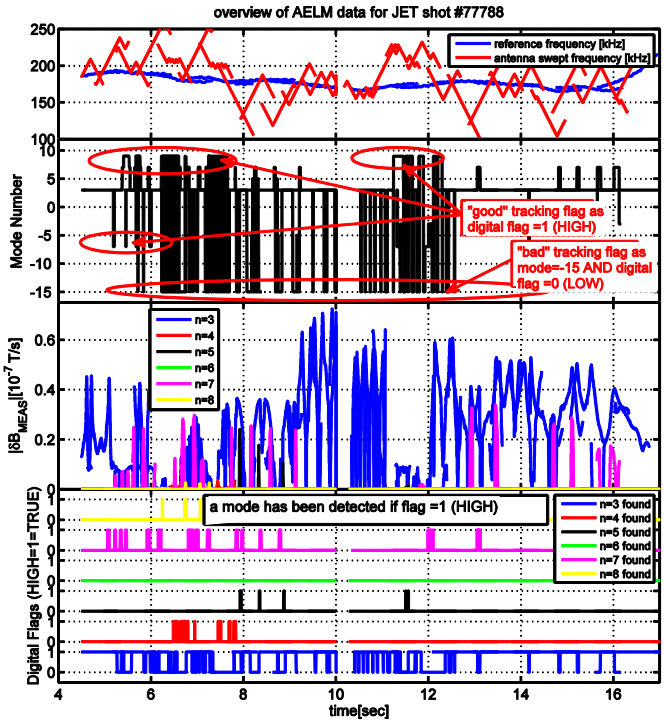

Fig. 5.1.1 *An example of real-time tracking of individual n=3-8 TAEs for the shot #77788; the analogue signal $|\delta B_{MEAS}|$ shows the amplitude of each individual mode as detected in real-time. Note that only very few even-n resonances (n=[4,6,8]) are detected in real-time (and confirmed by post-pulse analysis, see Fig. 5.1.1c), compared to the number of n=3 resonance; second, the n=3 mode dominates the detected spectrum, as this is the one for which the KC1T system produces the maximum drive.*

We show separately the detection of all modes with 3≤n≤8 (Fig. 5.1.1), and the detection of odd-n modes rotating in the co-current (positive n's, the preferential direction for the usual tokamak magnetic equilibrium) and counter-current (negative n's) direction, with |n|=[3,5,7] (Fig 5.1.2). All the digital signals shown at the bottom of Figa 5.1.1 and 5.1.2 indicate whether detection and tracking of a certain mode has been successful: if the flag is set to high (=1), then the corresponding mode has been correctly detected and tracking is occurring, otherwise the digital signal is set to low (=0). At the start of each real-time scan t, the global "mode" value is initialised to a "bad" tracking value of n=-15 and its associated digital validity flag is set to 0. When a mode is successfully detected, the "mode" value is set to n and the validity flag is set to 1. From Fig. 5.1.1, we note that only very few even-n resonances (n=[4,6,8]) are detected in real-time (and confirmed by post-pulse analysis), compared to the number of n=3 resonance; second, the n=3 mode dominates the detected spectrum, as this is the one for which the KC1T system produces the maximum drive. Finally, Fig. 5.1.2 demonstrates that not only co-and counter-rotating modes with the same |n| can be perfectly distinguished in real-time, but also that the plasma preferentially supports co-rotating modes (which are driven with the same amplitude as the corresponding counter-rotating modes). This result allows us to discriminate whether the pressure profile of any resonant fast ion population is peaked on axis (reducing the damping rate of co-rotating modes) or off-axis (reducing the damping

rate of counter-rotating modes), with important consequences for plasma control and burn optimization.

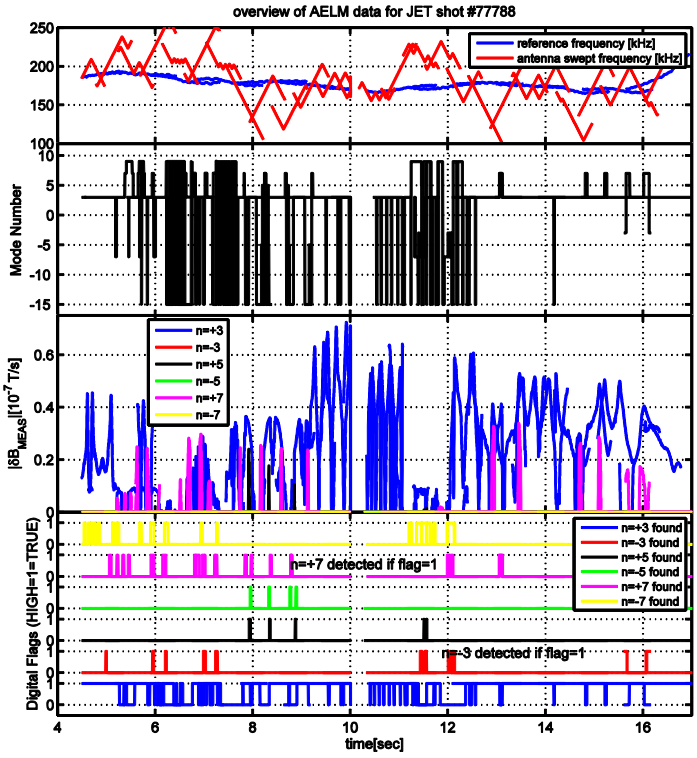

Fig. 5.1.2 *An example of real-time tracking of individual n=±3, n=±5, n=±7 TAEs for the shot #77788. Note that not only co-and counter-rotating modes with the same |n| can be perfectly distinguished in real-time, but also that the plasma preferentially supports co-rotating modes (which are driven with the same amplitude as the corresponding counter-rotating modes)*

For comparison, in Fig. 5.1.3 we show the results of the post-pulse analysis using the full implementation of the SparSpec algorithm. A statistical analysis of the real-time vs. the post-pulse data (performed over many different discharges) indicates that the toroidal mode number and the mode frequency are detected in real-time with a confidence level >90%, the confidence level in the damping rate data being ~70%; this confirms the overall accuracy of the real-time calculations. The mode amplitude cannot be directly compared as, due to computational reasons, in real-time we do not perform the renormalization needed because of the λ-penalization term.

During 2010 another important focus of our work has been a detailed analysis of the dependence of the damping rate of the n=3 and the n=7 TAEs as function of the edge elongation. In JET, the edge plasma shape and magnetic shear have been found to be key ingredients for increasing the damping rate of stable, antenna-driven low-n (n=1, n=2) and unstable, fast-ion driven, medium-n (n~3-10) TAEs. This has motivated experimental studies on the Alcator C-mod tokamak where it was found that the damping rate of an n=6 TAE remains essentially invariant when the average edge triangularity (δ_{95}) is scanned in the range $0.3<\delta_{95}<0.7$. Conversely, the data obtained for the n=3 and n=7 TAEs during the two otherwise similar JET discharges presented in Fig. 5.1.4 show an almost linear increase of the damping

rate as a function of the edge elongation (κ_{95}). Hence, increasing κ_{95} has in JET the same effect on the damping rate of these medium-n TAEs as on the n=1 and the n=2 TAEs. This result further confirms that the same damping mechanisms acting upon global, low-n modes, play also an important role for the stability of core-localised medium-n TAEs, opening interesting perspectives for their real-time control in burning plasma experiments.

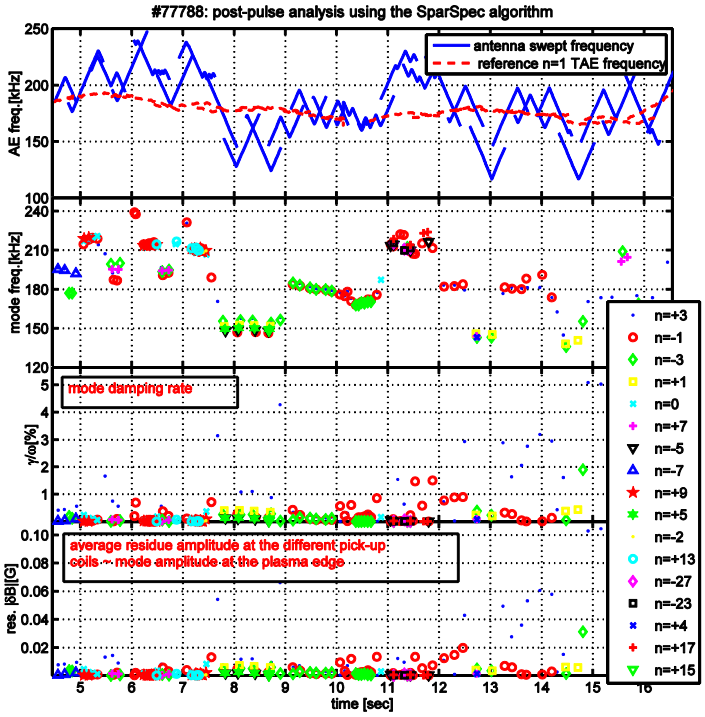

Fig. 5.1.3 *The results of the post-pulse analysis using the full implementation of the SparSpec algorithm, confirming the accuracy of the real-time measurements.*

The two discharges shown in Fig. 5.1.4 have been used for detailed comparisons with theory and models in the framework of the ITPA work-program. Figure 5.1.4 also shows the results of the simulations performed with the LEMan, TAEFL and CASTOR codes. Both the LEMan and the TAEFL codes model the actual plasma shape using a magnetic configuration which is up/down symmetric, but non-circular. This work has led to a number of conclusions, namely that in order to provide a quantitatively correct modelling of this damping rate measurements it is essential to (a) retain the up/down asymmetry in the plasma poloidal cross-section, (b) include a large number of poloidal harmonics in the calculations, and (c) have a very accurate reconstruction of the density and safety factor profiles.

The LEMan results show that, for the cases where the actual plasma poloidal cross section is sufficiently up/down symmetric, the mode frequency and damping rate are in good agreement with the measurements (mode frequencies within 10%, damping rates within ~50%), this exercise also demonstrating that a rather large number of poloidal harmonics needs to be used to reproduce quantitatively the measured γ/ω even for moderately low-n modes. Conversely, when the up/down asymmetry in the poloidal cross-section is not correctly retained in LEMan (i.e. for κ_{95}>1.45), there can be a much larger discrepancy, up to a factor ~4, between the

measured and the calculated damping rates, although a slightly different selection of the input profiles used for the analysis may also account for this difference.

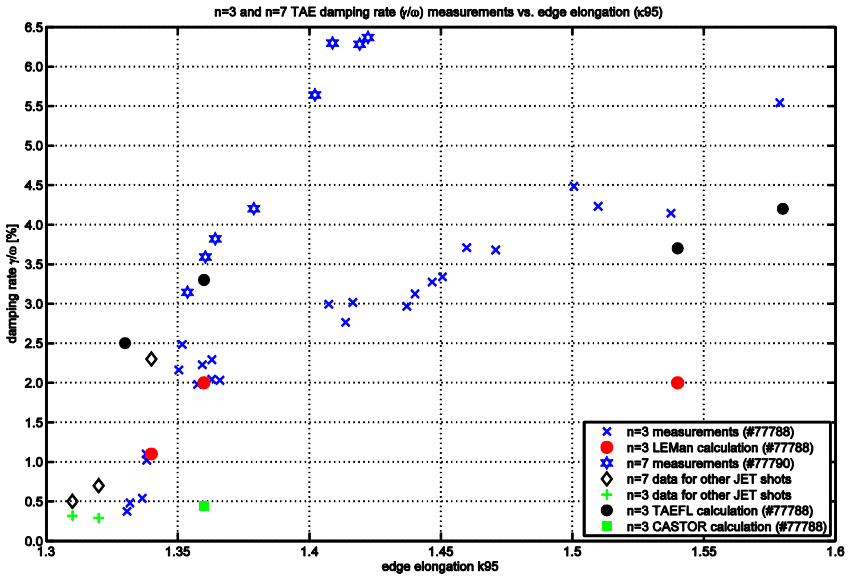

Fig. 5.1.4 *Damping rate data for the n=3 and n=7 TAEs as function of κ_{95}, showing a linear dependence $\gamma/\omega=f(\kappa_{95})$, compared with the results of the LEMan, TAEFL and CASTOR simulations.*

The TAEFL code is a reduced MHD initial value code that uses gyrofluid closure techniques for the energetic ions to incorporate the Landau resonance effects that destabilize Alfvén modes. Since only unstable modes can be analyzed by TAEFL, the technique used was to start with an unstable Alfvén mode, vary the fast ion drive and extrapolate back to zero drive in order to determine an effective damping rate. Fast ion profiles/parameters are chosen that lead to a mode very close to the frequency excited by the antenna. This model incorporates ion/electron Landau damping, continuum damping and radiative damping (due to finite ion Larmor radius) effects. It uses Fourier spectral representations in the poloidal and toroidal directions and finite differences in the direction normal to the flux surfaces. The TAEFL simulations of JET plasmas used 300-400 radial points and 26 Fourier modes (m=0→25). The TAEFL results are in very good agreement with the measurements for relative high values of the elongation (κ_{95}>1.45), whereas the discrepancy at lower values of κ_{95} is somewhat larger.

The CASTOR code predicts an n=3 mode at 184kHz (in good agreement with the measurement: f_{MEAS}=179kHz) with a damping rate γ/ω_{CASTOR}=0.44%, compared to γ/ω_{MEAS}~2.0%. The discrepancy with the measured damping rate can be due to small uncertainties in the q- and/or density profiles, and to the absence of kinetic effects. For instance, slightly different values of q- or density at ψ_N~0.55 can make the mode intersect the continuum and increase γ/ω_{CASTOR} by a factor of 2, and kinetic effects such as radiative and Landau damping have been shown to play an important role with other codes such as LEMan and LIGKA. Hence continuum damping, which is the only mechanism included in these CASTOR simulations, can only account for a fraction of the measured damping rate, which clearly suggests that other mechanisms make important contributions to the total damping.

5.1.3 General diagnostic support for JET operation

CRPP staff has been involved throughout 2010 in support of JET operation in ensuring data analysis for the low and high energy NPA diagnostics (KF1 and KR2) for the temperature and density profiles provided by the LIDAR systems, and for the observations of MHD instabilities using the KC1M and KC1T diagnostic system.

5.2 Collaborations on other fusion experiments

Collaboration on high-frequency magnetic sensors based on the Low-Temperature Co-fired Ceramic technology for FTU, ENEA, Frascati, Italy

The Low-Temperature Co-fired Ceramic (LTCC) technology is currently being considered as a possible option for the high-frequency (HF) magnetic diagnostic system in ITER. Therefore, the possible installation in currently operating devices of sensors similar to those that would be required for ITER would help in assessing the suitability of this technology for the measurement of high-frequency instabilities in fusion devices. CRPP has developed an expertise in manufacturing and testing this type of sensors. Following a visit in 2009, the possibility arose to install two such LTCC sensors in the FTU machine in Frascati (Rome, IT), which has been realized in the fall of 2010.

Initial measurements indicate a factor ~10 improvement in the measurement sensitivity for HF instabilities when using the CRPP-made LTCC sensors, compared to the usual conventional Mirnov-type HF pick-up coils in use on FTU. This work is expected to continue in 2011 to achieve full exploitation of these LTCC sensors.

Participation of Switzerland to the Broader Approach (BA) through the JT60-SA project [*]

In the context of the negotiation between EU and JA about ITER, it has been agreed that several projects relative to the fusion research will be integrated under the BA concept, in which both partners (EU and Japan) will collaborate in order to accelerate the development of fusion as a source of energy. Several EU countries participate to this project, and the Swiss government decided to support the ECRH part by supplying in kind the procurement of the High Voltage Power Supplies (HVPS) required to power the gyrotrons.

Following the redimensionning of the Swiss Voluntary contribution, the collaboration with a Swiss industry to study a supply topology for gyrotrons in the framework of JT60-SA and ITER will be supported as defined by contract. In this context, CRPP representatives have regularly participated to the meetings reviewing the progress made by industry on this task. An additional contribution of CRPP is in the evaluation of the operation parameters of the JT60-SA and ITER gyrotrons, in order to specify more accurately the EC HVPS requirements. This task is expected to continue in 2011.

[*] Work not belonging to the Euratom Association Work Programme

Collaboration with FAST and FTU, ENEA, Frascati, Italy

Collaboration has been established with ENEA-Frascati to install a new microwave line on FTU testing and exploiting one of the gyrotron at 170GHz foreseen for the FAST System. The new installation must be reusable (in the major part) on FAST.

The project is based on the possibility of having in short time (3 years) a gyrotron source at 1 MW of power with a frequency around 170GHz or at a frequency adequate for FAST and FTU. On FTU the maximum pulse length is around 2 sec (at fundamental resonance 6T) or 4-5 s for second harmonic field (3T). The considered tube should be capable at least of 200s pulse length for the "steady state" scenario of FAST.

Collaboration with the linear basic plasma device GyM at CNR-Milano, Italy

Both Institutes have a basic plasma device (TORPEX at CRPP and GYM at IFP) to perform basic investigations in several fields of plasma physics of interest for fusion, including turbulence, transport and wave-particle interactions.
Collaborations can take the form of exchange of ideas, personnel for discussions or during specific experimental campaigns, and hardware, in particular for plasma diagnostics. For this, an agreement has been reached for a shared usage of a plasma imaging system based on a visible fast framing camera and a recently purchased image intensifier.

Collaboration on the investigation of current filaments in magnetized plasmas with RFX, Consorzio RFX, Padova, Italy

A current probe allowing highly resolved spatial measurements of current structures in turbulent plasmas has been developed at CRPP in collaboration with RFX-Padova. First direct measurements of the 2D structure of the blob-induced parallel current have been obtained in simple magnetized plasmas in the TORPEX device. A dipolar structure of the current density has been measured, which results from Bohm condition at the sheath boundary. Furthermore, we showed that, in hydrogen plasmas, the parallel current to the sheath can efficiently damp the charge separation, and thus the blob radial speed.

Collaboration on measurements of edge turbulence and flows in TEXTOR H-mode plasmas by correlation reflectometry, FZJ, Jülich, Germany

An ongoing collaboration on reflectometry measurements exists between the TEXTOR and TCV devices. The TEXTOR tokamak features an advanced correlation reflectometry diagnostic, using two simultaneous frequencies and two launching antennae, one on the midplane and one at the top of the device. Four poloidally spaced receiving antennae are available at each location, and tuneable receivers permit a variety of turbulence correlation measurements with both poloidal and radial spacing. Time delay detection can additionally provide information on the ExB flow.

The measurement campaign at TEXTOR has continued in 2010 to measure correlation lengths and flows in the edge barrier region of H-mode plasmas with an ergodic divertor. Data analysis is currently underway in view of a publication.

Collaboration on the design of a phase contrast imaging diagnostic for MAST, Culham, U.K.

A phase contrast imaging diagnostic has been proposed for studying electron-scale turbulence in the MAST spherical tokamak. The CRPP is collaborating on this project owing to its long-standing expertise in this technique. The collaboration has so far involved remote technical discussions and visits to MAST by CRPP personnel are expected in the future.

Collaboration with LHD on real-time control of ECH polarization, NIFS, Japan

The NIFS collaboration on real-time control of ECH polarization resulted in a publication entitled "Feedback control of ECRH polarization on the LHD" in Nuclear Fusion.

Collaboration with Alcator C-Mod on rotation reversals in L-mode plasmas, MIT, USA

Abrupt rotation reversals have been observed in Alcator C-Mod L-mode plasmas, similar to those observed in TCV. The magnitude of the reversals is typically tens of km/s, and can be triggered by slight changes in the electron density or plasma current. The critical density for the reversal is itself a strong function of plasma current. There are no other changes in macroscopic parameters such as the electron temperature or energy confinement time. Subtle differences in the turbulence characteristics are sometimes observed. The reversals occur inside of the q=2 surface.

NIFS collaboration on LHD MHD stability, Japan

Diamagnetic drift stabilisation of ballooning modes is theoretically demonstrated for high beta LHD plasmas with anisotropic energetic beam ions.
The ideal MHD model predicts instability. The fast ions interact weakly with the modes because of their large drift frequencies. The diamagnetic drifts of the thermal ions then become sufficient to stabilise the structures. The theory is valid for hot ion fractions below 2% of the thermal component. At moderate beta, finite diamagnetic drifts displace the Weyl formula minima to smaller frequencies and magnitudes.

Collaboration with MAST, Culham, CCFC, U.K.

3D helical core MHD equilibrium states are computed in MAST with flat central pressure and weak internal reversed magnetic shear. The structures resemble saturated ideal MHD internal m/n=1/1 kinks and may constitute a very good model to describe the long-lived modes that are observed in the experiment.

Collaboration with RFX-mod, ENEA, Padova, Italy

The ideal MHD stability of SHAx (Single Helical Axis) RFX-mod equilibrium states that have 7-fold toroidal periodicity are explored with respect to sideband toroidal modes. Under weak central reversed shear, the plasma is stable when the central q is approximately 1/8. If the core shear reversal vanishes or if the central q decreases below 1/8, the plasma becomes unstable to a coupled m/n=1/8 and m/n=2/15 internal kink mode. We conjecture that this may explain the periodic relaxation of the SHAx quiescent state to the multiple helicity turbulent regime.

5.3 Plasma surface interactions in collaboration with the University of Basel

For development of the first mirrors for ITER several films deposition were carried out for tokamak exposure at the University of Basel. Rhodium and molybdenum films were deposited by both magnetron and evaporation technique. These mirrors were exposed in TEXTOR and demonstrated acceptable performance under mild erosion conditions. The total accumulated fluence in one experiment can be compared to more than 350 ITER-discharges for mirrors located in equatorial ports and to approximately 10 discharges for mirrors installed in the upper ports with gas fuelling. Estimates are given for mirrors in diagnostic ducts located close to the first wall position. In another experiment the accumulated fluence corresponded to about 850 ITER discharges for mirrors in equatorial ports or 25 discharges for mirrors in the upper port plug equipped with a gas fuelling system. Single crystal molybdenum mirrors preserved their optical properties, for Mo-coated mirror slight degradation of reflectivity in the UV range was noticed. Sputtering and particle implantation led to a drastic drop of the reflectivity of the Rh-coated mirror reaching ~25% in UV range.

The goals of another project are to assess the manufacturing feasibility of the mirrors coatings, study the manufacturing capability and associated performances for the mirrors cooling and polishing, and determine the costs and delay of the first prototypes of diameter 200mm and 500mm. Three kinds of ITER candidate mock-ups are being designed and manufactured: rhodium films on stainless steel substrate, molybdenum on TZM substrate, and dielectric silver films on stainless steel substrate. The University of Basel takes part of this project with the CEA Cadarache and the company SESO to manufacture ITER first mirror mock-ups.

5.4 Collaborations with other EURATOM Associations

J-F. Artaud, V. Basiuk, Association EURATOM-CEA, France, *"Coupling of the DINA-CH and CRONOS codes to simulate the ITER hybrid scenario"*

K. Avramidis, Association Euratom Hellenic Republic, Greece, *"Studies of high-power gyrotrons for ITER"*

A. Bottino, IPP-Garching, Germany, *"Global PIC gyrokinetic simulations of turbulence and code development"*

I. Chapman, CCFG, UK, *"Sawtooth Stability with Fast Ions", "MHD equilibrium and stability in MAST"*

A. dellaCorte, Association EURATOM-ENEA, Italy, *"Test in SULTAN of two poloidal field conductors for ITER"*

G. Conway, IPP-Garching, Germany, *"Turbulence and flow measurements in TCV"*

D. Coster, IPP-Garching, Germany, *"SOLPS simulations of scrape-off layer in TCV and JET elmy-H discharges"*

G. Cunningham, CCFE, UK, *"ECH-assisted breakdown studies and H-mode studies in TCV"*

C. Cianfarani, ENEA-Frascati, Italy, *"Development of low-temperature co-fired ceramic magnetic pick-up coils for the measurement of high-frequency instabilities in the FTU tokamak"*

J. Decker, Y. Peysson, CEA-Cadarache, France, *"Electron Bernstein Wave Heating and Current Drive in axisymmetric toroidal plasmas"*

T. Eich, IPP-Garching, Germany, *"Parallel transport dynamics of type-I ELMs in JET and comparison to PIC modelling"*

W. Fietz, KIT Karlsruhe, Germany, *"Planning of High Temperature Superconductivity activities for EFDA and Demo"*

X. Garbet, Ph. Ghendrih, V. Grandgirard, G. Falchetto, Association EURATOM-CEA, France, *"Gyrokinetic global turbulence simulations"*

G. Granucci, D. Ricci, EURATOM-ENEA-CNR Association, Italy, *"Fast imaging in basic plasma devices"*

P. Hill, S. Saurelma, CCFE-Culham, UK, *"Global PIX gyrokinetic simulations of turbulence with flows"*

M. Hirsch, IPP-Greifswald, **E. Holzhauer,** University of Stuttgart, Germany, *"Loan of two homodyne single-frequency reflectometers and participation in reflectometer measurements and analysis on TCV"*

F. Jenko, T. Goerler, F. Merz, IPP-Garching, Germany, *"Development and application of the gyrokinetic code GENE"*

T. Johnson, EURATOM-VR Association, Stockholm Univ., Sweden *"Ion cyclotron current drive, heating, and sawteeth"*

A. Koenies, V. Kornilov, A. Mishchenko, S. Sorge, IPP Greifswald, Germany, **A. Bottino, A. Peeters**, IPP Garching, Germany, **R. Hatzky**, Rechenzentrum MPG Garching, Germany *"Linear and nonlinear gyrokinetic code developments and simulations"*

A. Krämer-Flecken, S. Soldatov, Forschungszentrum Jülich, Germany, *"Fluctuation studies by reflectometry on the TCV and TEXTOR tokamaks"*

P. Lauber, IPP-Garching, Germany, *"Damping rates of Alfvén Eigenmodes: theory-experiment comparison"*

H.P. Laqua, IPP Greifswald, Germany, *"Electron Bernstein Waves on TCV"*

E. Lazzaro, **M. Lontano**, **G. Grosso**, EURATOM-ENEA-CNR Association, Italy, *"Development of a linear plasma device for basic wave-particle interactions studies"*

M. Lewandowska, EURATOM-Poland Association, Un. of Stectin, *"Hydraulic experiments and modeling of CICC"*

P. McDermott, IPP-Garching, Germany, *"Intrinsic rotation measurement comparison AUG & TCV"*

N. Mellet, Association EURATOM-CEA, Cadarache, France, *"Application of the LEMAN code for heating and stability"*

P. Nave, JET/IST Abingdon, UK, *"Plasma rotation measurement comparison between JET and TCV plasmas"*

Y. Peysson, J. Decker, Association EURATOM-CEA, France, *"Quasilinear Fokker-Planck simulations and modelling of hard X-ray emission in TCV"*

A. Rodrigues, N. Cruz, C. Varandas, CFN Lisbon, Portugal, *"Advanced plasma control for TCV"*

J. Romero, CIEMAT, Madrid, Spain, **M.G.S. Berasategui**, EHU, Spain *"Current profile control on TCV"*

G. Temmerman, FOM, the Netherlands, *"Inner-outer divertor power assymetries on TCV"*

D. Terranova, P. Martin, L. Marrelli, M. Gobbin, EURATOM-ENEA-CNR Association, Italy, "RFX-Mod Shax equilibrium and MHD stability"

I. Tigelis, G. Latsas, Association Euratom Hellenic Republic, Greece, *"Instability calculations in the 170GHz coaxial-cavity-gyrotron beam-duct"*

A. Torre, Association EURATOM-CEA, France, *"Test in SULTAN of two poloidal field conductors for ITER"*

J. Urban, IPP, Acad. Of Science of Czech Republic, Praha, CZ, *"Benchmarking of the AMR (Antenna Mode-Conversion Raytracing) and LUKE code for the TCV tokamak EBW experiments"*

G. Veres, M. Berta, B. Tal, S. Zoletnik, A. Bencze, Association EURATOM-HAS, KFKI Reasearch Inst. For Particle & Nuclear Physics, Budapest, Hungary, *"Plasma imaging and tomography" and "Mitigation disruption studies, particle transport studies in the SOL, high temporal resolution radiation measurements for ELMs"*

L. Vermare, P. Hennequin, Ecole Polytechnique, Palaiseau + CEA, France, *"Reflectrometry measurements on TCV"*

C. Wahlberg, EURATOM-VR Association, Uppsala University, Sweden, *"MHD aspects of the sawtooth instability"*

5.5 Other international collaborations

G. Annino, Istituto per i Processi Chimico-Fisici, CNR, via G. Moruzzi 1, 56124 Pisa, Italy, *"Development of THz-waves Instrumentation for DNP-NMR spectroscopy"*

L. Berry, S.P. Hirshman, ORNL, Oak Ridge, USA, *"Anisotropic equilibrium for ECRH heating applications"*

A. Bortolon, PPPL, Princeton, USA, *"Rotation comparison between NSIX and TCV"*

Y. Camenen, Univ. Marseille, France, *"Modelling of plasma rotation and momentum transport on the TCV tokamak"*

H. Carfantan, Laboratoire d'Astrophysique de Toulouse - Tarbes, Université de Toulouse - CNRS, Toulouse, FR, *"Development of the Sparse Signal Representation method for real-time and post-pulse decomposition and analysis of a frequency-degenerate spectrum"*

P. Chattopadhyay, Inst. For Plasma Research, Bhat, Gandhinagar, India, *"Electron Bernstein Wave heating", "Correlation ECE turbulence measurements"*

E. Edlund, C. Rost, M. Porkolab, MIT, USA, *"Turbulence measurements by phase-contrast imaging in TCV, C-Mod, DIII-D"*

R. Ganesh, J. Chowdury, Inst. For Plasma Research, Bhat, Gandhinagar, India, *"Effects of non-adiabatic electron dynamics in gyrokinetic simulations of microinstabilities"*

R. Gruber, EPF-Lausanne, Switzerland, **S.P. Hirshman**, **Y. Suzuki**, **Y. Asahi, S. Ohdachi,, R. Seki**, ORNL, USA, **K.Y. Watanabe, H. Yamada, S. Okamura, Y. Narushima**, NIFS, Japan, **K. Yamazaki**, Nagoya Univ., Japan, *"3D anisotropic pressure equilibrium and fluid magnetohydrodynamic stability"*

E. Gusakov, A. Popov, IOFFE Institute, St.-Petersburg, Russia, *"Parametric decay calculations for TCV"*

B. Harrison, Inst. of Materials Engineering, Australian Nuclear Science and Technology Organisation (ANSTO, Australia, *"Manufacturing of oxide dispersion strengthened steels"*

R.W. Harvey, A.P. Smirnov, E. Nelson-Melby, CompX, San Diego, CA, USA, *"Modelling of electron cyclotron wave propagation and electron cyclotron emission in TCV"*

W. Heidbrink, H. Boehmer, UC Irvine, USA, *"Sources for energetic ions for a simple magnetized torus"*

S.P. Hirshman, Oak Ridge National Laboratory, USA, *"Three-dimensional anisotropic pressure free boundary equilibria: the ANIMEC code"*

J. Hittinger, R. Berger, Lawrence Livermore National Laboratory, USA, **E. Valeo**, Princeton University, USA, and *"Development of numerical methods for Vlasov simulations"*

M.Yu. Isaev, Russian Research Centre Kurchatov Institute, Moscow, Russia, **A. Konies**, IPP-Greifswald, D, *"Development of the VENUS-df Code for Bootstrap Current and Neoclassical Transport and Alfvén mode stability in Stellarators"*

K. Kim, NFRI, South Korea, "*Assembly and test in SULTAN of the Korean ITER conductor sample KOTF3*"

N. Kirneva, RRC Kurchatov Institute, Moscow, Russia, *"Investigation of turbulent tokamak plasma self-organization and influence of the tokamak cross-section geometry on the plasma-pressure self-consistant radial profile"*

S. Lelekhov, Kurchatov Institute, Moscow, Russia, *"Test in SULTAN of the RFPF16 ITER conductor"*

S.Yu. Medvedev, A.A. Martynov, A.A. Ivanov, Yu.Yu. Poshekhonov, Keldysh Institute of Applied Mathematics, Moscow, Russia, **M.Yu. Isaev, V.D.Shafranov, A.A. Subbotin**, RRC Kurchatov Institute, Moscow, Russia, *"Equilibrium and Stability of 2D and 3D plasma configurations"*

M. Mikhailov, A. Subbotin, V.D. Shafranov, M.Yu. Isaev, M. Samitov, Russian Research Centre Kurchatov Institute, Moscow, Russia; J. **Nuehrenberg**, Max Planck Institut fuer Plasma Physik, Greifswald *"Optimisation of Advanced Stellarator Systems"*

N. Mitchell, **A. Devred**, **M. Jewell**, ITER Organisation, *"In-situ measurements of Tc for SULTAN samples", "Protective investments for SULTAN", "Thermal cycles at liquid nitrogen of SULTAN samples", "Preliminary development of a thermal-hydraulic code"*

G.R. Odette, Univ. California Santa Barbara (UCSB), Santa Barbara, CA, USA, *"Fracture mechanics and small specimen test technology"*

K. Okuno, **Y. Takahashi**, JAEA, Japan, *"Assembly and test in SULTAN of the Japanese ITER conductors JACS1, JATF5 and JATF6"*

A. ten Ouden, Radbaud University, Nijmegen, The Netherland, *"Assembly and test in SULTAN of a prototype conductor for a high field magnet"*

F. Poli, PPPL, Princeton, USA, *"Characterization of the linear and nonlinear spectral properties of plasma density fluctuations in the TORPEX device in a limited magnetic configuration"*

J. Rice, C-MOD, Boston, USA, *"Intrinsic rotation comparison between CMOD & TCV"*

B. Rogers, Dartmouth College, USA, *"Theoretical characterization of turbulence in TORPEX plasmas"*.

D. Ryutov, LLNL, USA, *"Snowflake divertor generation and characterization in TCV"*

P. Savrukhin, A. Sushkov, RRC Kurchatov Institute, Moscow, Russian Federation, "*Design and fabrication of a tangential X-ray diagnostic for TCV*"

Dr. T.Shimozuma, National Institute of Fusion Science, Japan, *"Real-time control of ECH polarization"*

P. Smeibidl, HZB, Berlin, Germany, *"Design and construction of a SC Cable-in-Conduit coil for a horizontal series-connected hybrid magnet system within the framework of the high field magnet project (HFM) at HZB"*

J. Snipes, R. Parker, M. Porkolab, J. Freidberg, J. Sears, **P. Woskov,** PFSC, MIT, USA, *"Fast particle physics, Alfven waves, and active MHD mode excitation on the Alcator C-Mod tokamak plasma"*

D. Tskhakaya, Innsbruck Univ., Austria, *"Comparison of SOLPS and PIC BIT-1 code simulations of the scrape-off layer in TCV and JET elmy-H mode discharges and TCV fast infrared measurements"*

A.D. Turnbull, General Atomics, San Diego, USA, *"Stability studies of ARIES stellarator configurations"*

Y. Wu, ASIPP, P.R. China, *"Assembly and test in SULTAN of the ITER conductors CNTF2 and CNTF3"*

J. Yu, China Institute of Atomic Energy (CIAE), Beijing, P.R. China, *"Modelling of radiation damage and radiation effects"*

5.6 Other collaborations within Switzerland

J.-Ph. Ansermet, EPFL/SB/LPMN; **A. Comment**, EPFL/SB/IPSB/LIFMET; **G. Bodenhausen**, EPFL/SB/ISIC/LRMB, **G. Boero**, EPFL/STI/IMT/LMIS1, *"Development of THz-waves Instrumentation for DNP-NMR spectroscopy"*

E. Cadoni, University of Applied Sciences of Southern Switzerland, Canobbio, *"High strain rate tensile testing of the EUROFER 97 RAFM steel"*

C. Hébert, CIME-EPFL, *"Microscopic analysis of nanoscale oxide particles"*

F. Holdener, WEKA, Bäretswil, *"Technology transfer for HTS current leads manufacture"*

Besides the activities in the field of plasma wall interaction with the University of Basel, of the socio-economics with the LASEN (EPFL) and CEPE (ETHZ), the CRPP also collaborates with the PSI in the field of materials under irradiation.

6 THE EDUCATIONAL ROLE OF THE CRPP

The CRPP plays a role in the education of undergraduate and postgraduate students, particularly in the Faculté des Sciences de Base (FSB) of the EPFL. Advanced education and training in fusion physics and technology and plasma physics topics is carried out as part of the research activities of the Association. Section 6.1 presents the 9 courses given to physics undergraduates and to engineering undergraduates. In their fourth and final year, physics undergraduates spend time with a research group at the EPFL, typically 12 hours per week for the whole year. During this period, they perform experimental or theoretical studies alongside research staff, discovering the differences between formal laboratory experiments and the "real" world of research. After successful completion of the first year of the Master Programme (4^{th} year of studies), physics students are required to complete a "master project" with a research group, lasting a full semester. This master project is written up and defended in front of external experts. The CRPP plays a role in all of these phases of an undergraduate's education, detailed in Sections 6.2 and 6.3.

As an academic institution, the CRPP supervises many Ph.D. theses, also in the frame of the Physics Section of the EPFL. 7 PhDs were awarded in 2010. At the end of 2010 we had 33 PhD students supervised by CRPP members of staff, in Lausanne and at the PSI site in Villigen. Their work is summarised in Section 6.4.

6.1 Undergraduate courses given by CRPP staff

S. Alberti, *Chargé de cours – "Plasma Physics I"*
This course is an introduction to plasma physics aimed at giving an overall view of the essential properties of a plasma and at presenting the approaches commonly used to describe its behaviour. We study single particle motion, the fluid description and the kinetic model. The relation between plasma physics and developing a thermonuclear reactor is presented and illustrated with examples.

N. Baluc - Professeure titulaire**, R. Schäublin** - Maître d'Enseignement et Recherche**, P. Spätig** - Maître d'Enseignement et Recherche**:** *"Fundamentals of radiation damage and effects"*
This 28-hours course is part of the EPFL's Minor in Space Technologies. The objective of this course is to provide a detailed description of fundamental interaction mechanisms between particles and matter, radiation damage and its characterization methods, and radiation effects with emphasis on the relationships between microstructure and mechanical properties. Various types of materials are being considered as well as various examples of applications related to nuclear, semi-conductor and aerospace industries.

N. Baluc, Professeur titulaire, *"Materials for fusion reactors"* and *"Multiscale modelling"*
The aim of these courses are to provide a basic introduction to candidate materials for fusion reactors, the status of their characterization, their advantages and key issues for use in fusion reactors, and to the numerical and analytic tools used for modelling radiation damage and effects. These courses were given within the frame of the Master in Nuclear Engineerings.

A. Fasoli, Professor – *"Plasma physics II"*
One semester option course presented to 4th year Physics students, introducing the theory of hot plasmas via the foundations of kinetic and magnetohydrodynamic theories and using them to describe simple collective phenomena. Coulomb collisions and elementary transport theory are also treated. The students also learn to use various theoretical techniques like perturbation theory, complex analysis, integral transforms and solutions of differential equations.

A. Fasoli, Professor – *"General Physics II"*
This course completes the introduction to mechanics provided in the first semester with the basic concepts of statics, oscillations and special relativity. It also covers the whole of thermodynamics, from the introduction to heat, temperature and kinetic theory to the first and second principles, including entropy and thermal engines, ending with a treatment of transport and non-equilibrium phenomena in open systems.

A. Fasoli, Professor and **M.Q. Tran**, Professor - *"Nuclear fusion and plasma physics"*
The aim of this course is to provide a basic understanding of plasma physics concepts of fusion energy, and of the basic principles of fusion reactors, including the main technological aspects. This course was given within the frame of the Master in Nuclear Engineering.

J.B. Lister, *Maître d'Enseignement et Recherche (MER) – "Plasma Physics III"*
An introduction to controlled fusion, presented as a one semester option to 4th year Physics students. The course covers the basics of controlled fusion energy research. Inertial confinement is summarily treated and the course concentrates on magnetic confinement from the earliest linear experiments through to tokamaks and stellarators, leading to the open questions related to future large scale fusion experiments.

M.Q. Tran, *Professor - "General Physics II and III"*
This course, given to the Mathematics Section, covers mechanics and thermodynamics (General Physics II) and hydrostatic, hydrodynamics waves and electromagnetism (General Physics III).

L. Villard, *Professeur Titulaire – "Computational Physics I-II"*
Full year course given to students in their 2nd year in Physics. The course covers various time and space integration techniques for ordinary and partial differential equations, and is applied to various physics problems ranging from particle dynamics, hydrodynamical equilibrium, electromagnetism, waves and quantum mechanics. It includes a strong practical work aspect.

6.2 Undergraduate work performed at the CRPP

EPFL Master students (4th year)

During the Spring semester of 2010, CRPP staff members have supervised 4 students performing their Advanced Physics Laboratory work. During the Automn semester of 2010, we had 6 students.

6.3 EPFL Master degrees awarded in 2010

Hassan Badreddine: "CFD simulation of flow distribution in Steam Generator"

Lucie Brocher: *"Investigate non-linear effects of AC loop voltage stimulation on the current profile of tokamak plasmas"*

David Martinet: *"Charactrisatiuon of a new, capacitively-coupled industrial RF plasma source"*

Imram Quaine: *"An analysis of MHD instabilities and their effect on plasma confinement in Heliotron J"*

Mikael Rancic*: "Effect of triangular plasma shape variations on plasma fluctuations correlation length measured by correlation ECE"*

Boris Roulet*: Experimental investigation of fast ion dynamics in TORPEX toroidal plasmas"*

Ralph Schnyder: *"Experimental investigation of a new structured RF plasma electrode"*

6.4 Postgraduate studies

Postgraduate courses given in 2010

R. Schäublin, Ph. Spätig: *"Multiscale Approach of Plastic Deformation of Metals and Alloys"* (28h course - EPFL Doctoral School in Materials Science and Engineering)
This course is aimed at introducing the fundamental phenomena of plastic deformation of metals and alloys, and at providing the necessary background to understand the multi-scale nature of the plastic deformation from the atomistic scale up to the continuum one. The course is divided into eight chapters: 1) elasticity, 2) plasticity, 3) finite element simulations, 4) dislocations, 5) strain hardening model, 6) molecular dynamics simulations, 7) kinetic Monte-Carlo simulations, 8) discrete dislocation dynamics simulations.

J. Graves, J.-M. Moret, A. Pochelon, O. Sauter, H. Weisen: *"Physics of magnetically confined plasmas", (*28h course, 28h exercise – EPFL doctoral programme in Physics)
The objective of the course is to provide the physics basis of magnetic fusion. Topic covered include magnetic equilibrium and magnetohydrodynamic stability properties in toroidal plasmas confined by magnetic fields, neoclassical cross field transport, heating and current drive by radio-frequency waves, and heating by energetic neutral atom beams.

Ch. Hollenstein and A. Howling: *"Plasma in industry: physics basis and applications"* (28h course, 28h exercises – EPFL doctoral programme in Physics)
The course covered basic plasma physics (plasma equation, equilibrium, collisions and transport) including interactions with surfaces (DC sheath, RF sheath, chemical reactions and surfaces). Industrial applications were explained

(deposition, etching) as well as the plasma techniques used in industry (DC, capacitive, and wave-heated discharges, and ion beam sources) and their diagnostics."

Doctorate degrees awarded during 2010

Seyed Masood HAFEZ HAGHIGHAT: *"Multiscale modeling of irradiation induced effects on the plasticity of Fe and Fe-Cr alloys"* (EPFL Thesis number: 4667/10)

Degradation of mechanical properties due to nanometric irradiation induced defects is one of the challenging issues in designing ferritic materials for future nuclear fusion reactors. Various types of defects, namely dislocation loops, voids, He bubbles and Cr precipitates may be produced in ferritic materials due to high doses of irradiation with the 14 MeV neutrons stemming from the deuterium-tritium fusion reaction. Multiscale modelling methods, namely molecular dynamics (MD) and dislocation dynamics (DD) methods, are used here to study the impact of irradiation-induced defects on the mechanical properties of model ferritic material.

MD simulation is used to study the state of a nanometric helium bubble in bcc-Fe as a function of temperature, 10 to 700 K, and He content, 1 to 5 He atoms per vacancy. The basic mechanisms of the interaction in bcc-Fe between a moving dislocation and a nanometric defect, as a function of temperature, interatomic potentials, interaction geometry and size are investigated using MD simulation. It appears that voids and He bubbles are strong obstacles to dislocation, which induce hardening and loss of ductility. A nanometric void is a stronger obstacle than a He bubble at low He contents, whereas at high He contents, the He bubble becomes a stronger obstacle. It also appears that different potentials give different strengths and rates of decrease of obstacle strength with increasing temperature. Temperature eases the dislocation release, due to the increased mobility of the screw segments appearing on the dislocation line upon bowing from the void or He bubble. Concerning the obstacle size at low content He bubble, where it is penetrable defect, size increase from 1 to 5 nm make them harder in agreement with the elasticity of continuum. At high He contents a size dependent loop punching is observed, which at larger bubble sizes leads to a multistep dislocation-defect interaction. Atomistic simulations reveal that the He bubble induces an inhomogeneous stress field in its surroundings, which strongly influences the dislocation passage depending on the geometry of the interaction.

Fe-Cr alloys are also studied using MD simulations as model alloys for the ferritic base steels. Studying the flow stress of a moving edge dislocation in Fe(Cr) shows that the flow stress is sensitive to temperature, strain rate and Cr concentration. The flow stress of a screw dislocation is temperature dependant and its value is much higher than that of edge dislocation. Interaction in a pure Fe matrix of an edge dislocation with a nanometric Cr precipitate having various Cr content inside (Cr/Fe ratio) indicates that with the Cr/Fe ratio the obstacle strength increases, with a strong sensitivity to the short-range order. Temperature induces a monotonous decrease of the strength for all studied Cr/Fe ratios.

DD calculation coupled to finite element method (FEM) is used to simulate the interaction of an edge dislocation with a void. DD calculations present a good match to the MD simulation results for the impact of image forces on the dislocation due to the free internal surface of the void. Using DD simulation, hardening due to the presence of nanometric defects, as immobile dislocation segments and spherical defect, are considered. The results of MD simulations for the strength of different defects are introduced in DD simulation. It appears that the presence of both immobile dislocation segments and nanometric defects may lead to the hardening of

bcc-Fe. However, the defect density has more significant importance on the DD simulation, obtained here, than the strength of a single defect.
TEM in-situ straining is used to validate simulations, in particular on the dislocation interaction mechanisms. Experiments were performed in ultra high purity Fe specimens. It appears that the microstructure of the material consists mainly in elongated screw dislocations. The in-situ straining tests led to the observation of the formation of <111> screw dislocation dipoles in consistency with the MD simulation results. The interaction between a dislocation and an obstacle, as nanometric defect or immobile dislocations, leading to their shear or to Orowan loop formation were successfully observed.
This work shows that using of different simulation methods can assist in the understanding of nano- and meso-scale phenomena occurring due to the presence of irradiation induced defects upon deformation of a-Fe. The information obtained from various microstructure mechanisms at lower scale simulations can be passed to higher scale simulation methods in order to realize the simulated phenomena. Experimental observations may validate what is observed in simulations provided the simulation scale is reachable in experimental observations.

Sudheer Kumar JAWLA: *"Phase Retrieval and Gaussian Beam Mode Decomposition of Gyrotron Beams"* (EPFL Thesis No. 4675 (2010))
One of the most important issues in designing the components of a quasi-optical launcher is to correctly know the characteristics of an RF beam coming out of a gyrotron. In this thesis, we have addressed this problem through emphasizing on an accurate phase retrieval and Gaussian beam modal decomposition technique. The later predicts that the RF beam Gaussian content must be defined by a coupling coefficient to an HE_{11} transmission line instead of a Gaussian content in free space. In order to analyze the phase reconstruction in detail, we have developed an accurate field propagation method using the complete scalar diffraction integral and the approximated Huygens-Fresnel diffraction integral, using a fast Fourier Transform based approach. The discretization of the two diffraction integrals is analyzed analytically and numerically. In the case of the Fresnel diffraction integral, a condition is found on the distance of propagation, where aliasing and replication are completely removed. It relates the distance of propagation z, the number of sampling points M, the grid cell size x and the wavelength λ as: $z = M(x)^2/\lambda$. The two formalisms are also studied using a zero-padding technique, which can be used to propagate the field to any arbitrary distance. These propagation methods are then used in an Iterative Phase Retrieval Algorithm for phase reconstruction. The effects of several parameters on the reconstruction e.g. the number of planes, the measurement plane size, the distance of propagation, the number of sampling points and the grid cell size, the misalignment along the optical axis, etc. are then analyzed. The experimental procedure to measure the beam intensity patterns using infrared thermography is explored extensively. Out of the many target materials used, Robax is the most appropriate in terms of dynamic range, temperature linearity and for the possibility to perform measurements from the front side and the back side. Further, infrared image data processing is investigated for intensity pattern enhancement. This includes various steps: Fixed Pattern Noise correction by subtracting the background image of the target taken before the microwave irradiation, defective pixels correction, perspective correction, image pattern enhancement by filtering and denoising. Further, the intermodal decomposition of the reconstructed phase and amplitude is analyzed in detail using two methods, in order to extract the Gaussian content: 1) Finding a set of Gaussian beam parameters and a mode content matrix which maximizes the power in the fundamental mode $|C_{00}|^2$. 2) Finding a set of Gaussian beam parameters and a mode content matrix which minimizes the error between the corresponding reconstructed field and the experimental field. As a general rule, the second method

gives more precise and more reliable results, but the solution is unfortunately not unique and depends both on the measured profile and the measurement parameters. In this analysis, we concluded that the concept of Gaussian content adopted by the community seems to be incomplete, and the corresponding optimized parameters should be associated to it. The definition of Gaussian content should then be reexamined, and completed by an analysis of the power coupling coefficient of the microwave beam to the corrugated waveguide.

Martin JUCKER: *"Self-consistent ICRH distribution functions and equilibria in magnetically confined plasmas"* (EPFL Thesis 4912(2010))
The deployment of high power radio frequency waves in the ion cyclotron range (ICRF) constitutes an important operational facility in many plasma devices, including ITER. Any charged particle describes a helical motion around a given magnetic field line, the so-called cyclotron motion. ICRF relies on the interaction between charged particles and an injected Radio Frequency (RF) wave, tuned to be at the same frequency as the helical cyclotron motion. It is applied not only for pure heating of the plasma, i.e. Ion Cyclotron Resonant Heating (ICRH), but also for the generation of non-inductive current through Ion Cyclotron Current Drive (ICCD). The numerical code package SCENIC has been developed for self-consistently simulating the effects of ICRH on the resonant ion species within the plasma, the resulting changes in the plasma equilibrium, and finally the back reaction onto the injected wave field. SCENIC is an iterated scheme, which advances the resonant ions' distribution function, the equilibrium and the wave field iteratively until a converged solution, representing a steady state, is reached. The constituents of SCENIC are the MagnetoHydroDynamic (MHD) equilibrium code VMEC, the full wave code LEMan and the Hamiltonian guiding centre drift following code VENUS. All of these codes are capable of dealing with 3D geometries, and have recently been updated to handle pressure anisotropy, where the energy density parallel and perpendicular to the magnetic field differ. This is important since the RF field resonates mainly with the particle's motion perpendicular to the magnetic field, thus creating pressure anisotropy. After the introduction and description of the different codes and their interfaces, this work verifies the consistency of the numerical results with expected results for simple cases, and a benchmarking effort against the similar code package SELFO is shown. After this validation, SCENIC is applied to different heating scenarios, which are relevant to present (Joint European Torus, JET) and future (ITER) devices. Low power heating simulations with a 1% helium-3 minority in background deuterium plasmas demonstrate that a pressure anisotropy is induced. We show that the hot particle distribution function can be adequately approximated with a particular bi-Maxwellian for the equilibrium and wave field computations. For high power, 3% hydrogen minority heating scenarios, the heating scheme alters the background equilibrium state. This justifies one of the main novelties introduced in this work, namely the inclusion of the equilibrium computation in the self-consistent scheme. Effects due to asymmetric wave injection and different heating locations on the hot particle distribution function, the hot dielectric tensor and the equilibrium will be studied. Here, the emergence of a high energy tail in the minority species distribution function is shown explicitly, and some of its exotic features are observed via the RF driven current, the density and the pressure evolution.

Xavier LAPILLONNE: *"Local and global Eulerian gyrokinetic simulations of microturbulence in realistic geometry with applications to the TCV tokamak"* (EPFL Thesis 4684(2010))
In magnetically confined fusion devices, the energy and particle transport is significantly larger than expected from purely collisional processes. This degraded

confinement mostly results from small-scale turbulence and prevents from reaching self-sustained burning plasma conditions in present day experiments. A better understanding of these nonlinear phenomena is therefore of key importance on the way towards controlled fusion. The small-scale microinstabilities and associated turbulence are investigated for Tokamak plasmas by means of numerical simulations in the frame of the gyrokinetic theory. This model describes the evolution of the particle distribution functions in phase space together with self-consistent electromagnetic fields, while neglecting the fast motion associated with the Larmor orbit of particles around the magnetic field lines.
In the course of this thesis work, substantial modifications to the existing Eulerian gyrokinetic code GENE have been carried out in collaboration with the Max-Planck-Institute für Plasmaphysik in Garching, Germany. The code has been extended from a local approximation, which only considers a reduced volume of a fusion plasma, to a global version which fully includes radial temperature and density profiles as well as radial magnetic equilibrium variations. To this end, the gyrokinetic equations have been formulated for general magnetic geometry, keeping radial variations of equilibrium quantities, and considering field aligned coordinates, suitable for their numerical implementation. The numerical treatment of the radial direction has been modified from a Fourier representation in the local approach to real space in the global code. This has in particular required to adapt the radial derivatives, the field solver, and to implement a real space dealiasing scheme for the treatment of the nonlinearity. A heat source was in addition introduced to allow for steady state global nonlinear simulations.
An important part of this work also focused on the description of the magnetic equilibrium. A circular concentric flux surface model as well as an interface with an MHD equilibrium code were implemented. A detailed investigation concerning the $s - \alpha$ model, previously used in local codes, was also carried out. It was shown that inconsistencies in this model had resulted in misinterpreted agreement between local and global results at large $\rho^* = \rho_s/a$ values, with ρ_s the Larmor radius and a the minor radius of the Tokamak. True convergence between local and global simulations was finally obtained by correct treatment of the geometry in both cases and considering the appropriate $\rho^* \rightarrow 0$ limit in the latter case.
The new global code was furthermore successfully tested and benchmarked against various other codes in the adiabatic electron limit in both the linear and nonlinear regime. A nonlinear ρ^* scan was in addition carried out showing convergence to the local results in the limit $\rho^* \rightarrow 0$ and also providing further insight on previous disagreements between two other global gyrokinetic codes concerning ρ^* convergence. Linear global simulations with kinetic electrons have shown consistent behavior with respect to local results.
Using the interface with the MHD equilibrium code, the effects of plasma shaping on Ion Temperature Gradient (ITG) instabilities were investigated by means of local simulations. A favorable influence of elongation and negative triangularity was observed. It was shown that these effects could be mostly accounted for by the modifications of the effective flux-surface averaged temperature gradient. Most importantly, a unique effective nonlinear critical temperature gradient could be determined for the different considered elongations and triangularities.
The local code was finally used to investigate particle and energy transport in the case of TCV discharges presenting an electron Internal Transport Barrier (eITB). It was shown that at the transition between ITG and Trapped Electron Mode (TEM) dominated turbulent regimes, the particle flux goes to zero. Interestingly, this effect could be well reproduced by a quasi-linear approach where all the different unstable wavenumbers are considered. The nonlinear simulations also revealed that a minimum of the electron heat diffusivity is observed at the transition between the TEM and ITG regimes. A strong dependence of this quantity was also noticed with respect to the density gradient. Quantitative comparisons with experimental

results have shown that a reasonable agreement could only be reached in regions where the density gradient is small while the flux tube simulations seem to overestimate the heat transport if one accounts for gradient values in the center of the transport barrier. Some first nonlinear global simulations appear to indicate that finite ρ* effects could potentially play an important role and thus reduce the heat diffusivity to realistic values.

Theodoros PANIS: *"Alfvén Eigenmode stability in tokamak plasmas"* (EPFL Thesis 4940(2010))

Direct damping rate measurements of AEs are obtained using the active MHD spectroscopy system installed on the JET tokamak. The system was recently equipped with new antennas, designed to study especially the modes of intermediate toroidal mode number n, $|n|$=3–15, as the AEs of this range are most prone to destabilization by the fast particles in JET and in future burning plasma experiments such as ITER.

The broad n-spectrum that is driven by the new antennas and the more localized structure of intermediate-n AEs has important implications for the ability to measure damping rates of intermediate-n. To obtain an extended database of high accuracy individual-n measurements, experimental work on technical and engineering aspects was indispensable both on the excitation side and on the detection side.

On the excitation side, the electrical model of the AE exciter has been constructed during this thesis. The model is used to determine the operational capabilities of the exciter with the new antennas, to optimize the antenna currents and to design the relevant impedance matching circuits.

On the detection side, the excitation of multiple-n, degenerate AEs at close frequencies prompted for a sophisticated method to correctly estimate the n-spectrum of the plasma response. To this end, a sparse spectrum representation method was adapted to deal with the complex and real-time data produced by the active MHD spectroscopy system. The n-decomposition of the plasma response requires an accurate relative calibration of the magnetic pick-up coils. An in situ method was developed and applied for the calibration of the coils using the direct coupling to the new AE antennas.

A large collection of damping rate measurements of, mainly, toroidal AEs (TAEs) was obtained during the 2008/2009 JET experimentalcampaigns following the technical optimization of the antenna system. Selected measurements of $|n|$=3, 4 and $|n|$=7 TAEs are compared to the plasma models of the numerical codes LEMan and CASTOR. The robustness of the results of the simulations is tested against uncertainties in density and safety factor profiles. The antenna-driven modes are characterized and the dominant damping mechanisms are identified in a number of cases, and confirm in general for a wide n-range the stabilizing role played by the edge magnetic shear. These comparisons underline the importance of the kinetic effects in order to achieve a realistic estimation of the TAE damping.

A database of approximately 3000 TAE damping rate measurements in ohmic plasmas is studied. The dependence of the damping rate measurements of $|n|$=2–7 TAEs on the edge magnetic shear, the edge elongation and the q profile is investigated. The analysis provides experimental evidence that the damping properties of TAEs with $|n|$= 2–7 change as the toroidal mode number n increases, showing that medium-n modes tend to be less damped than low-n modes. In JET plasmas, the turning point for the damping properties to change from low-n to medium-n behavior is found to be at $|n| \approx 3$–4 .

Andreas PITSCHKE: *"Pedestal Characteristics and MHD Stability of H-mode Plasmas in TCV"* (EPFL Thesis 4917(2010))

The tokamak à configuration variable (TCV) is unique in its ability to create a variety of plasma shapes and to heat the electron population in high density regimes using microwave power at the third harmonic of the electron cyclotron frequency. In the frame of this thesis, the impact of plasma shaping and heating on the properties of the edge transport barrier (ETB) in the high confinement mode (H-mode) was studied. This mode of operation is foreseen as one of the reference scenarios for ITER, the International Tokamak Experimental Reactor, which is being build to demonstrate the feasibility of thermonuclear fusion using magnetic confinement. A feature of H-mode regime operation are edge localized modes (ELMs), instabilities driven by the steep pressure gradients that form in the plasma edge region due to a transport barrier. During an ELM event, energy and particles are expelled from the plasma in a short burst. This will cause serious problems with respect to the heat load on plasma facing components in a tokamak of the size of ITER. Understanding of the phenomena associated with ELMs is thus required and dedicated investigations of their theory and experimental observations are carried out in many laboratories worldwide. This thesis presents several experimental and numerical investigations of tokamak behavior for configurations where the plasma edge plays an important role.

From the experimental viewpoint, studies of transport barriers are challenging, as plasma parameters change strongly within a narrow spatial region. As part of the work presented here, the TCV Thomson scattering system was upgraded to meet the requirements for diagnosing electron temperature and density with high spatial resolution in the region of internal and external transport barriers. Simultaneously, the data analysis was significantly improved to cope with statistical uncertainties and alleviate eventual systematic errors.

For measurements of the time evolution of density and temperature profile during the ELM cycle, the low repetition rate of the lasers used for Thomson scattering is a limiting. Although the system on TCV comprises 3 laser units that may be triggered in sequence with time separations down to 1ms, time evolution over longer periods can only be reconstructed from repetitive events. In this context, an adjustment of the laser trigger to improve the synchronization with the ELM event is an advantage. A method was developed and implemented to generate a synchronizing trigger sequence, by a real-time monitoring of the D-alpha emission, which provides a marker for the ELM event.

Recently, a "snowflake" (SF) divertor configuration, proposed as a possible solution to reduce the plasma-wall interaction by changing the divertor's poloidal magnetic field topology, was generated, for the first time, in TCV. A numerical code (KINX), based on a magnetohydrodynamic model (ideal MHD), was used to investigate the stability limits of this configuration under H-mode conditions and compare them with a similar standard single-null equilibrium. In a series of experiments, improved energy confinement was found and explained by improved stability of the edge region in the SF configuration.

The influence of the pedestal structure in ELMy H-mode plasmas on the energy confinement and on ELM energy losses was investigated. The different ELM regimes found in TCV were analysed, in particular the transition between type-III to type-I ELMs. The operational boundary of each ELM regime was characterized and verified by ideal MHD stability simulations for the ETB region. Recent studies on the scaling of the pedestal width with normalized poloidal pressure were confirmed. Using the capabilities of TCV, the influence of plasma shaping on pedestal parameters and MHD stability limits was investigated.

In the past, models were developed to describe the onset of type-I ELMs, which are associated with modes in the ETB region arising from a coupling of pressure- and current-driven instabilities (coupled kink-ballooning modes). Experimental studies were performed to trace the temporal evolution of pedestal parameters

characterizing the ETB during an ELM cycle. The results of these experiments were analyzed using information from MHD stability calculations. It is concluded that these models a capable of predicting limits as necessary conditions for ELM activity, but are not sufficient to fully explain ELM triggering.

Alexandra ZHUCHKOVA: *"A Far-Infrared Polarimetry Diagnostic for the Measurement of the Poloidal Magnetic Field in the TCV Tokamak"* (EPFL Thesis 4847 (2010))

Information about the poloidal field inside the plasma and about the current density profile is essential for the understanding of the behaviour of tokamak plasmas. One of the diagnostics permitting to measure the magnetic field distribution inside the plasma is polarimetry using beams of electromagnetic waves traversing the plasma.

This thesis is devoted to the design of a specific polarimeter system and its implementation on the TCV tokamak. The conceptual design took into account the particular

requirements of the TCV experiments and its experimental program with particular interest in measurements of current density profiles in low-density, EC-heated plasmas.

Aiming at optimum performance of the polarimeter in this parameter range, the FIR laser wavelength of 432.5 μm was chosen. Since TCV is already equipped with an interferometer (at 214 μm) for measurements of the line-integrated density along 14 chords, the polarimeter was built as a separate instrument. The number of 10 spatial channels to cover the plasma diameter was found as a compromise between desired spatial resolution, access constraints and cost. The measurement of the Faraday rotation angle is based on a method which uses optical beams with rotating linear polarization. In this case, the Faraday rotation angle is retrieved from a phase measurement comparing the modulated signals from the probe detectors with that from a reference detector and to first order is insensitive to amplitude variations of the signals. Waveguide detectors based on Schottky barrier diodes are used as detectors for their sensitivity and large electrical bandwidth. Signal processing and analysis is performed in two branches :

- using specifically built analog electronic phase detectors followed by slow (250kHz) ADCs
- using fast (5MHz) ADCs and numeric signal processing on a mainframe computer.

The thesis covers the description of the design and the various components of the polarimeter, presents initial tests and an evaluation of its performance based on simulations using real plasma configurations of TCV. The analysis of specific tests with the system installed on TCV revealed the presence of perturbations leading to parasitic contributions to the measured phase angles.

The results of first measurements of the Faraday rotation angle for different plasma conditions on TCV are presented. Comparing the measured Faraday rotation angles with the results of calculations showed qualitative agreement, in particular the effects of an increase in electron density and of the reversal of the current direction were clearly seen. The system is also capable to detect a radial displacement of the magnetic axis of the plasma, as was demonstrated by comparing measurements from two specific plasma configurations. However, the absolute values still show significant deviations from the expected ones based on calculations. The discrepancies increase with increasing Faraday angle and depend on the direction of the plasma current. At high electron densities beam refraction becomes a problem and may lead to significant errors in the measurements and eventually to complete loss of the signal in several channels. In its present status, the polarimeter cannot yet provide results that are suitable to reconstruct the poloidal

field or the current density profile of the plasma. Tentative explanations for this problem are given, but further specific tests are necessary to confirm them.
Even in its present state, the polarimeter may be used to detect transient relative changes in the profiles of electron density and current. This was demonstrated by a series of experiments in plasmas with sawtooth activity. Comparing the signals from the polarimeter with those from other multi-chord diagnostics (interferometer and soft X-ray detectors) clearly revealed correlations but also specific differences.
These experimental studies showed that the Far-Infrared Polarimetry still requires further improvements, but has potential to become a valuable diagnostic capable of directly measuring the current density profile in the TCV tokamak.

Ph.D. Theses supervised by CRPP staff at the end of 2010

Mattia ALBERGANTE: *"Microtubulence driven transport of energetic ions"*
A deeper insight into the physics of the anomalous transport of fast ions in ITER has been gained.
The analysis has been carried out with the employment of a newly developed numerical platform. First, the linear and nonlinear features of the background turbulent fields in ITER have been simulated with the gyrokinetic code GENE. The single particle code VENUS has then been employed for simulating the neutral beam slowing down in ITER. The unperturbed and collisional transport of these ions has been coupled with the anomalous diffusion driven by the turbulent fields described by the GENE code. Results have shown that for the 1MeV NBI in ITER only a minor redistribution is expected. At the same time, the employment of a lower energy neutral beam system could suffer from a more intense interaction with the turbulent fields.

Karim BESSEGHIR: *"Maintaining optimal ITER scenario trajectories"*
In presently operated tokamaks, optimality is mainly reached by trial and error, and the objective function being optimised is often implicit, even to the operator himself. This scheme is adequate for present tokamaks because disruptions are not a major issue. However, such an operation scheme cannot be performed on ITER since the occurrence of disruptions may lead to damage to the tokamak. Hence, automation of the present pulse scenario trajectories generation procedure will be required for ITER operation. Moreover, such automation will also allow 'on-the-fly' re-optimisation of the scenario trajectories – in other words, it will enable online modification of the scenario trajectories according to the actual state of the tokamak – and thus minimise the operation risk.
In order to demonstrate the feasibility of such an optimisation procedure, a simple plasma behavioural model was developed. We introduced an arbitrary objective function which consisted of weighted contributions of several costs: total flux consumption, proximity to the operational limits of the actuators, time necessary to reach the target, and tokamak hard constraints, and minimised it using a simple optimisation algorithm. This work enabled us to demonstrate the feasibility of automation of the scenario trajectories generation procedure using a basic optimal control algorithm. Moreover, it helped us understand the main issues that may be encountered when designing an optimal control algorithm for a full tokamak, namely the very high sensitivity of the solution to the weighting of the different costs in the objective function, the need for either high-dimensionality or infinite dimensional solution space, the need for fast simulations and rapidly converging optimisation algorithms, and some of the optimal control community vocabulary and techniques.

In order to test this approach on a more complex full tokamak simulator, we undertook the re-organisation of DINA-CH, which is a free-boundary equilibrium evolution solver, coupled with CRONOS, which is a transport solver. The initial equilibrium design is presently under investigation, so as to enable us to provide different initial equilibria in accordance to the desired simulated scenario. This work aims at providing a framework in which an optimal control algorithm may be designed and tested for a more complex modelling of tokamak behaviour.

Alexandre BOVET: *"Fast Ions experiment"*
The experimental setup to investigate fast ions transport in the TORPEX device used in the past years, consisting of a fast ions source and a double gridded energy analyzer mounted on a 2D movable system, was integrated in the control system permitting an automation of the process. A new lock-in system was developed for the synchronous detection of fast ions. This new device has the possibility to add a dead time to get free of the capacitive effect due to the modulation of the fast ions source. The control system and the BITBUS server were also upgraded

Ciro CALZOLAIO: *"Irreversible degradation in Nb_3Sn CICC"*
The Nb_3Sn filament axial strain has two components: the thermal strain, ε_{th}, due to the mismatch of the thermal expansion coefficients among the cable in conduit conductor (CICC) components and the operating strain, ε_{op}, due to the electromagnetic forces on the winding. Only the first contribution has been considered because it is the most relevant and the less known. Once the thermal strain is measured, it is possible to utilize it in the already available scaling laws in order to have a prediction about the reversible cable performance. The irreversible degradation is the difference between the actual performance and the scaling law prediction.
In order to measure ε_{th}, it was performed an experiment with the aim to compare the measurement of the critical temperature as a function of the applied field, $T_c(B)$, for a CICC and the $T_c(B, \varepsilon)$ data for a free standing strand. Without transport current, a small AC field was generated at the sample and its inductive response evaluated. At the superconducting transition the change from a diamagnetic to a paramagnetic response was found. Exploring a broad range of temperature and background field, a curve $T_c(B)$ was obtained and compared to the $T_c(B)$ curves for a free standing Nb_3Sn strand. From the difference of the two curves and using the available scaling laws, the strain in the Nb_3Sn filaments of the CICC was assessed.

Gustavo CANAL: *"Sawtooth Generated Magnetic Islands"*
Analysis of TCV data suggest that the island generation process is too fast to be resolved by temporal Fourier techniques, widely used in JET. Instead of using the usual temporal Fourier technique, toroidal mode decomposition at each time (instantaneous analysis) has been done. The aim of this work is to test the applicability of the forced-reconnection trigger model for "instantaneous" seed island formation in TCV and investigate its applicability on JET. It includes a good understanding of the sideband generation of the 1/1 perturbation at the q=1 surface (sawtooth) and their coupling to the 3/2 or 2/1 magnetic island. Since the generation of sidebands and the coupling of modes is expected to strongly depend on the plasma shape and the q-profile, the study include measurements of parametric dependencies of the sawtooth trigger of NTMs including parameters such elongation, triangularity, magnetic shear, and $q = 1$ flux surface radius.

Michael CHESAUX: *"A new low ion energy bombardment PECVD reactor for the deposition of thin film silicon for solar cell applications"*
The deposition of thin film silicon solar cells done with PECVD using a CCP at VHF lead to a deposition rate of few Å/s and the film thickness is in the range of 0.2 to 3μm. To obtain higher deposition rates more power is often used but this causes an increase of the ion bombardment intensity thus creating higher defects density of the produced films. It is thus necessary to reduce this bombardment in order to increase solar cells efficiencies and satisfy industry demand in term of production yield. This research aims to reduce this ion bombardment by changing the reactor design.
During 2010, Langmuir probes and Paschen curves measurements permitted to test several reactor configurations in order to reduce the breakdown voltage and obtain plasmas covering the whole electrode. A 2D OES (Optical Emission Spectroscopy) setup has been installed to measure the dissociation degree obtained in hydrogen plasmas with the new reactor configurations. The dissociation degree is measured by tacking the intensity ratio of molecular and atomic lines. This diagnostic has shown that the dissociation degree in the new reactor configuration was similar to the ones obtained in the original design.
In order to ensure that the new reactor configurations were indeed reducing the energy of ions falling to the reactor bottom (where a substrate is usually placed), a RFA (Retarding Field Analyser) was built. This diagnostic has shown (Fig. 1) that the new reactor design successfully reduces the ion energy.
The work on numerical simulations is continued. It provided useful numerical data for OES measurements and developments are done to better understand the impact of both argon and hydrogen properties on the plasma behaviour.

Loïc CURCHOD: *"Heating of High Density Plasmas in the TCV Tokamak"*
Oscillation analysis of the toroidal plasma flux response to X2 and X3 modulated ECH (MECH) in order to determine the EC power absorption reveals a strong perturbation of the method due to the sawtooth activity. The experimental frequency transfer functions of the perpendicular kinetic energy in response to the MECH indicate that the plasma behaves like a damped oscillator forced by the MECH, with a resonance at the sawtooth frequency, which yields erroneous estimates of the power absorption coefficient. In particular, an asymmetric improvement of the X3 power absorption in X2 pre-heated plasmas with respect to the sign of the X2 ECCD was observed in previous TCV experiments. This effect remained unexplained, despite intense efforts in Fokker-Planck simulations to investigate the effect of the fast electrons. This asymmetry can be now safely attributed to a strong sawtooth activity destabilized in the case of central co-ECCD and locking to the RF power modulation.
The lower-hybrid (LH) waves generated by a parametric instability (PI) expected to arise during the X-B mode conversion at the upper-hybrid resonance in electron Bernstein wave heating (EBH) experiments are studied thanks to a loop-antenna recently installed on TCV. Fast monitoring of the LHPI spectrum allows to show for the first time the correlation of the amplitude of the detected waves with the local LHPI threshold power at the mode conversion region, estimated from the experimental profiles data. In an EBW power scan, the LHPI threshold power is estimated to be less than 50kW, in good agreement with the value calculated using the experimental profiles data. The LHPI energy cascade from the low to high LH frequency bands, expected in high power EBH experiments, is demonstrated for the first time in TCV.

Cornelis DE MEIJERE: *"Experimental study of turbulence in TCV plasmas"*
In the framework of an ongoing collaboration with A. Kraemer-Flecken the candidate conducted a two week working visit to the Forschungzentrum Juelich in May. Experiments were conducted on the TEXTOR tokamak to measure correlation properties of the turbulence in the edge of limiter H-mode plasmas. Unfortunately, the H-mode transition could not be achieved. Bursts of fluctuations in electron density and magnetic field are observed in these and other neutral beam heated TEXTOR plasmas with weak toroidal magnetic field. The candidate performed an extensive analysis of reflectometer and Mirnov coil data which shed some light on the phenomenology of these bursts. A report on the findings is currently underway.
During part of the period June-August the candidate assisted in setting up the beam generation optics for the tangential phase-contrast imaging system on TCV. The candidate plans to focus entirely on this diagnostic once the aforementioned report on the TEXTOR work is finalized.

Wondwossen Wubie ESHETU: *"Vertical electron cyclotron emission (VECE) diagnostic on TCV"*
A vertically viewing electron cyclotron emission diagnostics is being installed to study non-thermal electrons which are believed to be produced during ECCD/ECRH and MHD activities like sawtooth events.
In the frame of this project a transmission line with ellipsoid mirror, telescope and oversized waveguide that collects the emission from TCV along a vertical and constant magnetic field has been installed. A vacuum compatible ceramic (MACOR) beam dump with a very low reflectivity was also mounted in the vessel to elliminate the wall radiation previous to last year campaign. The ECE radiometers which were being used for horizontal ECE are planned to be used for the VECE measurement. Nevertheless HFS radiometer was found to have very low signal level and even some of the channels were not working at all. The main reason for the low signal level was found to be a problem on the preamplifiers, and they were replaced with new preamplifiers. Plus to this the hetrodyne modules of some of the channels were found to be not working and couldn't be repaired in our expertise. However it is planned to take first measurement in the next experimental campaign with the working channels.
The limitations and the feasibility of the experiment was studied. Plasma parameters that could be feasible for this experiment has been designed. In addition a new analysis method for the calculation of the distribution function and an inversion technique to improve the energy resolution of the system has also been proposed and will be discussed in the coming few days.

Lucia FEDERSPIEL: *"CXRS diagnostic update and momentum transport in TCV across sawteeth events"*
During this year significant effort has been undertaken to update the entire CXRS system. Two new highly sensitive and high time resolution CCD cameras featuring on-chip gain with a full frame readout up to 500Hz (Andor iXon EM+ DU897) were installed so as two new reducers and a new water cooling system. The entire CXRS acquisition process had to be re-integrated into the TCV plant control system and the analysis routines (providing the temperature, velocity and density profiles) were updated for the new CXRS cameras. During the last TCV opening, the mirrors of the horizontal CXRS systems, damaged by glow exposure, were replaced with a pair featuring a Beral coating. The re-installation of the CXRS diagnostic has required a verification of the chord alignment in the lab and on TCV. An absolute calibration, essential in the derivation of density profiles, has also been performed for both the horizontal (LFS) and the vertical (VER) systems directly on TCV. An integrating

sphere together with a support structure was built to place the sphere inside the tokamak vacuum vessel.
The main investigated rotation topic has been a thorough study of the toroidal plasma rotation evolution across sawteeth (ST) events. Several modifications in the CXRS acquisition, analysis and standard TCV operation had to be introduced to obtain time resolved velocity measurements between ST crashes. A scan of ST period has been performed by varying the ECCD deposition just outside the ST inversion radius (STIR). For limited plasmas, it has been observed that inside the STIR (just after the ST crash) there is a strong co-current acceleration in the core of the plasma, whereas in the outer region a small cnt-current acceleration (slower relaxation) is measured. Further measurements with the new cameras need to be performed in order to increase the available radial resolution inside the plasma core and confirm this effective central co-current torque.
Final measurements were performed to confirm that an up-down asymmetry of the magnetic configuration, producing a radial toroidal momentum flux, affects the toroidal rotation gradient in the outer region of TCV plasmas as theoretically predicted. Moreover, support has been given to perform experiments studying the role of Ip and ECH deposition as well as the effect of MHD modes (such as tearing modes) on the rotation profiles.

Federico FELICI: *"Real-time control and simulation of tokamak plasma profiles and MHD activity"*
Recent work has focused around the development of a new 1D finite-element based plasma transport simulation code called RAPTOR. This has two main goals. The first is to allow simulation of the plasma current density profile based on a first-principle model, to be applied in real-time on the TCV tokamak using kinetic data from diagnostic measurements. The code makes have multiple plasma parameters, which are usually available only after post-shot transport analysis, available in real-time during the shot such that they can be used for monitoring or feedback control purposes. This has been successfully implemented and tested on TCV plasmas by programming the interpretative transport code in the new distributed digital control system (SCD). At the same time, a predictive version of the code has developed which can simulate both poloidal flux and electron temperature diffusion. This code has been applied to open-loop optimization studies of tokamak actuator time-trajectories. After definition of an appropriate cost function, tools from nonlinear optimal control can be used to generate an increasingly optimal set of actuator trajectories satisfying a given set of constraints. This methodology has been used to numerically optimize plasma current ramp-up scenarios, both for a hybrid confinement mode with flat core q profile, and for an eITB formation with strong negative shear. TCV experimental work on tearing mode stabilization has progressed with the deployment of the new digital control system and the development of algorithms for MHD-activity triggered actuator scans, phase tracking of magnetic perturbation signals and in-phase RHVPS firing for modulated-ECCD NTM stabilization efficiency studies. First experiments have shown promising results and now await modeling and further experimental confirmation.

Silvano GNESIN: *"Suprathermal electron dynamics in the TCV tokamak"*
A dedicated four camera (24 CdTe semiconductor detectors each) spectroscopic HXR system, providing full coverage of the TCV plasma poloidal plane and opening the possibility of 2D tomographic inversion, is currently in the commissioning phase. Extensive tests of a prototype detector-collimator assembly are currently ongoing in the TCV environment. Dedicated experiments have been performed in TCV to study the synergetic EC power absorption at the 2nd and 3rd harmonics at

the same frequency (f2=82.7GHz). The experiments have been analyzed numerically with the help of the LUKE quasilinear Fokker-Planck code and compared with linear results. Excess X3 absorption is numerically predicted on the plasma LFS and is explained by its interaction with the suprathermal electron population generated by X2 ECCD on the HFS; HXR and ECE emission trends are found to be in good agreement with the simulated synergy level. The parametric dependence of the X2/X3 synergy in density and power scans has also been analyzed. Ongoing work concerns simulations with appropriately tailored radial and velocity space transport in an attempt to quantitatively reproduce measured HXR signal.

Nazar ILCHUK: *"Characterization and modeling of neutron irradiation, pre-deformation and warm prestressing effects on the fracture behavior of the tempered martensitic steel Eurofer97"*
First, experimental activities were undertaken to investigate the fracture toughness behavior of tempered martensitic steel Eurofer97 irradiated up to 0.35dpa at two different temperatures, 150°C and 350°C, respectively. Irradiated sub-sized pre-cracked compact tension fracture specimens were tested accordingly to the ASTM-E1820 standard with a shielded machine in the PSI Hot Laboratory. Vickers micro-hardness tests were performed on the fracture specimens to quantify the irradiation hardening. Finite element modeling (FEM) of Vickers micro-hardness test was performed from which we showed that moderate modifications of Oliver-Pharr's model are necessary to determine the indenter-specimen contact area to calculate the hardness number correctly. Second, characterization of a cold-forged plate of Eurofer97 was performed by micro-tests together with the compression tests of non-standard specimens such as micropillars prepared using the focused ion beam technique. This cold-forged plate is intended to reproduce similar effects on the fracture properties as those induced by irradiation. The pre-cracking of sub-sized compact tension fracture specimens fracture specimens is in progress. Finally, a geometry of notched tensile fracture specimens used to investigate the effect of warm prestressing treatment and residual stresses on the fracture and notch toughness was developed using FEM. Notched tensile fracture specimens of high-chromium tempered martensitic steel F82H were produced and later pre-loaded at room temperature to different loads to create a region with residual stresses around the notch. Measurements of those residual stresses were performed by the time-of-flight neutron diffraction method using POLDI-SINQ instrument at Paul Scherrer Institute showing a good agreement with the modeled results.

Davoud IRAJI: *"Tomographic reconstruction of turbulent plasma emissivity in TORPEX"*
To complement electrostatic probe measurements of plasma turbulence and study of plasma structures smaller than the spatial resolution of probes array, a non-perturbative direct imaging system has been developed on TORPEX, including a fast framing Photron-APX-RS camera and an image intensifier unit. From the line integrated camera images we compute the poloidal emissivity profile of the plasma by applying a tomographic reconstruction technique, using a pixel method and solving an over-determined set of equations by singular value decomposition. This allows comparing statistical, spectral and spatial properties of visible light radiation with electrostatic fluctuations. The shape and position of the time-averaged reconstructed plasma emissivity are observed to be similar to those of the ion saturation current profile. In the core plasma, excluding the electron cyclotron and upper hybrid resonant layers, the mean value of the plasma emissivity is observed to vary with $T_e \hat{}\alpha\ n_e \hat{}\beta$, which α =0.25-0.7 and β=0.8-1.4, in agreement with collisional radiative model. The tomographic reconstruction is applied to the fast

camera movie acquired with 50 kframes/s rate and 2μs of exposure time to obtain the temporal evolutions of the emissivity fluctuations. Conditional average sampling is also applied to visualize and measure sizes of structures associated with the interchange mode. The ω-time and the 2D k-space Fourier analysis of the reconstructed emissivity fluctuations show the same interchange mode that is detected in the ω and k spectra of the ion saturation current fluctuations measured by probes. Small scale turbulent plasma structures can be detected and tracked in the reconstructed emissivity movies with the spatial resolution down to 2 cm, well beyond the spatial resolution of the probe array.

Josef KAMLEITNER: *"Hard X-ray diagnostics, measurement and modeling of suprathermal electron population"*
The hard x-ray diagnostics at TCV are essential to measure the suprathermal electron population in the fusion plasma. The Tangential X-ray Detector Array (TXDA) diagnostic system observes the hard x-ray bremsstrahlung emission of high energy electrons in the range 1.5 to 200 keV. Its high time resolution of 125 kHz enables the analysis of the acceleration of these electrons during fast MHD events such as sawtooth crashes and disruptions. A preliminary analysis of data collected during the last campaign was performed and is being compiled in a report.
Additionally, a Hard X-Ray Tomographic Spectrometer (HXRS) is being installed on TCV and will enable a two-dimensional tomographic reconstruction of the suprathermal electron population with energy resolution. Detector testing and characterization for this system was carried out in 2010.

Sohrab KHOSH AGHDAM: *"Study of the non-adiabatic response of electrons in ITG/ETG-type microturbulence"*
To study microinstabilities, the starting point is the gyrokinetic equation, which describes in a kinetic frame the dynamics of each plasma particle distribution function (PDF) in a 6-dimensional phase-space. Within the gyrokinetic ordering, one can average out the fast gyromotion of particles and thus reduce the dimensionality of the problem from 6 to 5. Concerning this project, we make use of the Eulerian gyrokinetic GENE code.
When considering the full kinetic dynamics of electrons, the response from the passing fraction may become non-adiabatic around so-called mode rational surfaces characterized by a rational safety factor $q_s=m/n$, where m and n are relatively low integer numbers. In the vicinity of such a surface, the parallel wave number $k_\parallel$ of the Fourier mode components with poloidal-toroidal mode number pairs (m,n) goes to zero and the corresponding parallel phase velocity $\omega/k_\parallel$ becomes large compared to the electron thermal velocity, to the point that electrons are unable to respond adiabatically. As a result of this non-adiabatic response, fine radial structures compared to the Larmor radius $\rho_L = v_{thi}/\Omega_i$ develop. Essential physics may thus be lost if these radial structures are not correctly resolved numerically.
The first step was thus to study in detail these regions for linear eigenmodes, so as to identify appropriate numerical parameters. In a second step, preliminary simulations were carried out to address the issue of whether these structures are still prevailing in the nonlinear regime or if they are wiped out by nonlinear mode interaction. In case such structures are persistent, the key question is how significantly they affect the turbulent transport levels.
In the current version of the GENE code, electrons are either considered to be fully kinetic or represented by a reduced model assuming a fully adiabatic response. In order to be able to selectively turn off the kinetic response of the passing fraction, a hybrid reduced model has been implemented in GENE, evolving trapped particles

kinetically and setting passing particles to be adiabatic. This hybrid model enables to effectively turn off the non-adiabatic response around mode rational surfaces and thus better assess their importance. This feature will thus be essential for characterizing these special structures both in a local and global geometry framework. A benchmark with another gyrokinetic code (ORB5) will be very helpful as well.
Finally, to enable a more flexible access to GENE simulation results, the output files have been extended to the standard HDF5 format. Thus, GENE becomes independent of its "in-house" diagnostic tools and can be easily accessed by most data analysis softwares (IDL, Matlab, etc).

Doohyun KIM: *"Plasma Simulations of TCV plasmas with ECCD sawtooth control"*
Transport phenomena are one of the most important parts of tokamak physics. By solving transport equations and using some simulation tools, we can understand this. As a first step of my study, I reviewed the neoclassical transport theories and particularly, derived transport coefficients for bootstrap current. From this work, I will be able to extend my understanding to the other transport phenomena and the link with ECH/ECCD.

Boris LEGRADIC: *"Arcing in Very Large Area Plasma-Enhanced Chemical Vapour Deposition Reactors"*
Small gaps are present in plasma enhanced chemical vapour deposition reactors to insulate the RF electrode from the grounded parts of the reactor in the showerhead. These gaps are supposed to be small enough that no glow discharge can form, but wide enough to prevent arcing. RF breakdown in these small gaps is of high interest for the thin-film industry, since arcing and parasitic plasmas in small gaps in PECVD reactors represent a failure point preventing the upscaling to larger substrates and/or higher power regimes for micro-crystalline silicon deposition.
In the last year more research into RF breakdown for parallel plate electrodes with holes or protruding features took place. Experiments in argon and hydrogen and fluid simulations show that the breakdown curves in typical gas pressures used in PECVD reactors are not influenced by sharp edges or ridges. Rather, the breakdown voltage mostly depends on the maximum and minimum distance between the electrodes. These results, together with analytical work explaining the physics behind them, were published in Physics of Plasmas, and presented at the ICOPS and GEC conferences.

David LESCURE: *"Breakdown events and potential wells in gyrotron guns"*
Although vacuum is used extensively for the insulation of high voltage in such devices as X-ray tubes, particle accelerators, gyrotron guns etc., the reliability of its performance is limited by
the operational risk of an unpredictible arcing event between high voltage electrodes, when the insulationg capability of the vacuum gap is suddenly lost. We then talk about electrical breakdown.
In the case of gyrotron gun, such events can be more or less dramatic, from small leak currents in various parts of the gyrotron to real arcing events in the cavity.
The consequences vary from small damage on the walls of the cavity, to real crack in the ceramic parts of the gun for example. Even more problematic, these events can interrupt the discharge
of the gyrotron and are suspected to be the cause that prevented the first prototype of the ITER 170 GHz gyrotron to withstand a discharge longer than a few nanoseconds.

Part of this thesis work is based on the idea that these breakdown events in gyrotron guns may be due to an accumulation of charges in charged particles traps. These particles may create
a growing space charge which could eventually lead to a discharge. A simulation and an experiment have actually been developped to study and confirm this idea, which lead to very encouraging results in terms of votage stand off for example.

Joaquim LOIZU: *"Simulation of plasma turbulence in the TORPEX basic plasma physics experiment"*
An effort is being put in the improvement of the current 3D two-fluid model that simulates the TORPEX device, first focusing on the physics of the plasma sheath. Indeed, boundary conditions determine the plasma losses at the vessel, thus strongly affecting the steady state profiles. A kinetic approach is needed in order to describe the plasma-wall transition (PWT), where the drift-reduced approximation breaks (magnetic presheath), followed by a breaking of quasi-neutrality (electrostatic sheath). For this purposes a fully kinetic, 1D3V particle-in-cell (PIC) code has been developed to study the properties of the plasma in the PWT region. The simplest case of a magnetic field perpendicular to the wall has been first explored. In this regime, the magnetic field does not affect the PWT, and only an electrostatic sheath is present. A combined fluid and kinetic description of the plasma, supported by the numerical results, has been used to rigorously derive the position of the sheath entrance and to understand how the fluid quantities are related at this point. In particular, it has been found that the Bohm criterion, stating that ions need to be accelerated up the sound speed c_s in order for a sheath to exist, is valid in floating potential conditions or in the presence of ion current to the wall, but fails to describe the transition to the non-neutral region in the presence of an electron current to the wall. In fact, the electron velocity distribution function is a Maxwellian that is truncated as approaching the wall, and such phenomenon can have a strong effect on the ion velocity at the sheath edge, in the case of a large electron current. The more general situation of an oblique magnetic field is now being studied in detail, using the same PIC code and a similar analytical procedure.

David MARTINET: *"Development of industrial gas-metal plasma sources for the deposition of nanostructured GaN semiconductor layers for lighting applications"*
Wide direct band-gap gallium nitride is a promising material for short-wavelength optoelectronic device applications such as light-emitting diodes (LEDs), laser diodes (LDs) and nitride-based solar cells. Gallium nitride-epitaxial films with low dislocation density are very important for improving device performance. Currently, GaN-related materials are predominantly grown on sapphire substrates on which there are large differences between the lattice constant and thermal expansion coefficient of the GaN layer and the substrate.
This results in high dislocation densities in the epitaxial films, reducing device performance and yield and also adds a significant contribution to the cost of producing a device.
GaN films can be grown by several techniques, the most common of which are metal organic chemical vapour deposition (MOCVD) and molecular beam epitaxy (MBE). To expand the range of applications of GaN it is necessary to develop processes that operate at lower temperatures, with cleaner precursors and which can be applied to larger scale fabrication.
This new CTI project, initially funded by seed money from March to October 2010, and subsequently by CTI No. 11548.1 PFIW-IW, in collaboration with Sulzer METCO and the Laboratory of Advanced Semiconductors for Photonics and Electronics (LASPE) at the EPFL, will try to modify the existing RF and DC plasma

sources in order to grow GaN films on SiC or sapphire substrates, by evaporating Ga in nitrogen plasma. During this first year, efforts have been made to characterize the plasmas created by the two sources, using Langmuir probe, Faraday cup (FC) and optical emission spectroscopy (OES) measurements. The principal plasma parameters, such plasma density, different temperatures and plasma composition can be found, and the homogeneity of the plasma at the substrate has been checked.
The complex RF inductively coupled -ECR combined plasma source has been tested with two major configurations: with and without a grid at the exit of the source, leading to two completely different plasmas. The insertion of the grid creates an ion beam, composed with both N^+ and N_2^+ (seen with OES) which quickly disappear in the downstream plasma. The impact of this beam with the insertion of Ga in this downstream plasma will be investigated in the next months.
Electrical properties and plasma composition and stability of the DC source with two different configurations have been investigated. A conical point anode shows a better stability than a circular one, due to the straight path of the electrons. But for depositions this configuration will certainly require more efforts to get acceptable film homogeneity. For this reason the circular anode configuration is preferred and will be further investigated.

Annamaria MOSETTO: *"Linear and non-linear modelling of scrape off layer instabilities"*
I started my PhD at the beginning of April, 2010, and I am working with Prof. Paolo Ricci for the development and the upgrade of the GBS two fluids code for the simulation of the scrape off layer (SOL) in a Tokamak configuration.
During this period of time I firstly studied the theoretical model on which the code is based and the main instabilities expected in this Tokamak region. Therefore a detailed linear analysis of the drift wave instability, of the ballooning mode and of the ion temperature gradient mode, based on the model equations, has been perfomed. After on I started implementing a simple linear code for the prediction of the growth rate of the possible instabilities. The aim of this code is to give a first insight on the non linear behaviour of the system that will be globally simulated by the GBS code. Finally we included some new features in the global code, in order to take into account some physical effects that were neglected before: firstly the SOL geometry was implemented, then the effects of the magnetic shear. We already performed some simulations including the new influences and now we are analyzing the results taking advantage of the linear code prediction, too. The next steps will be the addition of the electromagnetic effects and of the ion temperature in the global and in the linear code, in order to achieve a complete physical description of the system.

Francesco PIRAS: *"Plasma shape control of TCV"*
The snowflake divertor has been proposed and theoretically studied by Dr. D.D.Ryutov from the Lawrence Livermore National Laboratory. In Ryutov's articles, this configuration was proposed to alleviate the problems of the plasma-wall interaction and possibly affect the plasma edge stability. The TCV tokamak was the first to report the creation and control of a snowflake configuration.
An edge-localized mode (ELM) H-mode regime, supported by electron cyclotron heating, has been successfully established in a snowflake. This regime exhibits 2 to 3 times lower ELM frequency but only a 20%-30% increase in normalized ELM energy compared to an identically-shaped, conventional, single-null, diverted H-mode. Enhanced stability of mid- to high-toroidal- mode-number ideal modes is consistent with the different snowflake ELM phenomenology. Finally, the capability

of the snowflake to redistribute the edge power on the additional strike points has been confirmed experimentally.

Anna PROKHODTSEVA: *"Primary Radiation Damage in Ultra High Purity Iron and Model Iron Cromium Alloys"*
TEM in situ dual beam irradiation/implantation experiments are being conducted in the JANNuS facility in Orsay, France, on specimens of ultra high purity (UHP) Fe, Fe-5Cr, Fe-10Cr and Fe-14Cr, at room temperature to 0.5 dpa with or without He at levels up to 1000 appm. Defect densities and sizes were calculated from the TEM micrographs. Defect number densities in the presence of He are strongly dependent on the Cr content, with a minimum for the Fe–10Cr alloy. However, in the case of the single beam irradiation, without He, the defect density shows no clear trend with the Cr content.
Defects Burgers` vectors are being identified in using the Convergent Weak Beam Technique (CWBT), whose application to the present project lead to further development. It consists in tilting the incident beam to achieve a range of diffraction conditions during a single exposure of the photographic negative, which allows circumventing oscillations of diffraction contrast and hence providing better statistics.
Bulk samples for the ex situ irradiation campaign were prepared and sent to Saclay.

Silvia PUDDU: *"Spectroscopy in visible light"*
For this diagnostic a complete analysis programme has been done for spectrum analysis, time evolution of spectral lines and time evolution of bremsstrahlung (in progress).
The aim is to study the presence of impurities in tokamak.
In particular the study of bremsstrahlung will allow us to know the Z_{eff} of the plasma and its evolution. This can be done by isolating zones without lines in the spectrum.

Marina RICCI: *"On the powder formation in the plasma enhanced chemical vapor deposition process for the deposition of SiOx barrier coatings"*
The powder formation in the plasma enhanced chemical vapor deposition process for coating polymer films has been used for investigating SiO_x powder particle formation. By studying processes made in a capacitively coupled reactor, it has shown that operating with hexamethyldisiloxane (HMDSO) and O_2, at high RF power, high pressure and high O_2 content, plasma crystals appear. The polymerization process, which normally comes before powder formation, is overtaken by immediate comparison of big powder particles. The analysis of the RF harmonics shows that plasma crystals seem to appear in correspondence of a reduction of the TO/LO mode ratio visualized in the in-situ infrared absorption spectra. The ATR infrared spectrum of the collected powder shows the reduction of the carbon content due to the introduction of the oxygen amount in the plasma admixture.

Jonathan ROSSEL: *"Edge localized modes: analysis and control in TCV"*
A detailed report on the physics design of a saddle coil system for TCV has been written. This includes the physical justification of the proposed design, the electrical characterization of the coil system in the presence of a conducting wall and other aspects like the electrical impact of plasma disruptions, magnetic forces and coil cooling. A number of hardware-related problems concerning the fast

magnetic probe diagnostics have been solved. The data analysis routines have been completed and packed in a common modular framework, including a number of new features and a documentation. A statistical analysis of type I ELM precursors based on magnetic diagnostics data has been carried out with no conclusive results. An experimental program has been prepared to study ELM control by plasma edge heating. Simulations have been run to assess heating accessibility and efficiency in different plasma configurations.

Ralf SCHNYDER: *"Arc Phenomena in Space Environment and Equipment"*
Arc phenomena are one of the oldest topics in plasma physics. Arcing is again a key issue in the application of plasmas in industry and also in space environment and space equipment. Modern satellites, in particular transmission satellites are being equipped with larger and larger power systems. Since the weight aspect is very important the dimensions of the conducting paths, for instance in slide rings, are small. Unfortunately several incidents showed that arcs producing short circuits of the power system can dangerous for the satellite. Arcing also starts to be the limiting factor in several other applications of plasmas, thus triggering intense research and development on this topic.
In the present work for the space agency ESA in collaboration with RUAG Aerospace in Nyon and the Haute École d'Ingénierie et de Gestion du Canton de Vaud (HEIG/VD-IESE) laboratory, the necessary fundamentals of arcing shall be established and be applied to space equipment in order to reduce or suppress arcing in space environment.
The first aim of the work was a breakdown limit test for DC high voltages with a simplified setup compared to a real slip ring assembly. With this setup, parameters such gas environment (various gases from 10^{-6} to 10^{3} mbar), global geometry and material of both conductors and insulators have shown impact on breakdown voltages. The next steps will be to understand exactly the different observations in particular the transition limit from vacuum arcs to corona discharge in these conditions. Furthermore we will purchase with a high voltage generator constructed by HEIG which simulates the voltages at the input of the satellites to test the robustness of a real slip ring assembly provided by RUAG Aerospace.

Christian THEILER: *"Basic investigations of turbulent structures and blobs of relevance for magnetic fusion plasmas"*
During year 2010, I have further explored possibilities of controlling the cross-field propagation of plasma filaments (blobs). I have found that increasing the neutral gas pressure or shortening the field line length reduces blob velocity. Shortening the field line length is only effective for blobs in light gases in TORPEX (H2 and He), but not for Neon or Argon blobs. These trends are in agreement with our blob velocity formula.
We have further advanced in the TORPEX code validation project, where I have conducted the experimental work. Based on a relatively large set of observables, we have compared experimental measurements and simulation outputs for different target plasmas. A metric was introduced to quantify the agreement between experiments and a given numerical model. This metric clearly shows the improved performance of a global 3D code compared to a 2D code and further highlights aspects of time averaged and turbulent properties that are or are not well represented by the codes.
Finally, together with a TP student (Aurélie Kuenlin), we have studied and overcome limitations of the triple Langmuir probe technique. A new probe design with new electronics allows us now to obtain local, time-resolved measurements of density, electron temperature and plasma potential.

Lyubomira VELEVA: *"Development and Characterization of Tungsten-Base Materials for Fusion Reactor Applications"*
Recent activities were focused on manufacturing, W-2Y material (in weight percent) by conventional powder metallurgy methods including dry mechanical alloying of elemental powders in an argon atmosphere, followed compaction by sintering in the PLANSEE Company in Austria. The density of the compacted W-2Y material was found to be the highest, equal to about 95% of the theoretical density. Specimens for scanning electron microscopy and transmission electron microscopy (TEM) observations were prepared from the W-2Y material. TEM observations showed that the W-2Y material is composed of grains with a size between 200 and 500 nm, it also contains big oxide particles with a mean size up to 100 nm. The small particles appear homogeneously distributed in the tungsten matrix. The rest of activates were focused on the preparation and writing of the PhD thesis with topic: "Contribution to the development and characterization of W-Y, W-Y2O3, and W-TiC for Fusion Reactors".

Thibaud VERNAY: *"Collision operators in the gyrokinetic code ORB5: neoclassical transport and turbulence studies"*
The first objective of the work is to implement different collision algorithms, based on the Langevin approach, into the gyrokinetic Particle-In-Cell code ORB5 and to test them. One possibility to achieve such tests is to use them in situations which are simplifications of the final system of interest. One may start solving for axisymmetric solutions to the collisional gyrokinetic equations in tokamak plasmas, thus addressing the topic of so-called neoclassical transport, for both electrons and ions. One will also focus on the way the collisionality affects the dispersion relation of the electrostatic wave itself, in the linear regime. The main work will then consist in studying the effects of collisions on the electrostatic micro-turbulence in the non-linear regime, and especially on the anomalous transport closely related to the turbulence. In addition to further developments brought to the collision algorithms in ORB5, the main 2010 activity was related to the publication of a paper in the journal *Physics of Plasmas*. Extensive tests of the collision operators within the frame of the neoclassical transport theory have been performed, through benchmarks against other codes as well as analytical theories. A new algorithm for carrying out collisional runs has been proposed. It has been shown that a coarse graining procedure in ORB5 is able to reduce the numerical noise. A controlled noise in collisional runs opens interesting perspectives for simulations of micro-turbulence. The newly implemented algorithms have also been introduced into the new electromagnetic version of the code, NEMORB. Preliminary runs for studying microturbulence, considering gyrokinetic ions and both adiabatic and kinetic electrons, have been carried out.

David WAGNER: *"Experimental and theoretical study of Impurity Transport on TCV"*
In TCV H-mode plasmas significant flattening of the density profile is observed when electron cyclotron resonance heating is applied. In 2010, linear flux tube gyrokinetic simulations with the GS2 code have been undertaken to understand the physical phenomena that can cause the reduction of the density gradient.
In other machines (e. g. JET, ASDEX-U) the collisionality is considered as the most influential parameter on the density peaking. However in the simulations corresponding to TCV cases, the stationary value of the density gradient changes little with this parameter. It is also found that the electron to ion temperature ratio has the most important effect and the reduction of the density peaking is mainly

due to this parameter. Other parameters like α and the Ware-pinch seem to play a role as well.
In most fusion devices the ion and electron temperature values and their gradients are close to each other. This parameter regime is relatively well studied and understood and it was shown that the so-called stationary value of the density gradient leading to zero particle flux is adjusted by the balance between the ion temperature gradient modes (ITG) driving inward particle flux and the trapped electron modes (TEM) driving outward flux. However, at TCV in particular in H-mode plasmas, the ion temperature gradient is lower than that of the electrons, therefore the ion dynamics can be suppressed and especially at low density gradients the most unstable modes are not ITG but slab-like electronic modes. These modes are due to the non-adiabatic passing électron response on the mode-rational surfaces.
In addition to the turbulence, the neoclassical Ware-pinch can contribute significantly to the density peaking. This effect is non-negligible for the ohmic H-mode cases.

7 PUBLIC RELATION ACTIVITIES IN 2010

The salient activities in the public relation domain were the open doors of the EPFL and the launch of a new web site. In parallel, we continued to welcome visitors and produce several documents aiming at different types of public.

The open doors of the EPFL attracted more than 20'000 people in 2 days (29-30 May). The CRPP hosted the centre dedicated to the energy. The visitors, more than 2000, mostly families, were proposed guided tours around our devices: TCV, Torpex and the plasma processing reactors. They had the oportunity to see and play with basic experiments showing for instance how magnetic fields can guide charged particles. Manned booths presented activities from other labs such as research in fuel cells, super caps, ... At this occasion, a flyer presenting fusion on one side and our activities on the other side was published and widely distributed.

Beside this major event another 1000 persons visited the CRPP in 2010. As usual, most of them were classes or adults belonging to professionnal or political groups which either were invited or asked for a visit (through the web site). In particular, we welcome, every year, 200 children (12-13 years old) in one morning.

In 2010, the EPFL launched a new graphic design for all its web sites. It was accompanied by a series of new tools to manage the information (CMS: Jahia). A large fraction of the CRPP web site was migrated to the new system. We took advantage of this migration to restructure, revisit and rewrite our public web site. In particular, animated images were produced.

8 FUSION & INDUSTRY RELATION

The mission of the Industrial Liaison Officer (ILO) was pursued in 2010 to encourage the contribution of Swiss industry to the realization of ITER. Several actions were undertaken to reach this goal, among which one can mention:

- January 20, 2010: Information Day addressed to professional associations in Switzerland, for them to relay the information on ITER to their members

- September 27 to October 1st, 2010: SOFT (Symposium on Fusion technologies) Conference in Porto bringing together the entire Fusion Community (researchers and industry at the exhibition booths). The ILO set up with the support of OSEC a Swiss Pavilion housing 11 Swiss companies. All Swiss firms reported their satisfaction of having come to Porto.

Other activities fall within the scope of standard promotional activities, e.g.: visits to enterprises, personal emails to potential suppliers drawing the attention to published Calls for Tenders issued either by F4E or ITER Organization (IO) in Cadarache, periodically updating the information on the Swiss WEB site (www.iter-industry.ch) and attending the routine meetings which F4E convenes for the European ILO's. Issues common to all ILO's are debated at these meetings, e.g.: contractual conditions, IPR, upcoming tenders, possibilities of collaboration amongst ILO's and amongst industries in Europe.

F4E performs 2 actions for early warning to industry on upcoming Calls:
A first action concerns the elaboration of so-called Mappings of competencies. With the help and feed-back from the ILO's and Industry, F4E lists all companies interested in a particular field of expertise in an excel-table (mapping). This table is published in F4E's WEB site. Companies therefore now have the opportunity of exchanging and making preliminary arrangements prior to the Call for tender.
A second action deals with carrying out Information Days on specific topics in Barcelona. Companies interested by the subject and attending the event not only gain first-hand information on upcoming Calls but also have the opportunity of networking with colleagues having similar interests.
The support of the ILO to F4E and to Industry is indispensable in both cases.

APPENDICES

APPENDIX A Articles published in Refereed Scientific Reviews during 2010

(see CRPP archives at http://crppwww.epfl.ch/archives)

M. Albergante, J. Graves, A. Fasoli, X. Lapillonne, *Microturbulence Driven Transport of Energetic Ions in the ITER Steady-State Scenario,* Nuclear Fusion **50**, 084013 (2010).

S. Alberti, M.Q. Tran, D.R. Whaley, *The Thirteenth Special Issue on High-Power Microwave Generation,* IEEE Transactions on Plasma Science **38**, 1138-1140 (2010).

D. Alves, R. Coelho, A. Klein, T. Panis, A. Murari, *A Real-Time Synchronous Detector for the TAE Antenna Diagnostic at JET,* IEEE Transactions on Nuclear Science **57**, 577-582 (2010).

J.F. Artaud, V. Basiuk, F. Imbeaux, M. Schneider, J. Garcia, G. Giruzzi, P. Huynh, T. Aniel, F. Albajar, J.M. Ané, A. Bécoulet, C. Bourdelle, A. Casati, L. Colas, J. Decker, R. Dumont, L.G. Eriksson, X. Garbet, R. Guirlet, P. Hertout, G.T. Hoang, W. Houlberg, G. Huysmans, E. Joffrin, S.H. Kim, F. K Chl, J. Lister, X. Litaudon, P. Maget, R. Masset, B. Pégourié, Y. Peysson, P. Thomas, E. Tsitrone, F. Turco, *The CRONOS Suite of Codes for Integrated Tokamak Modelling,* Nuclear Fusion **50**, 043001 (2010).

M. Bagnasco, D. Bessette, L. Bottura, C. Marinucci, *Progress in the Integrated Simulation of Thermal-Hydraulic Operation of the ITER Magnet System,* IEEE Trans. Appl. Supercond. **20**, 411-414 (2010).

M. Bagnasco, L. Bottura, M. Lewandowska, *Friction Factor Correlation for Cicc's Based on a Porous Media Analogy,* Cryogenics **50**, 711-719 (2010).

A. Bottino, B. Scott, S. Brunner, B.F. McMillan, T.-M. Tran, T. Vernay, L. Villard, S.B. Jolliet, R. Hatzky, A. Peeters, *Global Nonlinear Electromagnetic Simulations of Tokamak Turbulence,* IEEE Transactions on Plasma Science **38**, 2129-2135 (2010).

L. Brocher, W.A. Cooper, J.P. Graves, G.A. Cooper, Y. Narushima, K.Y. Watanabe, *Drift Stabilization of Ballooning Modes in a High,* Nuclear Fusion **50**, 025009 (2010).

P. Bruzzone, *Superconductors for Fusion: Achievements, Open Issues, Roadmap to Future,* Physica C **470**, 1734-1739 (2010).

P. Bruzzone, B. Stepanov, R. Wesche, M. Bagnasco, F. Cau, R. Herzog, M. Calvi, M. Vogel, M. Jenni, M. Holenstein, H. Rajainmaki, *Status Report of the Sultan Test Facility,* IEEE Trans. Appl. Supercond. **20**, 455-457 (2010).

P. Bruzzone, R. Wesche, F. Cau, *Results of Thermal Strain and Conductor Elongation Upon Heat Treatment for Nb3Sn Cable-in-Conduit Conductors,* IEEE Trans. Appl. Supercond. **20**, 470-473 (2010).

A. Burckel, O. Sauter, C. Angioni, J. Candy, E. Fable, X. Lapillonne, *On the Effects of the Equilibrium Model in Gyrokinetic Simulatins: From S-Alpha to Diverted MHD Equilibrium,* J. of Physics: Conference Series **260**, (2010).

M. Calvi, P. Bauer, F. Cau, C. Marinucci, P. Bruzzone, *Design Proposal for ITER Feeder Busbar System,* IEEE Trans. Appl. Supercond. **20**, 407-410 (2010).

Y. Camenen, A. Bortolon, B.P. Duval, L. Federspiel, A.G. Peeters, F.J. Casson, W.A. Hornsby, A.N. Karpushov, F. Piras, O. Sauter, A.P. Snodin, G. Szepesi, *Experimental Evidence of Momentum Transport Induced by an up-Down Asymmetric Magnetic Equilibrium in Toroidal Plasmas,* Physical Review Letters **105**, 135003 (2010).

Y. Camenen, A. Bortolon, B.P. Duval, L. Federspiel, A.G. Peeters, F.J. Casson, W.A. Hornsby, A.N. Karpushov, F. Piras, O. Sauter, A.P. Snodin, G. Szepesi, T.C.V.T. The, *Experimental Demonstration of an up-Down Asymmetry Effect on Intrinsic Rotation in the TCV Tokamak,* Plasma Physics and Controlled Fusion **52**, 124037 (2010).

F. Cau, P. Bruzzone, *Dependence of the AC Loss on the Aspect Ratio in a Cable in Conduit Conductor,* Supercond. Sci. Technol. **23**, (2010).

F. Cau, P. Bruzzone, M. Calvi, *Interstrand Resistance and Contact Resistance Distribution on Terminations of ITER Short Samples,* IEEE Trans. Appl. Supercond. **20**, 478-481 (2010).

F. Cau, P. Bruzzone, M. Vogel, *Design Study of a Superconducting Magnet System for the European Synchrotron Radiation Facility,* Supercond. Sci. Techn. **23**, (2010).

I.T. Chapman, R.J. Buttery, S. Coda, S. Gerhardt, J.P. Graves, D.F. Howell, A. Isayama, R.J. La-Haye, Y. Liu, P. Maget, M. Maraschek, S. Sabbagh, O. Sauter, *Empirical Scaling of Sawtooth Period for Onset of Neoclassical Tearing Modes,* Nuclear Fusion **50**, 102001 (2010).

I.T. Chapman, J.P. Graves, C. Wahlberg, *The Effect of Plasma Profile Variation on the Stability of the n=1 Internal Kink Mode in Rotating Tokamak Plasmas,* Nuclear Fusion **50**, 025018 (2010).

I.T. Chapman, M.D. Hua, S.D. Pinches, R.J. Akers, A.R. Field, J.P. Graves, R.J. Hastie, C.A. Michael, *Saturated Ideal Modes in Advanced Tokamak Regimes in MAST,* Nuclear Fusion **50**, 045007 (2010).

I.T. Chapman, R. Scannell, W.A. Cooper, J.P. Graves, R.J. Hastie, G. Naylor, A. Zocco, *Magnetic Reconnection Triggering Magnetohydrodynamic Instabilities During a Sawtooth Crash in a Tokamak Plasma,* Physical Review Letters **105**, 255002 (2010).

J. Chowdhury, R. Ganesh, P. Angelino, J. Vaclavik, L. Villard, S. Brunner, *Sluggish Response of Untrapped Electrons and Global Electrostatic Micro-Instabilities in a Tokamak,* J. of Physics: Conference Series **208 (2010)**, 012058 (2010).

J. Chowdhury, R. Ganesh, S. Brunner, J. Vaclavik, L. Villard, *Toroidal Universal Drift Instability: A Global Gyrokinetic Study,* Physics of Plasmas **17**, 102105 (2010).

A. Collazos, R. Bertizzolo, R. Chavan, F. Dolizy, F. Felici, T.P. Goodman, M.A. Henderson, J.D. Landis, F. Sanchez, *Progress on the ITER H&CD EC Upper Launcher Steering-Mirror Control System,* IEEE Transactions on Plasma Science **38**, 441-447 (2010).

W.A. Cooper, L. Brocher, J.P. Graves, G.A. Cooper, Y. Narushima, K.Y. Watanabe, W. Ebeling, G. Gussman, T. Klinger, K.H. Spatsche, *Drift Stabilization of Ballooning Modes in an Inward-Shifted LHD Configuration,* Contributions to Plasma Physics **50**, 713 (2010).

W.A. Cooper, J.P. Graves, A. Pochelon, O. Sauter, L. Villard, *Tokamak Magnetohydrodynamic Equilibrium States with Axisymmetric Boundary and a 3d Helical Core,* Physical Review Letters **105**, 035003 (2010).

A. Della Corte, V. Corato, A. Di Zenobio, C. Fiamozzi Zignani, L. Muzzi, G.M. Polli, L. Reccia, S. Turt II, P. Bruzzone, E. Salpietro, A. Vostner, *Successful Performances of the EU-AltTF Sample, a Large Size Nb3Sn Cable-in-Conduit Conductor with Rectangular Geometry,* Supercond. Sci. Technol. **23**, 045028 (2010).

A. Encheva, G. Vayakis, A. Karpushov, *Design Optimisation of the ITER Divertor Magnetic Probes Using Fem Analyses,* Fusion Engineering and Design **85**, 18-23 (2010).

E. Fable, C. Angioni, O. Sauter, *The Role of Ion and Electron Electrostatic Turbulence in Characterizing Stationary Particle Transport in the Core of Tokamak Plasmas,* Plasma Phys. Control. Fusion **52**, 015007 (2010).

A. Fasoli, A. Burckel, L. Federspiel, I. Furno, K. Gustafson, D. Iraji, B. Labit, J. Loizu, G. Plyushchev, P. Ricci, C. Theiler, A. Diallo, S. Müller, M. Podesta, F.M. Poli, *Electrostatic Instabilities, Turbulence and Fast Ion Interactions in the TORPEX Device,* Plasma Physics and Controlled Fusion **52**, (2010).

A. Fasoli, D. Testa, T. Panis, A. Klein, J.A. Snipes, J. Sears, M. Gryaznevich, R. Martin, S.D. Pinches, JET-EFDA Contributors, *Active Excitation and Damping Rate Measurement of Intermediate-n Toroidal Alfvén Eigenmodes in JET, C-Mod and MAST Plasmas,* Plasma Phys. Control. Fusion **52**, 075015 (2010).

F. Felici, T. Shimozuma, S. Kubo, Y. Yoshimura, O. Sauter, T.P. Goodman, LHD Experiment Group, *Feedback Control of ECRH Polarization on LHD,* Nuclear Fusion **50**, 105003 (2010).

A. Feltrin, B. Strahm, G. Bugnon, F. Sculati-Meillaud, C. Ballif, A.A. Howling, C. Hollenstein, *Input Silane Concentration Effect on the a-Si:H to μc-Si:Hμc-Si:H Transition Width,* Solar Energy Materials and Solar Cells **94**, 432-435 (2010).

X. Garbet, Y. Idomura, L. Villard, T.H. Watanabe, *Gyrokinetic Simulations of Turbulent Transport,* Nuclear Fusion **50**, 043002 (2010).

T. Goerler, X. Lapillonne, S. Brunner, J. Chowdhury, T. Dannert, F. Jenko, B. Mcmillan, F. Merz, D. Told, L. Villard, *Nonlocal Effects in Gyrokinetic Turbulence Simulations Using Gene,* J. of Physics: Conference Series **260**, 012011 (2010).

J.P. Graves, I.T. Chapman, S. Coda, T. Johnson, M. Lennholm, *A New Sawtooth Control Mechanism Relying on Toroidally Propagating Ion Cyclotron Resonance Frequency Waves: Theory and Joint European Torus Tokamak Experimental Evidence,* Physics of Plasmas **17**, 056118 (2010).

J.P. Graves, I.T. Chapman, S. Coda, T. Johnson, M. Lennholm, B. Alper, M. Baar, K. Crombe, L.G. Eriksson, R. Felton, D. Howell, V. Kiptily, H.R. Koslowski, M.L. Mayoral, I. Monakhov, I. Nunes, S.D. Pinches, *Experimental Verification of Sawtooth Control by Energetic Particles in Ion Cyclotron Resonance Heated JET Tokamak Plasmas,* Nuclear Fusion **50**, 052002 (2010).

S.M. Hafez Haghighat, R. Schaublin, *Influence of the Stress Field Due to Pressurized Nanometric He Bubbles on the Mobility of an Edge Dislocation in Iron,* Philosophical Magazine **90**, 1075-1100 (2010).

C. Hellesen, M. Albergante, E.A. Sundén, L. Ballabio, S. Conroy, G. Ericsson, M.G. Johnsson, L. Giacomelli, G. Gorini, A. Hjalmarsson, I. Jenkins, J. Källne, E. Ronchi, H. Sjöstrand, M. Tardocchi, I. Voitsekhovitch, M. Weiszflog, JET-EFDA Contributors, *Neutron Spectroscopy Measurements and Modeling of Neutral Beam Heating Fast Ion Dynamics,* Plasma Physics and Controlled Fusion **52**, 085013 (2010).

A.A. Howling, R. Sobbia, C. Hollenstein, *Hydrogen-Dominated Plasma, Due to Silane Depletion, for Microcrystalline Silicon Deposition,* Journal of Vacuum Science & Technology A: Vacuum, Surfaces, and Films **28**, 989 (2010).

F. Imbeaux, J.B. Lister, G.T.A. Huysmans, et al., *A generic data structure for integrated modelling of tokamak physics and subsystems*, Computer Physics Communications, **181**, 987 (2010)

D. Iraji, I. Furno, A. Fasoli, C. Theiler, *Imaging of Turbulent Structures and Tomographic Reconstruction of TORPEX Plasma Emissivity,* Physics of Plasmas **17**, (2010).

X. Lapillonne, B.F. McMillan, T. Goerler, S. Brunner, T. Dannert, F.Jenko, F. Merz, L. Villard, *Nonlinear Quasisteady State Benchmark of Global Gyrokinetic Codes,* Physics of Plasmas **17**, 112321 (2010).

B. Legradic, A.A. Howling, C. Hollenstein, *Radio Frequency Breakdown between Structured Parallel Plate Electrodes with a Millimetric Gap in Low Pressure Gases,* Physics of Plasmas **17**, 102111 (2010).

C. Marinucci, L. Bottura, M. Calvi, *A Parametric AC Loss Model of the ITER Coils for Control Optimization,* Cryogenics **50**, 187-199 (2010).

C. Marinucci, M. Calvi, L. Bottura, F. Cau, A. Portone, *Analysis of the EDIPO Temperature Margin During Current Ramp-Up,* IEEE Trans. Appl. Supercond. **20**, 604-607 (2010).

N.N. Martovetsky, D.R. Hatfield, J.R. Miller, P. Bruzzone, B. Stepanov, B. Seber, *Qualification of the U.S.-Made Conductors for ITER Toroidal Field (TF) Magnet System,* IEEE Trans. Appl. Supercond. **20**, 466-469 (2010).

B.F. McMillan, S. Jolliet, A. Bottino, P. Angelino, T.M. Tran, L. Villard, *Rapid Fourier Space Solution of Linear Partial Differential Equations in Toroidal Magnetic Confinement Geometries,* Computer Physics Communications **181**, 715 (2010).

B.F. McMillan, X. Lapillonne, S. Jolliet, L. Villard, A. Bottino, T. Görler, F. Jenko, *System Size Effects on Gyrokinetic Turbulence,* Physical Review Letters **105**, 155001 (2010).

S.Y. Medvedev, A.A. Ivanov, A.A. Martynov, Y.Y. Poshekhonov, R. Behn, Y.R. Martin, J.M. Moret, F. Piras, A. Pitzschke, A. Pochelon, O. Sauter, L. Villard, *Edge Stability and Pedestal Profile Sensitivity of Snowflake Diverted Equilibria in the TCV Tokamak,* Contributions to Plasma Physics **50**, 324 (2010).

L. Muzzi, A. Della Corte, S. Di Zenobio, S. Turtu, P. Barabaschi, P. Bruzzone, A. Baldini, *The JT-60SA Toroidal Field Conductor Reference Sample: Manufacturing and Test Results,* IEEE Trans. Appl. Supercond. **20**, 442-445 (2010).

D.K. Oh, S.-H. Park, K. Kim, P. Bruzzone, *Performance Test of TFK02 Qualification Sample of ITER TF Conductor,* IEEE Transactions on Applied Superconductivity **20**, 458-461 (2010).

Z. Oksiuta, E. Boehm-Courjault, N. Baluc, *Relation between Microstructure and Charpy Impact Properties of an Elemental and Pre-Alloyed 14Cr ODS Ferritic*

Steel Powder after Hot Isostatic Pressing, Journal of Materials Science **45**, 3921-3930 (2010).

T. Panis, D. Testa, A. Fasoli, A. Klein, H. Carfantan, P. Blanchard, *Optimization of the Active MHD Spectroscopy System on JET for the Excitation of Individual Intermediate and High-N Alfven Eigenmodes,* Nuclear Fusion **50**, 084019 (2010).

G. Pintsuk, Z. Oksiuta, J. Linke, N. Baluc, *High heat flux testing of 12-14 Cr ODS ferritic steels*, Journal Nuclear Materials **396**, 20 (2010)

F. Piras, S. Coda, B.P. Duval, B. Labit, J. Marki, S.Y. Medvedev, J.M. Moret, A. Pitzschke, O. Sauter, TCV Team, *Snowflake Divertor Experiments on TCV,* Plasma Physics and Controlled Fusion **52**, 124010 (2010).

F. Piras, S. Coda, B.P. Duval, B. Labit, J. Marki, S.Y. Medvedev, J.M. Moret, A. Pitzschke, O. Sauter, TCV Team, *"Snowflake" H Mode in a Tokamak Plasma,* Physical Review Letters **105**, 155003 (2010).

F. Piras, J.M. Moret, J.X. Rossel, *Measurement of the Magnetic Field Errors on TCV,* Fusion Engineering and Design **85**, 739-744 (2010).

P. Ricci, B.N. Rogers, *Turbulence Phase Space in Simple Magnetized Toroidal Plasmas,* Physical Review Letters **104**, 145001 (2010).

P. Ricci, B.N. Rogers, W. Dorland, *Collisional Damping of Zonal Flows Due to Finite Larmor Radius Effects,* Physics of Plasmas **17**, 072103 (2010).

B.N. Rogers, P. Ricci, *Low-Frequency Turbulence in a Linear Magnetized Plasma,* Physical Review Letters **104**, 225002 (2010).

J.X. Rossel, J.M. Moret, Y. Martin, TCV Team, *A 3D Multi-Mode Geometry-Independent Rmp Optimization Method and Its Application to TCV,* Plasma Phys. Control. Fusion **52**, 035006 (2010).

O. Sauter, M.A. Henderson, G. Ramponi, H. Zohm, C. Zucca, *On the Requirements to Control Neoclassical Tearing Modes in Burning Plasmas,* Plasma Phys. Control. Fusion **52**, 025002 (2010).

A. Shikov, V. Pantsyrny, A. Vorobieva, R. Vasilyev, N. Kozlenkova, K. Abramushin, V. Sytnikov, A. Taran, A. Rychagov, P. Bruzzone, B. Stepanov, *The Result of Russian ITER TF Conductor Sample Test in Sultan,* IEEE Trans. Appl. Supercond. **20**, 462-465 (2010).

F. Simon, Y. Ilin, B. Su Lima, F. Cau, R. Herzog, B. Stepanov, *Reliability Considerations of the ITER Poloidal Field Coils,* IEEE Trans. Appl. Supercond. **20**, 423-426 (2010).

B. Stepanov, P. Bruzzone, R. Wesche, N. Martovetsky, D. Hatfield, A. Vostner, A. Devred, *Impact of Sample Preparation Procedure on the Test Results of Four US ITER TF Conductors,* IEEE Trans. Appl. Supercond. **20**, 508-511 (2010).

B. Strahm, C. Hollenstein, *Powder Formation in SiH[Sub 4] -H[Sub 2] Discharge in Large Area Capacitively Coupled Reactors: A Study of the Combined Effect of Interelectrode Distance and Pressure,* Journal of Applied Physics **107**, 023302 (2010).

D. Terentyev, S.M. Hafez Haghighat, R. Schaeublin, *Strengthening Due to Cr-Rich Precipitates in Fe-Cr Alloys: Effect of Temperature and Precipitate Composition,* Journal of Applied Physics **107**, 061806 (2010).

D. Terranova, D. Bonfiglio, A.H. Boozer, A.W. Cooper, M. Gobbin, S.P. Hirshman, R. Lorenzini, L. Marrelli, E. Martines, B. Momo,

N. Pomphrey, I. Predebon, R. Sanchez, G. Spizzo, M. Agostini, A. Alfier, L. Apolloni, F. Auriemma, M. Baruzzo, T. Bolzonella, F. Bonomo, M. Brombin, A. Canton, S. Cappello, L. Carraro, R. Cavazzana, S.D. Bello, R. Delogu, G. De Masi, M. Drevlak, A. Fassina, A. Ferro, P. Franz, E. Gaio, E. Gazza, L. Giudicotti, L. Grando, S.C. Guo, P. Innocente, D. L Pez-Bruna, G. Manduchi, G. Marchiori, P. Martin, S. Martini, S. Menmuir, S. Munaretto, L. Novello, R. Paccagnella, R. Pasqualotto, G.V. Pereverzev, R. Piovan, P. Piovesan, L. Piron, M.E. Puiatti, M. Recchia, F. Sattin, P. Scarin, G. Serianni, A. Soppelsa, S. Spagnolo, M. Spolaore, C. Taliercio, M. Valisa, N. Vianello, Z. Wang, A. Zamengo, B. Zaniol, L. Zanotto, P. Zanca, M. Zuin, *A 3D Approach to Equilibrium, Stability and Transport Studies in Rfx-Mod Improved Regimes,* Plasma Physics and Controlled Fusion **52**, 124023 (2010).

D. Testa, H. Carfantan, R. Chavan, J. Lister, J.M. Moret, M. Toussaint, *Functional Performance Analysis and Optimization for the High-Frequency Magnetic Diagnostic System in ITER - Part 2: Detailed Overview of the Analysis Method and of the Test Calculations,* Fusion Science and Technology **57**, 238-273 (2010).

D. Testa, H. Carfantan, R. Chavan, J.B. Lister, J.M. Moret, M. Toussaint, *Functional Performance Analysis and Optimization for the High-Frequency Magnetic Diagnostic System in ITER - Part 1: Overview of the Results,* Fusion Science and Technology **57**, 208-237 (2010).

D. Testa, H. Carfantan, A. Goodyear, T. Panis, P. Blanchard, A. Fasoli, A. Klein, JET-EFDA Contributors, *The JET Alfvén Eigenmode Local Manager for the Real-Time Detection and Tracking of MHD Instabilities,* Europhysics Letters **92**, 50001 (2010).

D. Testa, N. Mellet, T. Panis, P. Blanchard, H. Carfantan, A. Fasoli, A. Goodyear, S. Pinches, JET-EFDA Contributors, *The Dependence of the Damping Rate of Medium-N Toroidal Alfvén Eigenmodes on the Edge Plasma Elongation in JET,* Nuclear Fusion **50(8)**, 084010 (2010).

D. Testa, M. Toussaint, R. Chavan, J. Guterl, J.B. Lister, J.-M. Moret, A. Perez, F. Sanchez, B. Schaller, G. Tonetti, A. Encheva, G. Vayakis, C. Walker, Y. Fournier, T. Maeder, A. Le-Luyer, P.J. Moreau, G. Chitarin, E. Alessi, R. Delogu, A. Gallo, N. Marconato, S. Peruzzo, M. Preindl, H. Carfantan, E. Hodgson, J. Romero, R. Vila, B. Brichard, L. Vermeeren, *The Magnetic Diagnostic Set for ITER,* IEEE Transactions on Plasma Science **38**, 284-294 (2010).

T. Vernay, S. Brunner, L. Villard, B. Mcmillan, O. Sauter, S.B. Jolliet, T.M. Tran, A. Bottino, *Global Collisional Gyrokinetic Simulations of ITG Microturbulence Starting from a Neoclassical Equilibrium,* J. of Physics: Conference Series **260**, 012021 (2010).

T. Vernay, S. Brunner, L. Villard, B.F. Mcmillan, S. Jolliet, T.M. Tran, A. Bottino, J.P. Graves, *Neoclassical Equilibria as Starting Point for Global Gyrokinetic Microturbulence Simulations,* Physics of Plasmas **17**, 122301 (2010).

L. Villard, A. Bottino, S. Brunner, A. Casati, J. Chowdhury, T. Dannert, R. Ganesh, X. Garbet, T. Görler, V. Grandgirard, R. Hatzky, Y. Idomura, F. Jenko, S. Jolliet, S. Khoshaghdam, X. Lapillonne, G. Latu, B.F. Mcmillan, F. Merz, Y. Sarazin, T.M. Tran, T. Vernay, *Gyrokinetic Simulations of Turbulent Transport: Size Scaling and Chaotic Behaviour,* Plasma Physics and Controlled Fusion **52**, 124038 (2010).

F. Wagner, A. Becoulet, R. Budny, V. Erckmann, D. Farina, G. Giruzzi, Y. Kamada, A. Kaye, F. Koech, K. Lackner, N. Marushchenko, M. Murakami, T. Oikawa, V. Parail, J.M. Park, G. Ramponi, O. Sauter, D. Stork, P.R. Thomas, Q.M. Tran, D. Ward, H. Zohm, C. Zucca, *On the Heating Mix of ITER,* Plasma Physics and Controlled Fusion **52**, 124044 (2010).

L. Zani, P. Barabaschi, P. Bruzzone, D. Ciazynski, P. Decool, B. Lacroix, M. Nannini, B. Stepanov, A. Torre, J.M. Verger, *Tests and Analyses of Two TF Conductor Prototypes for JT-60SA,* IEEE Trans. Appl. Supercond. **20**, 451-454 (2010).

APPENDIX B Conferences and Seminars

(see CRPP archives at http://crppwww.epfl.ch/archives)

B.1 Conference and conference proceedings published in 2010

M. Albergante, J.P. Graves, A. Fasoli, M. Jucker, X. Lapillonne, W.A. Cooper, *Numerical Modelling of the Electromagnetic Turbulent Transport of Energetic Ions in Burning Plasmas,* Varenna Lausanne International Workshop, Theory of Fusion Plasmas, Varenna, Italy, 30 August - 03 September 2010.

M. Albergante, J.P. Graves, F. Fasoli, W.A. Cooper, M. Jucker, X. Lapillonne, *Influence of Fine Scale Turbulence on the Transport of High Energy Populations in Burning Plasmas,* 37th EPS Conference on Plasma Physics, Dublin, Ireland, 21-25 June 2010.

S. Alberti, J.-P. Hogge, I. Pagonakis, T.-M. Tran, M.Q. Tran, *Design Studies of the Dual-Frequency Operation of the W7-X/140Ghz/Mw Gyrotron at 126Ghz for TCV and 168Ghz for ITER,* 35th International Conference on Infrared, Millimeter and Terahertz Waves, Rome, Italy, September 5-10, 2010 (IRMMW-THZ 2010)

D. Borba, A. Fasoli, N.N. Gorelenkov, S. Gunter, P. Lauber, N. Mellet, R. Nazikian, T. Panis, S.D. Pinches, D. Spong, D. Testa, JET-EFDA Contributors, *The Influence of Plasma Shaping on the Damping of Toroidal Alfven Eigenmodes,* presented at 23rd IAEA Fusion Energy Conference, Daejeon, Republic of Korea, 11-16 October 2010.

P. Bruzzone, *Review of Design Aspects for High Current Nb3Sn Conductors,* Applied Superconductivity Conference, ASC-2010, Washington, DC, USA, August 1-6, 2010 (2010).

P. Bruzzone, B. Stepanov, R. Wesche, M. Bagnasco, R. Herzog, C. Calzolaio, M. Vogel, *Operation and Test Results from the Sultan Test Facility, Presented at: Applied Superconductivity Conference, ASC-2010, Washington, DC, USA, August 1-6, 2010.*

P. Bruzzone, B. Stepanov, R. Wesche, S. Turtu, V. Corato, A. Devred, D. Bessette, A. Vostner, T. Boutboul, S. Lelekhov, W. Yu, *Test Results of Two ITER Poloidal Field Conductor Samples in Sultan,* Applied Superconductivity Conference, ASC-2010, Washington, DC, USA, August 1-6, 2010.

P. Bruzzone, B. Stepanov, R. Wesche, R. Herzog, C. Calzolaio, M. Vogel, *Test of ITER Conductors in Sultan: An Update,* SOFT 2010, Porto, Portugal, September 27 - October 1, 2010.

R. Chawla, J.-P. Ansermet, J.M. Cavedon, P. Hirt, W. Kroeger, H.M. Prasser, M.Q. Tran, *The Swiss Master in Nuclear Engineering: A Collaboration between Universities Research Centre and Industry,* Icone 18, Xi'an, P.R. China, May 2010.

S. Coda, T.C.V. Team, *Progress and Scientific Results in the TCV Tokamak,* 23rd IAEA Fusion Energy Conference, Daejon, Korea, 11-16 October 2010, Proceedings of the 23rd IAEA Fusion Energy Conference, OV/5-2 (2010).

S. Goekce, P. Peschke, C. Hollenstein, P.N.L. Leyland, P. Ott, S. Pavon, *Surface DBD'ss and Plasma-Flow Interaction,* Euromech Fluid Mechanics Conference 8, Bad Reichenhall, D, September 13-16, 2010.

S. Goekce, P. Peschke, C. Hollenstein, P. Ott, P.N.L. Leyland, *Aero Engine Flow Control by Surface Discharge Plasma,* III International Scientific and Technical Conference Aeroengines of XXI Century, Moscow, RU, November 30 - December 3, 2010.

J.P. Graves, S. Coda, I. Chapman, T. Johnson, M. Lennholm, *Sawtooth Control Relying on Toroidally Propagating Icrf Waves,* 23rd IAEA Fusion Energy Conference, Daejon, Korea, 11-16 October 2010.

B. Labit, A. Pochelon, M. Rancic, F. Piras, *Transport and Turbulence with Innovative Plasma Shapes in the TCV Tokamak,* 23rd IAEA Fusion Energy Conference, Daejeon, Korea, October 11-16, 2010.

B. Legradic, A. Howling, C. Hollenstein, *RF Breakdown in Low Pressure Gases between Small (Millimetric) Gap Parallel Plate Electrodes with Surface Structures,* Proceedings of the 7th ICRP and 63rd GEC conference, Paris, France, October 4-8, 2010, TF1-003 (2010).

B. Legradic, A. Howling, C. Hollenstein, *RF breakdown in low pressure gases in small (millimetric) gaps with non-planar surfaces*, 37th IEEE International Conference on Plasma Science (ICOPS), Norfolk, USA, October 4-8, 2010

C. Marinucci, L. Bottura, M. Calvi, R. Wesche, *Quench Analysis of a High-Current Forced-Flow Hts Conductor Model for Fusion Magnets,* Presented at: ASC, Washington, DC, USA, August 1-6, 2010. (2010).

A. Macor, E. De Rijk, G. Boero, J.-P. Ansermet, S. Alberti, *Millimeter Waves for NMR Enhancement,* 35th Int. Conference on Infrared, Millimeter and Terahertz Waves, Roma, Italy, September 5-10 2010 (IRMMW THz 2010).

Y. Martin, E. Fable, C. Angioni, Y. Camenen, D. Wagner, B.P. Duval, L. Federspiel, A. Karpushov, V. Piffl, O. Sauter, H. Weisen, *Impurity Transport in TCV: Neoclassical and Turbulent Contributions,* 23rd IAEA Fusion Energy Conference, Daejon, Korea, 11-16 October 2010.

R. Narkovic, M. Siegrist, P. Moreau, J.-P. Hogge, R. Raguotis, R. Brazis, *Third Harmonic Generation with a 118ghz Gyrotron,* 18th Int. Conf. on Microwaves, Radar & Wireless Communications (MIKON 2010).

Y. Nunoya, Y. Nabara, M. Yoshikawa, K. Matsui, T. Hemmi, Y. Takahashi, T. Isono, N. Koizumi, H. Nakajima, B. Stepanov, P. Bruzzone, *Test Results for a Full Size Nb3Sn Conductor Developed for the ITER TF Coils,* Applied Superconductivity Conference, ASC-2010, Washington, DC, USA, August 1-6, 2010.

Z. Oksiuta, M.Ç. Lewandowska, K. Kurzydlowski, N. Baluc, *Reduced Activation ODS Ferritic Steel - Recent Development in High Speed Hot Extrusion Processing,* Fall meeting of the European Materials Research Society, Warsaw, Poland, September 14-18, 2009, Physica Status Solidi A **207**(5), 1128-1131 (2010).

I. Pagonakis, J.-P. Hogge, S. Alberti, B. Piosczyk, S. Illy, S. Kern, C. Liévin, *An Additional Criterion for Gyrotron Gun Design,* IEEE 35th Int. Conference on Plasma Sciences (ICOPS 2010).

I.G. Pagonakis, J.P. Hogge, S. Alberti, S. Illy, B. Piosczyk, S. Kern, C. Liévin, M.Q. Tran, *Status of the EU 170 GHz/2MW,CW coaxial cavity gyrotron for ITER: the dummy gun experiment,* 35th International Conference on Infrared, Millimeter and Terahertz Waves, Rome, Italy, September 5-10, 2010 (IRMMW-THZ 2010)

J.I. Paley, S. Coda, B.P. Duval, F. Felici, J.M. Moret, TCV Team, *Architecture and Commissioning of the TCV Distributed Feedback Control System,*

17th Real Time Conference IEEE NPSS Technical Committee on Computer Applications in Nuclear and Plasma Sciences, Lisboa, Portugal, 24-28 May 2010.

A. Perez, D. Fasel, J.B. Lister, B. Marlétaz, P. Marmillod, U. Siravo, *ITER-Earthing,* Fusion Engineering and Design, 26th Symposium on Fusion Technology, Porto, Portugal, 27 September – 1 October 2010 (2010).

A. Portone, M. Bagnasco, B. Baker, P. Bruzzone, F. Cau, E. Fernandez-Cano, E. Salpietro, B. Stepanov, P. Testoni, E. Theisen, R. Wesche, *Status Report of the EDIPO Project,* Applied Superconductivity Conference, ASC-2010, Washington, DC, USA, August 1-6, 2010.

M. Silva, F. Felici, T.P. Goodman, L. Porte, *Fast Polarizers Installation for ECRH and ECE in TCV,* Fusion Engineering and Design, 26th Symposium on Fusion Technology, Porto, Portugal, 27 September - 01 October 2010.

D. Testa, H. Carfantan, M. Toussaint, R. Chavan, Y. Fournier, J. Guterl, J.B. Lister, T. Maeder, J.M. Moret, A. Perez, F. Sanchez, B. Schaller, C. Slater, M. Stoeck, G. Tonetti, *Assessment of the ITER High-Frequency Magnetic Diagnostic Set,* Proceedings 26th Symposium on Fusion Technology (SOFT 2010 Conference), Porto (Portugal), September 27th to October 1st, 2010 (2010).

D. Testa, N. Mellet, T. Panis, S.E. Sharapov, D. Spong, P. Blanchard, H. Carfantan, A. Fasoli, A. Goodyear, J.-E. Contributors, *Recent JET Experiments on Alfven Eigenmodes with Intermediate Toroidal Mode Numbers: Measurements and Modelling,* 23rd IAEA Fusion Energy Conference, Daejon, Korea, 11-16 October 2010, IAEA-FEC Fusion Energy Conference 2010.

F. Wagner, A. Becoulet, R. Budny, O. Sauter, M.Q. Tran, C. Zucca, *On the Heating Mix of ITER,* 37th EPS European Physical Society Conference, Dublin, Ireland, 21-25 June, 2010.

R. Wesche, M. Bagnasco, P. Bruzzone, R. Felder, M. Guetg, M. Holenstein, M. Jenni, S. March, F. Roth, M. Vogel, *Test Results of the 18 kA EDIPO HTS Current Leads,* SOFT 2010, Porto, Portugal, September 27 - October 1, 2010.

B.2 Seminars presented at the CRPP in 2010

D. Lescure, Ecole Nationale Supérieure des Mines de Paris, F, *"Etude thermo-hydraulique des propriétés de mélange d'un nouveau type de combustible pour REP et REB"*

Dr. F. Li, SUPA, Dept. Of Physics, Univ. of Strathclyde, Glasgow, Scotland, UK, *"Millimeter wave gyrotron research at the University of Strathclyde"*

A. Mosetto, Politecnico di Torino, I, *"Two phase flow instrumentation and CFD analysis for the SPES3 facility"*

Dr. W. Suttrop, Max-Planck-Institute für Plasmaphysik, Garching, D, *"In-vessel saddle coils for MHD control in ASDEX Upgrade"*

Y. Sadeghi, ENEA Frascati, I, *"Real-time reconstruction of magnetic flux in FTU tokamak"*

J. Guterl, EPFL, CH, *"Simulation of return plasma flow in the ionization region"*

Dr. M. Barns, Oxford University, UK, *"Direct multi-scale coupling of a transport code to gyrokinetic turbulence codes, with comparisons to tokamak experiments"*

Dr. X. Lapillonne, CRPP-EPFL, CH, *"Local and global Eulerian gyrokinetic simulations of microtrubulence in realistic geomertry with applications to the TCV tokamak"*

Dr. S. Jawla, CRPP-EPFL, CH, *"Phase retrieval and Gaussian beam mode decomposition of gyrotron beams"*

Dr. A. Macor, Inst. de Physique des Nanosctructures, EPFL, CH, *"Advancement of the Gyro DNP project"* and **E. de Rijk**, Univ. van Amsterdam, NL, *"Coupling between millimeter waves and matter in nuclear magnetic resonance spectroscopy"*

F. Felici, CRPP-EPFL, CH, *"Feedback control of ECRH polarization on LHD"*

W. Vijvers, FOM Institute for Plasma Physics, Rijnhuizen, NL, *"Development of a high power plasma source to simulate ITER divertor conditions"*

Dr. M. Faganello, Lab. de Physique des Plasmas, Ecole Polytechnique Palaiseau, F, *"Multiple scale behaviour of luid plasmas, strong feedback between large scale and small scale dynamics"*

Dr. J. Urban, Inst. for Plasma Physics, Praha, CZ, *"EBW heating and current drive modelling for spherical tokamaks" and "EBW emission on COMPASS"*

G. Hornung, Inst. für Plasmaforschung, Univ. Suttgart, D, *"Characterization of the turbulent structures in the torsatron TJ-K"*

Dr. A. Degeling, Dept. Of Physics, Univ. of Alberta, CA, *"Modeling of ultra low frequency wave activity and relativistic electron dynamics within the earth's magnetosphere"*

R. Futtersack, Ecole Centrale Paris, F, *"Modular Fokker-Planck solver for neutral beam injection in CRONOS"*

F. Halpern, CNRS, Ecole Polytechnique Palaiseau, F, *"Oscillation regimes of the internal kink mode in two-fluid MHD simulations"*

Dr. N. Kirneva, RRC "Kurchatov Institute" Moscow, RU, *"Plasma confinement and transport in experiments with different EC heating profile width"*

Dr. B. Teaca, Université Libre de Bruxelles, B, *"Energy transfers between scales in fully developed magnetohydrodynamic turbulence"*

J. Kamleitner, Vienna University of Technology, A, *"The Na beam plasma edge diagnostic at ASDEX Upgrade and further previous work"*

Dr. A. Martynov, Univ. du Québec, Montréal, CA, *"Paramétrage avancé de la surface terrestre dans les modèles du climat: lacs et mers internes"*

C. Reux, CEA Cadarache, F, *"Disruption mitigation using massive gas injection – experiments and modelling"*

D. Kim, CRPP-EPFL, CH, *"Numerical simulation on ELM control capability of RMP in the KSTAR tokamak"*

A. Bovet, EPFL, CH, *"Anomalous diffusion of fat ions in the presence of fishbone instabilities in tokamaks" and "One year as a physics teacher in Cameroon"*

G. Avvisati, Univ. of Naples "Federico II", I, *"Dynamics of dust particles in tokamak plasmas"*

Dr. G. Annino, Scuola Normale Superiore, Pisa, I, *"Millimeter and submillimeter wave dielectric characterization by means of whispering gallery mode resonators"*

Dr. C. Chaston, Space Sciences Lab., Univ. of California, Berkeley, USA, *"Current sheets, flow shears and particle acceleration in auroral plasmas"*

Dr. M. Jucker, CRPP-EPFL, CH, *"Self-consistent ICRH distribution functions and equilibria in magnetically confined plasmas"*

S. Zhou, McWilliams Plasma Lab., Univ. of California, Irvine, USA, *"Turbulent transport of fast ions in the large plasma device (LAPD)"*

Dr. L. Vermare, Lab. de Physique des Plasmas, Ecole Polytechnique, Palaiseau, F, *"Doppler reflectrometry in Tore Supra: Application to plasma turbulence and transport studies"*

D. Pfefferlé, CERN, Genève, CH, *"Hitch-hiking through particle physics from the standard model to the 5th dimension"*

Dr. W. Bertsche, CERN, Genève, CH, *"Trapped antihydrogen for spectroscopy"*

Dr. J. Romero, CIEMAT, Madrid, SP, *"Inductive control at TCV: transformer model and internal inductance real time observer"*

APPENDIX C External activities of CRPP Staff during 2010

C.1 National and international committees and ad-hoc groups

MEMBERSHIP

N. Baluc	Member of the HPC-FF board Member of the EFDA Scientific and Technical Advisory Committee (STAC) International Organizing Committee of the SOFT Conference (Symposium on Fusion Technology) International Advisory Committee of the ICFRM Conference (International Conference on Fusion Reactor Materials) IEA Annex II Executive Committee IEA Fusion Materials Agreement Executive Committee Swiss Society for Optics and Microscopy (SSOM) Task Coordinator of the subproject entitled 'Radiation-Resistant Materials' of the EXTREMAT Integrated Project (IP) of the 6th European Framework Programme
P. Bruzzone	International Magnet Technology Conference Organizing Committee European Magnet Expert Group 22st Magnet Technology Conference, Programme Committee SST-1 (India), Magnet Review Group Series Connected Hybrid Magnet, Project Review Group
B.P. Duval	TTG-rotation/transport working group chair, EU-TTG
A. Fasoli	Visiting Professor, MIT Physics Department EFDA Steering Committee ASDEX Upgrade Programme Committee, Germany International Tokamak Physics Activities: Energetic Particles Topical Group Scientific Committee, 12th IAEA Technical Meeting on Energetic Particles in Magnetic Confinement Systems, 2011 Expert for the Review of projects submitted to the French National Agency for Research (ANR) Member of Scientific Committee of the EFDA Transport Topical Group US Department of Energy National Spherical Torus Experiment Review U.S. Department of Energy SciDAC: Advanced Simulation of Fusion Plasmas Review. Review of projects using large research infrastructure for the Government Commissioner for European Research of the Czech Republic Professor Committee for APS Marshal Rosenbluth Outstanding Doctoral Thesis Award, 2010 Evaluation of research programme of the University of Padua, Italy Chair of the Basic and astrophysical plasma of Programme Committee of EPS Conference 2011
Ivo Furno	Member of the SPS Committee
Ch. Hollenstein	Member of the Wissenschaftlicher Beirat Leibniz-Institut für Oberflächenmodifizierung Leipzig Editorial Board Plasma Chemistry and Plasma Processing Kluwer Academic/Plenum Publisher Member of the IUVSTA Plasma Division

	President of the Swiss Vacuum society
C. Marinucci	CHATS-AS, Board
A. Pochelon	Member of the Committee of the SWISS NUCLEAR FORUM Secretary and Member of the Swiss Physical Society Committee Member of the FORATOM Committee, in particular of the "Research and Development Task Force (R&D.TF) Associate member of IUPAP (International Union of Physics and Applied Phyiscs), Commission C16: Commission on plasma physics
O.Sauter	International Tokamak Physics Activities: MHD, Disruption and Control Topical Group Chairman of the scientific committee of the Joint Varenna-Lausanne International Workshop on Theory of Fusion Plasmas
R. Schäublin	Member of the board of the Swiss Society for optics and microscopy Member of the Program Committee of the ICFRM Conference (Int. Conf. on Fusion Reactor Materials)
P. Spätig	Member of the Program Committee of the ICFRM Conference (Int. Conf. on Fusion Reactor Materials)
M.Q. Tran	Director of the Inst. of Physics of Energy and Particle, EPFL Consultative Committee for the Euratom Specific Research and Training Programme in the field of Nuclear Energy, Fusion (CCE-FU) Chairman of the Technical Advisory Panel of the Joint Undertaking Fusion for Energy (F4E) Swiss expert to the Governing Board of F4E Member of the Core Commission for nomination of Max-Planck Plasma Physics Committee of the International Symposium on Fusion Nuclear Technology Member of the Steering Committee of the Center of Competence on Energy and Mobility of the the CEPF Member of the International Committee of the IRMWW and THZ conference Swiss delegate at the Fusion Power Coordinating Committee Member of the EU Delegation and vice-chair of ITER STAC
L. Villard	Expert, High Performance Computing for Fusion, EFDA Special working group 1 of the HPC-IFERC-Broader Approach
H. Weisen	Seconded to EFDA-JET CSU, programme department Member of the Diagnostics Working Group within the ITPA Member of the expert panel for evaluating PhD and post-doc research proposals submitted to the Fonds National de la Recherche, Luxembourg

PARTICIPATION

S. Alberti	Member of the Local Organizing Commitee of the "3rd International Meeting on Dynamic Nuclear Polarization" to be held at EPFL, 7-10 September 2011
B. Duval	Remote Participation Users Group, EFDA-JET EU-TTG Meeting, Cordoba, Spain
Y.R. Martin	International Tokamak Physics Activity: Transport and Confinement Modelling Topical Group

C.2 Editorial and society boards

S. Alberti	Guest Editor for the Special Issue on High-Power Microwave Generation, IEEE Transactions on Plasma Science, June 2010 Editorial Board IEEE Transaction on THz Science and Technology (Topical editor: THz plasma science and instruments)
S. Coda	Editorial Board of Plasma Physics and Controlled Fusion
Ch. Hollenstein	Editorial Board Plasma Chemistry and Plasma Processing Kluwer Academic/Plenum Publisher
J.B. Lister	Member of the International Advisory Board of Plasma Physics and Controlled Fusion
Y.R. Martin	Member of the EFDA Public Information Group (PIG) Chairman of the Association Vaudoise des Chercheurs en Physique
A. Pochelon	Auditor of the Swiss Physical Society Committee Set up of a "Network of Experts in the domain of Energy in Switzerland", Swiss Physical Society Committee
M.Q. Tran	Guest Editor for the Special Issue on High-Power Microwave Generation, IEEE Transactions on Plasma Science, June 2010

C.3 EPFL committees and commissions

N. Baluc	Commission Ecole Doctorale en Science et Génie des Matériaux Commission Ecole Doctorale en Physique
A. Fasoli	Commission Stratégique de la Physique, EPFL Direction de la Faculté FSB Comité de Coordination Joint Doctoral Initiative EPFL-IST Lisbon Conseiller d'études pour la Physique - Master
J-Ph. Hogge	Commission du Doctorat de la Section de Physique, FSB-EPFL
O. Sauter	Commission du Doctorat de la Section de Physique, FSB-EPFL
M.Q. Tran	Commission du Doctorat de la Section de Physique, FSB-EPFL Commission stratégique de la Section de Physique, EPFL Membre du Comité de Sélection du Prix de la meilleure thèse EPFL
T.M. Tran	Groupe de travail technique du Comité de Pilotage HPC/MPC, EPFL
L. Villard	Délégué à la mobilité, Section de physique, FSB-EPFL Commission d'Ethique, EPFL Commission d'Enseignement de la Section de Physique, FSB-EPFL Groupe de travail technique HPC (High Performance Computing) – EPFL Steering Committee, HPC (High Performance Computing) – EPFL

APPENDIX D The basis of controlled fusion

D.1 Fusion as a sustainable energy source

Research into controlled fusion aims to demonstrate that it is a valid option for generating power in the long term future in an environmentally, politically and economically acceptable way. Controlled fusion is a process in which light nuclei fuse together to form heavier ones: during this process a very large amount of energy is released. For a fusion reactor it is planned to use the two isotopes of hydrogen: deuterium (D) and tritium (T), which fuse together much more readily than any other combination of light nuclei according to the following reaction:

$$D^2 + T^3 \rightarrow He^4 + n + 17.6MeV$$

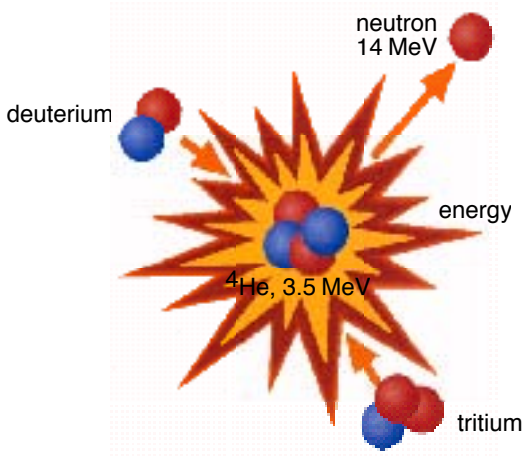

Fig. D.1 *Schematic of a fusion reaction between deuterium and tritium nuclei. The products are 3.5MeV ^{4}He, the common isotope of helium, and a 14MeV free neutron.*

The end products are helium and neutrons (n). The total energy liberated by fusing one gram of a 50:50% mixture of deuterium and tritium is 94000kWh, which is 10 million times more than from the same mass of oil. 80% of this energy is carried by the neutrons with an energy of 14MeV while the remaining 20% is carried by the helium nucleus. Most of this energy eventually becomes heat to be stored or converted by conventional means into electricity.

The temperature at which fusion reactions start to become significant are above a few tens of millions of degrees. For the D-T reaction, the optimal temperature is of the order of 70-200 million degrees. At such temperatures the D-T fuel is in the plasma state.

Deuterium is very abundant on the earth and can be extracted from water (0.034g/l). Tritium does not occur naturally, since its half-life is only 12.3 years, but it can be regenerated from lithium using the neutrons produced by the D-T fusion reactions. The two isotopes of natural lithium contribute to this breeding of tritium according to the reactions:

$$Li^6 + n \rightarrow He^4 + T^3 + 4.8MeV$$

$$Li^7 + n \rightarrow He^4 + T^3 + n - 2.5MeV$$

The relative abundance of the two lithium isotopes Li^6 and Li^7 are 7.4% and 92.6%, respectively. The known geological resources of lithium both in the earth and in the sea water are large enough to provide energy for an unlimited time.

D.2 Attractiveness of fusion as an energy source

The inherent advantages of fusion as an energy source are:

- The fuels are plentiful and their costs are negligible because of the enormous energy yield of the reaction;
- The end product of the reaction is helium, an inert, non-radioactive gas;
- No chain reaction is possible: the neutron emitted by the fusion process does not trigger subsequent reactions;
- Only a very small amount of fuel is present in the core of the reactor: the plasma weights a fraction of gram;
- Any malfunction would cause a quick drop of temperature and all fusion reactions would stop within seconds;
- No after-heat problem can lead to thermal runaway even if the case of a loss of coolant accident;
- None of the materials required by a fusion power plant are subject to the provisions of the non-proliferation treaties.

Its further potential advantages are:

- Radioactivity of the reactor structure, caused by neutrons, can be minimised by careful selection of low-activation materials resulting in a manageable quantity of long lived radioactive waste;
- The release of tritium in normal operation can be kept at a very low level. The inventory of tritium on the site can be sufficiently small so that even the worst possible accident could not lead to a harmful release to the environment requiring evacuation of the nearby population.

APPENDIX E Sources of Financial Support

In 2010, the work carried out at the CRPP and presented in this annual report was financed from several sources. The major financial support is provided by:

Swiss public institutions:

- the Ecole Polytechnique Fédérale de Lausanne (EPFL)
- the Conseil des Ecoles Polytechniques (CEPF)
- the Centre de Compétence "Energie-Mobilité" of the CEPF
- the Swiss National Science Foundation
- the Paul Scherrer Institute (PSI), which hosts the Supraconductivity and the Materials science activities
- the Swiss Secrétariat d'Etat à l'Education et à la Recherche (SER)
- the Swiss "Departement Fédéral de l'Intérieur" in the frame of the Broader Approach
- the Swiss "Commission pour la Technologie et l'Innovation" (CTI)

International public institutions:

- EURATOM
- ITER
  - ITER Organization
  - Domestic Agencies in China, Europe (F4E), Japan, Korea
- Helmholtz-Zentrum Berlin, D

Private organisations

- Inspire AG
- OC Oerlikon
- Roth&Rau AG
- Ruag AG
- Sulzer Metco AG
- Swiss Electric AG
- Tetra Pak SA.

The CRPP is the Host of Euratom Fellows:

- MM. A. Collazos and M. da Silva, EC-TECH “Electron cyclotron system technology for ITER”
- F. Cau, M. Bagnasco, MATEFU “Magnet Technology for Fusion”
- Dr. A. Bencze, WP08-FRF-HAS “Spatio-temporal characterization of edge localised mode filamentary and turbulent transport in tokamaks”

APPENDIX F Glossary

A general purpose glossary for the field of controlled fusion and plasma physics is provided in the CRPP Annual Report every two years. Since it was part of the Annual Report 2009, it will not be provided here. (http://crpp.epfl.ch/page-48260-fr.html)